EXPERIMENTAL INVESTIGATION AND NUMERICAL SIMULATION OF THERMAL PERFORMANCE OF COATING-BASED INSULATION IN BUILDINGS

BY

AHMED ABDULLAH ALAWI AL-NAGHI

A Dissertation Presented to the

DEANSHIP OF GRADUATE STUDIES

KING FAHD UNIVERSITY OF PETROLEUM & MINERALS

DHAHRAN, SAUDI ARABIA

In Partial Fulfillment of the

Requirements for the Degree of

DOCTOR OF PHILOSOPHY

In

CIVIL ENGINEERING

OCTOBER 2018

KING FAHD UNIVERSITY OF PETROLEUM & MINERALS
DHAHRAN 31261, SAUDI ARABIA
DEANSHIP OF GRADUATE STUDIES

This thesis, written by **AHMED ABDULLAH ALAWI AL-NAGHI** under the direction of his thesis advisor and approved by his thesis committee, has been presented and accepted by the Dean of Graduate Studies, in partial fulfillment of the requirements for the degree of **DOCTOR OF PHILOSOPHY IN CIVIL ENGINEERING**.

Prof. Omar S. Baghabra Al-Amoudi
(Advisor)

Dr. Muhammad Kalimur Rahman
(Co-Advisor)

Dr. Salah U. Al-Dulaijan
Department Chairman

Dr. Salah U. Al-Dulaijan
(Member)

Prof. Salam A. Zummo
Dean of Graduate Studies

Dr. Ahmed Saad Al-Gahtani
(Member)

22/11/18
Date

Dr. Ali H. Al-Gadhib
(Member)

عمادة الدراسات العليا
DEANSHIP OF GRADUATE STUDIES


وَقُل
رَّبِّ زِدۡنِي عِلۡمٗا

This humble work is dedicated to:

The Soul of My Mother

May Allah shower her his mercy

ACKNOWLEDGMENT

Praise and thanks be to Allah Almighty, for giving me the health, knowledge and patience to complete this work. I acknowledge the financial support given by KFUPM and Thamar University during my graduate studies.

My sincerest gratitude goes to my advisor Prof. Omar Al-Amoudi for the continuous support during my MS and PhD studies and related research, for his patience, motivation, and imparting me immense knowledge. I express my deepest thank to my co-advisor Dr. Muhammad Kalimur Rahman for his extensive guidance during the course of my PhD research in all areas of this research. I am also grateful to my Committee Members, Dr. Salah Al-Dulaijan, Dr. Ahmed Saad Al-Gahtani and Dr. Ali Al-Gadhib for their constructive guidance and support. Thanks are also extended to the department's faculty members and to the other staff members of the Department.

Special thanks and appreciation to Mr. Mohammad A. Al-Oraini; SouthMed Company, Dammam, Saudi Arabia; for providing all the necessary equipment, materials and venue for the test rooms to conduct this research.

My heartfelt gratitude is given to my beloved dead mother and father, my wife and my children Marya, Meera, Hassan and Hossam, who always support me with their love, patience, encouragement and constant prayers. I would like to thank my beloved sister, brother, and all members of my family in Yemen. Finally, I would like to thank my friends in Yemen and KFUPM for their encouragement and support.

TABLE OF CONTENTS

LIST OF TABLES

LIST OF FIGURES

THESIS ABSTRACT

NAME: **AHMED ABDULLAH ALAWI AL-NAGHI**

TITLE: **EXPERIMENTAL INVESTIGATION AND NUMERICAL SIMULATION OF THERMAL PERFORMANCE OF COATING-BASED INSULATION IN BUILDINGS.**

DEPARTMENT: **CIVIL AND ENVIRONMENTAL ENGINEERING**

DATE: **October 2018**

This study was planned to investigate experimentally and numerically the thermal performance and energy efficiency of a new coating-based thermal insulation as compared with other insulation materials that are currently being used in buildings. The experimental investigation was based on full-scale in-situ measurements of four test rooms located in eastern Saudi Arabia during the summer months. The walls of the first test room were constructed using the prevalent hollow-core concrete blocks and a 3-mm coating-based thermal insulation was applied on cement plaster layer from both inner and outer sides. The second test room was the control room, which was similar to the first room except the coating insulation was not applied on the walls. The walls of the third test room were made from concrete blocks incorporating expanded polystyrene board. A new generation and state-of-the-art insulation system, which included insulate-aerated concrete blocks, insulate plaster and thermal coating, was used to construct the walls of the fourth test room. The test rooms were instrumented with thermocouples, heat flux meters, temperature/relative humidity data loggers and power meters. Thermal scanning of the test room walls and roofs using infrared camera and thermal transmittance measurements using commercial U-value equipment were also conducted. The weather station installed at the site provided all the meteorological data.

The data collected from all these equipment were analyzed and validated using numerical simulation programs (DesignBuilder 5.3 and ABAQUS 6.13). The agreement

between the experimental measurements and simulation results was more than 90%, which is considered excellent from practical point of view. These results indicated that the coating-based thermal insulation has excellent thermal properties that included low thermal conductivity, high solar reflectivity and low heat convective coefficient.

The total thermal resistance of the walls in the fourth test room was more than three times that of the total thermal resistance of walls constructed from normal hollow-core concrete block. In comparison with the control room, the energy saved due to the usage of the insulate coating on walls of the first test room, concrete blocks incorporating expanded polystyrene board in walls of the third test room and the new insulation system in walls of the fourth test room was 34.57, 28.73 and 58.04 %; respectively. Hence, the new coating-based thermal insulation was found to be very effective in reducing the heat transfer through the walls of new buildings (as well as existing buildings) whereby the energy consumption in buildings during the summer months could be reduced by about 35%. The new insulation system of walls is highly recommended to be used in new buildings for saving the energy consumption by about 58%. Though the cost of constructing walls using this new insulation system would be marginally more than the other systems, this increase in the initial cost can be repaid within about two years of the saving in energy consumption.

DOCTOR OF PHILOSOPHY
KING FAHD UNIVERSITY OF PETROLEUM AND MINERALS
DHAHRAN 31261
SAUDI ARABIA

ملخص الرسالة

الإســــــــــم: أحمد عبدالله علوي النجحي

عنوان الرسالة: دراسة تجريبية ومحاكاة عددية عن الأداء الحراري للطلاء العازل في المباني

التخصـــــص: الهندسة المدنية والبيئية

تاريخ التـخرج: أكتوبر 2018م

تم تنفيذ هذه الدراسة للتأكد تجريبياً وعددياً من الأداء الحراري وكفاءة الطاقة لطلاء عزل حراري جديد مقارنةً مع مواد العزل الأخرى المستخدمة حالياً في المباني. أستند التحقيق التجريبي على قياسات واسعة النطاق في الموقع لأربع غرف أختبار تقع في شرق المملكة العربية السعودية، خلال أشهر الصيف. تم بناء جدران غرفة الاختبار الأولى باستخدام الطابوق الخرساني المجوف وطبقة 3 مم من طلاء العزل الحراري الجديد على طبقة الجص الأسمنتية من الجانبين الداخلي والخارجي للجدران. غرفة الاختبار الثانية هي الغرفة المرجعية، وكانت مشابهة لغرفة الاختبار الأولى بإستثناء أن طلاء العزل الحراري لم يتم تطبيقة على الجدران. بُنيت جدران غرفة الأختبار الثالثة من طابوق خرساني يشتمل على ألواح البوليسترين الممتدة. تم إستخدام جيل جديد ونظام عزل حديث، والذي يتضمن الطابوق الخرساني الخلوي العازل والجص العازل وطلاء العزل الحراري الجديد، لبناء جدران غرفة الاختبار الرابعة. جُهزت غرف الاختبار بمستشعرات الحرارة، وعدادات تدفق الحرارة، وأجهزة تسجيل بيانات درجة الحرارة/الرطوبة النسبية وعدادات الطاقة. تم إجراء مسح حراري لجدران وأسقف غرف الاختبار بإستخدام كاميرا الأشعة تحت الحمراء. كما تم قياس النفاذية الحرارية باستخدام جهاز تحديد قيمة-U التجاري. وتم تركيب محطة الطقس في الموقع لقياس جميع بيانات الأرصاد الجوية.

تم تحليل البيانات التي جُمعت من جميع هذه الأجهزة والتحقق منها باستخدام برامج محاكاة عددية (DesignBuilder 5.3 و ABAQUS 6.13). كانت المطابقة بين نتائج القياس التجريبية ونتائج المحاكاة العددية أكثر من 90٪ والتي تعتبر ممتازة من الناحية العملية. وأشارت نتائج القياسات التجريبية وتحليل المحاكاة العددية إلى أن طلاء العزل الحراري الجديد يمتلك خصائص حرارية ممتازة. والتي تتضمن: موصلية حرارية منخفضة وأنعكاسية عالية للأشعة الشمسية ومعامل حمل حراري منخفض.

بالمقارنة مع الغرفة المرجعية، فإن الطاقة التي تم توفيرها نتيجة استخدام طلاء العزل الحراري على جدران غرفة الاختبار الأولى، والطابوق الخرساني الذي يضم لوحة البوليسترين الممتدة في جدران غرفة الاختبار الثالثة

ونظام العزل الجديد لجدران غرفة الاختبار الرابعة كانت 34.57 و 28.73 و 58.04٪ ؛ على التوالي. وبالتالي، فأن طلاء العزل الحراري الجديد فعّال للغاية للحد من انتقال الحرارة عبر جدران المباني الجديدة (وكذلك المباني القائمة) حيث يمكن توفير الطاقة المستهلكة في المباني خلال أشهر الصيف بنسبة 35٪ تقريبًا. كما يُوصى بإستخدام نظام العزل الجديد للجدران في المباني الجديدة لتقليل استهلاك الطاقة بنسبة 58٪ تقريبًا. وعلى الرغم من أن تكلفة بناء الجدران باستخدام نظام العزل الجديد أكثر من الأنظمة الأخرى، إلا أنه يمكن إسترداد قيمة هذة الزيادة في التكلفة الأولية خلال عامين تقريباً مقابل التوفير في إستهلاك الطاقة.

درجة الدكتوراة

جامعة الملك فهد للبترول والمعادن

الظهران 31261

المملكة العربية السعودية

CHAPTER ONE

INTRODUCTION

1.1 General

Over the past four decades, the building industry in Saudi Arabia, in both the residential and commercial sectors, has expanded significantly because of the population growth and the development of the necessary infrastructure associated with the upsurge in oil prices [1]. The population of Saudi Arabia is expected to rise by about 28% between 2015 and 2030, as shown in Figure 1.1 and, hence, the housing stock demand is estimated to increase from 5.7 million in 2015 to about 9.4 million housing units in 2030, which is a growth of about 65%, as depicted in Figure 1.2 [1,2].

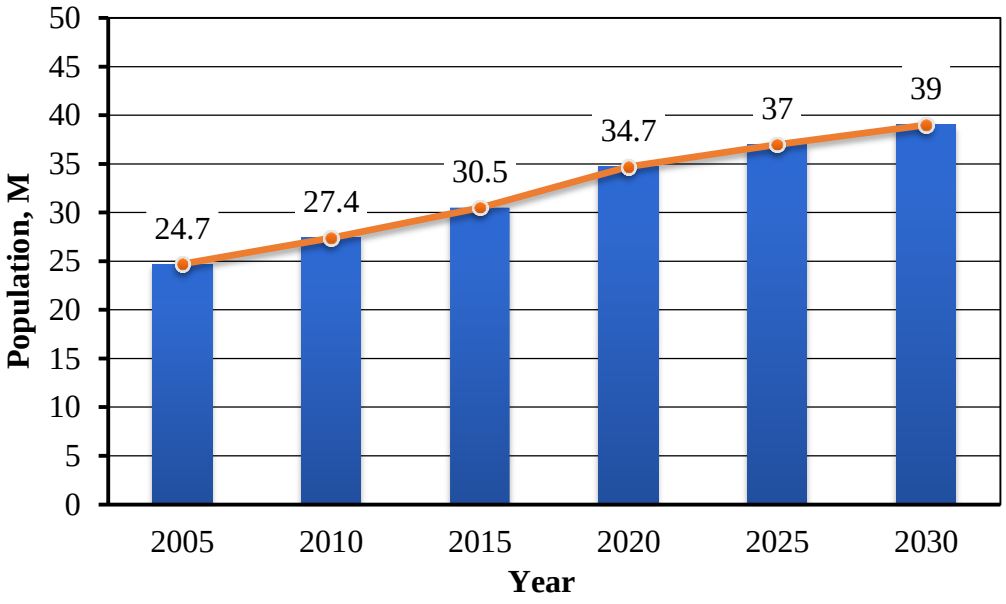

Figure 1.1: Population of Saudi Arabia [2].

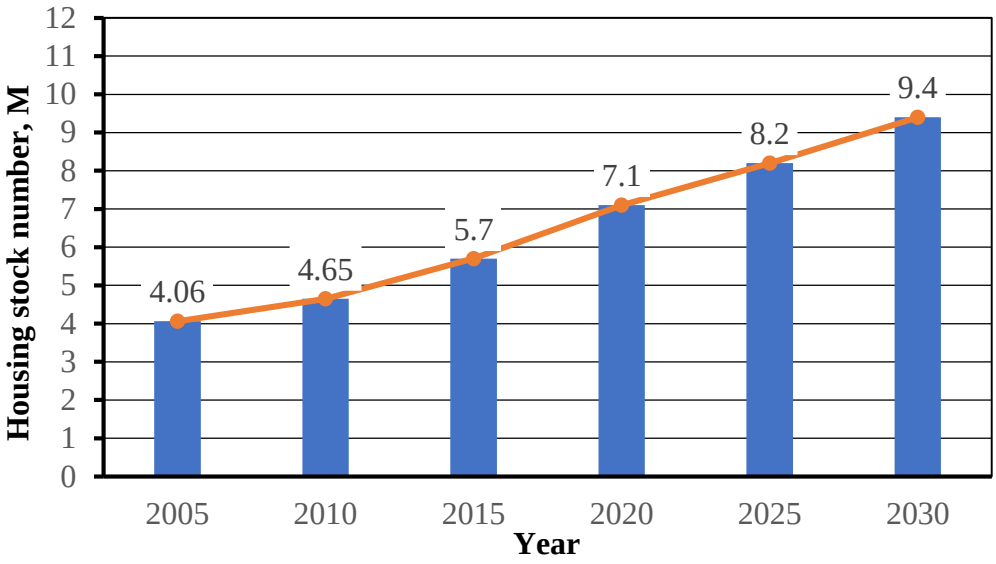

Figure 1.2: Housing stock number in Saudi Arabia [1].

1.2 Energy consumption in Saudi Arabia

With the increase in the population and housing units, the electricity consumption in Saudi Arabia has increased dramatically over the past 30 years, where the consumption per capita; 9.2 kWh; reaches about three times the world average; 3.2 kWh [3]. The largest consumption of electricity in Saudi Arabia is in the residential sector, as shown in Figure 1.3 [3], whereby 52% of the total electricity consumption goes to the residential sector [3] and 60% of this amount is consumed by air conditioners that provide the human "cooling" comfort, especially with the high ambient temperature during the summer and most part of the year, as depicted in Figure 1.4 [4].

Figure 1.5 demonstrates the monthly average outdoor air temperature in Dammam. It can be noted that the average air temperature reaches to as high as 43°C in July and such a

high temperature will certainly increase the electricity demand for air conditioning inside the buildings for providing comfortable and working media [4].

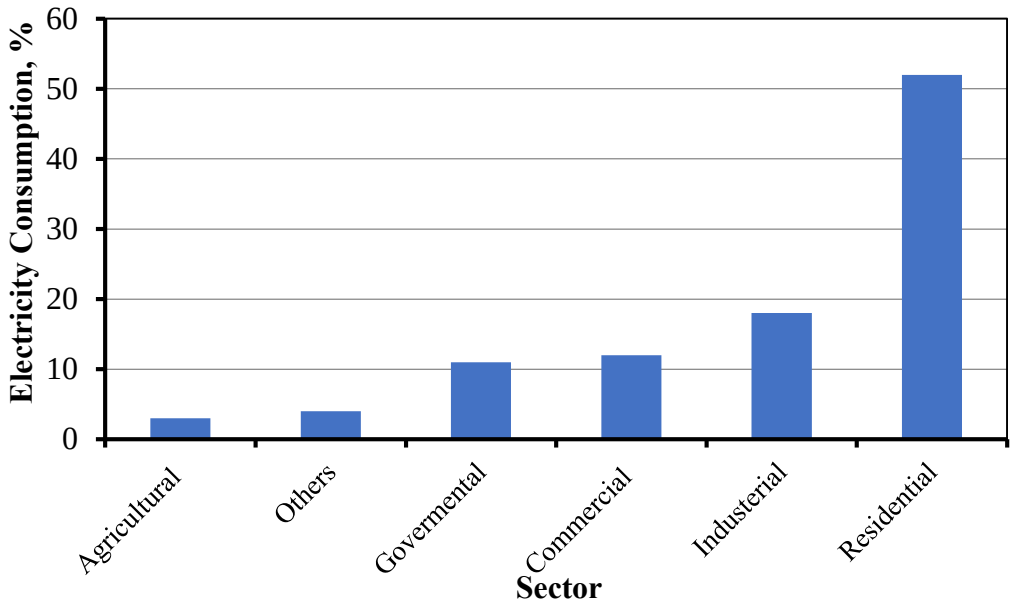

Figure 1.3: Electricity consumption sectors in Saudi Arabia [3].

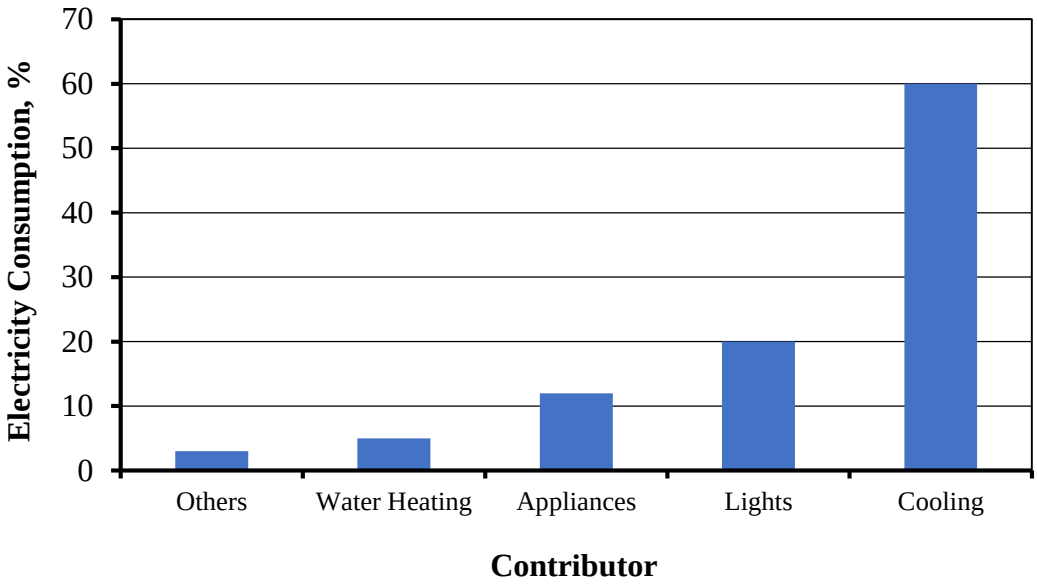

Figure 1.4: Electricity consumption contributors [4].

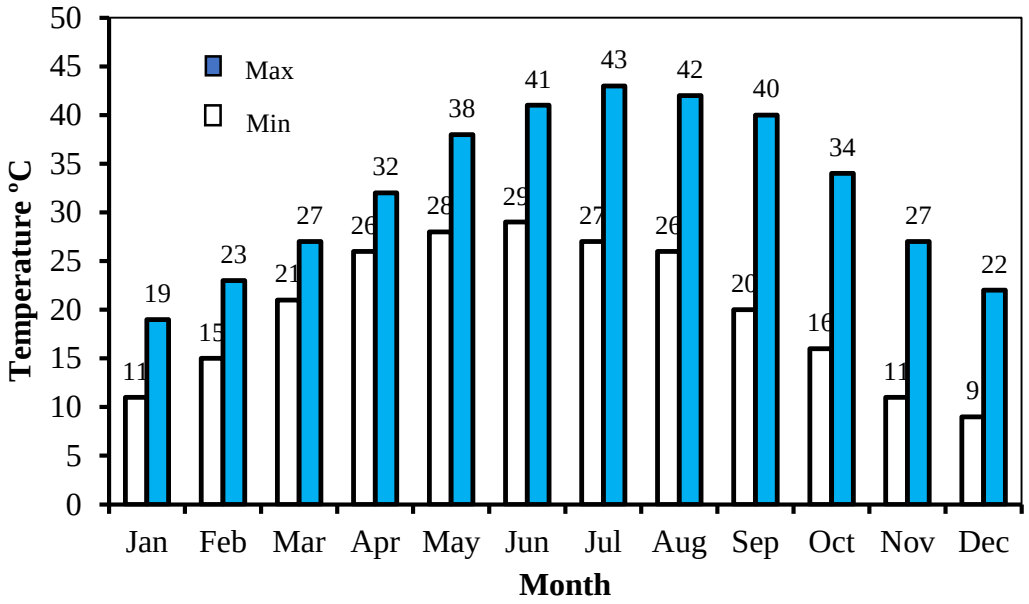

Figure 1.5: Mean temperatures of Dammam during year [4].

1.3 Electricity demand in Saudi Arabia

Over the past thirty years, the population in Saudi Arabia increased rapidly which caused a rise in primary energy consumption. Figure 1.6 depicts the growth of primary energy demand in Saudi Arabia. In 2004, the consumption of energy was 1050 terawatt hours (TWh) and it increased to 1366 TWh in 2006. Between 2006 and 2008, it almost remained constant with 1366 TWh. However, the energy consumption is predicted to rise to 2035 TWh in 2020 and to 2539 TWh in 2030 [5].

In 2008, the consumption of oil and gas was more than one billion barrels and it is expected to be doubled in the next twenty years [5]. Power stations and desalination plants for generating electricity consume 78% of the primary energy in Saudi Arabia [5].

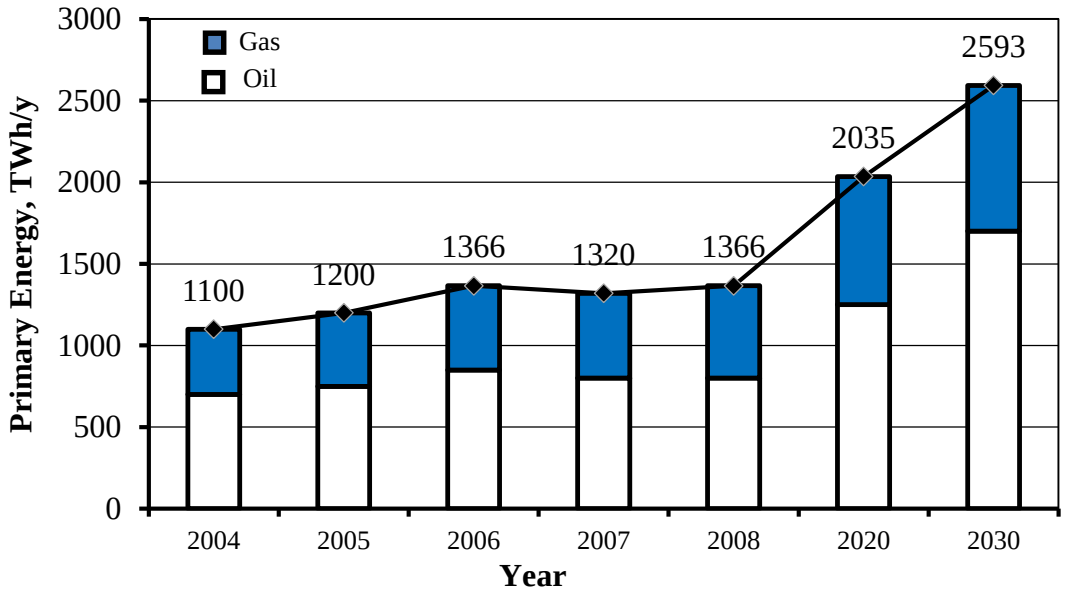

Figure 1.6: Energy consumption in Saudi Arabia [5].

1.4 Need for energy conservation in Saudi Arabia

The Saudi Electricity Company spent at least SR 380 billions in investments during the period 2009-2017 to meet its capacity increase targets [5]. Saudi Arabia utilizes a substantial portion of its oil and gas resources in providing the necessary electricity for its increasing population, leading to reduction in oil export and high environmental pollution in terms of CO_2 emission. Therefore, the Saudi Energy Efficiency Center (SEEC) was established in November 2010, to develop the necessary policies and regulations to mitigate the overwhelming electrical energy consumption in the private and governmental sectors (www.seec.gov.sa). With SEEC regulations and a three-fold increase in the electricity tariff, since January 2018, energy efficiency measures must be undertaken to reduce the cooling load in the residential, commercial and other sectors.

1.5 Significance of this research

The energy consumption in Saudi Arabia and the other Arabian Gulf as well as many other countries in the world has recently become of great importance to the society due to the large increase in the electricity tariff. Therefore, this PhD dissertation was timely conducted to scientifically and practically assess the role and mechanisms of thin layers of nan-ceramic coatings in reducing the energy consumption. Unlike most of insulating materials, these types of coating materials can also be applied for both new and existing structures thereby studying the effectiveness of these coating in decreasing the energy consumption is very important.

The literature review in Chapter 2 indicated that there are some studies that have been carried out on the use of thermal insulations in buildings in both the Arabian Gulf and other countries. However, most of these studies were conducted in the laboratory. Therefore, there is need for comprehensive and genuine experimental and simulaion studies in which insulation materials are invistigated in the field for their effectivness, espicially the new generation of coating-based thermal insulation that was used in this study.

The thermal performance of this coating insulation cannot be evaluated using the thermal parameters stipulated in the codes which are the thermal transmission (U-value)/thermal resistance (R-value) computation, especially under local conditions because it has new thermal properties which are still under investigation. Therefore, a full-scale monitoring of the performance in field test rooms was essential to investigate

the reduction in energy consumption as conducted in this research. In addition, numerical modeling, that was carried out in this study, provides an important tool for simulating the response of the insulating materials under various scenarios. Therefore, the outcomes of this research will also be useful to update the local and international building codes.

1.6 Objectives

The general objective of this research program was to assess the effectiveness of thermal insulations for decreasing the energy consumption and providing the thermal comfort in buildings by conducting full-scale experimental program and simulation. The specific objectives of this work were as follows:

1- To evaluate the thermal performance of four test rooms with and without a new generation of coating-based thermal insulation in typical Saudi Arabian buildings under field local conditions;
2- To monitor the electrical energy savings that were achieved using the proposed insulation system;
3- To conduct numerical simulation with the aim of analyzing the thermal behavior of the four test rooms with and without the new generation of coating-based thermal insulation; and
4- To provide appropriate recommendations on the usage of the new thermal insulation coating in the buildings in Saudi Arabia based on the findings of this research work.

CHAPTER TWO

LITERATURE REVIEW

2.1 Energy consumption in buildings

Energy consumption in buildings has been evaluated from different aspects in many studies [6–13]. Energy consumption in buildings based on their age has been studied using a statistical method and it was found that old buildings performed better than new buildings because of the less number of storeys, gross floor and residential areas [6]. However, it was reported that bad envelope quality of old dwellings will increase the energy consumption [7].

Case studies on the energy consumption in buildings have been conducted by several researchers [8–10]. Lu et al. [8] conducted a study to quantify the uncertainty of energy consumption in buildings. The results of this study were valuable to assess to the energy consumption inventory by providing information which reduces the uncertainty of the overall energy consumption inventory [8].

Lombard et al. [11] studied the energy consumption in buildings using HVAC system and required thermal comfort. In another study, the energy consumption in buildings according to the usage type of building has been evaluated to provide the measurers and policies for saving energy in these types of buildings [12].

Policy measures required to replace some elements in new buildings and accelerate this replacement to achieve energy efficiency have been investigated by Uihlein and Eder

[13]. The results showed that energy saving in residential buildings increased with accelerated installation of efficient energy windows and roofs [13].

2.2 Thermal insulation materials

There are many materials that could be used in buildings to reduce the heat transfer and to save the energy consumed in heating/cooling. These materials decrease the heat flow by their low thermal conductivity or by their ability to reflect solar radiation [14]. Some of these materials are recommended by ASTM, ISO and SASO, while others are still under investigation. In this study, the following materials have been reported in the literature for their effectiveness in reducing heat transfer in buildings and in saving the energy used for providing thermal comfort:

2.2.1 Autoclave aerated concrete block

This block is made from lime, sand, cement and aluminum powder. The thermal conductivity (k) of autoclave aerated concrete block, which was tested in Dubai Central Laboratory for ESPAC company, was 0.17 W/(m.K) as compared to 0.54 W/(m.K) for hollow-core normal concrete blocks [15,16].

2.2.2 Polystyrene concrete block

This commonly-used type of block is a normal block with a sandwiched polystyrene layer in the middle of it. There are two types of polystyrene boards used in construction of buildings in Saudi Arabia as insulation materials which are extruded and expanded polystyrene. The extruded polystyrene is characterized by low thermal conductivity ranging between 0.026 to 0.03 W/(m.K), while thermal conductivity of the expanded

polystyrene ranges between 0.04 to 0.06 W/(m.K). However, the price of extruded polystyrene is higher than that of the expanded polystyrene. Therefore, the expanded polysterene boards are usually used in construction of buildings due to its low price compared with other insulation materials [17,18].

2.2.3 Insulate plaster

This type of plaster is made of mineral cementitious material with low thermal conductivity of 0.05 W/(m.k) [19]. It is composed of virgin polystyrene microspheres, flame retardant with high density, and specific admixtures. For applying, it is mixed with water and it should be dried for 2 to 3 days before being used and it is utilized for internal and external applications [19].

2.2.4 Reflective coating

These liquid coatings are nano-ceramic coatings composed from nano-ceramic microspheres and silicon which make their thermal conductivity (k) very low [20]. According to some researchers, k for these types of coatings ranges between 0.03 to 0.1 W/(m.k) [20]. It was claimed that the good quality of these coatings is not only due to their low thermal conductivity, but it is attributed to their high solar radiation reflectivity [21] or to their low convective heat transfer coefficient which enhances their surface heat transfer resistance [22–26].

2.3 Thermal insulations in buildings and their effectiveness

In the past three decades, a host of experimental and numerical studies on thermal insulations in buildings and their effectiveness were conducted. Laboratory tests on nano-

ceramic thermal insulation coating to evaluate its thermal properties were conducted by Bozsaky [20]. The primary objective of this research was to check what was claimed in previous researches about the thermal conductivity for this thermal coating. Some of these reports mentioned that the thermal conductivity of this coating is between 0.001 and 0.003 W/mK. However, other studies mentioned that this thermal coating has high thermal conductivity that ranges between 0.01 and 0.14 W/mK. Therefore, thermodynamic tests were carried out on this thermal insulation coating and thermal conductivity of it was determined based on MSZ European Standard [20]. The results showed that the thermal conductivity of this type of coating was 0.069 W/mk, which was far from those published in previous papers. It was also concluded that the good quality of this coating is not primarily attributed to its low thermal conductivity but also for its heat transmission resistance between air and the surface of the building structure [20].

Shen et al. [21] evaluated the effect of reflective coatings on indoor environment and energy consumption in buildings. In this study, the performance of three types of coatings applied on building walls with a thickness of 30 to 40 µm was compared experimentally during summer and winter. In this experimental investigation, the effect of coatings on exterior and interior surface temperature, the reduction of electricity consumption due to the usage of coatings and the properties of envelope material equipped with coatings were evaluated. It was observed that the average reduction of the exterior surface temperature due to the usage of coatings was 7ºC, while the average reduction of the interior surface temperature due to the usage of coatings was 2ºC. Further, annual reduction in electricity consumption of 116 kWh can be achieved by using these coatings [21].

Soubdhan et al. [27] evaluated experimentally the effect of reflective insulation integrated to building envelope (i.e., "the physical separator between the conditioned and unconditioned environment") on heat transfer under tropical climate in France. The effectiveness of this insulation material was compared with the traditional insulations; such as mineral wools and polystyrene; to determine which one is better for reducing the heat flux through the building's roof. In this experimental study, four test cells were used as depicted in Figure 2.1 and Figure 2.2. The roof in the first cell was equipped with polystyrene, while a reflective insulation was applied on the roof in the second cell. In the third, the roof was equipped with fiberglass and the fourth cell was the control one. Temperature, conductive and radiative heat fluxes of walls and ceilings were measured. The results indicated that the reflective insulation can decrease the heat flux by 37%. The reflective insulation was comparable to the polystyrene and fiber glass with no ventilation. However, the radiant barrier for reflective insulations provided better insulation when the airspace was ventilated [27].

The impact of paints containing mineral micro-particles in reducing thermal dissipation in walls was evaluated by Sheikhzadeh et. al. [28]. Figure 2.3 describes the details of wall and ceiling of the test room. The heat transfer and temperature distribution were assessed in the room with coatings containing mineral micro-particles under different climatic conditions. The results indicated that these coatings decreased the energy consumption by about 20% [28].

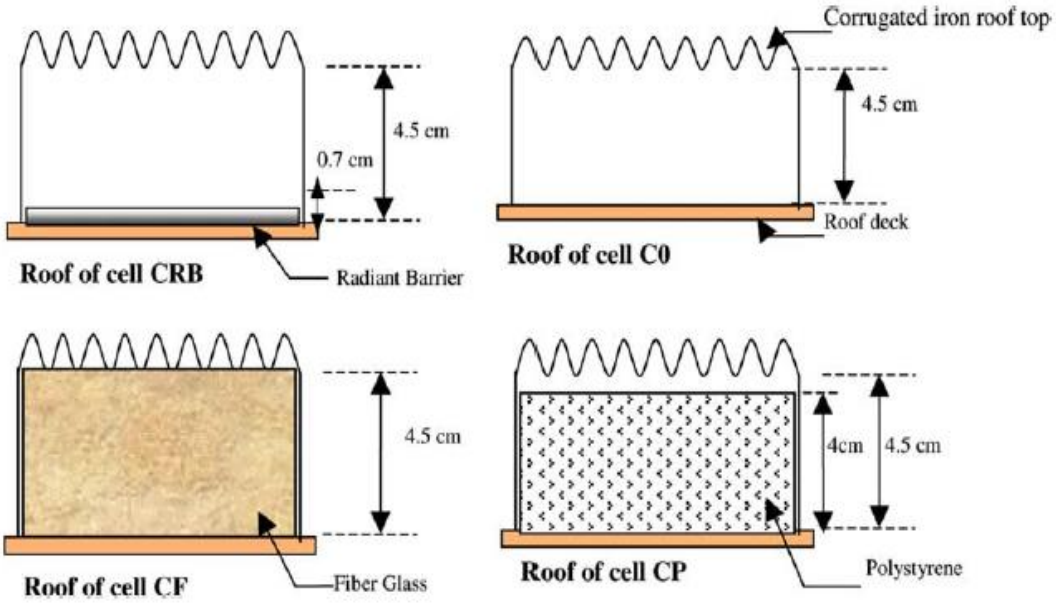

Figure 2.1: Roof systems under test [27].

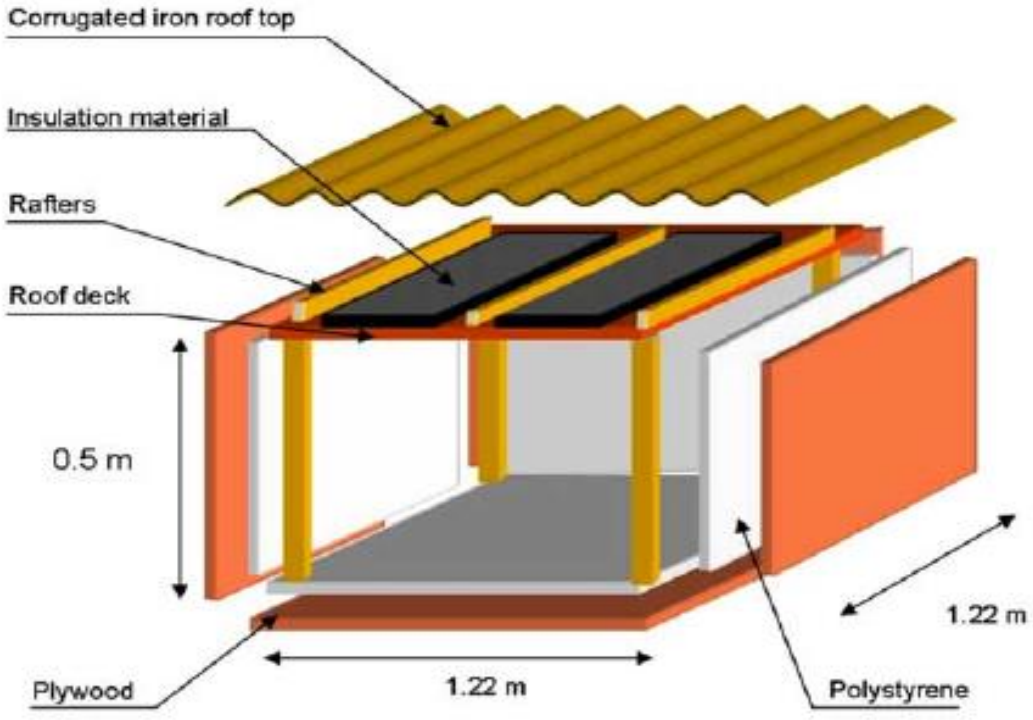

Figure 2.2: Cell components [27].

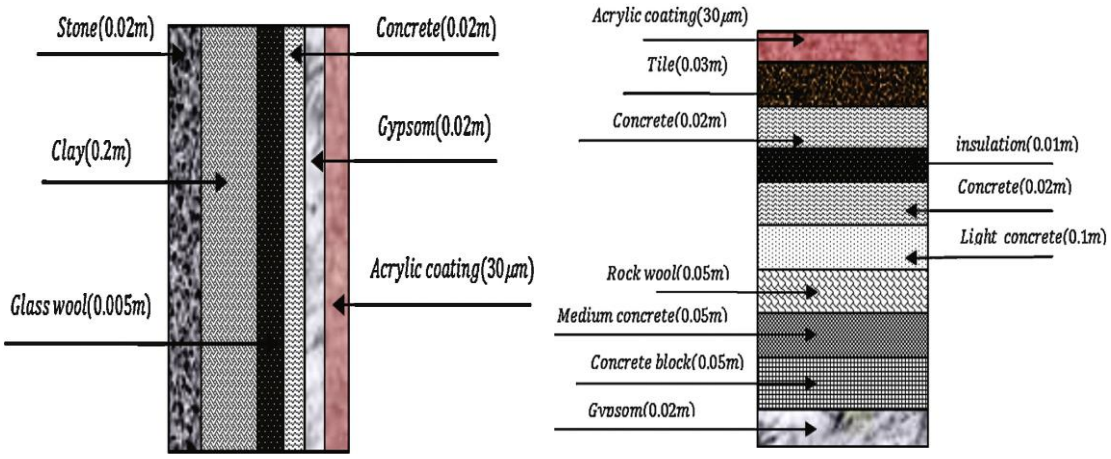

(a) (b)

Figure 2.3: a) Wall details, b) Ceiling details [28].

Joudi et al [29] evaluated the thermal performance of reflective coatings applied on cladding of small cabins under different conditions of climate. The potential energy saving as a result of applying this coating was also simulated. The results indicated that applying the reflective coating on the exterior surfaces of cladding would be beneficial in warmer climate to save energy consumption, while applying this coating on the interior surfaces of cladding would be better in colder climate. The application of reflective coating on both interior and exterior surfaces of cladding is the best solution to save energy in milder climate [29].

Laboratory tests on insulate plaster, which is gypsum consisting of light weight aggregate, were conducted to evaluate its thermal properties [30]. The results indicated that the addition of cork to gypsum produces plaster with low density and low thermal conductivity of 0.11 W/(m.ºC) [30]. The thermal conductivity and thermal diffusivity of gypsum plaster incorporating palm fibers with different percentages were assessed

experimentally by Amara et al [31]. It was found that palm wood enhances the thermal properties of gypsum plaster thereby reducing its thermal conductivity and diffusivity [31]. The thermal conductivity of normal plaster and plaster consisting of 90% of granular aerogel was compared by Buratti et al [32]. It was concluded that considering 90% of granular aerogel in natural plaster decreased the thermal conductivity from 0.50 W/(m.K) to 0.050 W/(m.K) [32].

Walker and Pavía [33] evaluated the thermal performance of seven internal insulations; "thermal paint, aerogel, cork lime, hemp lime, calcium silicate board, timber fiber board and polyisocyanurate (PIR) board"; in brick wall of historic building and their effect on reducing the energy consumption of buildings. The thermal performance of these insulations was assessed using heat flux sensors, infrared camera, thermocouples and U-value meter and it was compared with the thermal the performance of traditional lime plaster finish. Moreover, the density and specific heat of these insulations were measured in the laboratory. Figure 2.4 shows the thermal performance and insulated walls with the monitoring setup. The results from the various thermal measurements showed that all internal insulations, except thermal paint, reduced the U-value of the wall within the range of 34 to 61%. Thermal paint had no effect on the U-value. The comparison between in-situ insulations results and manufacturer's specified properties indicated that the wall U-value was higher by 13 to 25% for all internal insulations with the exception of cork lime [33].

The properties of concrete blocks with thermal insulation used to produce masonry walls in Oman were reported in a study conducted by Al-Jabri et al. [17]. As shown in Figure 2.5, different types of lightweight concrete blocks using different hole arrangement or concrete blocks with thermal insulation materials were evaluated in this study. The thermal insulation materials used to produce concrete blocks were vermiculite and polystyrene beads (PolyBlock1) that were compared with the thermal insulation blocks (PolyBlock2) and ordinary blocks. Thermal conductivity and compressive strength tests were conducted on blocks and walls that were constructed with these different types of blocks. The results indicated that the blocks with thermal insulations were effective to decrease the thermal conductivity and the one with polystyrene was the best (i.e., the thermal conductivity for polystyrene blocks was 0.616 W/m.ºC and for ordinary blocks was 1.6 W/m.ºC). All the blocks with different insulation materials satisfied the requirements of compressive strength for non-bearing load walls [17].

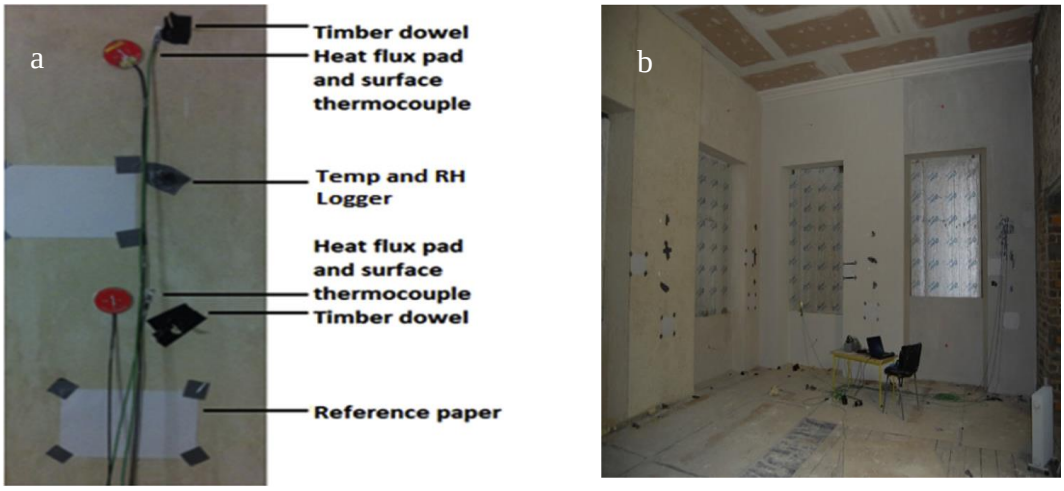

Figure 2.4: a) Set-up of thermal performance monitoring, b) Walls with monitoring set-up [33].

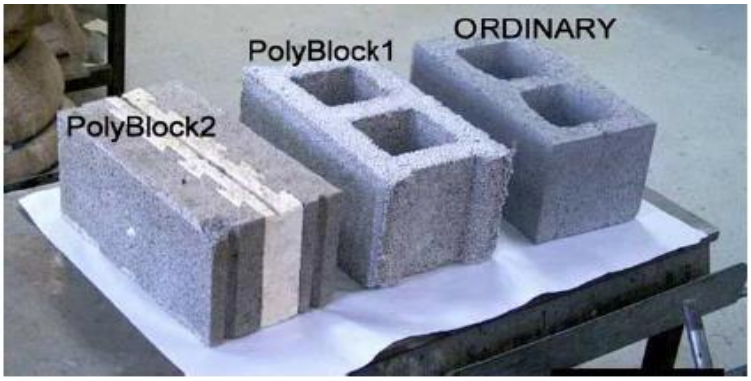

Figure 2.5: Different types of blocks [17].

The thermal properties and energy efficiency of autoclave aerated concrete block used for constructing walls in buildings have been investigated in many studies [34–37]. Autoclave aerated concrete blocks have low density and their thermal resistance is 11 times higher than of that for ordinary concrete blocks with the same size [36,37]. The low thermal conductivity of autoclave aerated concrete block that may reach to 0.133 W/(m.K) will certainly minimize the loss of heat through walls in buildings thereby decreasing their energy consumption in buildings [34,35].

Decreasing the energy used in buildings by reducing the thermal conductivity of building bricks was investigated experimentally by Othman [38]. In his research, the insulation materials were mixed with the buildings bricks as follows: "Polystyrene of 2.5, 5, 10 & 15 wt %, polycarbonate of 2.5, 5, 10 & 15 wt %, polyethylene of 2.5, 5, 10 & 15 wt %, wood dust of 1, 2, 3, & 4 wt %, natural cork of 1, 2, 3, & 4 wt %, glass wool and rock wool layer of 24, 36, 48 and 60 g". Thermal conductivity of these insulation materials was investigated. The compressive strength and water absorption were also conducted on bricks. The test results indicated that the thermal conductivity was reduced by about 70% with glass wool and natural cork additions. The water absorption and

compressive strength were decreased with the addition of polystyrene, polycarbonate, polyethylene, glass wool and rock wool [38].

Castell et al. [39] conducted an experimental study to compare two different types of bricks; conventional brick and alveolar brick; the latter being used for decreasing the thermal demand of buildings. Five cubicles were constructed where conventional brick was used to build four of them and insulation materials (i.e. polyurethane, mineral wool and polystyrene) were used in these cubicles. The fifth cubicle was built with alveolar brick which is considered as a thermal insulator by itself. Figure 2.6 depicts cross-section of the cubicles investigated. All cubicles had air conditioners. The energy consumption in all cubicles was registered and the results showed that the alveolar brick reduced significantly the energy consumption by about 40% in comparison with conventional brick without insulation materials. However, the conventional brick with 5 cm of other insulations (i.e. polyurethane, mineral wool and polystyrene) was 5 to 8% better than alveolar brick in reducing the energy consumption [39].

To preserve the energy consumed by buildings, Emadi [40] investigated the reduction in energy consumption of buildings by applying thermal insulation; polystyrene; on external walls. The thermal comfort and energy cost in two apartments; the first apartment was without thermal insulation, while the second one was with walls havings thermal insulation; were evaluated during the cold months of the year to assess the effectiveness of thermal insulation in decreasing the loss of temperature from inside the buildings. From the results, it was proven that using thermal insulation on external walls helps provide thermal comfort for 3 hours after switching off the heater whereas without

the insulation, the thermal comfort was for 1 hour. Consequently, this leads to save the energy consumed in buildings [40].

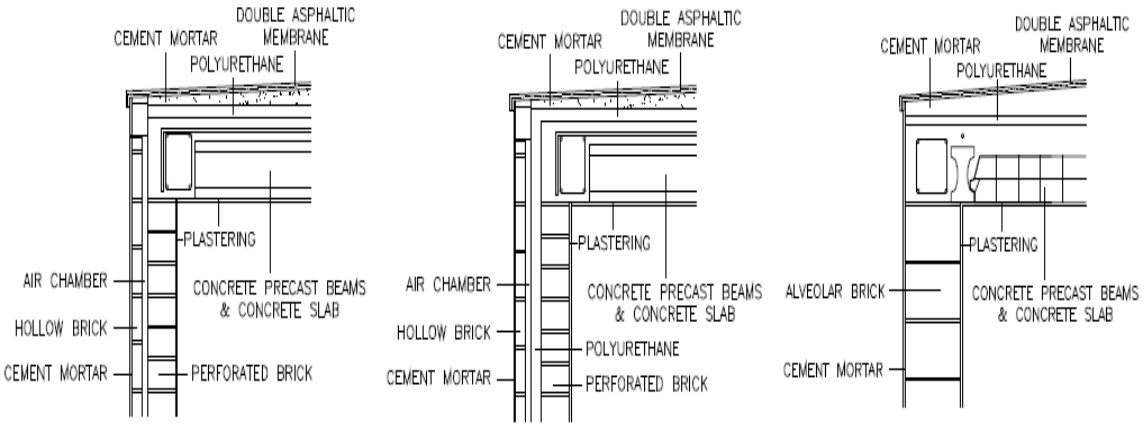

Figure 2.6: Section of the cubicles analyzed. Left: Reference; Middle: Insulated; Right: Alveolar [39].

The effectiveness of internal insulations to reduce energy consumption in buildings was evaluated on test chambers at the Edilmaster site, Trieste, Italy [41]. These internal insulations were wooden and metallic studs. In the experimental work, specimen under test was placed between two isothermal chambers. The temperature was controlled to keep the temperature with a constant difference. Figure 2.7 shows the insulation materials and a picture of the chamber. The wall superficial temperature, chamber's air temperature and heat flux were measured using thermal sensors. Further, numerical simulation of the insulated system was carried out using ANSYS Fluent 14.5 software. The results from both the experiments and simulation indicated that the conductance values neglecting of studs effect causes an overestimation of the insulation performance of refurbished walls. The conductance values obtained by the numerical simulation were 10% less than that obtained by the experimental work [41].

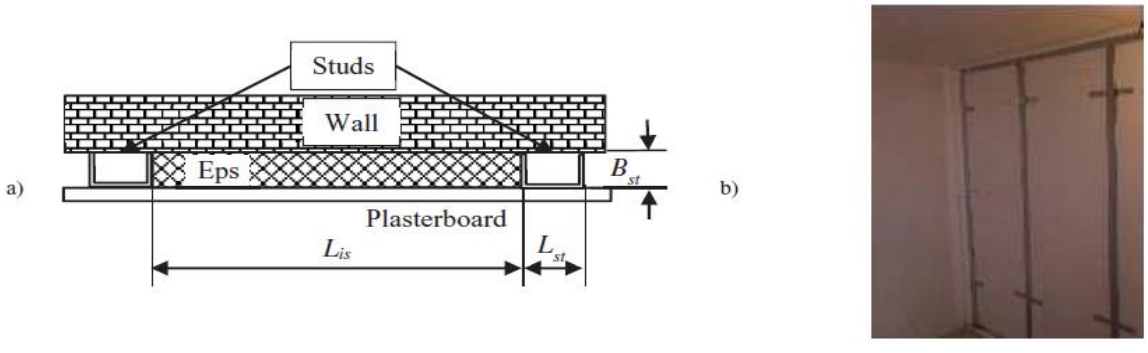

Figure 2.7: a) Insulation materials, b) Picture of the chamber [41].

2.4 Thermal performance and energy consumption of buildings with and without insulations

Experimental analysis of thermal comfort in buildings has been reported in many studies [42–45]. The thermal performance of vernacular buildings using solar passive techniques was studied by Singh et al. [46]. They conducted a field study on typical traditional vernacular dwellings in different bioclimatic zones to investigate their thermal performance. Survey of 150 vernacular dwellings was also conducted to get the range of comfort temperature in these buildings. Temperature, humidity, illumination level and building design parameters were measured. The results indicated that these buildings performed satisfactorily except in the winter months and the occupants feel comfortable in a wider range of temperature [46].

Ozkan et al. [47] studied the thermal performance of traditional buildings in Anatolian village of Şahmuratli in Turkey. They focused on the thermal performance of traditional materials such as mud brick and a straw bale. Also, the thermal performance of an under-

construction aerated concrete building was investigated. The assessment was based on measuring the temperature and humidity within the constructed buildings and energy consumption in them. Computer simulations on different building systems using Ecotect 5.01 were also conducted. It was concluded that these traditional materials were effective in decreasing energy consumption. However, they need higher maintenance requirements [47].

In Riga, Latvia, long-term monitoring study was conducted by Gendelis et al. [48] to get detailed data about the energy consumption and thermal comfort in small test buildings equipped with different heating systems cosisting of "a standard electric convectors, an air-air heat pump and an air-water heat pump" as shown in Figure 2.8. Electric/heating powers, temperature and humidity inside the rooms were measured. For outside monitoring, temperature, humidity and solar irradiation were measured. The energy consumption and thermal comfort factors were calculated during the heating seasons. It was concluded that the type of heating system affects the heating energy need and the thermal comfort conditions in buildings where actual energy efficiency ratio for heating systems as compared with standard electric convector was high between 0.94 and 2.5 [48].

Figure 2.8: Test buildings [48].

Ozel [49] studied the impact of dynamic thermal conditions on the thermal performance of building walls with different structural materials. The optimum insulation thickness in building walls was also investigated. In this research, building walls constructed of concrete, briquette, brick, blokbims (i.e., Turkey block is made from volcanic stone to resist physical and chemical effects) and autoclaved-aerated concrete were assessed for thermal performance with and without insulation. The insulations selected for walls were extruded and expanded polystyrene. An economic model under dynamic thermal conditions was carried out to investigate the optimum insulation thicknesses based on the climatic conditions of Elazıg, Turkey, and the parameters obtained from the local market costs and local conditions. It was concluded that the optimum insulation thicknesses was between 2 and 8.2 cm and the energy saving was between 2.78 and 102.16 $/m^2 [49].

The thermal performance of masonry and wood frame walls was investigated by Fiorato and Cruz [50]. In this investigation, the thermal conductance and resistance properties under steady state temperature conditions and the thermal response under dynamic condition of six walls depicted in Figure 2.9 were measured. The walls were put in the indoor chambers to get a constant temperature, while the temperature was varied for outdoor conditions. The temperature was measured using thermocouples and the energy required for heating and cooling the indoor chamber was monitored using a watt-hour meter. Thereafter, the temperature and energy measurements were used to calculate the thermal conductance and resistance. The results indicated that the heat transfer characteristics were considerably affected by the thermal inertia and with increased wall

weight, thermal lag increased. The increment of thermal resistance resulted in significant reduction in dynamic energy requirements [50].

The thermal performance of building elements subjected to non-steady state heat flow was measured in quantitative method conducted by Danielski and Fröling [51]. In this method, heat flux meters and thermography were used to measure the convection heat transfer coefficient. Then, thermography was used to measure the overall heat transfer coefficient of a complete building element to include all non-uniformities. Figure 2.10 shows the laminated timber wall that was assessed for thermal performance. It was exposed to the outdoor weather conditions between January and February, 2014. The difference between the results for a small uniform wall segment from thermography and the heat flux meter measurements was 4%. However, the overall heat transfer coefficient of a large wall area using heat flux meters was 11% lesser in comparison to thermography. It was concluded that a more representative result could be gotten using thermography when it is applied on areas of imperfections [51].

The thermal performance and comfort conditions of many buildings in Umbria Region, Italy, were assessed by Asdrubali et al. [52]. Further, energy consumption and environmental aspect for these buildings were considered. Regarding thermal performance assessment, infrared analysis and thermal transmittance measurements were carried out using infrared camera, temperature and relative humidity sensors. At the end of monitoring for many buildings, it was found that the green buildings perform better than the conventional building in reducing heat transfer and energy consumption [52].

The thermal performance of a social housing building was evaluated using grey box model. Grey model is considered as a solution for predicting the thermal performance of buildings and it is applied to energy systems. Temperature, heat flux, solar radiation, wind velocity and atmospheric pressure on an empty social house were monitored for three months. After that, the monitoring data was used to develop grey box model. The outcome of this research was a methodology proposal to be applied by the public administrations, as depicted in Figure 2.11 and to explore the possibility of using grey box model as an accurate way to represent the thermal performance of buildings [53].

A study on measuring the temperature and humidity of concrete structures using radio frequency integrated circuits was conducted by Hung et al. [54]. The aim of this study was to monitor the thermal performance of concrete structure without wiring requirements that may cause discontinuity of monitoring and high costs. This was done using radio frequency integrated circuits combined with thermocouples and fiber optics sensors that were applied on five simulated roofs and walls where that data was recorded automatically, regularly and continuously. At the end of this study, the authors mentioned that their long-term monitoring of temperature and humidity using this wireless system was successful and it was observed that the temperature was influenced by the insulation material performance, weather, absorption and radiation rates, direction of wall and solar radiation amount [54].

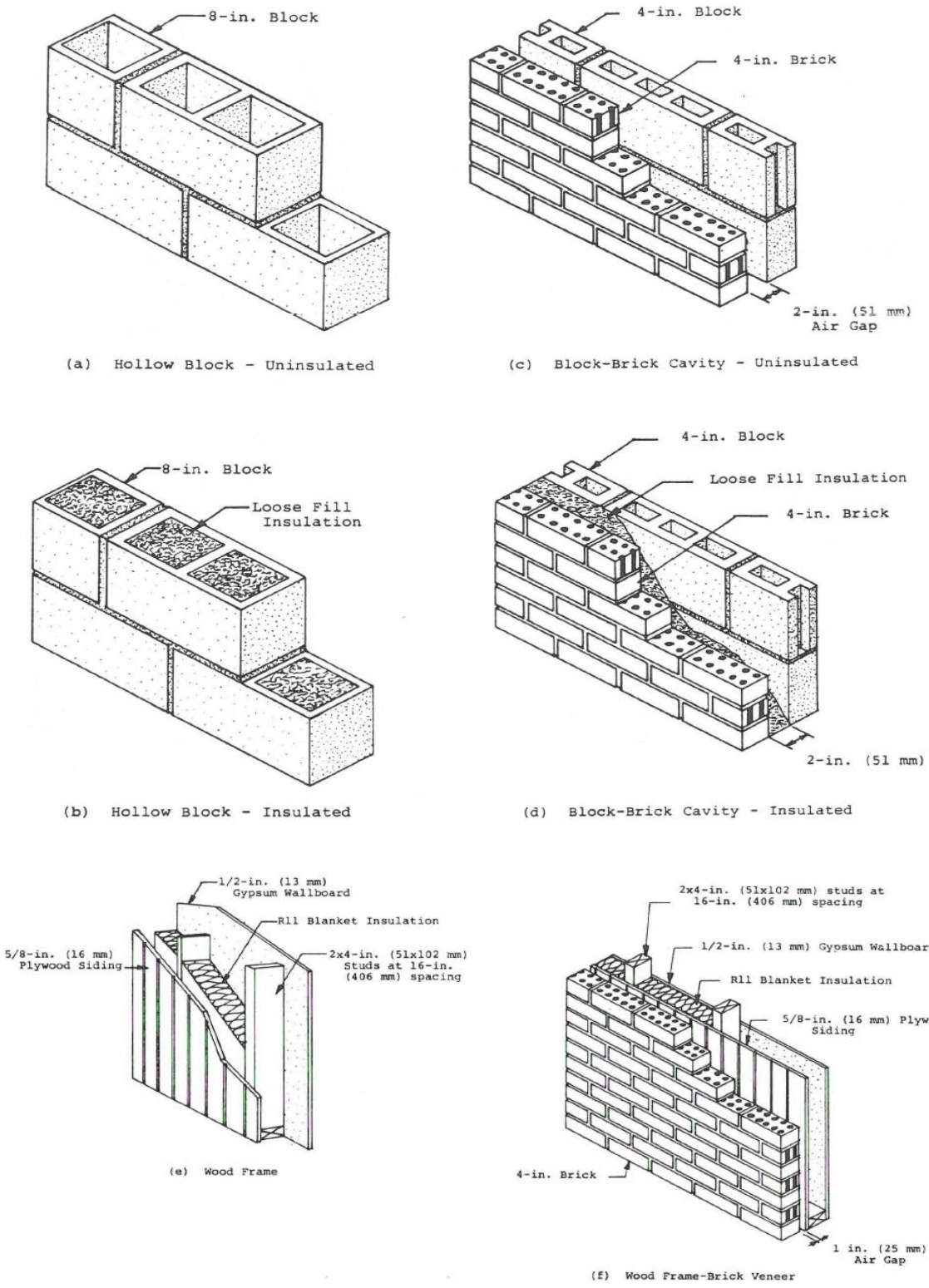

Figure 2.9: Test specimen details [50].

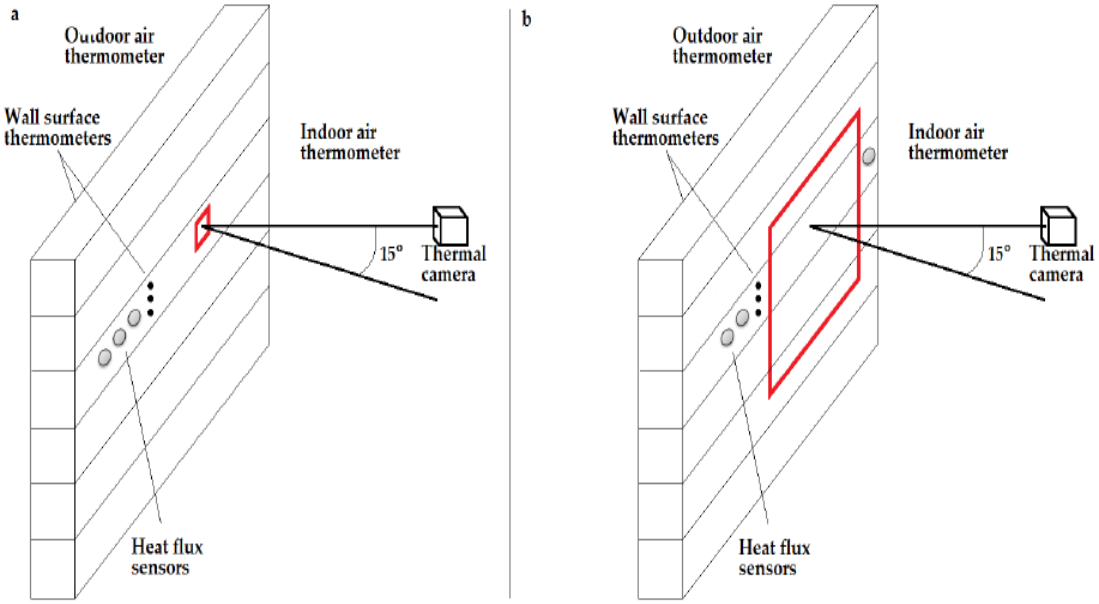

Figure 2.10: Laminated timber during measurement of (a) Small element (b) Large element [51].

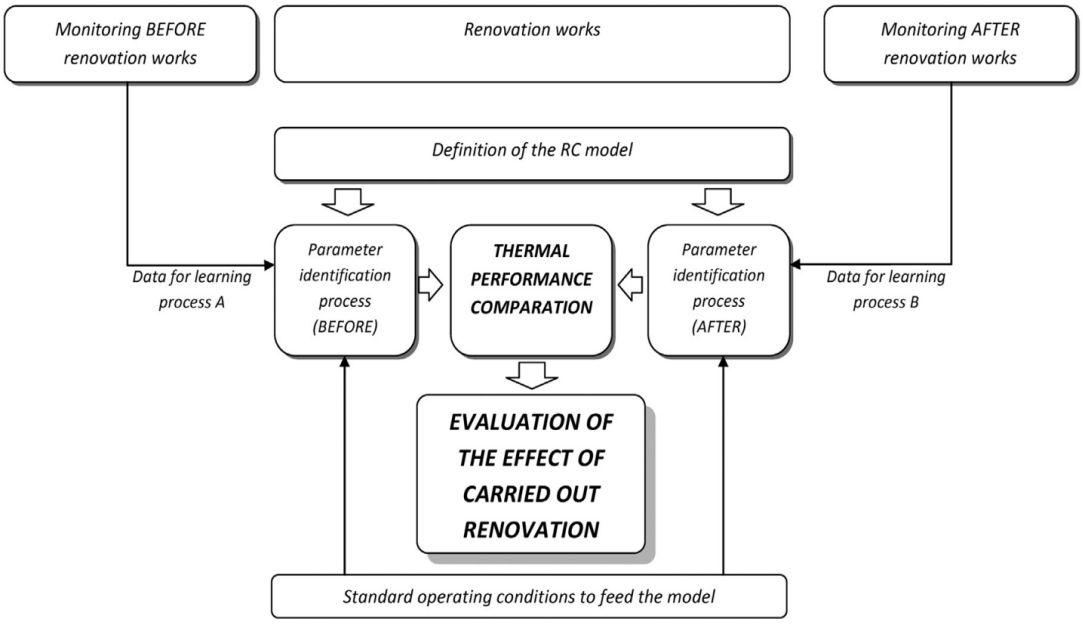

Figure 2.11: Evaluation of energy renovation effect in social housing [53].

2.5 Numerical simulation of thermal performance and energy consumption of buildings

During the past ten years, a number of numerical studies have been carried out to evaluate the thermal comfort for occupants inside buildings with different conditions [55–57]. A numerical study of dynamic thermal characteristics of insulated walls in buildings having the same thermal mass was conducted by Al-Sanea and Zedan [58]. The aim of this study was to optimize insulation; molded polystyrene; thickness for walls to achieve the best thermal performance of buildings based on climatic data of Riyadh, Saudi Arabia. The results showed that the best thermal performance and effective energy consumption were achieved using three layers of insulation on wall. However, the cost increased with increasing the insulation layers [58].

Herbinger et al. [59] developed a model of an office room in COMSOL 4.4 to evaluate the thermal comfort by simulating the heat transfer and studying the effect of placing phase change materials; "A phase-change material (PCM) is a substance with a high heat of fusion which, melting and solidifying at a certain temperature, is capable of storing and releasing large amounts of energy. Heat is absorbed or released when the material changes from solid to liquid and vice versa; thus, PCMs are classified as latent heat storage (LHS) units". Figure 2.12 depicts COMOSOL geometry of the office room. The results showed that using phase change material; butyl stearate; in the ceiling and in the floor did not change the temperature of the room remarkably after one hour. Also, the phase change material incorporated in the floor beside the window proved to raise the

temperature in the room slightly because of the high absorption of the phase change material enclosure. However, the room temperature decreased at the end of the simulation. Further study is needed to find optimal phase change materials surface properties for achieving optimal performance during the day [59].

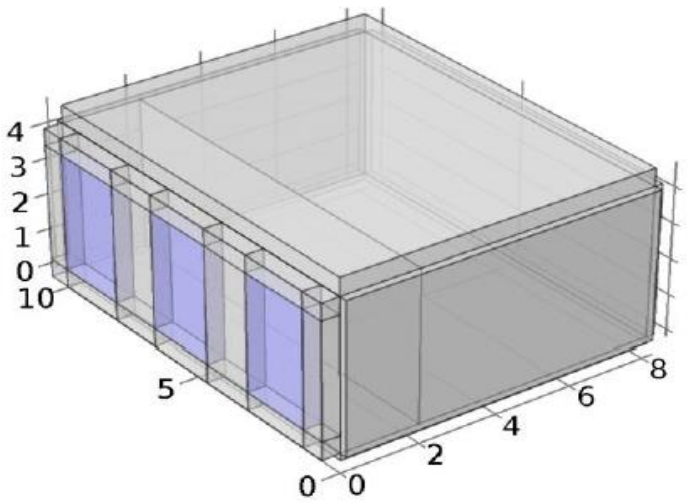

Figure 2.12: COMOSOL geometry of the office room [59].

An experimental and numerical study to evaluate the energy efficiency improvement in buildings due to using phase change materials was conducted by Kheradmand et al. [59]. Two prototype test cells were prepared. The first cell was with hybrid phase change material plastering mortar and the second one was without phase change material. Thereafter, the cells were exposed to daily temperature and comparison between their behaviors was carried out. Furthermore, numerical model using ANSYS-FLUENT was developed to validate experimental results. Figure 2.13 depicts the prototype and the 3D model. The results indicated that incorporating hybrid phase change material in plastering mortar reduced heating/cooling temperature demands to maintain the interior temperature

within comfort levels when compared to mortar without hybrid phase change material [59].

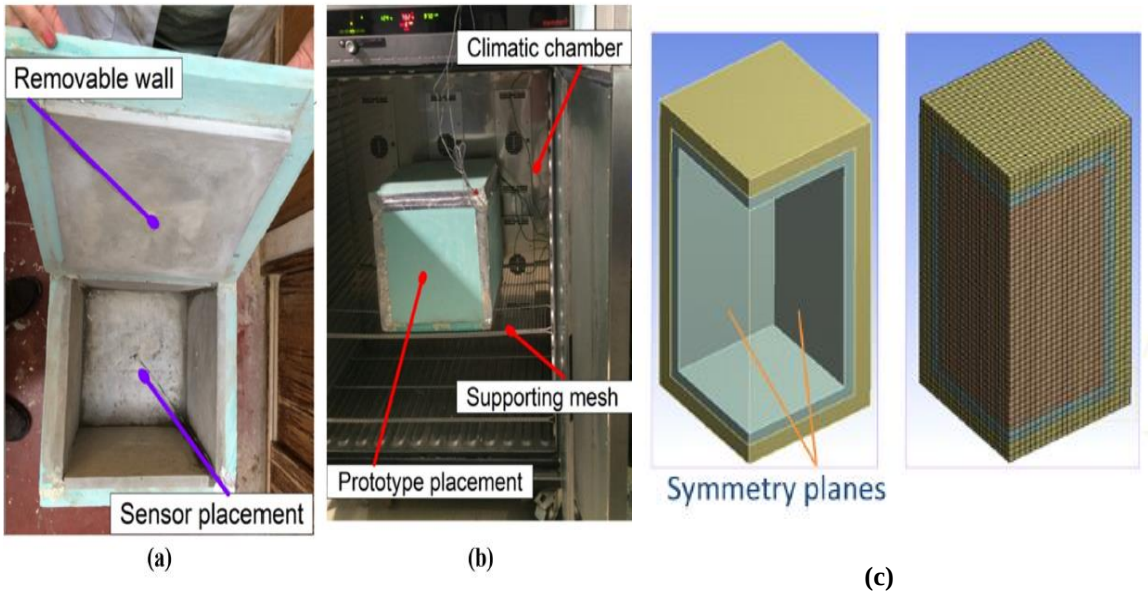

Figure 2.13: (a) The prototype with sensor placement; (b) The prototype in the climatic chamber, (c) The 3D geometric model and mesh model [59].

Sabanskis and Virbulis [60] conducted a monitoring study on five experimental buildings with size of 3x3x3 m located in Riga, Latvia, to investigate the change of temperature, humidity and air flow velocity. Different heating systems were used in these experimental buildings and sensors were installed and connected to data loggers for automatic collection data. Numerical model using OpenFOAM software was also developed to simulate heat transfer, air flow and radiation in experimental buildings. Their results indicated that there was good agreement between experimental and modeling results [60].

Numerical modeling using FLUENT computational fluid dynamics software was developed to analyze the impact of air flow of AC unit on temperature and air velocity

under standard conditions with and without solar radiation [61]. In this model, a 3D case of air flow and heat transfer was introduced for indoor space cooling with AC unit during the summer in Rijeka, Croatia. The results indicated that solar radiation must be considered in numerical modeling to get more accurate prediction of heat and thermal comfort parameters in the indoor space due to noticeable deviations from thermal comfort conditions that were observed [61].

To enhance the thermal insulation of buildings and to save the energy consumed by cooling/heating systems, a new design of concrete wall panel was presented by Zhou et al [62]. This new design was achieved by adding a gypsum layer inside concrete wall. Monitoring of temperature variation in concrete walls with the new design and in conventional concrete wall was conducted. All walls were under a heat radiation source. Moreover, numerical models using ABAQUS software of two three-story buildings with different wall designs were developed to understand the thermal effect of these walls in buildings. Figure 2.14 depicts the numerical model used in this study. The results from experimental work and numerical simulation showed that the gypsum layer delayed the heat transfer across the wall by about 1.1ºC thereby improving the thermal insulation of buildings [62].

Ibrahim et al. [63] conducted a numerical study to investigate the impact of aerogel-based rendering/mortar; exterior insulation system; on the thermal performance and energy efficiency of buildings. This aerogel-based rendering/mortar is applied on new buildings and it is also used for retrofitting of existing buildings because of its high insulation properties, the ease of its application and its compatibility with masonry

facades. In this study, the modeling approach included three different scales; 1D, 2D and 3D envelopes scale; to evaluate the effect of aerogel rendering on the thermal and moisture transfer of exterior walls, the heat losses through some types of thermal bridges; "the thermal bridge is generated at the junction between the vertical walls and the intermediate floor and the thermal bridge generated at the window reveals"; and the reduction of heating demand, respectively. It was concluded that aerogel rendering on the exterior walls reduced significantly the moisture and it decreased the wall heat losses. It was recommended to use 5 cm of aerogel when the needed heating increases by about 10%. Moreover, it is suitable to use aerogel in places where traditional insulation cannot be applied, such as the exterior facades of buildings [63].

Azemati et al. [64] developed a 2D model of a room with mineral insulator in coatings. These mineral coatings were ceramic particle and acrylic coatings. The 2D model was constructed using FLUENT software to simulate the heat flow and temperature distribution and to investigate the effect of coatings position on wall temperature and absorption coefficient. It was concluded that the best position of these mineral coatings was on the exterior walls and they can reduce the energy consumption by about 17%. The loss of energy with ceramic coating on the walls was about 14%, while without coating on the walls, it was about 40% [64].

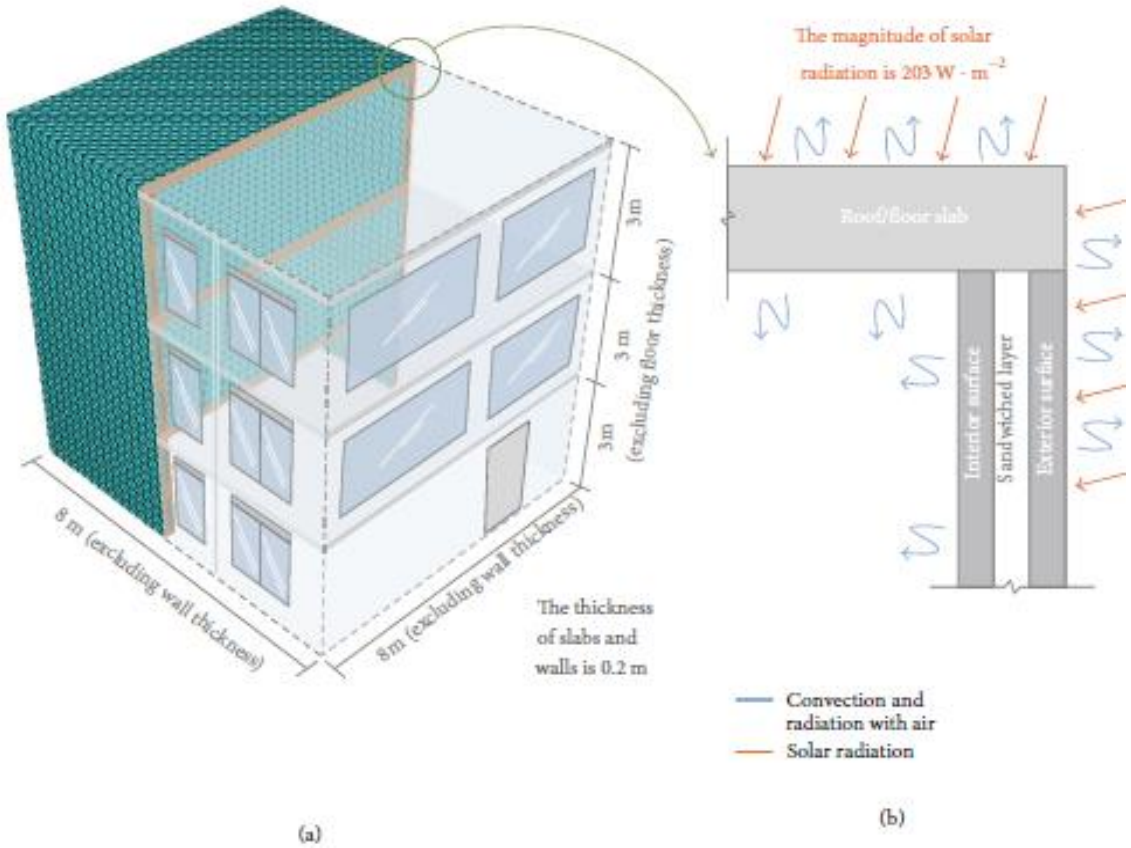

Figure 2.14: (a) 3D view of building with meshing; (b) 2D diagram of roof and wall with boundary conditions [62].

The impact of shape-stabilized phase change material (PCM) floor on thermal performance passive solar building was modeled and simulated by Xu et al. [65]. In their research, the effect of the thickness and thermal conductivity of PCM floor, temperature and heat fusion on the thermal performance of the room was analyzed to evaluate the energy consumption due to heating or cooling space of the room. The analytical model was validated by the experimental results, as depicted in 2.15 that describes the results of indoor temperature from modeling and experiments. It was found that the model and the analysis were helpful for the application of shape-stabilized PCM floor in solar energy buildings [65].

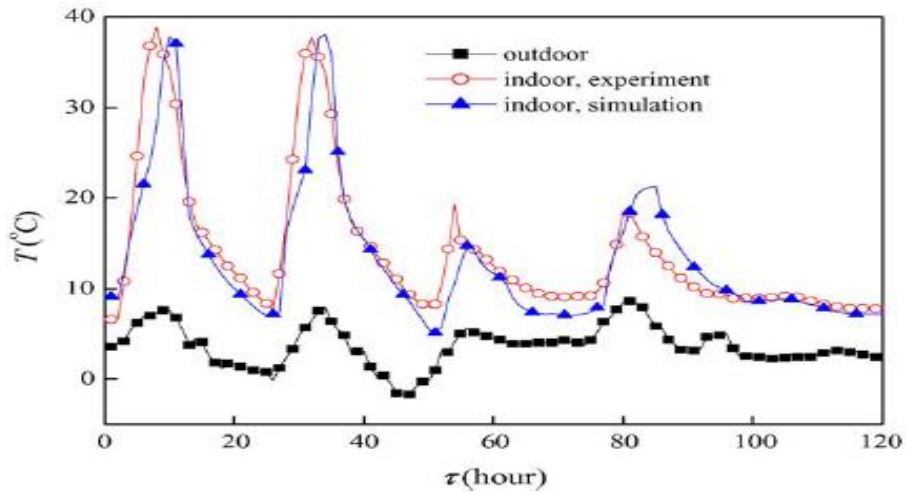

Figure 2.15: The simulated and experimental results comparison [65].

Simulation of energy consumption and thermal performance of buildings using DesignBuilder software has been investigated in a number of studies [66–68]. The simulation results were compared with the experimental results and it was found that there was good agreement between the results. This software is discussed in detail in Chapter 5.

CHAPTER THREE

EXPERIMENTAL PROGRAM

3.1 General

In this PhD dissertation, the experimental program was basically planned to assess the thermal performance of a new generation of an insulated coating applied on the walls in buildings. This assessment was based on comparing the effectiveness of this coating in reducing the heat flow through walls in reducing the energy consumption in the building for providing the thermal comfort with the other currently used materials in eastern Saudi Arabia. The following major operational tasks were conducted to achieve the objectives of this investigation:

1. Testing the thermal properties of the materials used in this research.
2. Constructing four test rooms with different insulation materials. One of these test rooms was constructed without any insulation material to be the reference room.
3. Monitoring the environmental conditions (i.e. solar radiation and wend speed) around each test room.
4. Placing weather station on top of building beside test rooms to provide the meteorological data during the period of investigation.
5. Supplying test rooms with the required equipment to monitor the thermal performance of insulation materials.
6. Measuring the electricity consumption in the test rooms during the summer used for cooling.

The details of all the above-mentioned tasks and all the information about the designations of test rooms and their sizes, preparation of test rooms, tests procedures, and the tests set-ups are discussed in the following sections.

3.2 Laboratory tests

The thermal properties of the insulation materials used in this investigation were tested to diagnose their thermal performance and to use them in analysis and simulation. These properties are:

3.2.1 Thermal conductivity (k)

According to ASTM C-518:2010 [69], the thermal conductivity of autoclave aerated concrete block, polystyrene concrete block, normal hollow concrete block, insulate coating and insulate plaster was measured in the Material-Lab in Dubai, UAE.

3.2.2 Reflectivity (α)

The solar reflectivity of insulate coating was measured in the Laser Lab in Building 28 at KFUPM using A JASCO, V-670 double beam spectrophotometer. In this test, two light beams were applied and passed through the test sample and reference sample were alternately collected by the detector, as reported in standard and some studies [70–72].

3.2.3 Microstructural analysis

In the Research Institute laboratories at KFUPM and according to ASTM C1723-16 [73], the micro-structure of autoclave aerated concrete block, insulate coating, insulate plaster and primer was identified using Scanning Electron Microscopy whereas

quantitative analysis of these materials was conducted using Energy-Dispersive Spectroscopy. Further, X-ray diffraction (XRD) analysis was used to identify the phases of crystalline components and to provide information on the unit cell dimensions for these materials [74].

3.3 Field monitoring

3.3.1 Construction of the test rooms

Four test rooms were constructed at Al-Faisaliah District in Dammam, eastern Saudi Arabia. The size of the test rooms was 4x5 m in plan and 3 m in height, as demonstrated in Figures 3.1 and 3.2. Ground reinforced concrete slab was cast below each test room with a size of 4x5 m in plan and 0.15 m in thickness. Figure 3.3 shows the steps for casting these slabs. These steps can be summarized as follows:

a) Preparing the ground: The ground under concrete slab was cleaned and leveled manually and its perimeter was restricted using wooden boards.

b) Reinforcing and casting: Concrete slabs, measuring 4mx5mx150mm, with 12 mm diameter steel bars (5 bars per meter) at bottom in both two directions, were cast. The concrete slabs were prepared with the following mixture composition: Cement content = 350 kg/m^3, Coarse aggregate = 1120 kg/m^3, Dune sand = 750 kg/m^3 and w/c = 0.5. Plastic sheet was placed under the concrete slab to prevent absorption of concrete water by the ground.

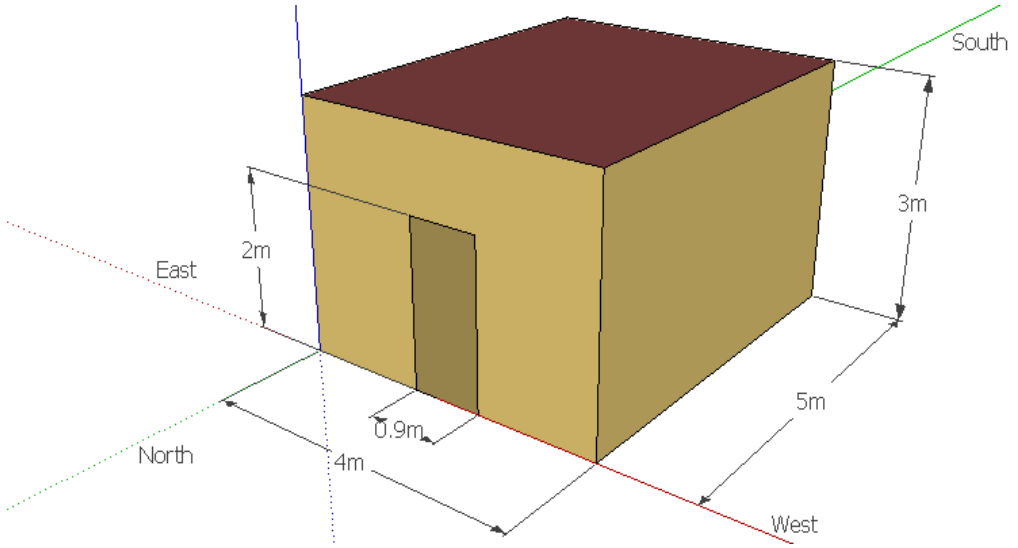

Figure 3.1: Test room in 3D view.

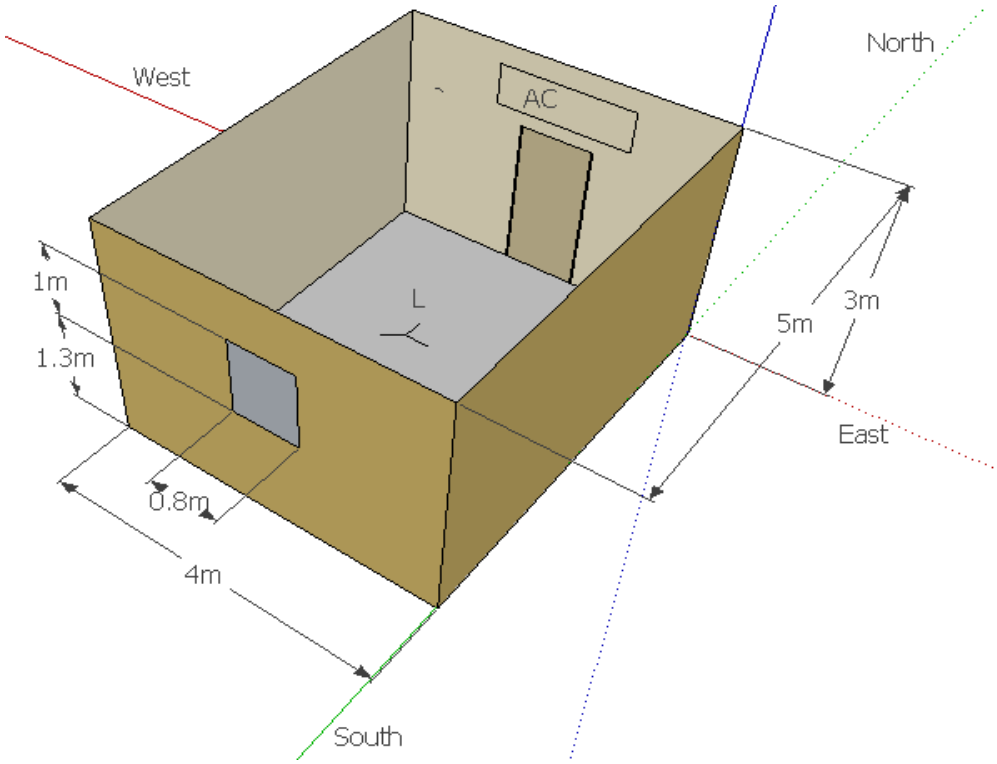

AC: Air conditioner, L: Light unit in the same point but in ceiling.

Figure 3.2: Test room from another view.

a) Preparing the ground.

b) Reinforcing.

c) Casting.

Figure 3.3: Steps in casting a ground reinforced concrete slab.

The characteristics of the walls, which were constructed with or without thermal insulation materials, in the four test rooms were as follows:

3.3.1.1 Test Room 1 (TR1)

This test room used a traditional system of walls that is often being commonly used in eastern Saudi Arabia, in villas and multi-storeyed buildings. The walls were made from normal hollow-core blocks with head and bed mortar and 10-mm thick plaster on the exterior and the interior walls. The block size was 20x20x40 cm. A 3-mm thick Insulate-Retherm (IR) coating was applied to the exterior wall and 2-mm thick IR coating was also

applied on both the inner walls and the ceiling of the room. After applying the Insulate coating, the normal exterior acrylic paint was applied from both outside and inside. The roof of the test room was fully insulated using a polystyrene/foam insulation with 7-cm thickness that is currently used in practice in the region. Figure 3.4 shows the details of TR1 walls.

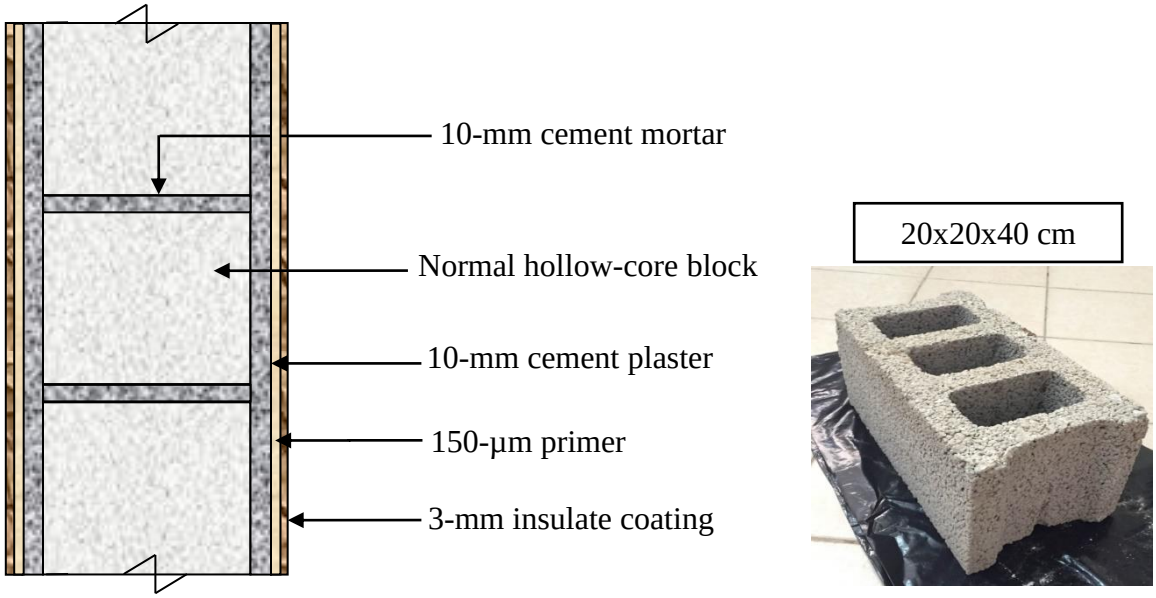

(a) Cross section of TR1 wall. (b) Normal hollow block.

Figure 3.4: Details of TR1 walls.

3.3.1.2 Test Room 2 (TR2)

This test room was similar to TR1. However, a 3-mm thick Insulate-Retherm (IR) coating was not applied to the exterior and inner walls. TR2 was served as the Reference Test Room and the performance of the insulations was compared with this test room. Figure 3.5 depicts the cross section of TR2 walls.

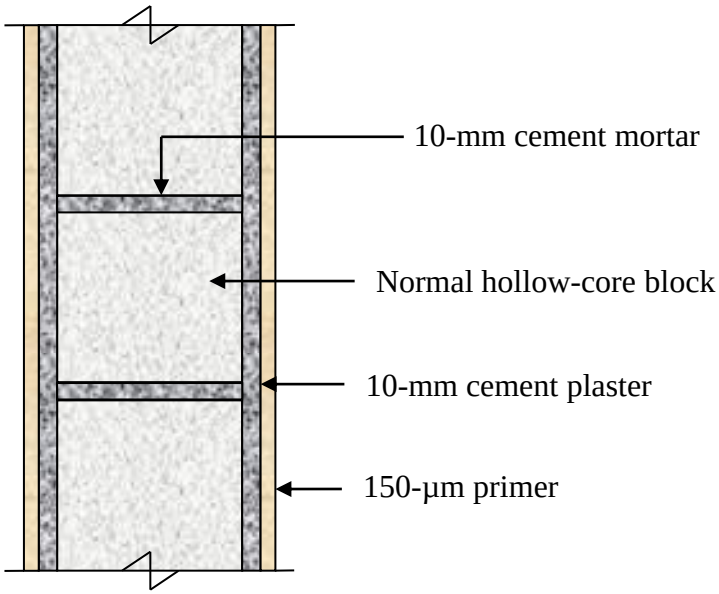

(a) Cross section of TR2 wall.

(b) Normal hollow-core block.

Figure 3.5: Details of TR2 walls.

3.3.1.3 Test-Room 3 (TR3)

This test room was similar to TR2. However, the normal hollow-core blocks were replaced by insulated blocks, which are also used in villas and multi-storeyed residential and commercial buildings. These blocks incorporate expanded polystyrene board and they are often used in eastern Saudi Arabia. Figure 3.6 depicts the cross section of TR3 walls.

3.3.1.4 Test-Room 4 (TR4)

This test room used a new generation and state-of-the-art system. The walls were made from INSULATE thermal block (20x20x60 cm in size). The head and bed joints were made from a special INSULATE thermal mortar. 15-mm INSULATE thermal plaster was applied on both inside and outside the walls. The INSULATE plaster was

subsequently coated by 3-mm thick Insulate-Retherm coating from outside and inside. Figure 3.7 depicts the cross section of TR4 walls.

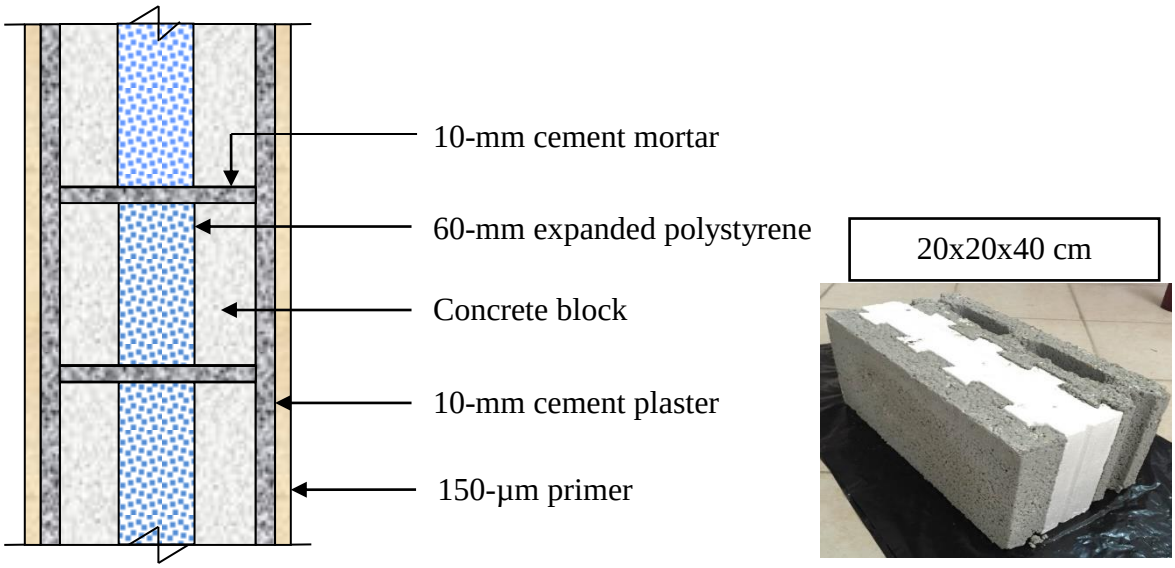

(a) Cross section of TR3 wall. (b) Insulate block (polystyrene).

Figure 3.6: Details of TR3 walls.

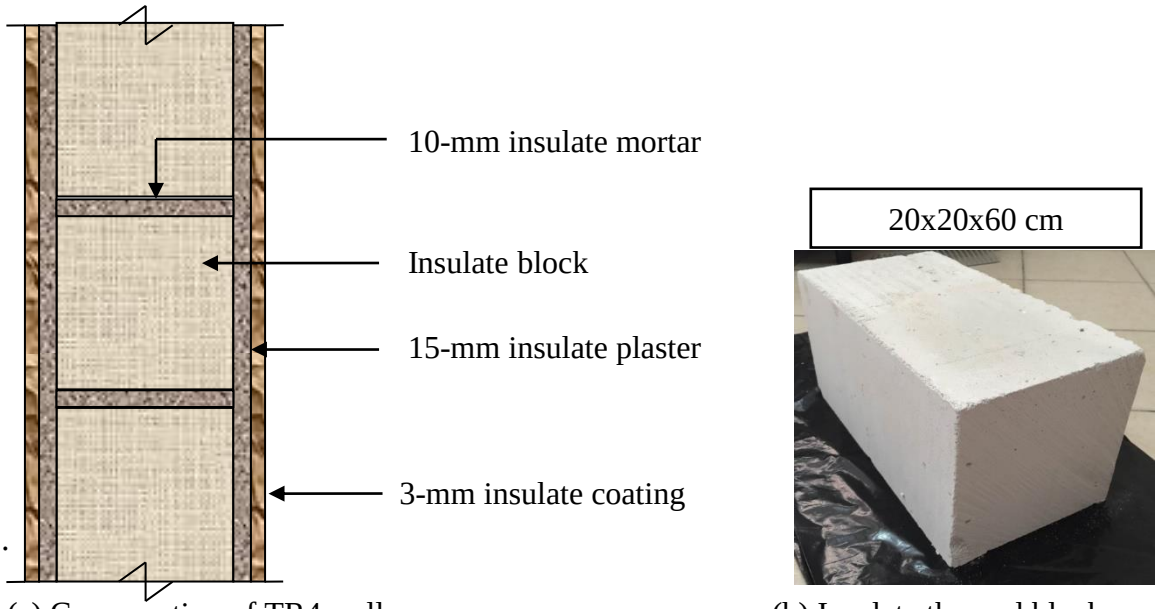

(a) Cross section of TR4 wall. (b) Insulate thermal block.

Figure 3.7: Details of TR4 walls.

Table 3.1 describes the various features of the walls in the four test rooms.

Table 3.1: Components of the walls in the four test rooms.

Test Room #	Block Type for Walls	Mortar Type between Blocks	Plaster Type	Paint Type
1	Normal Hollow Core Blocks	Cement Mortar	Cement Mortar	Insulate-Retherm Coating + Emulsion paint
2	Normal Hollow Core Blocks	Cement Mortar	Cement Mortar	Emulsion paint
3	Insulated Blocks (Polystyrene)	Cement Mortar	Cement Mortar	Emulsion paint
4	INSULATE Thermal Block	INSULATE Thermal Mortar	INSULATE Thermal Plaster	Insulate-Retherm Coating+ Emulsion paint

All the test rooms (TR1, TR2, TR3 and TR4) had the following common features:

1. All the test rooms were constructed with the dimensions of 4x5 m in plan and 3 m in height, as shown in Figures 3.1 and 3.2. The distance between the test rooms was 2 m on North-South direction and free space on Eastside. However, there was external boundary wall on Westside of test rooms with distance of 1.5 m. Therefore, all test rooms were exposed to the same shading.
2. The roof of all the test rooms was 150-mm thick reinforced concrete slabs that were simply supported on the four walls.
3. All the test rooms had one standard hollow door in the northern wall, 0.9x2 m in size, for access inside each room.

4. All the test rooms had one standard double-glasses window in the southern wall, 0.8x1 m in size, for lighting each room during the day.
5. All the test rooms were equipped with one digital control 18000 BTU split air conditioner installed on the north wall of each test room.
6. All the test rooms were equipped with a standard stand-alone electric meter approved by Saudi Electricity Company (SEC) to measure the power consumption in each room.
7. A 220V, 50Hz A/C current was made available in each room for the two tube lights and the air conditioner as well as for the measuring devices.
8. All the doors were equipped with an automatic door closer unit.
9. All the openings for door, window, A/C unit and holes were closed with silicon sealant or silicon foam to ensure that the air and humidity did not penetrate the room.
10. All the test rooms were constructed facing the east direction so that the front walls were subjected to solar radiation in the morning and the back wall in the afternoon.
11. The air conditioning units were originally new and thereafter they were properly maintained to ensure similar efficiency of A/C units in all the test rooms.

Figure 3.8 (a to l) explains the steps for constructing test rooms, while Figure 3.9 shows the test rooms after construction.

(a) Constructing walls.

(b) Casting slabs.

(c) Applying plaster.

(d) Applying inside paint.

(e) Applying outside paint.

(f) Applying Insulate-coating.

(g) Measuring thickness of Insulate-coating.

(h) Composing windows and doors.

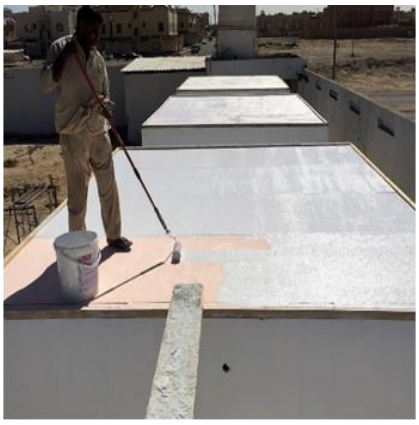

(k) Applying insulation on roof.

(l) Installation of A/C's.

Figure 3.8: Various construction stages.

Figure 3.9: Test rooms after construction.

3.3.2 Checking conditions around each test room

After constructing the test rooms, the air movement and temperature around each room were checked using vane anemometer testo 417, as shown in Figure 3.10. Wall of wood was constructed beside TR4 to keep the temperature and wind speed the same around each test room. Figure 3.11 shows wooden wall and test rooms.

Figure 3.10: Vane anemometer testo 417.

Figure 3.11: Wooden wall beside TR4.

3.3.3 Monitoring thermal performance of the test rooms

The proposed research was conducted for the period of summer session to monitor the thermal performance of the four test rooms. During this period, there was a continuous

monitoring of indoor and outdoor environmental conditions. The field monitoring tasks involved the following:

3.3.3.1 Weather monitoring

A complete unit of wireless weather monitoring system from Davis (Wireless Vantage Pro 2) was installed on the top of the building beside test rooms [75]. The weather station had its own data displayers and a data logger with the capability of recording and storing the data (Davis Console or Envoy8x) using special programs (weather-link or weather-transfer) as demonstrated in Figure 3.12. In this study, two data loggers were used and the two programs for checking the data collected by both of them. The wireless weather monitoring station measured the following:

a) Rainfall (mm);
b) Wind speed (km/h);
c) Wind direction;
d) Ambient temperature (ºC);
e) Ambient relative humidity (%);
f) Solar radiation (W/m^2); and
g) UV index

All monitored weather data were collected and stored continuously in computer every 10 minutes.

(a) Wireless Vantage Pro 2

(b) Davis Console.

(c) Envoy8x.

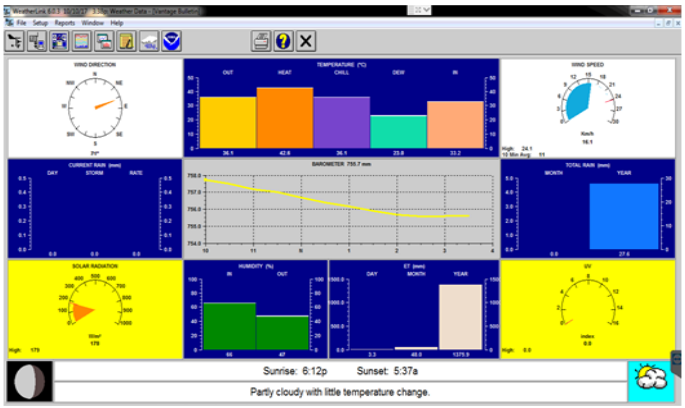

(d) Weather-link program.

Figure 3.12: Wireless weather station components.

3.3.3.2 Infrared thermograph assessment

FlirE6 camera was used to assess the temperature distribution across the interior and exterior surfaces of the walls in all the four test rooms aiming at investigating the effectiveness of insulation materials in reducing the heat transfer from the outside surface to inside surface of the walls [76–78]. Further, the thermal leakage from doors and windows was monitored using this camera in order to block the voids and cracks using

silicon foam before the start of the measurements. Thermal images showed the variations of surface temperature and helped locate the installation places for thermocouples and heat flux meters. Figure 3.13 shows the FlirE6 camera used in this study.

Figure 3.13: FlirE6 camera.

3.3.3.3 Temperature monitoring on walls

Thermocouples (T/C) type K were used to measure the temperature on surfaces (ºC or ºK) according to ASTM C 1046-95 for evaluating the effectiveness of insulation materials in reducing the inside surface temperature of the walls and for calculating the thermal parameters, thermal resistance and thermal conductance, of the walls [79]. The temperature of both exterior and interior faces of the walls and roof slab was measured continuously every 10 minutes using T/C grids connected in parallel [75]. 56 T/C's were fixed on the external and internal faces of the walls and roof in each room, as follows: 8 T/C's were fixed on the external and internal faces of the East and West walls. 6 T/C's were fixed on the external and internal faces of the South wall. 4 T/C's were fixed on the external and internal faces of the North wall. 4 T/C's were fixed on the external and internal faces of the roof. All T/C's were connected to the walls and roofs using putty and strong plastic tapes. All monitored temperature data from T/C's was collected and stored

continuously by the data logger (AT4532X) and AT4500 program every 10 minutes. Figure 3.14 depicts all the procedures and equipment used to monitor the temperature on walls.

(a) Making holes on walls. (b) Extra T/C'S extension module-8 channels.

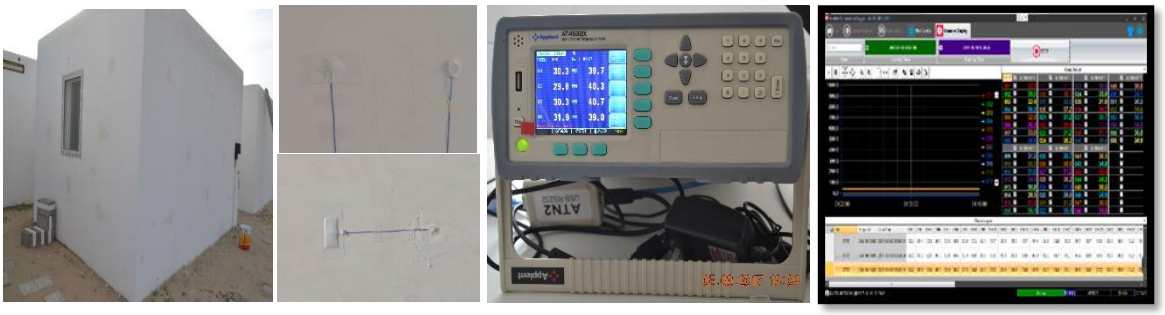

c) T/C's on walls. d) AT4532X data logger. d) AT4500 program.

Figure 3.14: Procedures and equipment for monitoring temperatures on walls.

3.3.3.4 Heat flux monitoring

Heat flux meters (HFS-PHFS-09e) were installed on the interior faces of the walls to measure the heat flow across the walls for calculating their thermal parameters, thermal resistance and thermal transmittance [75,79]. All monitored heat flux data from HFS was collected continuously by the data logger (FluxDAQ) and FluxTeq program every five seconds. Figure 3.15 depicts the heat flux measurement instruments. In all standards (ASTM and ISO), the heat flux (q) can be calculated using the following equation:

$$q = k \frac{dT}{dx} \quad 3.1$$

where:

q = heat flux (W/m^2)

k = thermal conductivity (W/m.K).

dT = temperature profile (K).

dx = thickness (m).

According to ASTM C 1046-95 [79], the heat flux can be measured in the site using the Equation 3.2.

$$q = \frac{\Delta V}{S} \quad 3.2$$

where:

ΔV = voltage obtained from heat flux meter (µV).

S = calibrated sensitivity of the sensor [µV/(W/m^2)].

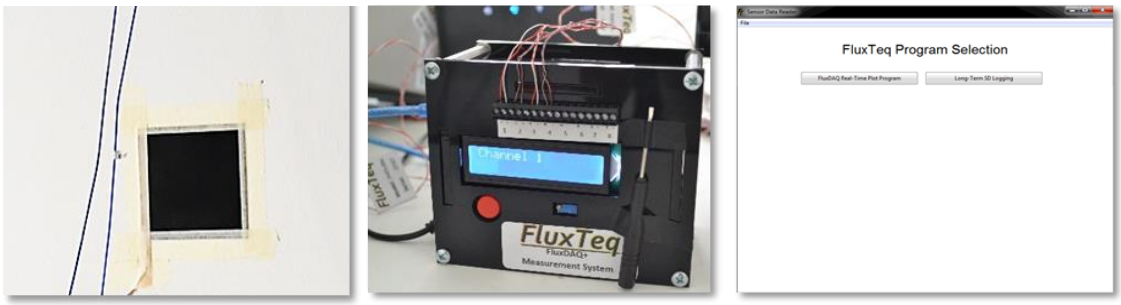

(a) HFS-PHFS-09e. (b) FluxDAQ data logger. (c) FluxTeq program.

Figure 3.15: Heat flux measurement instruments.

3.3.3.5 Temperature/relative humidity monitoring

Temperature and relative humidity inside the test rooms were measured continuously using T/RH data logger for calculating thermal transmittance of the walls and evaluating the effect of RH on the surface temperature of walls and the inside temperature of the test rooms [79]. In all standards (ASTM and ISO), the relative humidity can be calculated using Equation 3.3.

$$RH = \frac{Pa}{Ps} * 100 \quad (\%) \qquad 3.3$$

where:

P_a = actual vapor density (g/m^3).

P_s = saturation vapor density (g/m^3).

The inside temperature and relative humidity of each test room were measured using testo data logger (testo 175 H1) connected in the middle of each test room every 10 minutes. This data logger was programed, and the data was transferred to a computer using testo comfort software, as show in Figure 3.16.

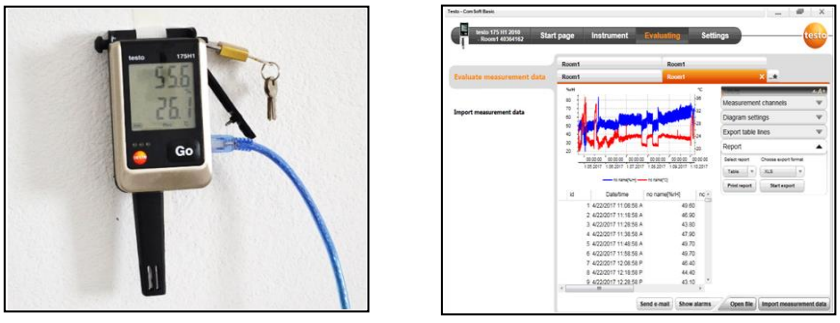

a) testo 175 H1. b) testo comfort software program.

Figure 3.16: testo 175 H1 and its software program.

3.3.3.6 Moisture monitoring

The moisture on the surface of the walls was monitored from time to time using testo 606-2 material humidity meter, as depicted in Figure 3.17.

Figure 3.17: Measuring the moisture on the surface of walls.

3.3.3.7 Thermal transmission (U-value) monitoring

The thermal transmission coefficient (U-value) for walls in all the test rooms was measured using U-value set (testo 635-2) [80]. This measurement was used for comparison with the actual U-value calculated from other sensors and data loggers in Sections 3.3.3.3 and 3.3.3.4. Figur 3.18 depicts the equipment used to measure U-value of walls. The total thermal resistance of these walls can be easily calculated (as it is the inverse of U-value). According to ASTM C1155 and ISO 9869, the thermal resistance (R) and thermal transmission coefficient (U) can be calculated using Equations 3.4 and 3.5, respectively.

$$R = \frac{L}{K} = \frac{dT}{q} \quad (\text{m}^2.\text{K/W}) \qquad 3.4$$

where:

L = length of material (m).

k = thermal conductivity (W/(m.K)).

dT = temperature profile (K).

q = heat flux (W/m^2).

$$U = \frac{1}{R} = \frac{k}{L} = \frac{q}{dT} \quad (\text{w/(m}^2.\text{K)}) \qquad 3.5$$

where:

R = total thermal resistance $(m^2.K/w)$.

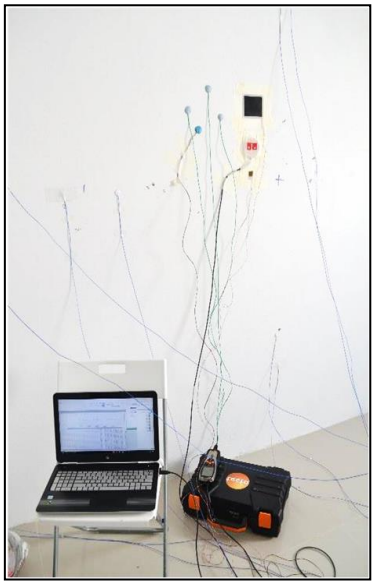

(a) U-value set (testo 635-2).

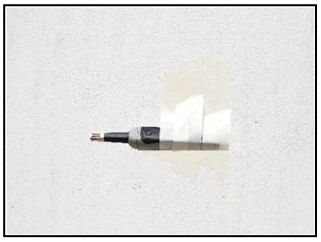

(b) Remote sensor outside.

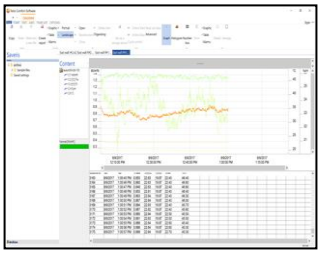

(c) testo U-value software program.

Figure 3.18: Equipment used to measure U-value of walls.

3.4 Electricity consumption monitoring

The electricity consumed by each of all the four test rooms during the monitoring period was continuously measured using an approved SEC power and energy meter. Further, the electricity consumption in each test room was also measured continuously every 10 minutes using Acuvim II Series meter and its software program, as shown in Figure 3.19.

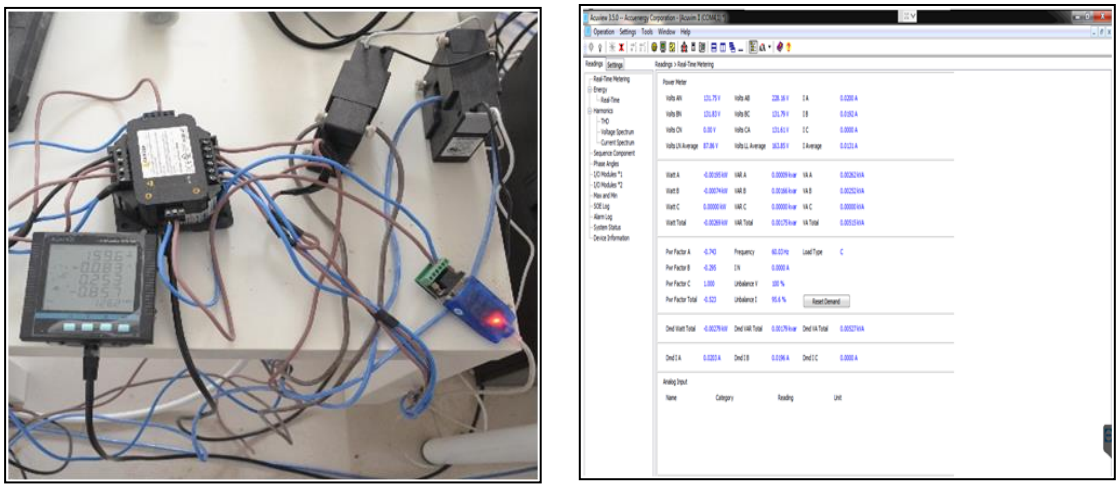

a) Acuvim II Series meter. b) Typical Acuview program.

Figure 3.19: Electricity consumption measurement set-up.

Figure 3.20 demonstrates one test room during monitoring. The performance of all equipment and software programs in all test rooms was monitored from KFUPM every 5 hours using the available software programs like Teamviewer and Chrome Remote Desktop.

Figure 3.20: Test rooms during monitoring.

CHAPTER FOUR

LAB TESTS AND FIELD MONITORING RESULTS

4.1 General

The thermal performance of the four test room's walls incorporating different insulation materials and the effectiveness of these insulation materials in decreasing the energy consumption in the test rooms for providing the thermal comfort during summer months were evaluated by following the flow chart shown in Figure 4.1. Data from surface temperatures and heat flux monitoring on walls were utilized to assess the thermal resistance and conductance of walls. Heat flux monitoring data with outside weather and inside Temp./RH data were used to calculate thermal transmittance (U-value) of the walls. This calculated U-value of walls was compared with that obtained from the U-value set (testo 635-2).

Simulation of the test rooms was conducted using input measured data which were the thermal properties of the materials from lab tests, inside Temp./RH, weather monitoring and measured energy data. After that, the simulation results were compared with the experimental thermal performance, measured energy data and the lab test results were utilized in the final evaluation.

In this Chapter, the resulted data for the lab tests and field monitoring would be presented to investigate the thermal performance and energy consumption of the fours test rooms. In Chapter 5, the simulation using lab tests results, weather data, inside Temp./RH and electricity consumption results would be presented. Finally, the final evaluation of the

insulation materials would be concluded by combining all the results from the experimental work and computer simulation.

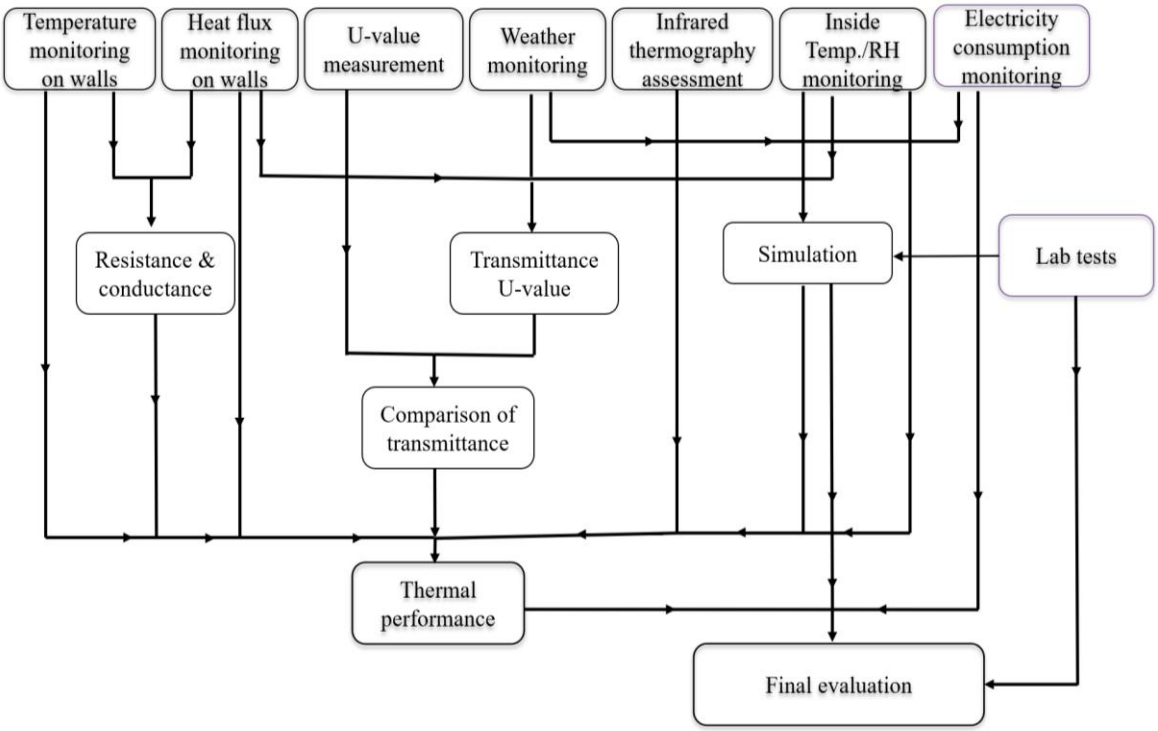

Figure 4.1: Flow chart of evaluation.

4.2 Laboratory test results

4.2.1 Thermal conductivity (k) test results

The thermal conductivity of the various materials used in this investigation was tested in the in Materials-Lab in Dubai, UEA, and the results are summarized in Table 4.1. INSULATE coating has the lowest thermal conductivity among all the insulation materials used in this project with a k value of 0.03 W/(m.K). However, the thickness of INSULATE coating on walls ranges between 2 to 4-mm. Since the thermal resistance of a material depends on its thermal conductivity and thickness (as demonstrated in Equation

3.4), the thermal resistance of INSULATE coating is low and this indicates that the high effectiveness of this coating in decreasing the heat flow through walls depends on reflecting the solar radiation as the manufacturer claims and explained in the next test [21].

Table 4.1: Thermal conductivity from lab tests.

#	Material	Test room	Image	Thermal conductivity (k), W/(m.K)
1	Normal Hollow Core Blocks	TR1 and TR2		0.52
2	Blocks with polystyrene board	TR3		0.10
3	Insulate Block	TR4		0.16
4	Insulate Coating	TR1 and TR4		0.03
5	Insulate plaster	TR4		0.06

4.2.2 Reflectivity (α) test results

From the solar reflectivity test results that were conducted at the Environment Monitoring and Remote Sensing Laboratory in Building 28 at KFUPM, the INSULATE coating has very high reflectivity for solar radiation. Figure 4.2 depicts the ability of INSULATE coating to reflect the solar radiation based on its wavelength. INSULATE coating can reflect 85% of ultraviolet rays, 90% of visible rays and more than 90% of infrared ray. The ultraviolet rays constitute only 6.6% of the total solar radiation, while the visible and infrared rays constitute more than 93% of the total solar radiation, as shown in Figure 4.3. Therefore, INSULATE coating reflects more than 90% of the solar radiation. This high reflectivity for solar radiation is due to the microspheric structure; explained in the next section; of INSULATE coating that improves the smoothness of its surface thereby permitting the reflection of solar radiation and reducing the heat transfer through the walls.

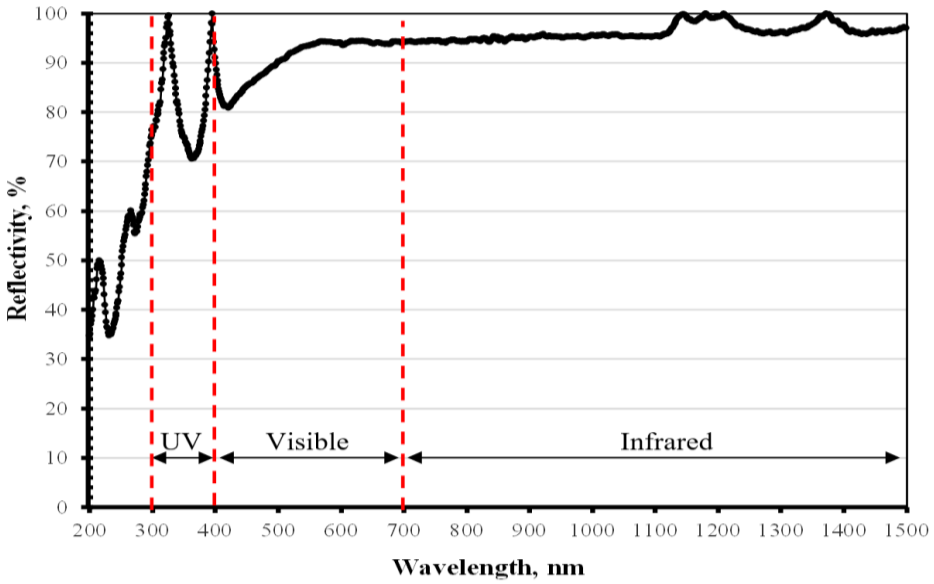

Figure 4.2: Solar reflectivity of INSULATE coating.

The reflectivity of INSULATE coating for solar radiation is very high (more than 90%) as compared with other materials such as primer paint and concrete. The reflectivity of primer paint ranges between 25 to 60%, while it ranges between 10 to 30% for concrete [81].

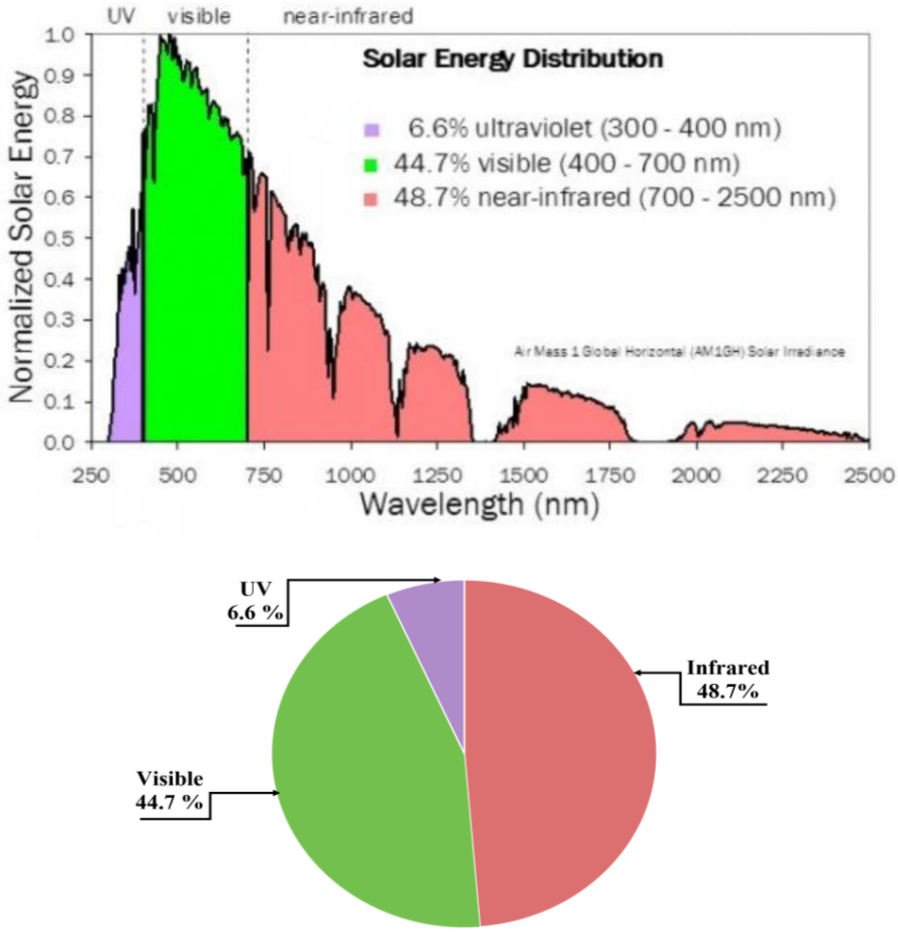

Figure 4.3: Spectrum of solar radiance.

4.2.3 Microstructural analysis results

SEM images; a, b, c and d; in Figure 4.4, show the microstructure of INSULATE coating, primer, insulate plaster and aerated concrete layers; respectively. The hollow microspheres which form the INSULATE coating layer decrease considerably the heat

flow thereby reducing the thermal conductivity of this coating [82]. On the contrary, the solid structure of primer layer enhances the thermal conductivity of the primer. Further, these hollow microspheres reflect most of the solar radiation applied on the coating passing between them [21]. This increases the effectiveness of INSULATE coating in reducing the heat transfer through walls coated with it. The voids distributed in insulate plaster and aerated concrete layers decrease the weight and thermal conductivity of these materials thereby reducing efficiently their heat transfer [82].

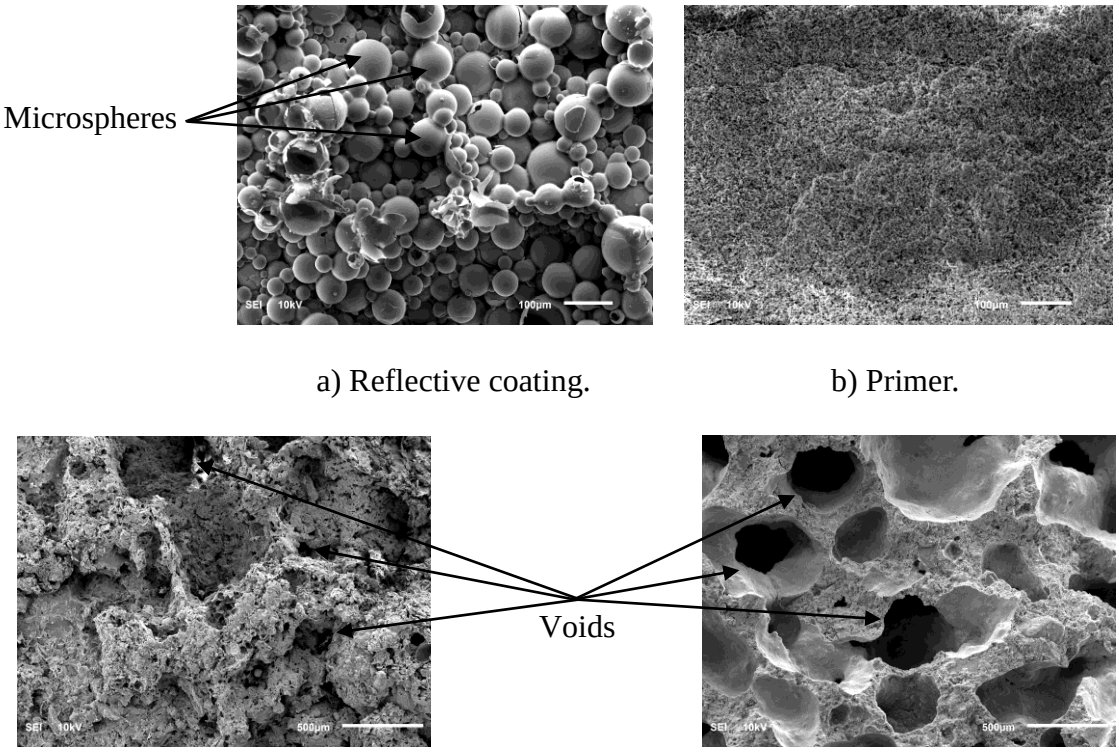

a) Reflective coating. b) Primer.

c) Insulate plaster. d) Aerated concrete.

Figure 4.4: Microstructure of materials.

The semi-quantitative analysis results from XRD analysis for INSULATE coating, primer, insulate plaster and aerated concert is demonstrated in Table 4.2 and presented in Figure 4.5. The Dihydro-phenanthry (material contains five carbon atoms and one

oxygen atom) represents 98% of INSULATE coating, while 2% was Rutile (a material composed primarily of titanium dioxed, TiO_2). The primer was 95% Calcite ($CaCO_3$) and 5% Dolomite ($CaCO_3$) whereas the insulate was 100% Calcium Sulfite ($CaSO_3$). 75% of aerated concrete was Quartz, 24.6% Calcite and 4% Tobermorite (calcium silicate hydrate mineral).

EDS analysis results of INSULATE coating, primer, insulate plaster and aerated concert are presented in Figure 4.6; a, b, c and d; respectively. INSULATE coating consists of oxygen, carbon, silicon, calcium, sodium and titanium. Primer has the same components of INSULATE coating but instead of sodium, it contains magnesium. Insulate plaster consists of carbon, oxygen, silicon, calcium, aluminum, potassium and sodium. Finally, insulate aerated concrete block consists of oxygen, calcium, silicon, carbon and aluminum. In INSULATE coating and primer paint, calcium, silica, carbonate and titanium are used as pigment [83], while silicon is used to improve adherence [84]. Using aluminum powder in insulate plaster and block is used to generate cellular structure [85].

Table 4.2: XRD analysis of materials.

Material	Phase name	Content (%)
INSULATE coating	Rutile, syn	2
	Dihydro-phenanthry	98
Primer	Calcite	95
	Dolomite	5
Insulate plaster	Calcium Sulfite	100
Aerated concrete	Quartz, syn	75
	calcite high, syn	24.6
	Tobermorite-11A, syn	0.4

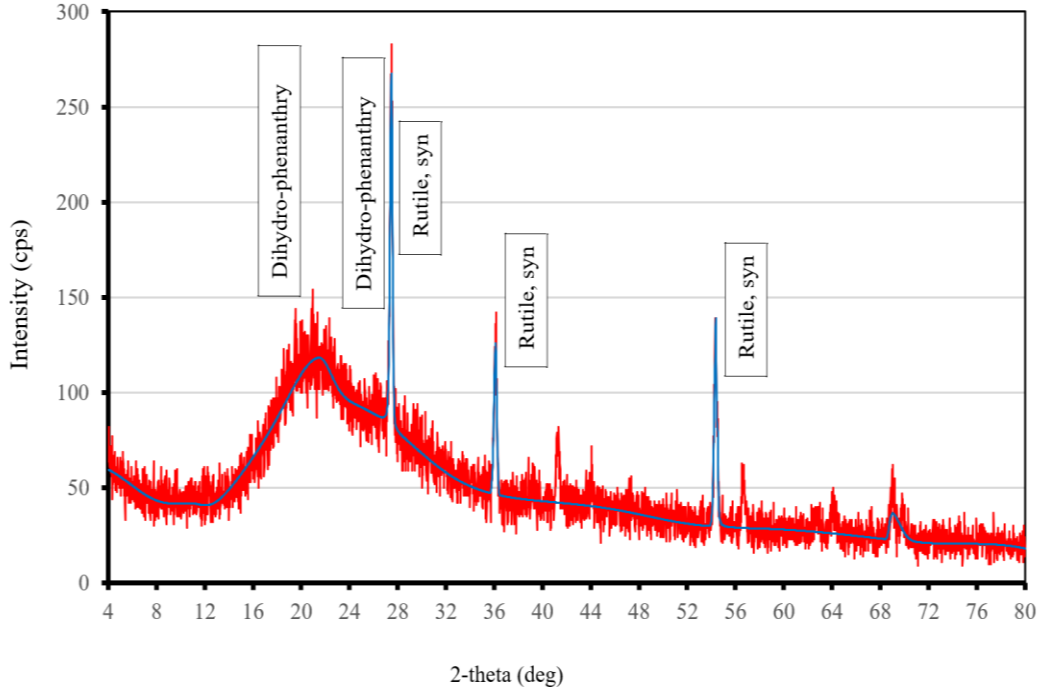

(a) INSULATE coating.

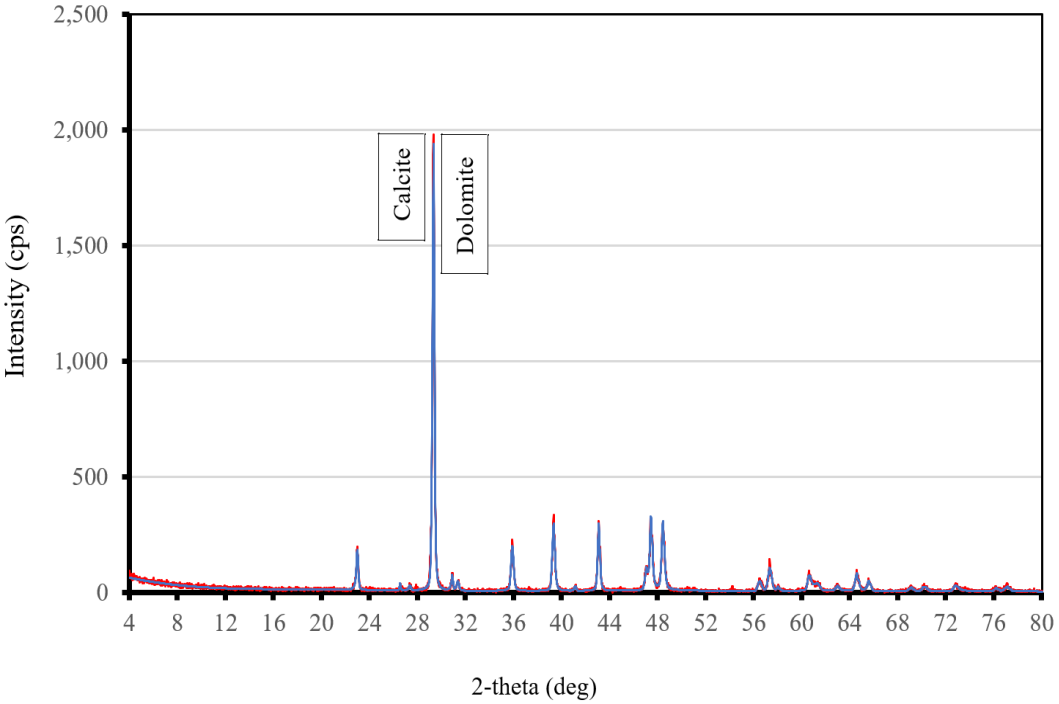

(b) Primer.

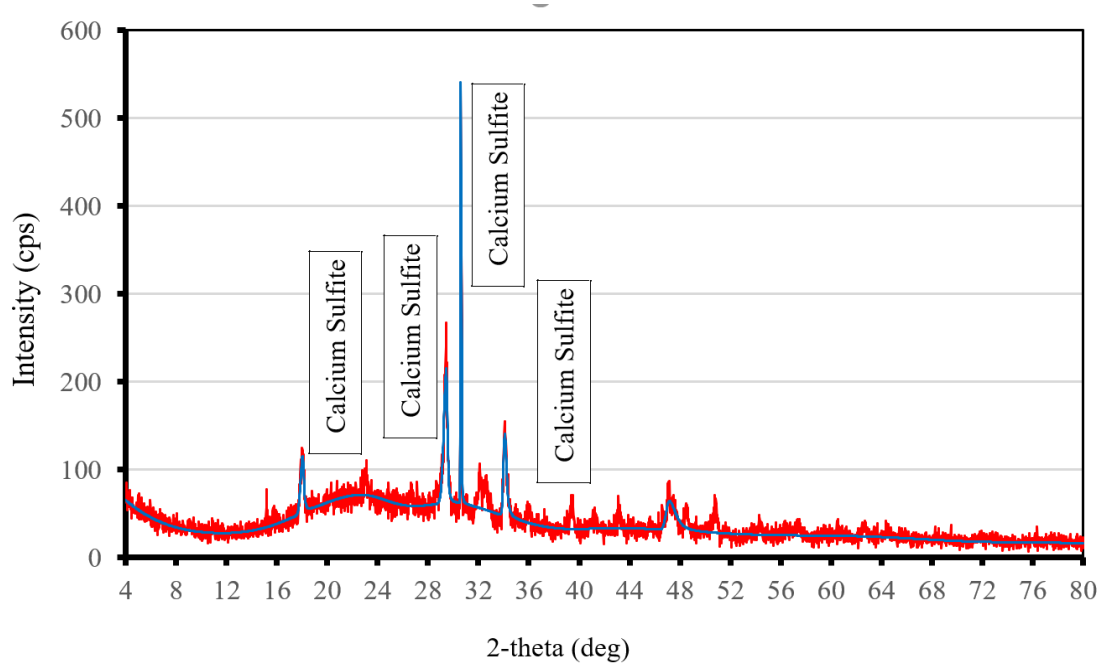

(c) Insulate plaster.

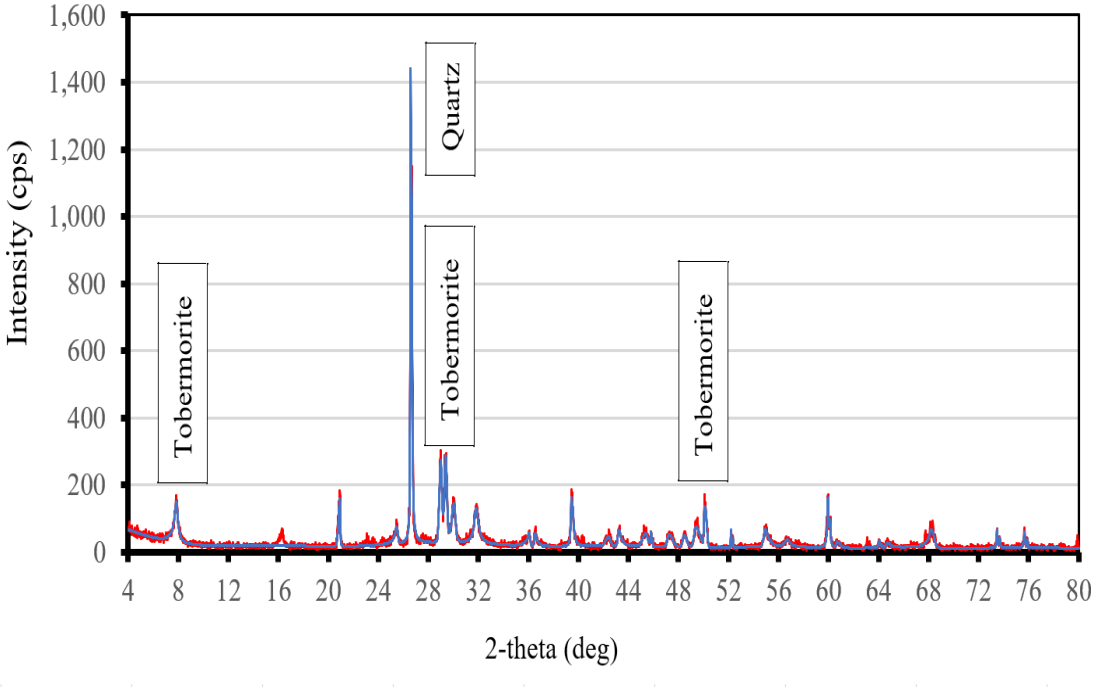

(d) Aerated concrete.

Figure 4.5: XRD analysis of materials.

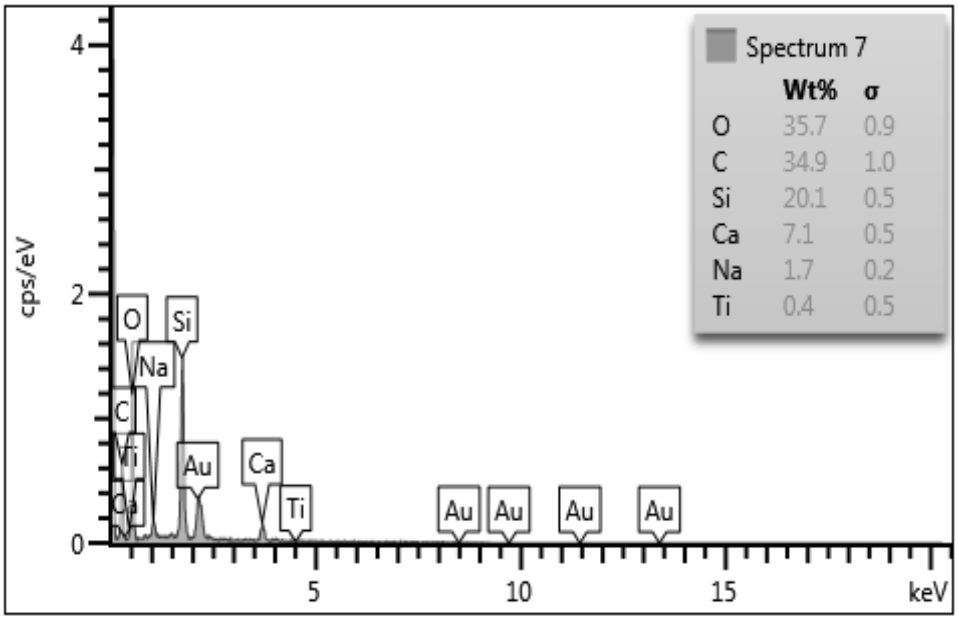

a) INSULATE coating.

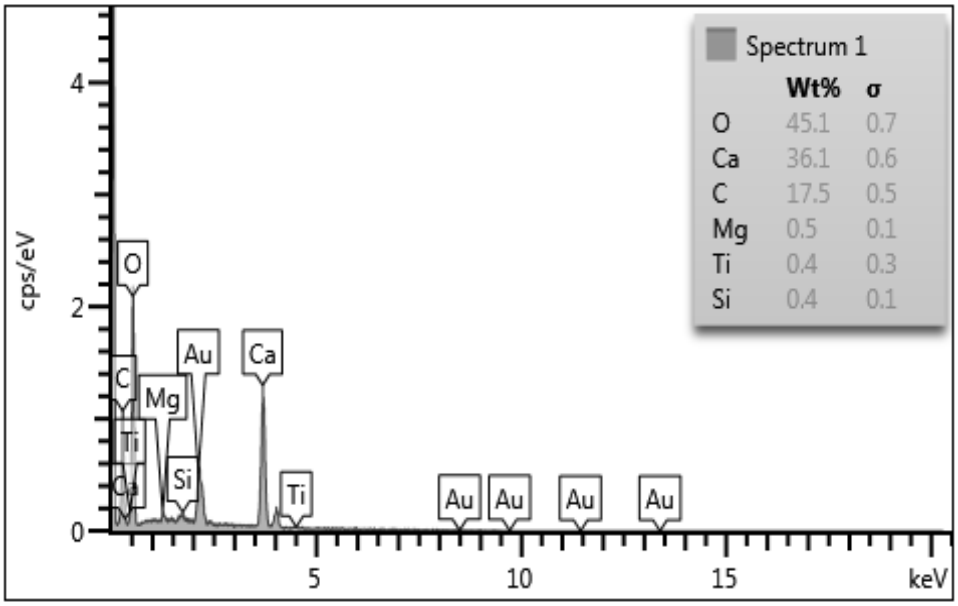

b) Primer.

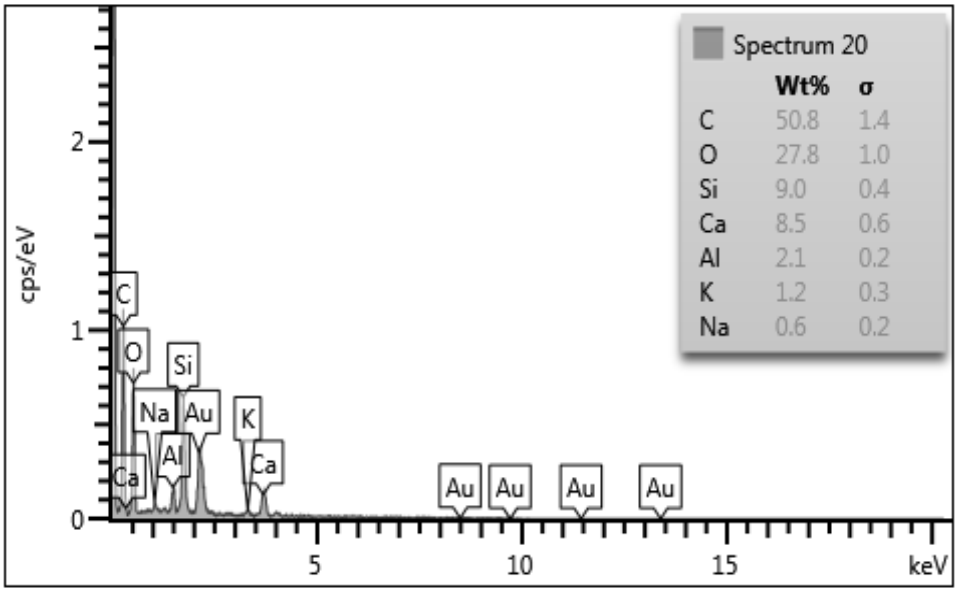

c) Insulate plaster.

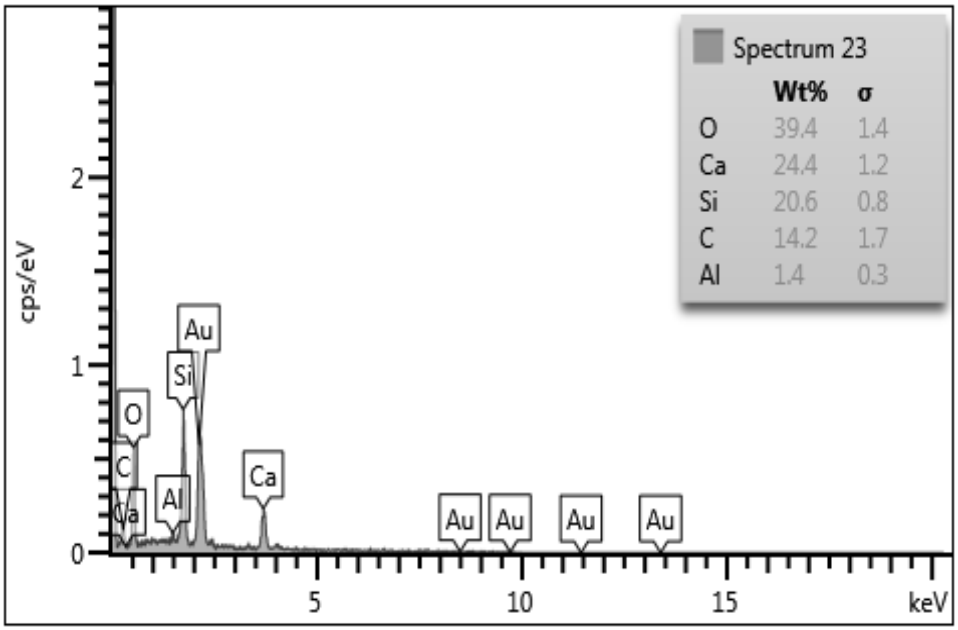

d) Aerated concrete.

Figure 4.6: EDS analysis of materials.

4.3 Weather data results

4.3.1 Outside temperature and relative humidity (RH)

The daily outside temperature for the hottest summer months are shown in Figure 4.7. The daily temperature was very high during July and August where it ranged between 32 and 49 °C. However, it decreased gradually from the end of August and it was the lowest at the end of September where it ranged between 28 °C and 41 °C. In contrary to the daily temperature, the daily RH was higher on August and September than on July, as depicted Figure 4.8. The average daily temperature and RH during the three months are depicted in Figure 4.9, while during July, August and September are demonstrated in Figures 4.10 to 4.12, respectively.

It can be easily obscured that the average daily RH increases with decreasing the temperature. On 9th of July, the maximum daily RH was 60% when the temperature was the minimum of 37.4 °C, while the maximum temperature was 40.6^{o}C with RH of 22% on 14th of the same month. On August, the maximum daily RH was 60% whereas the temperature was about 40°C. The average daily temperature on September decreased where the maximum value was about 39^{o}C at the beginning of this month. However, it decreased gradually to about 33°C at the end of this month. The average daily RH on September was very high, reaching to about 70% at the middle of the month. Figure 13 shows a typical week for the temperature and RH data from 8th to 14th August, while the first of July was selected as typical day in Figure 4.14. The temperature reaches the maximum value of 46°C during the day at 2:00 pm and it decelerates to the minimum

value of 33°C at 5:00 am. However, RH was maximum at mid night with rate of 24% and, thereafter, it reduces to the lowest value of 9% at 3:00 pm.

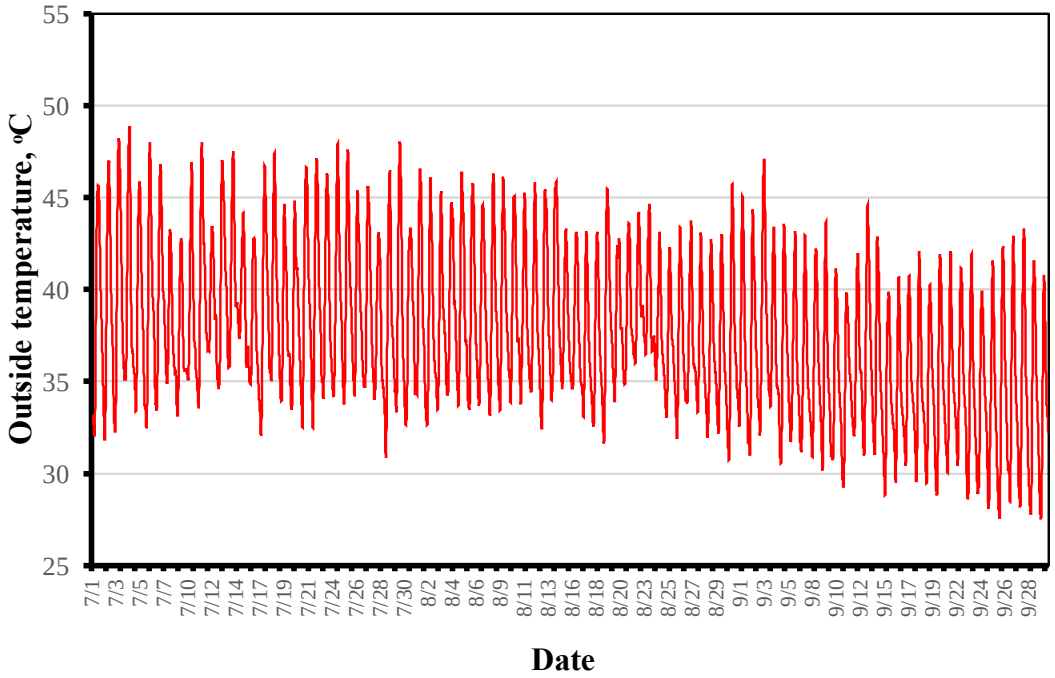

Figure 4.7: Outside temperature during the hottest summer months.

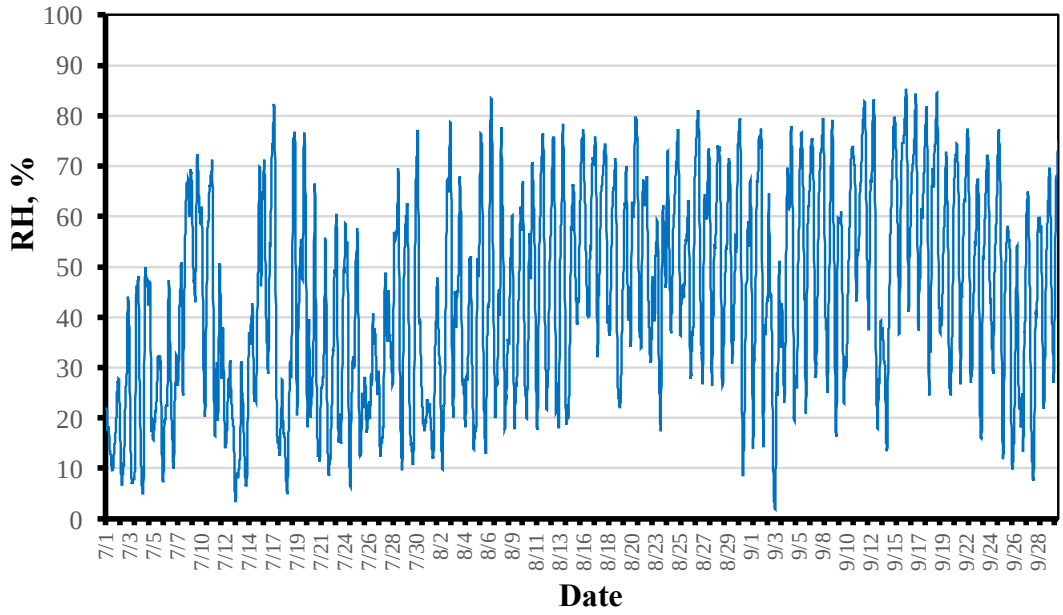

Figure 4.8: Outside RH during the hottest summer months.

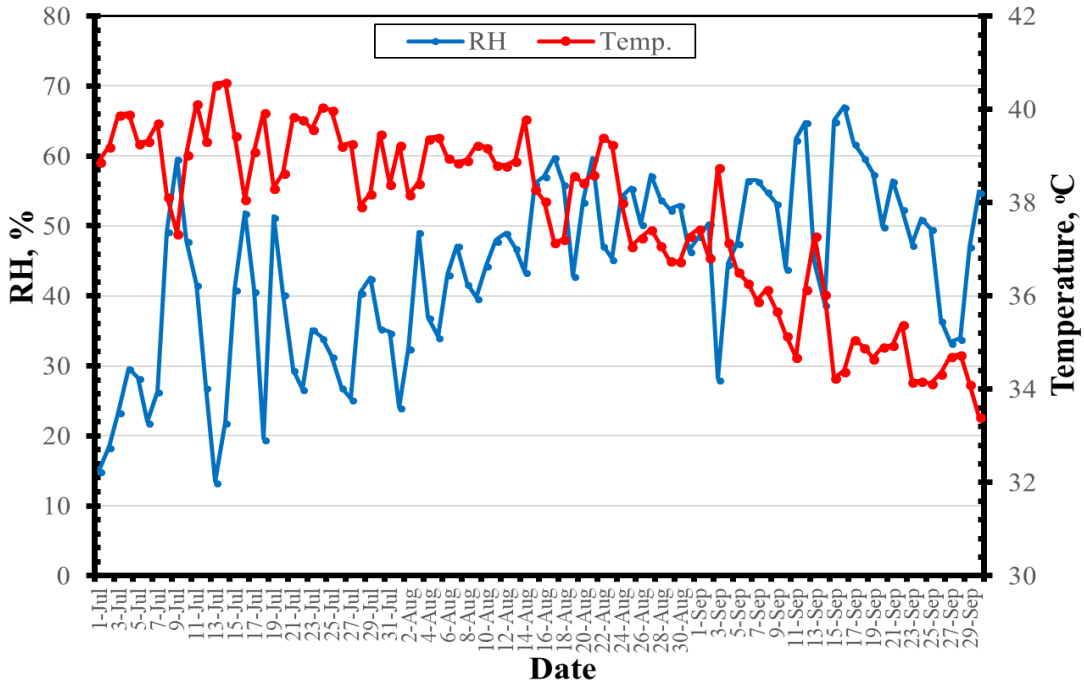

Figure 4.9: Average daily temperature and RH during the hottest summer months.

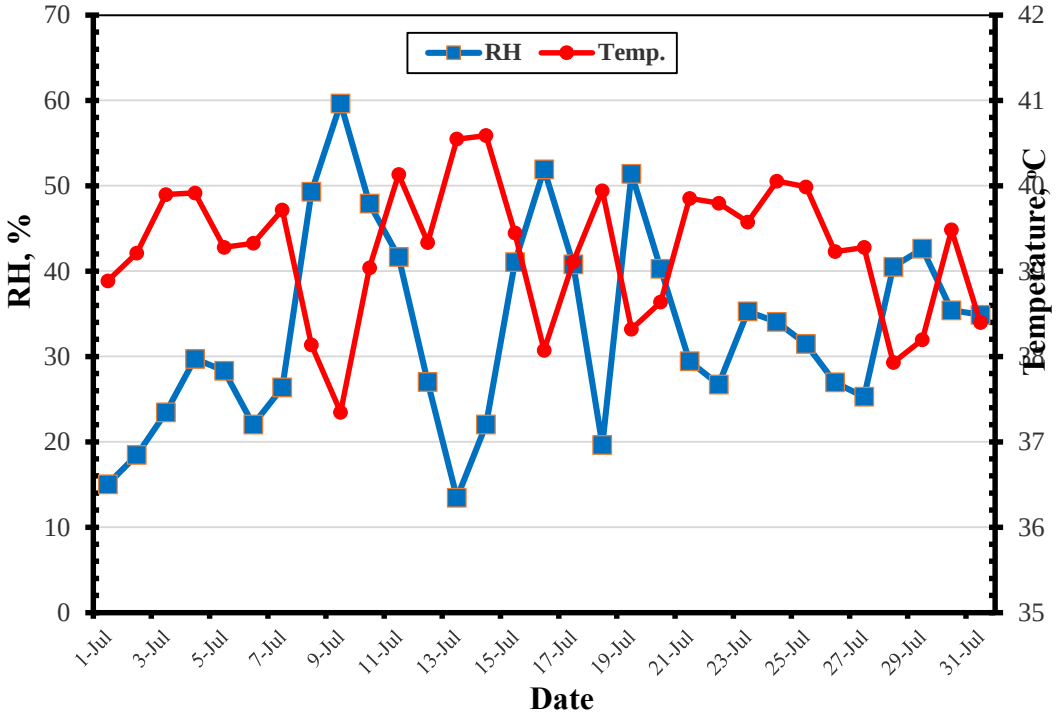

Figure 4.10: Average daily temperature and RH on July.

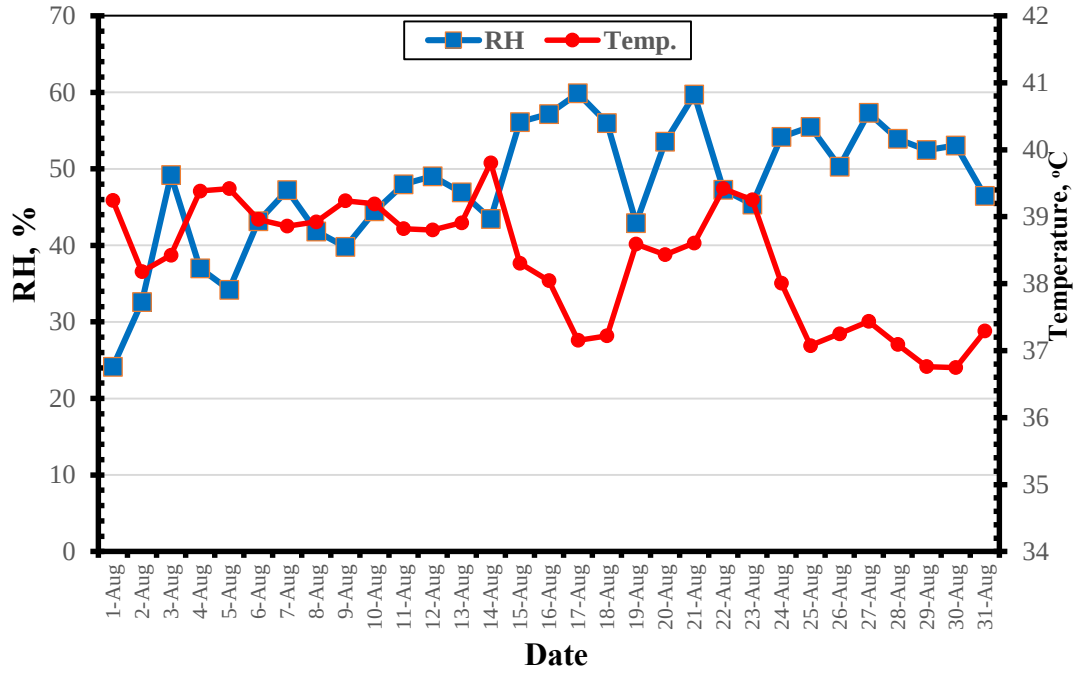

Figure 4.11: Average daily temperature and RH on August.

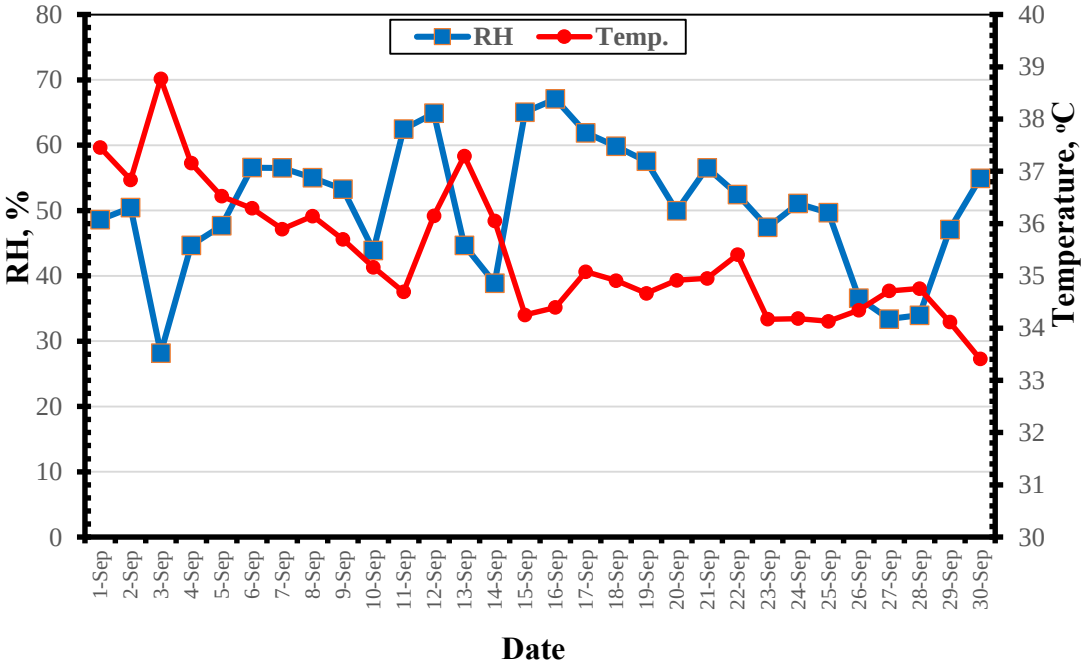

Figure 4.12: Average daily temperature and RH on September.

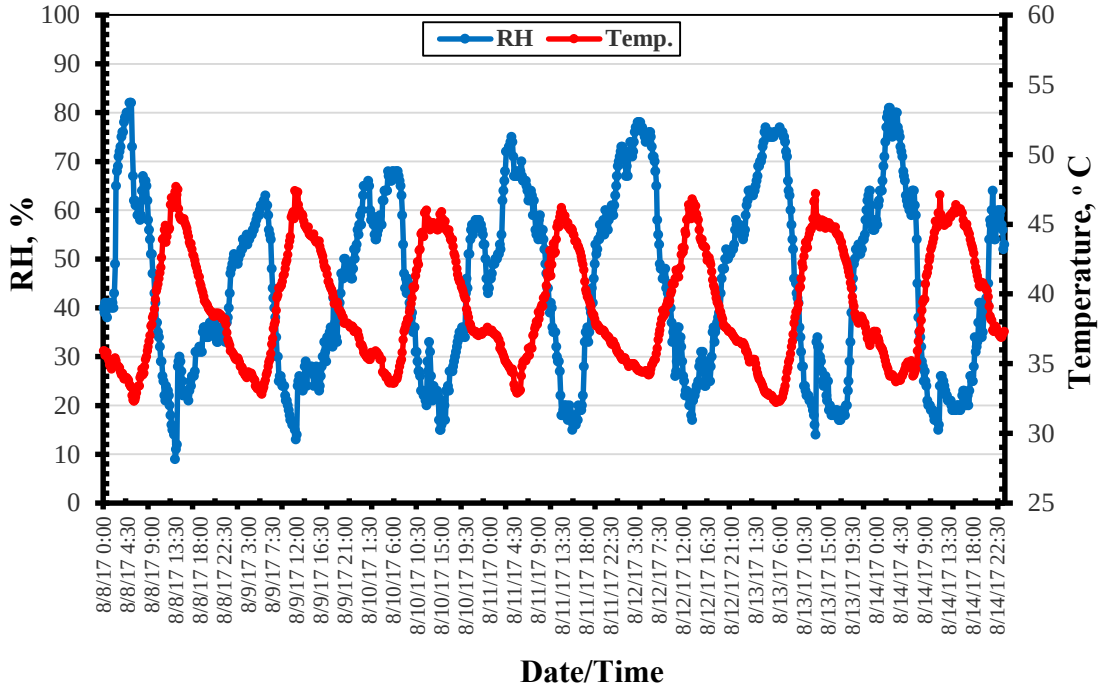

Figure 4.13: Typical temperature and RH on representative week (8 to 14 August).

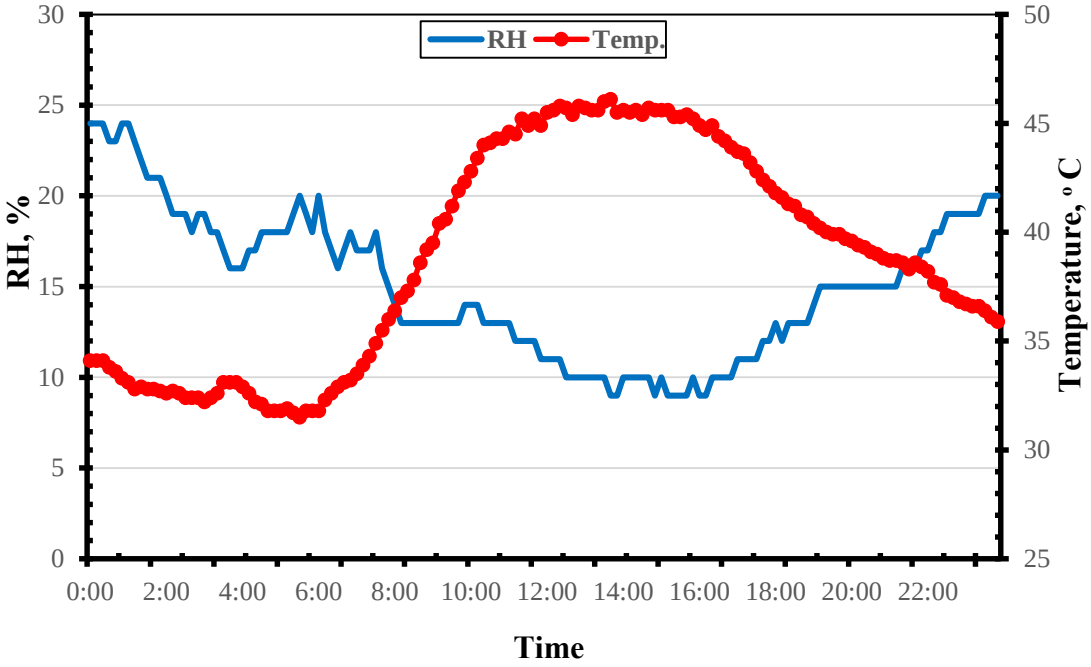

Figure 4.14: Typical temperature and RH on representative day (1st of July).

4.3.2 Solar radiation and Ultraviolet-index (UV-Index)

The solar radiation and UV-index during the day during the period of the hottest summer months are shown in Figures 4.15 to 4.21. The solar radiation and UV index on July and August were more than on September in accordance with the rise in the temperature, as described above. The maximum solar radiation and UV index on July, August and September during the day are 895, 861, 810 W/m² and 5.7, 5.5, 4.7, respectively. Figures 4.22 and 4.23 depict the solar radiation and UV index on a typical week. Similarly, the data for a representative day are shown in Figures 4.24 and 4.25. The highest values of solar radiation and UV-index were at 12:00 pm when the rays of sun are perpendicular to surface of the Earth.

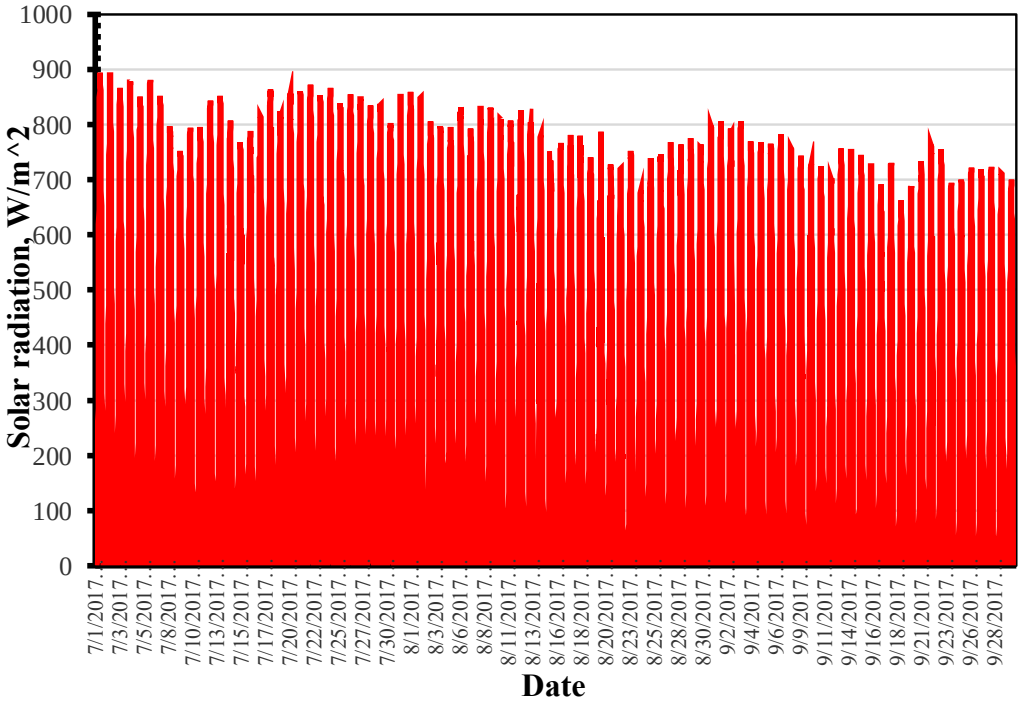

Figure 4.15: Solar radiation during the hottest summer months.

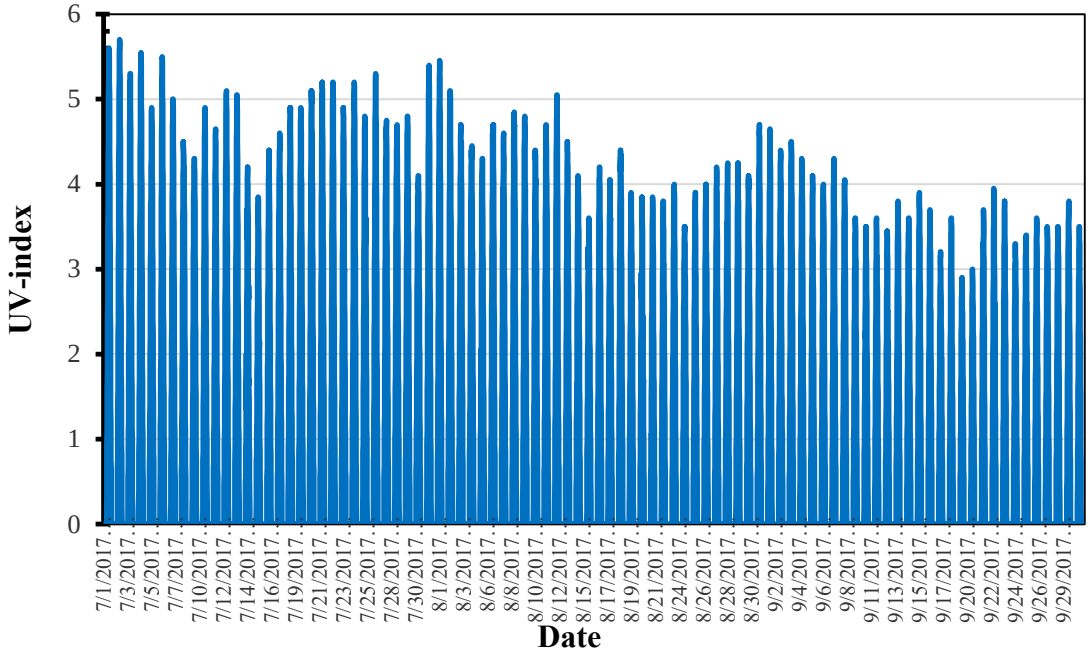

Figure 4.16: UV index during the hottest summer months.

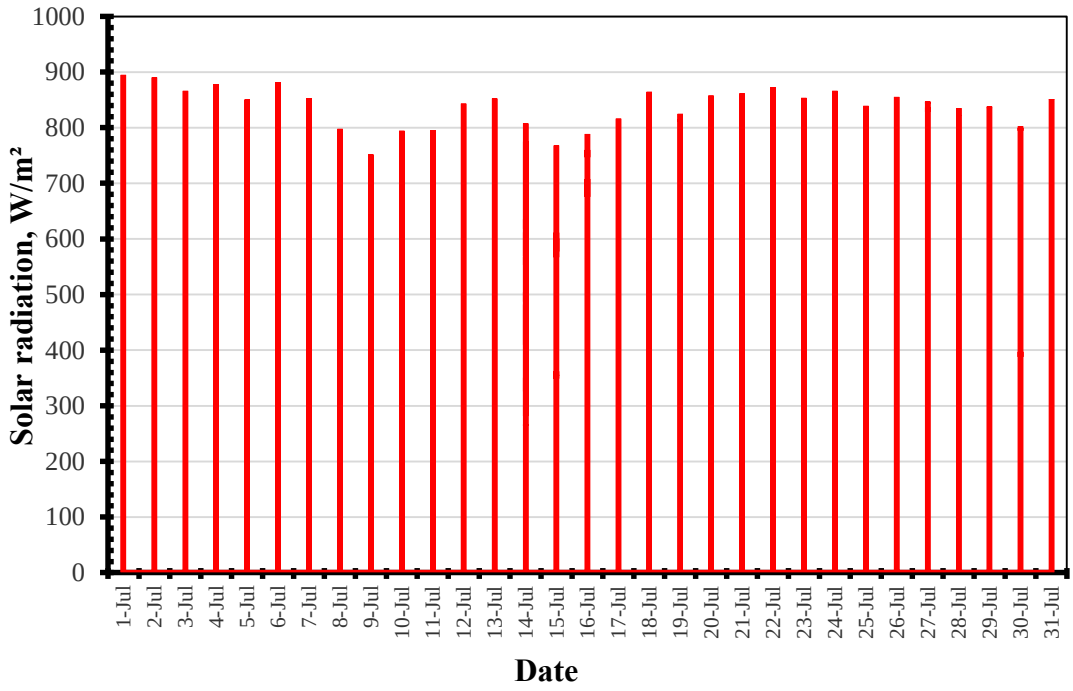

Figure 4.17: Solar radiation during July.

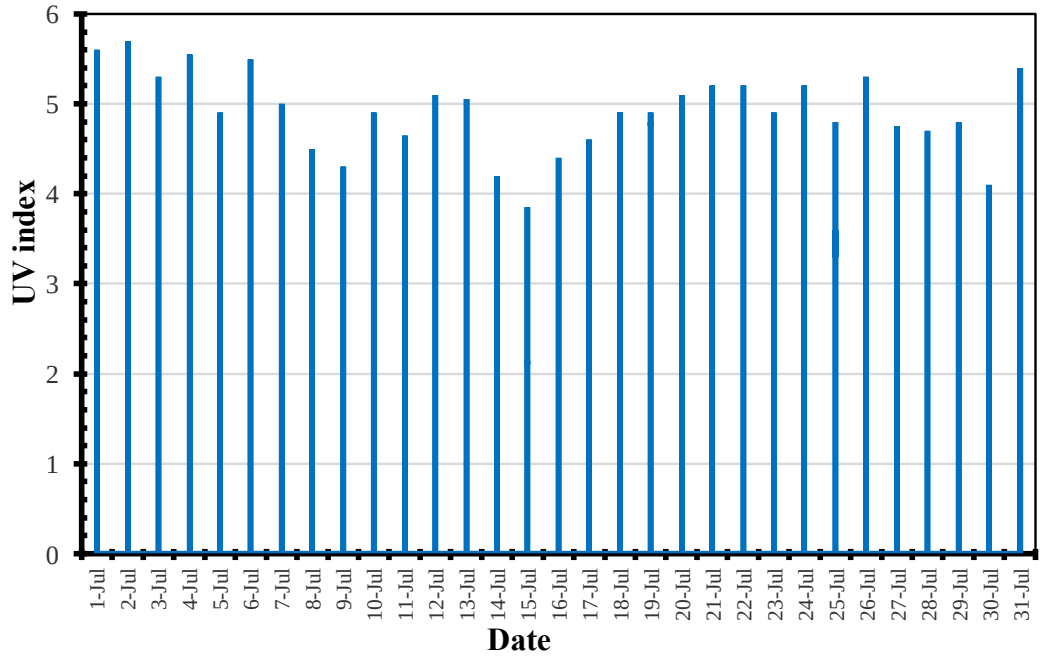

Figure 4.18: UV index during July.

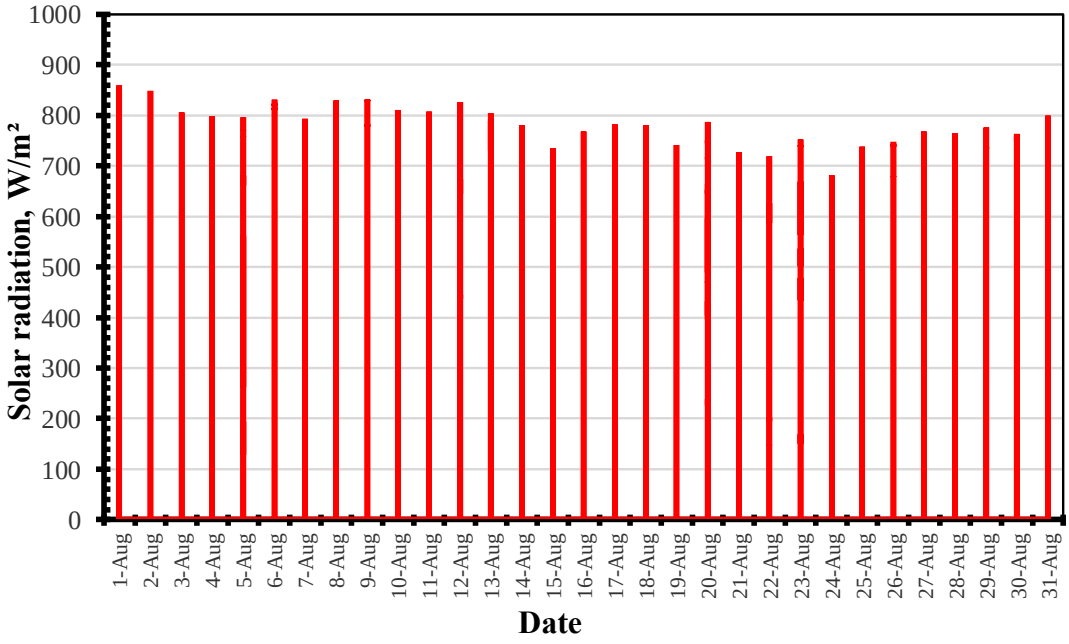

Figure 4.19: Solar radiation during August.

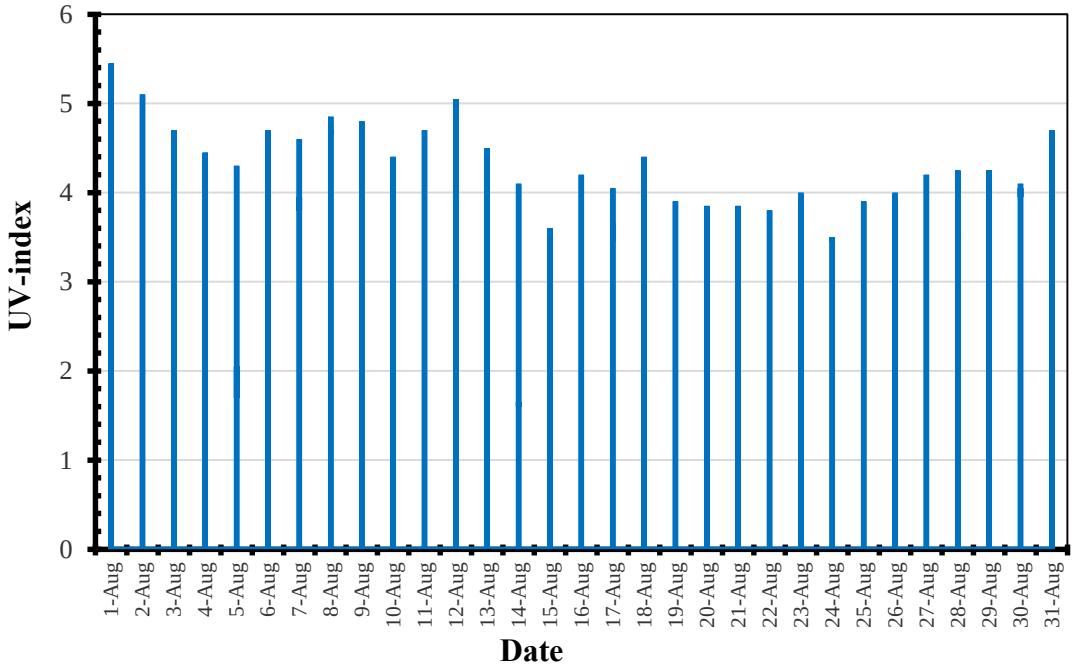

Figure 4.20: UV index during August**.**

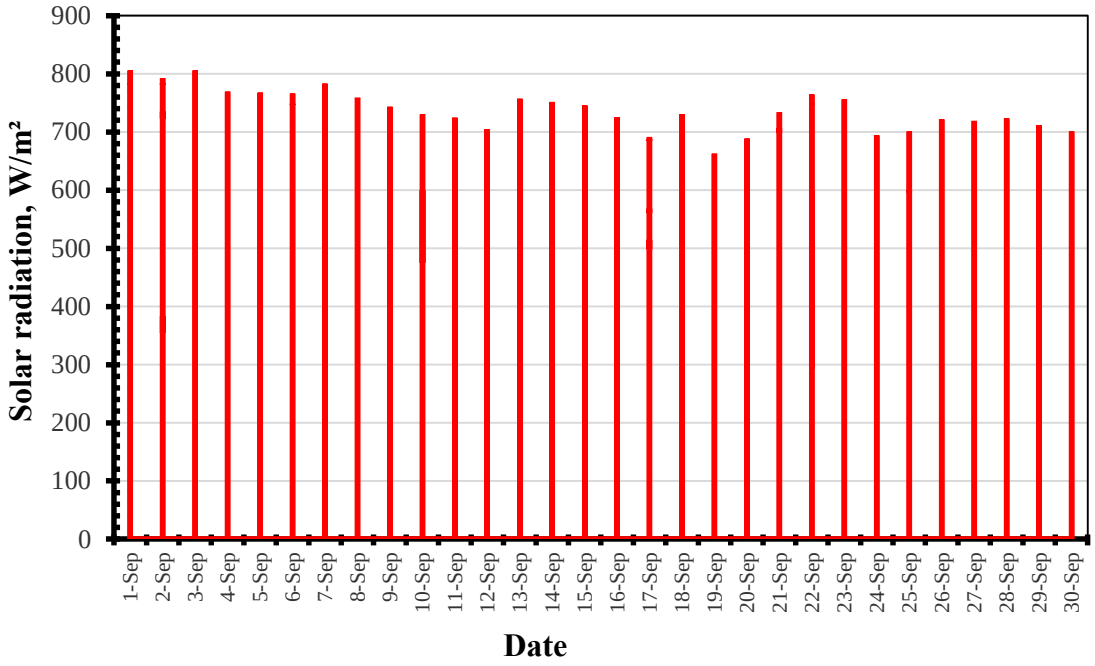

Figure 4.21: Solar radiation during September.

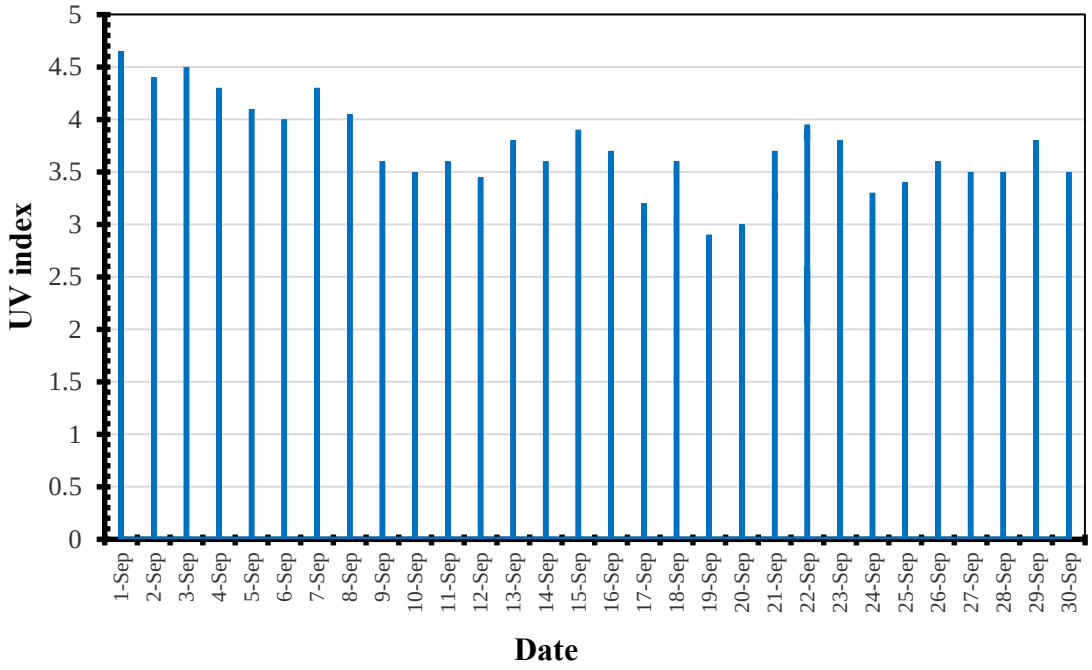

Figure 4.22: UV index during September.

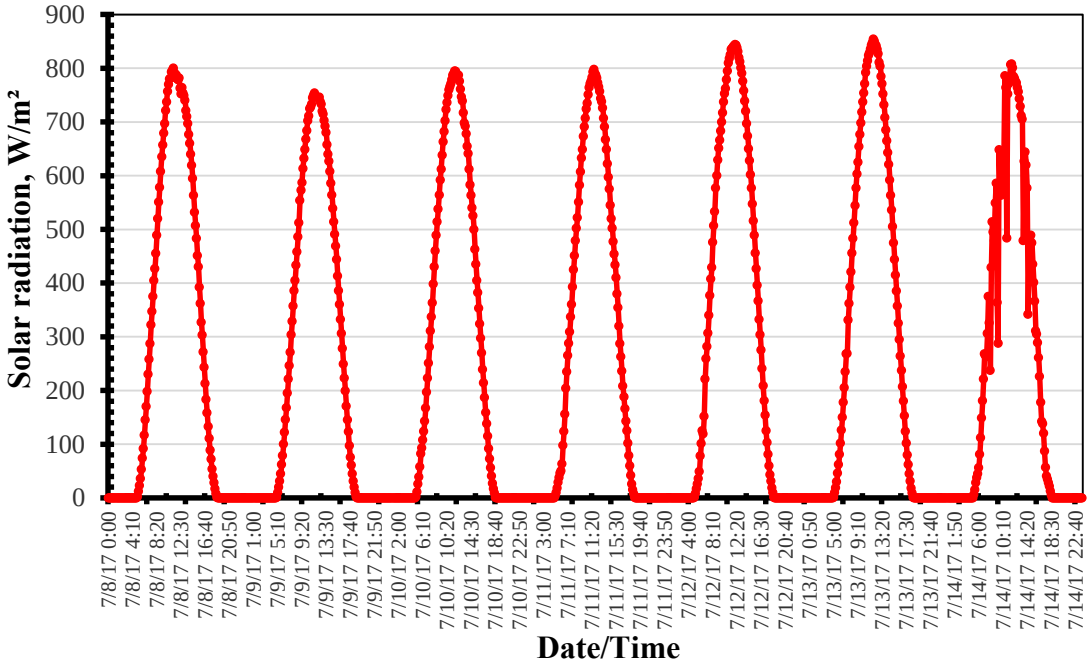

Figure 4.23: Typical solar radiation on a representative week (8 to 14 July).

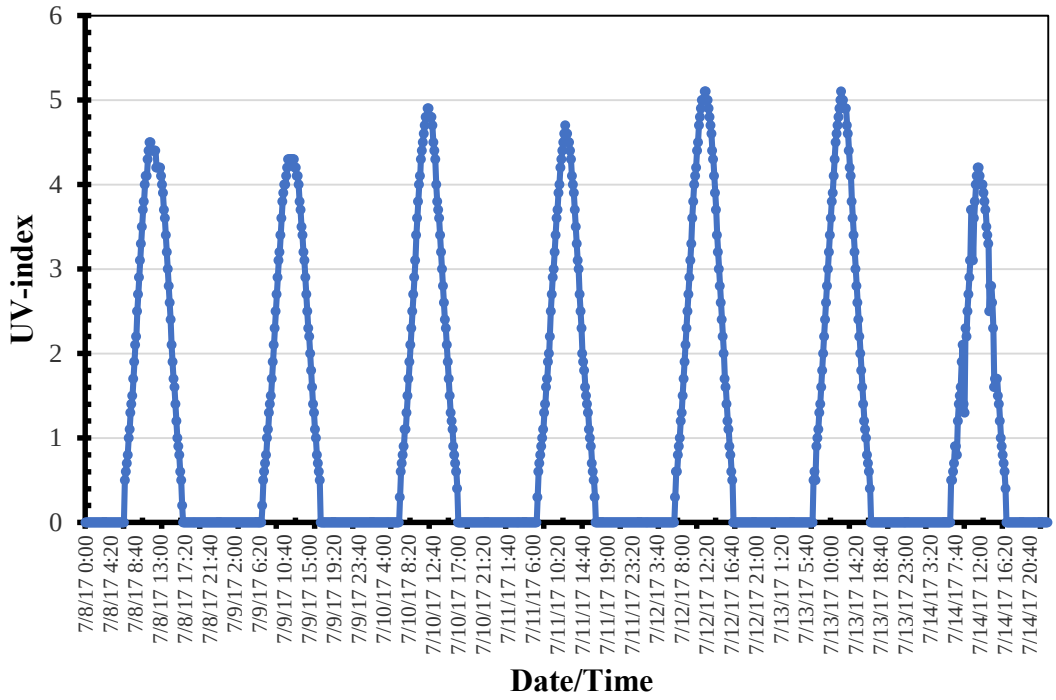

Figure 4.24: Typical UV index on a representative week (8 to 14 July).

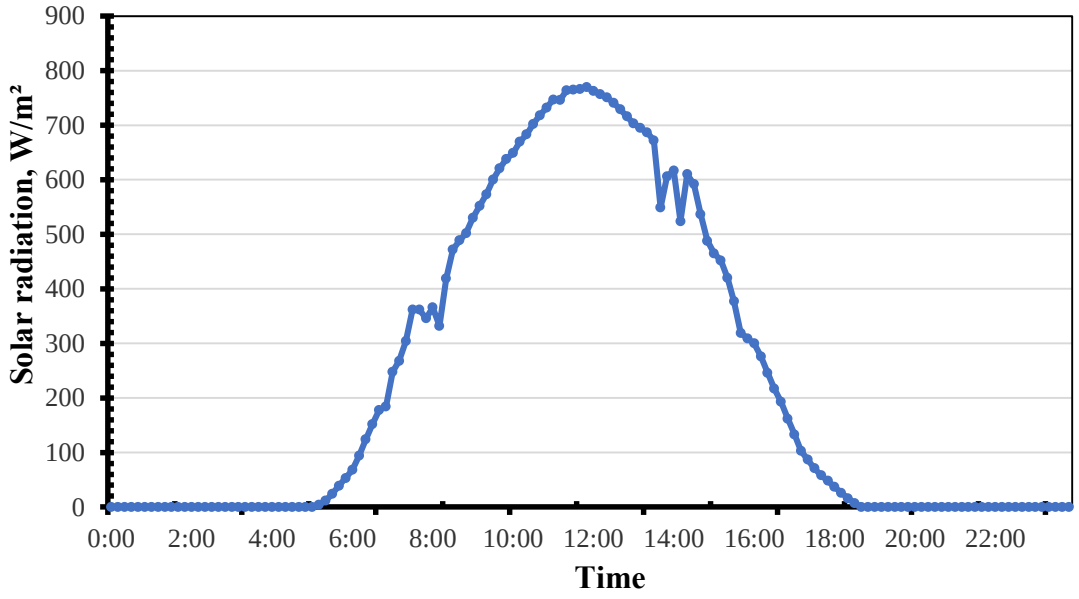

Figure 4.25: Typical solar radiation on a representative day (15th July).

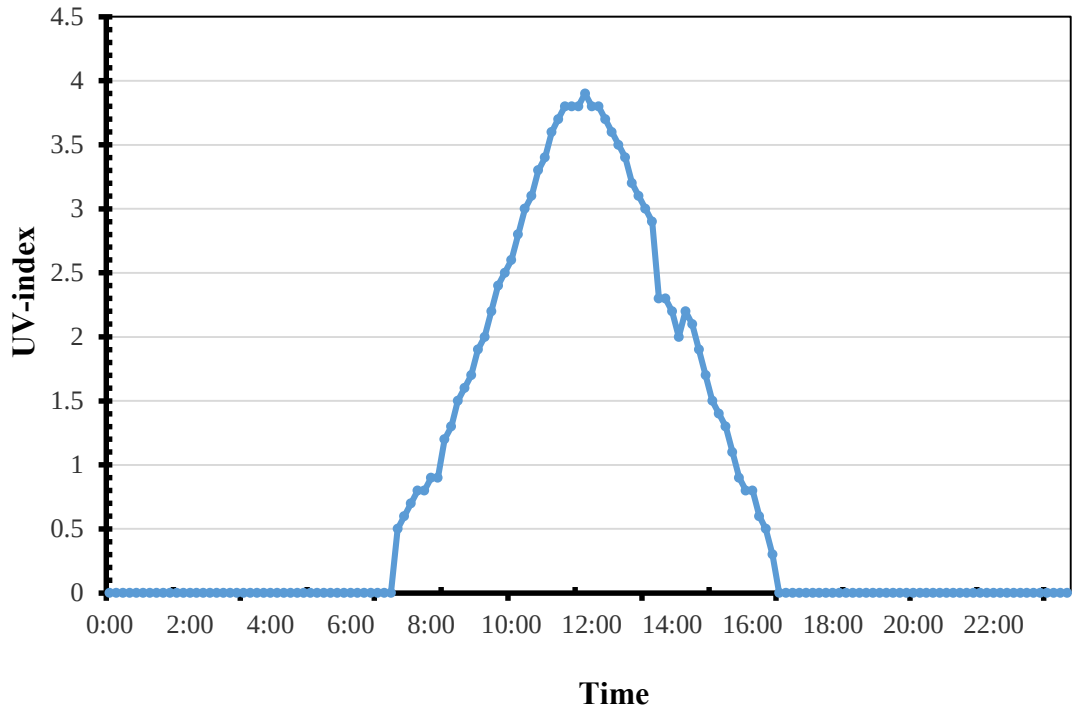

Figure 4.26: Typical solar radiation on a representative day (15th July).

4.3.3 Wind speed

The wind speed during the summer months is demonstrated in Figure 4.27. It can be noticed that the wind speed in July was more than that in August and September. Figure 2.8 depicts the change of wind speed during a representative day; 15th September. The wind speed varies during the day where it was about 3 km/h at midnight and increased to reach 15 km/h between 6:00 pm to 8:00 pm.

The average daily weather station data during the monitoring period is presented in Appendix A.

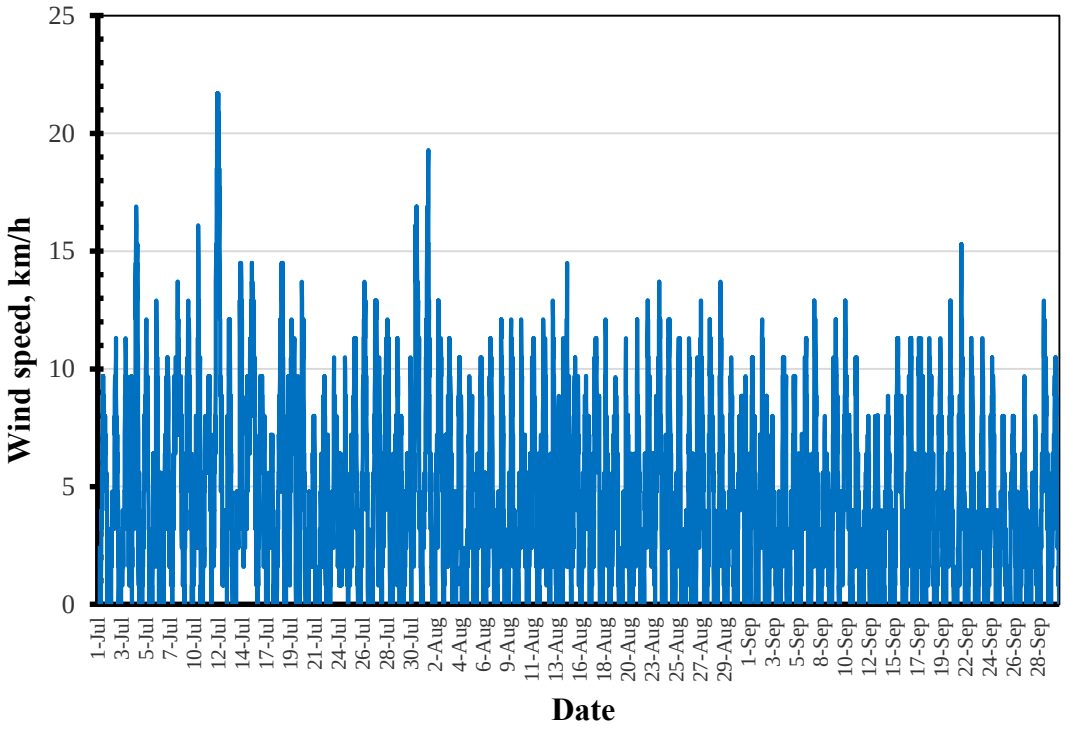

Figure 4.27: Wind speed during the period of the hottest summer months.

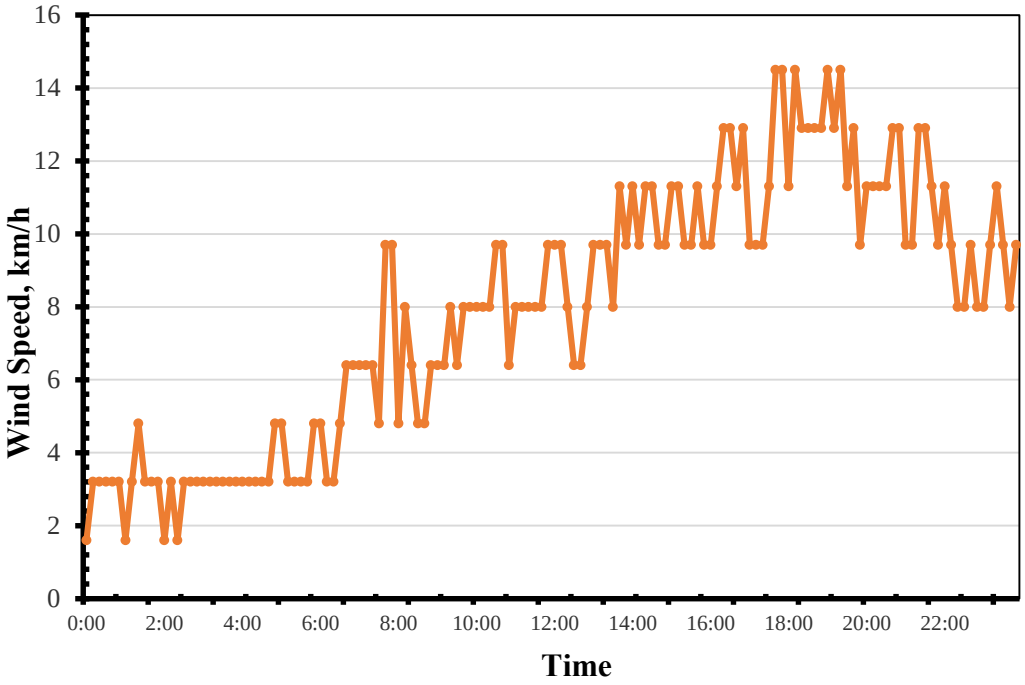

Figure 4.28: Typical wind speed on representative a day; 15th September.

4.4 Inside temperature/humidity of rooms

The temperature and RH inside the test rooms when the air conditioner (A/C) was working all the time during the hottest months of summer are presented in Figures 4.29 and 4.30, respectively. A/C was set with different values of temperature to investigate the energy consumption with different thermal comfort conditions. The A/C was initially set with 24°C all the period except from 22th to 30th July and from 7th to 15th August when the A/C was set with 20°C to investigate the electricity consumption at different temperatures of A/C. In these two figures, the period with 20°C was denoted by A. When the setting temperature of A/C was 24 °C, the inside temperature of TR1, TR2 and TR3 was almost the same as can be noted by the curves of these three test rooms in Figure 4.30. The inside temperature of TR4 was less than the other test rooms by about 1°C. However, during the period of changing the setting temperature of A/C to 20 °C, the inside temperature of TR1 and TR2 was 21°C, while it was 20.5°C in TR3 and 20 °C in TR4. This indicates that TR4, which has full insulation system, was very effective in reducing the inside temperature through decreasing the heat transfer from outside to inside, even when the inside temperature is controlled. The same trend was noted from the weekly inside temperature plot presented in Figure 4.31.

Figures 4.33 and 4.35 show the inside temperature on representative days; 10th July and 10th August; when the setting temperature of A/C was 24°C and 20°C, respectively. The temperature seems to be constant during the whole day in all the test rooms and it was relatively less in TR4 than the remaining test rooms by about 1°C. The inside temperature in TR2 was more than that in the other test rooms by about 1°C during noon

when the temperature of A/C was set at 20°C because the walls of this room were constructed without insulation materials.

With different setting temperature of A/C, the inside RH of TR1, TR3 was almost the same. However, it was less by about 10% when the A/C temperature was 20°C than with 24° C because A/C was working longer with 20°C thereby removing the moisture from the ambient air in the test rooms. The inside RH in TR4 was more than that in TR1 and TR3 by about 10% at all the times because the moisture of the construction materials used in TR4 was higher than those used in TR1 and TR3. The same observation was noted from the weekly inside RH plot demonstrated in Figure 4.32. Figures 4.34 and 4.36 show the inside RH on representative days; 10th July and 10th August; when the temperature of A/C was set at 24°C and 20°C, respectively. The inside RH in TR2 was less than that in the other test rooms. The average daily inside temperature and RH data in the test rooms during the monitoring period are presented in Appendix B.

4.5 Moisture monitoring results

The average moisture on the surfaces of walls in all the four test rooms, which was measured on 7th August, is shown in Table 4.3. The moisture of the surface materials on walls of TR2 and TR3 was 9%, which was much less than that on the walls of TR1 and TR4 which were 25% and 27%, respectively. This is ascribed to the coating on walls of TR1 and TR4 which has moisture content more than that of the primer paint applied on walls of TR2 and TR3. This explains why the inside RH in TR4 was higher than that in TR2 and TR3.

Table 4.3: Average surface moisture of inside walls for all test rooms on 7th August.

Test room	Moisture (%)
TR1	25
TR2	9
TR3	9
TR4	27

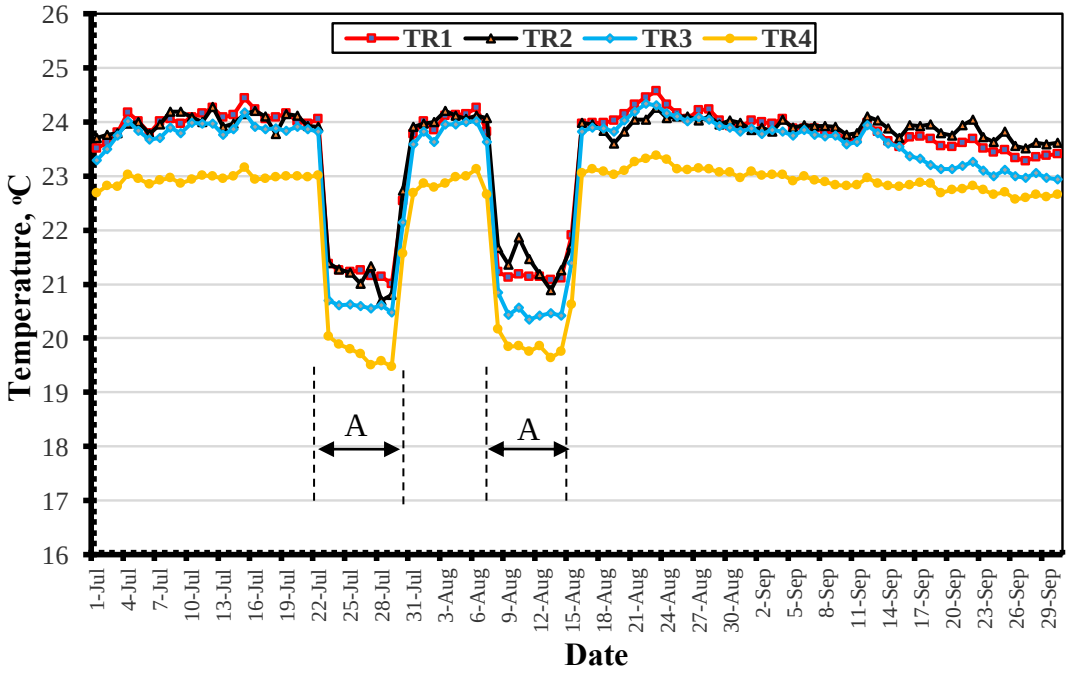

Figure 4.29: Inside temperature during the summer months.

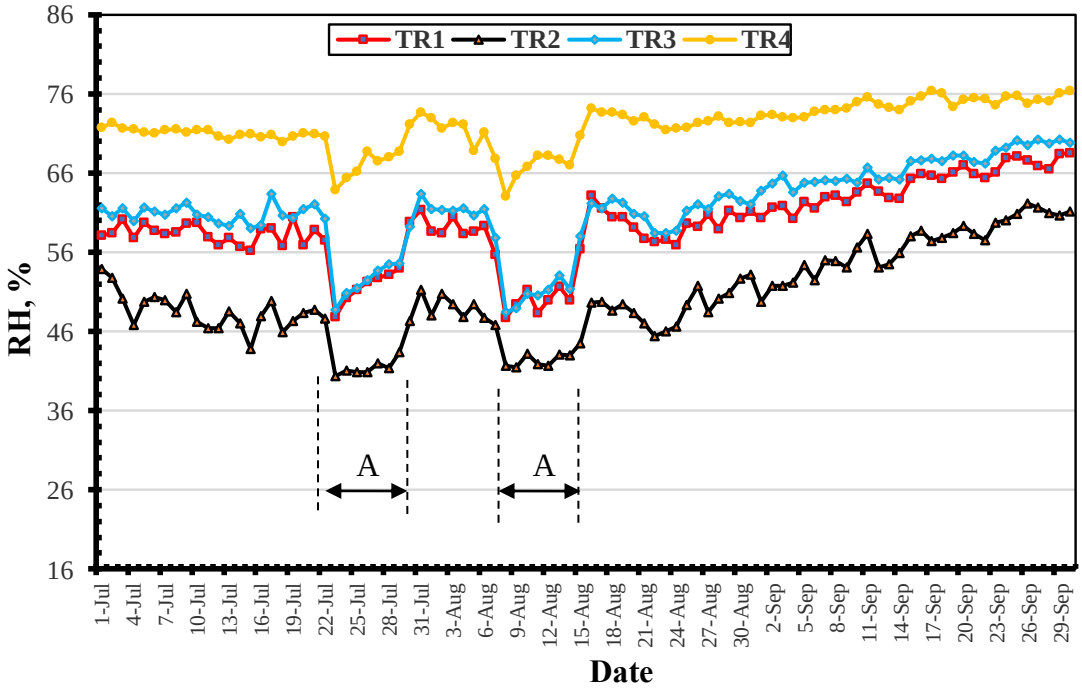

Figure 4.30: Inside RH during the summer months.

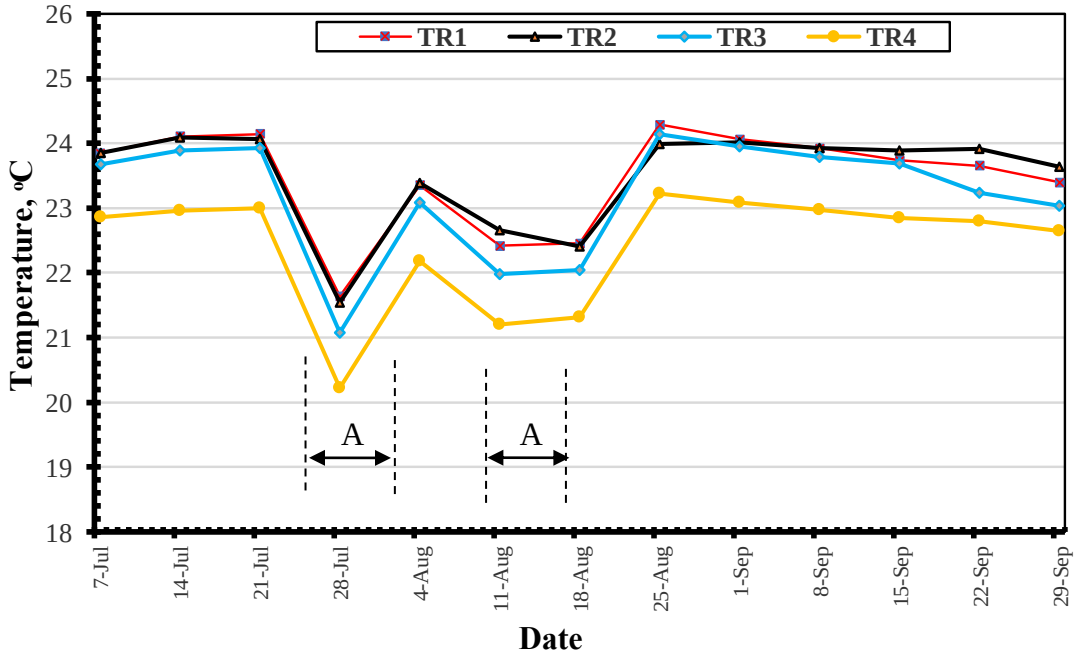

Figure 4.31: Weekly inside temperature.

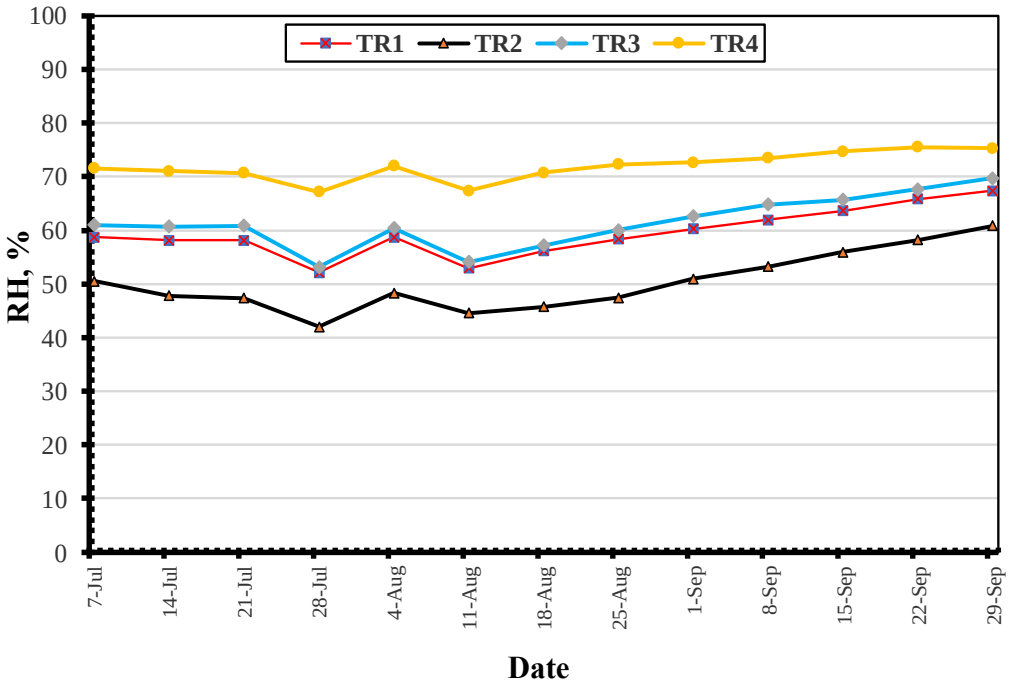

Figure 4.32: Weekly inside RH.

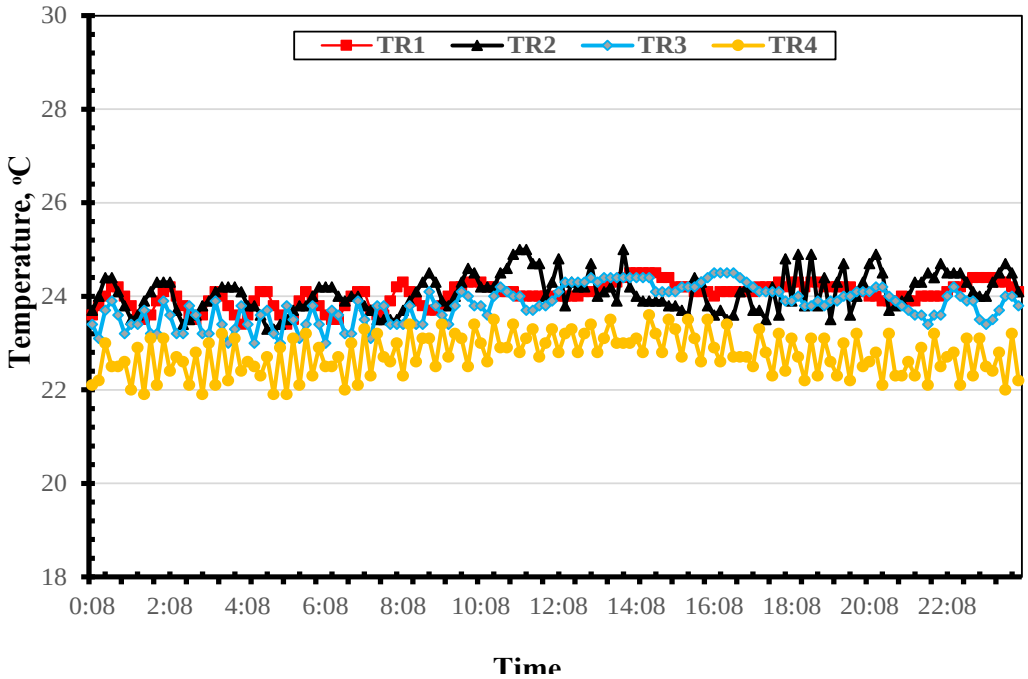

Figure 4.33: Temperature during representative day (10th July); A/C temp.=24°C.

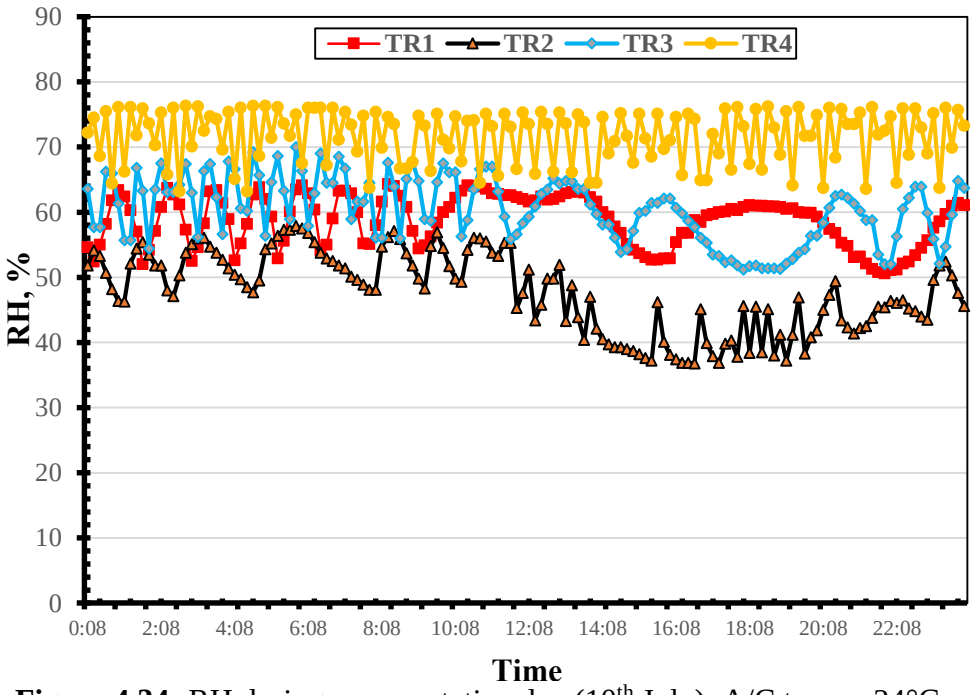

Figure 4.34: RH during representative day (10th July); A/C temp.=24°C.

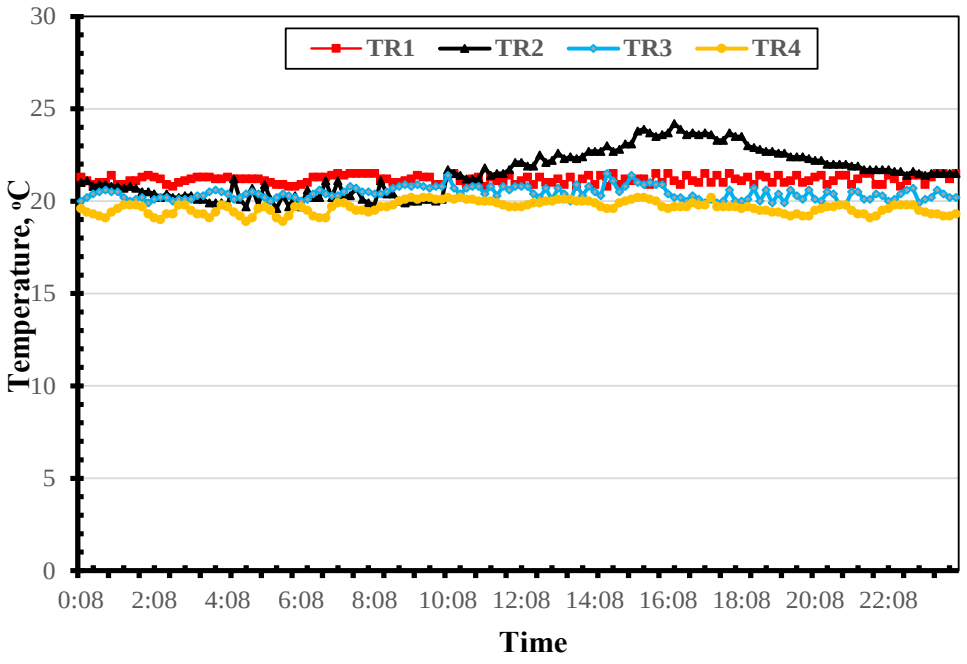

Figure 4.35: Temperature during representative day (10th August); A/C temp.=20°C.

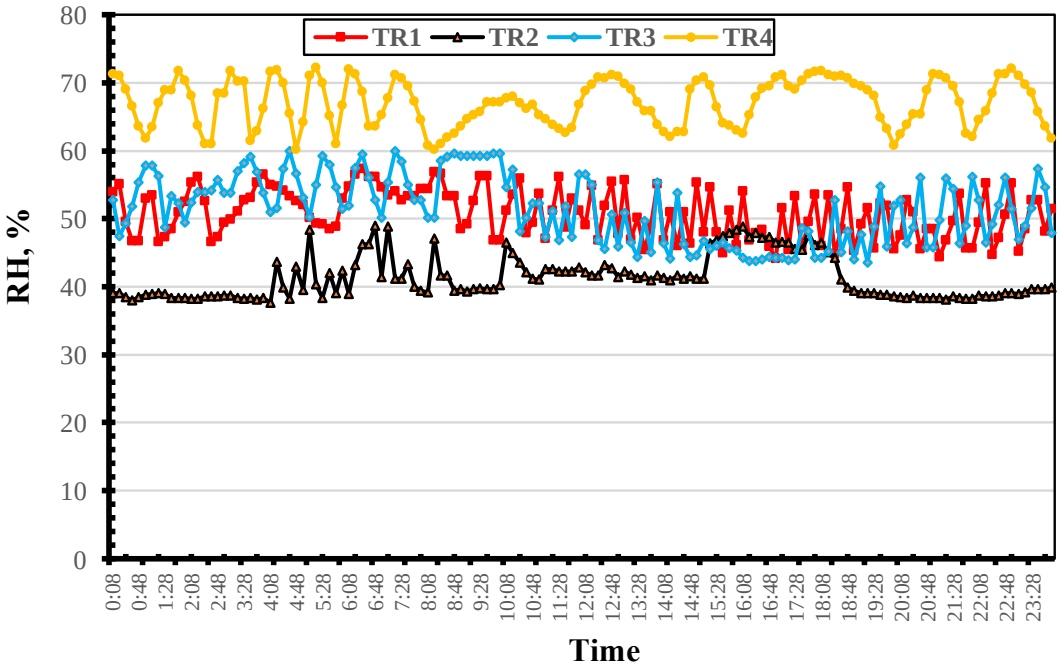

Figure 4.36: RH during representative day (10th August); A/C temp.= 20°C.

4.6 Thermograph assessment results

The thermal images of walls and roof in each test room, which explain the effectiveness of insulation materials in reducing the heat transfer from outside to inside, taken on August 7, 2017 at 12:00 noon when the outside temperature was 45.1°C and solar radiation was 791 W/m² are demonstrated in Figures 4.37 to 4.40. Temperature variation scale on the surface is shown in the left of each thermal image, while the temperature at the middle of the surface is presented in the top right of each thermal image. The decrease of inside surface temperature on walls and roof in TR1, TR3 and TR4 compared with TR2 are summarized in Table 4.4. From the data in this table, it is obvious that the insulation materials used in TR4 was the most effective in decreasing the heat flow followed by those used in TR3 and finally by those used in TR1. In comparison

with TR2, the insulation system used in TR4 decreased the surface temperature on walls by 4.3 to 5.9°C, while concrete blocks incorporating expanded polystyrene board reduced the surface temperature on walls by 2.7 to 3.4°C. The reflective coating applied on TR1 walls decreased the the surface temperature on walls by 1.6 to 1.9°C. However, the low heat convective coefficient of coating in TR1 must be considered because it results in raising the surface temperature of walls in TR1 [22–26]. This effect of heat convective coefficient was not clear in TR4 because most of the heat flow from outside to inside through walls are prevented by the insulate block and insulate plaster. This effect of heat convective coefficient will be elucidated in Section 5.5.

Table 4.4: Decrease of inside surface heat on walls and roof in TR1, TR3 and TR4 as compared with TR2 (August 7, 2017 at 12:00 noon).

Location	TR1	TR3	TR4
East wall	1.9°C	3.0°C	5.9°C
South wall	1.8°C	2.9°C	4.6°C
West wall	1.7°C	3.4°C	4.0°C
North wall	1.6°C	2.7°C	4.3°C
Roof	1.4°C	1.6°C	3.2°C

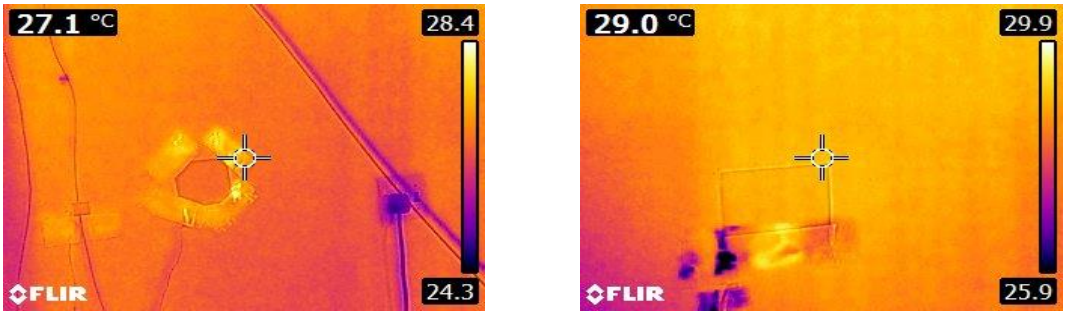

TR1 **TR2**

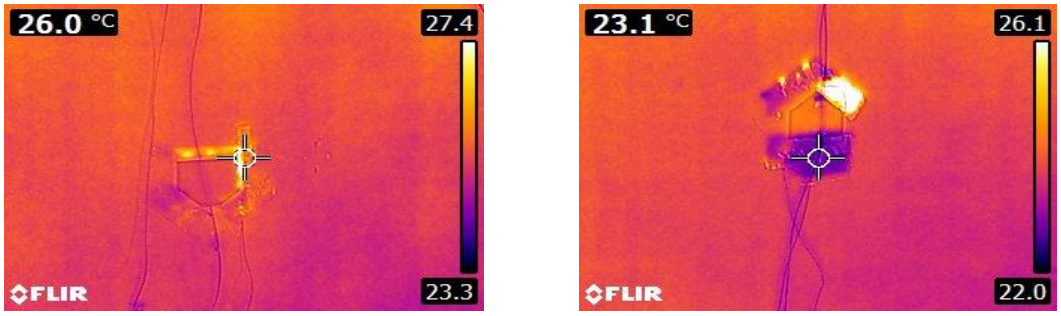

TR3 **TR4**

Figure 4.37: Typical thermal images on East wall.

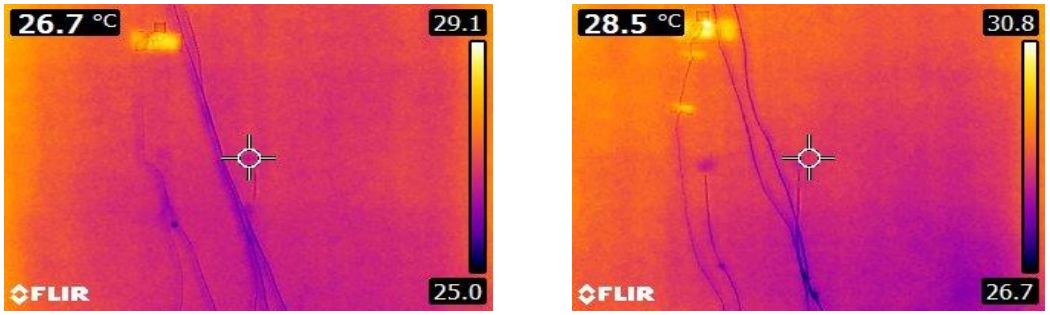

TR1 **TR2**

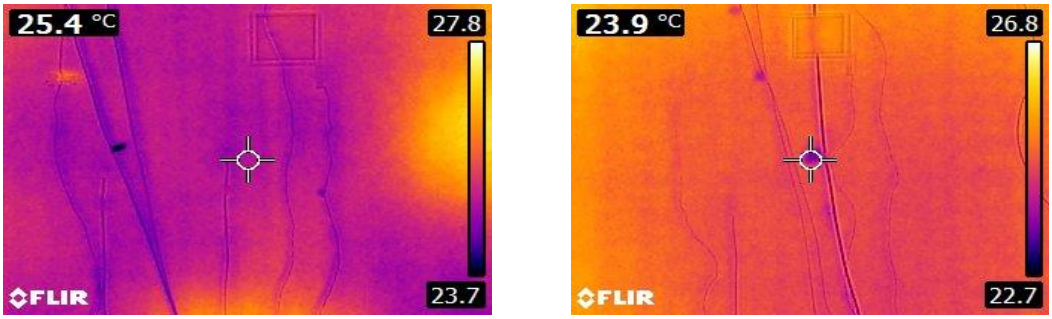

TR3 **TR4**

Figure 4.38: Typical thermal images on South wall.

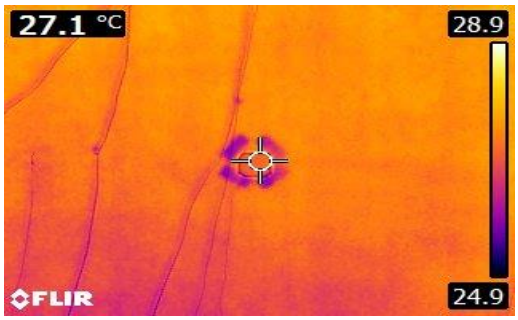

TR1

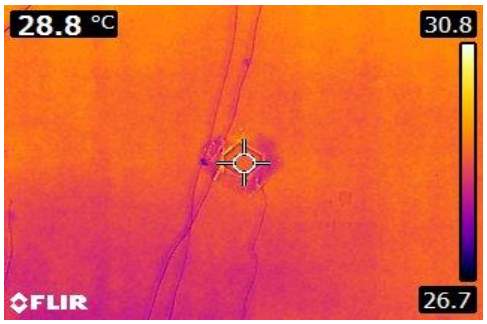

TR2

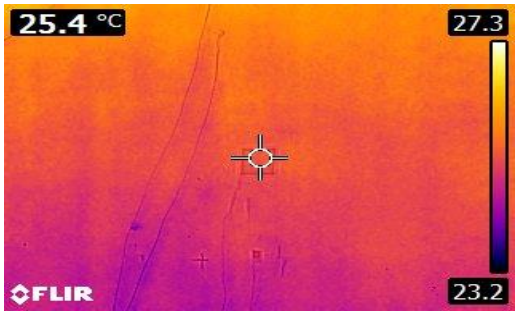

TR3

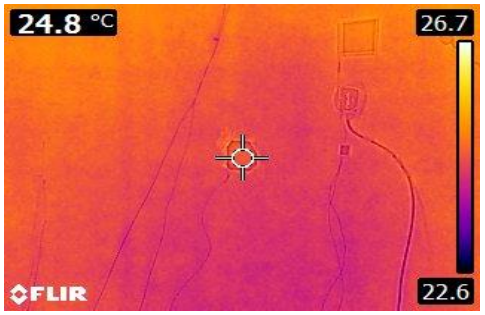

TR4

Figure 4.39: Typical thermal images on West wall.

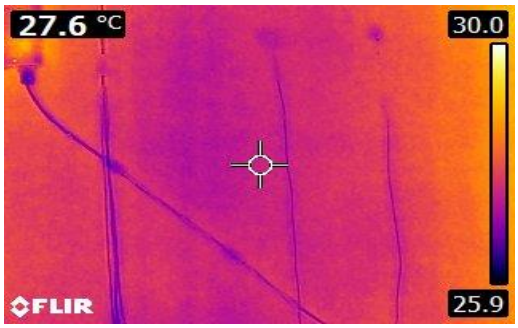

TR1

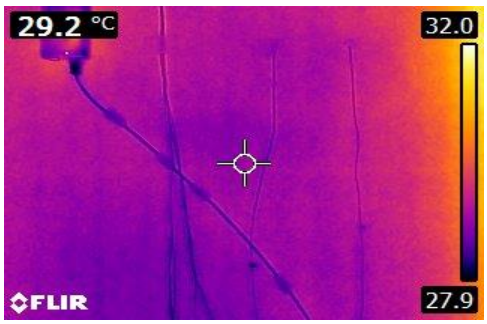

TR2

TR3

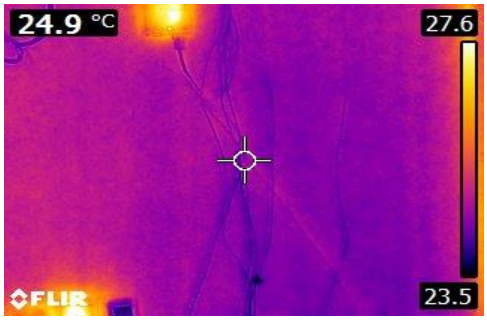

TR4

Figure 4.40: Typical thermal images on North wall.

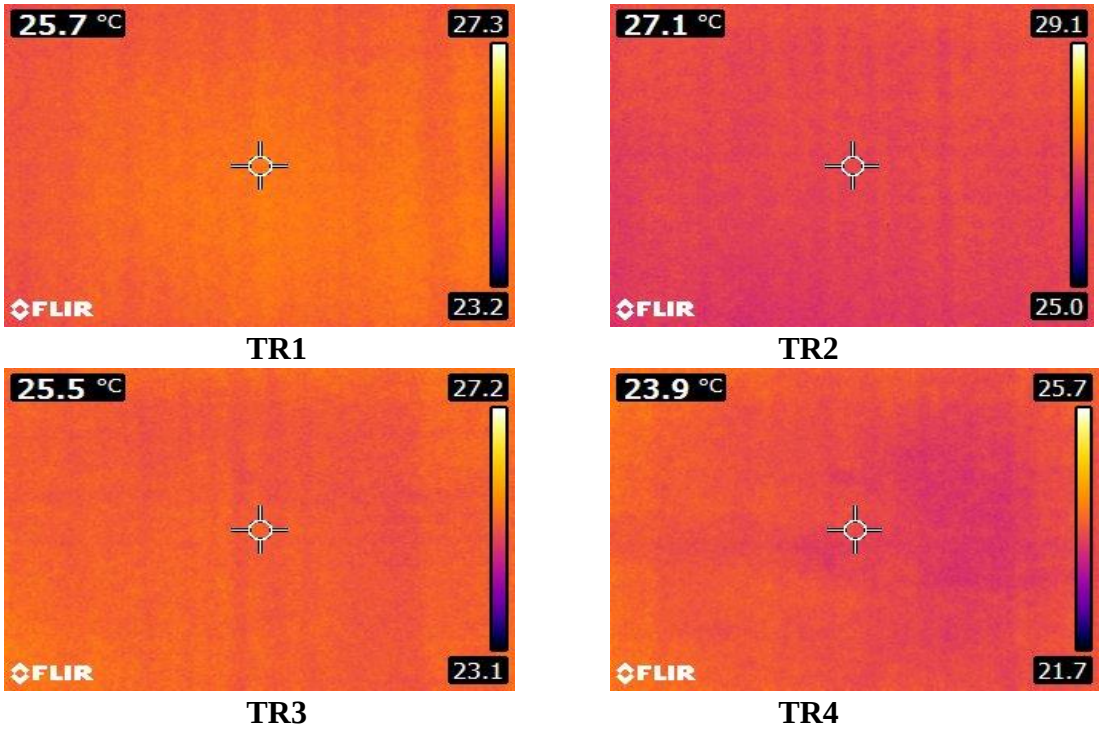

Figure 4.41: Typical thermal images on Roof.

4.7 Temperature on surfaces of walls

The temperature on the surface of East wall, South wall, West wall, North wall and Roof in each test room from inside during the summer monitoring are presented in Figures 4.42 to 4.46; respectively. The results of the temperature were at two different setting temperatures of A/C; 20°C and 24°C. With A/C setting temperature of 24°C, the average surface temperature on TR1, TR2, TR3 and TR4 was 26.5, 28.5, 25.5, 24°C; respectively. The temperature on surface walls and roof from inside in TR2 was, as expected, the highest among all test rooms, while it was the lowest in TR4 because the walls of TR2 did not include any insulation materials, while the walls of TR4 were constructed from full insulation system.

In TR1 and TR3, the temperature on surfaces of the walls and roof from inside for these two test rooms was close to each other. However, it was marginally lower in TR3 than in TR1 due to the low convective coefficient of the coating in TR1 which prohibits the exchange of heat between the surface of walls and the inside air [22–26].

With A/C setting temperature of 20°C, which is indicated in Figures 4.42 to 4.47 by A, the average surface temperature on TR1, TR2, TR3 and TR4 was 24, 26.5, 23, 22°C; respectively. The same indication was noted but the difference between TR1 and TR3 was more. TR4. The data of the inside surface temperature on the walls explained in Figures 4.42 to 4.46 indicate that the insulation materials used in TR4 were the most effective in decreasing the heat flow followed by those used in TR3 and thereafter TR1. However, it must be noted that the low heat convective coefficient of the coating on the walls in TR1 makes the surface temperatures of walls of TR1 marginally higher than the walls of TR3 [22–26].

Figure 4.47 depicts the inside temperature on representative month; July; of West wall with two different setting temperatures of A/C; 20 and 24°C. It is obvious that the lowest surface temperature of West wall was in TR4, while the highest was in TR2. With a setting temperature of 24◦C, the difference between the surface temperature of West wall in TR1 and TR3 was small. However, it was higher with the lower setting temperature of A/C; 20°C. This indicates that low heat convective coefficient of coating on walls of TR1 keeps the surface temperature high with the low temperature of A/C, as will explained in Section 5.5.

The surface temperate of the roof from inside on representative month; September; is shown in Figure 4.48. The temperature was almost similar in TR1 and TR3, while the difference in this temperature between TR2 and TR4 was 3°C. The surface temperature of walls and roof from inside in TR4 seems to be constant during the day and night and during the whole period with each setting temperature of A/C and this means that the insulation materials used in this room kept the temperature constant all the times. The above observations could be verified from the plots for a representative week of surface temperature on walls and roof, as shown in Figures 4.49 and 4.50. Further, the high percentage of RH inside TR4 due to high moisture content of the materials used to construct the walls of this room led to keep the inside surface temperature on the walls and roof low and constant. Figure 4.51 demonstrates the change in the surface temperature of west wall during a representative day; 1st August. As expected, the temperature during the day was more than that during the night and this is clear in TR2, which is without any insulation materials when the solar radiation on walls and convection between air and outside surface are high.

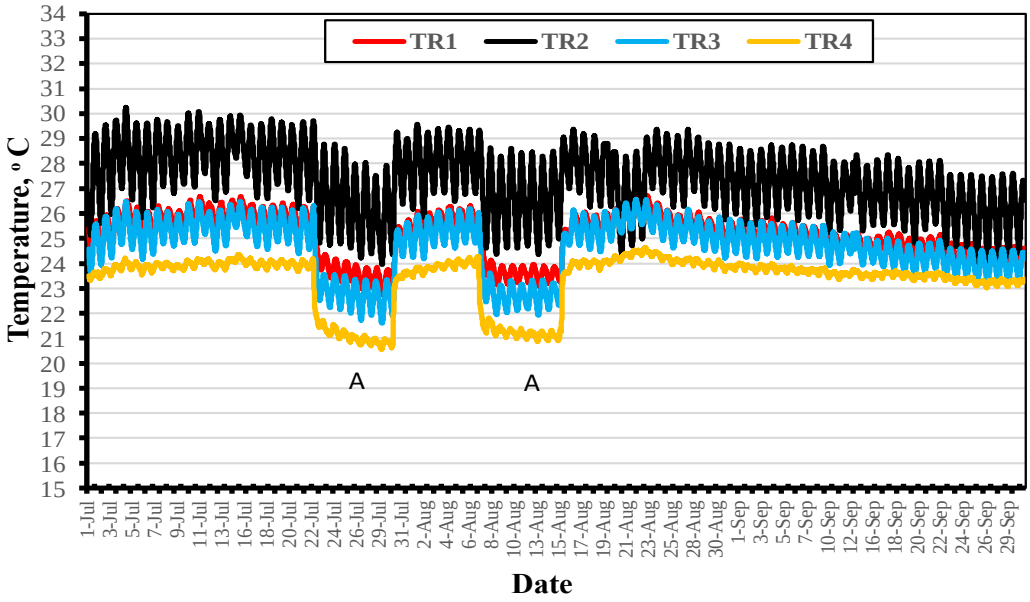

Figure 4.42: Inside surface temperature of East wall.

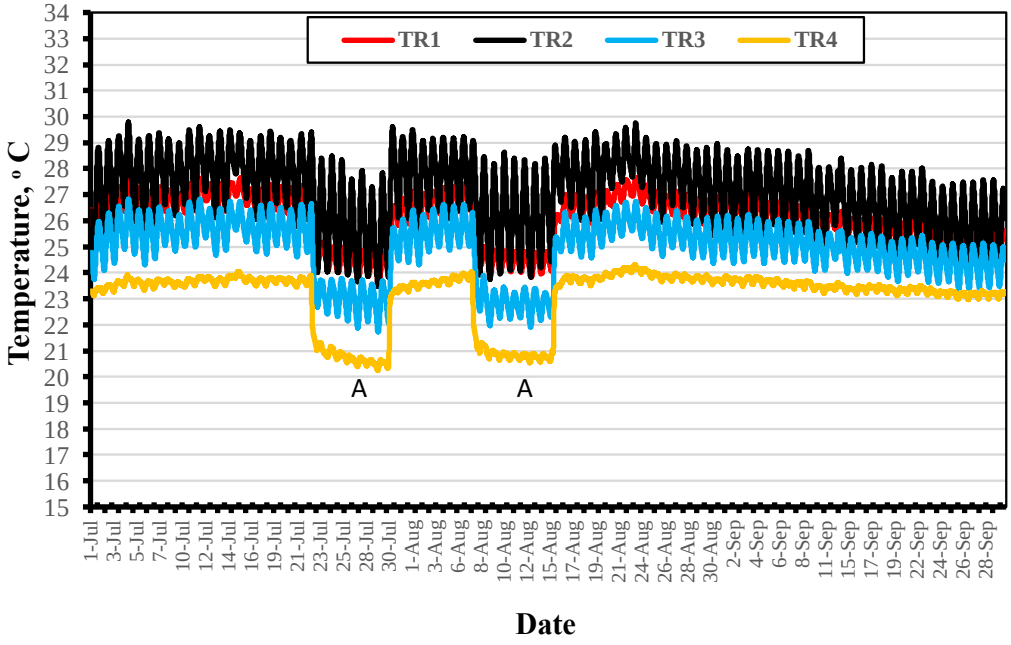

Figure 4.43: Inside surface temperature of South wall.

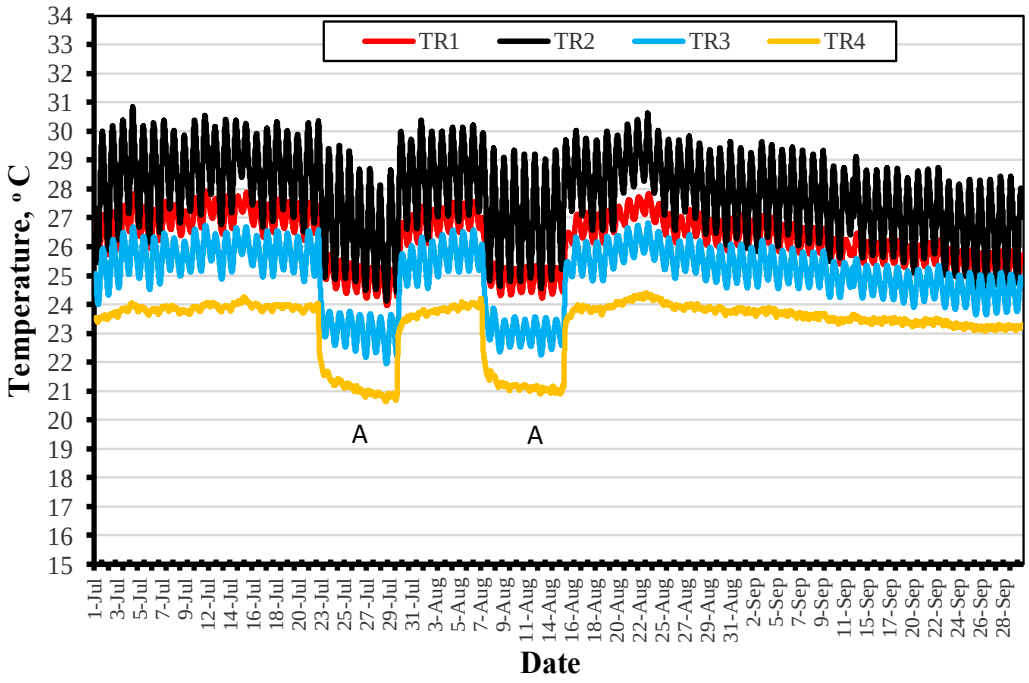

Figure 4.44: Inside surface temperature of West wall.

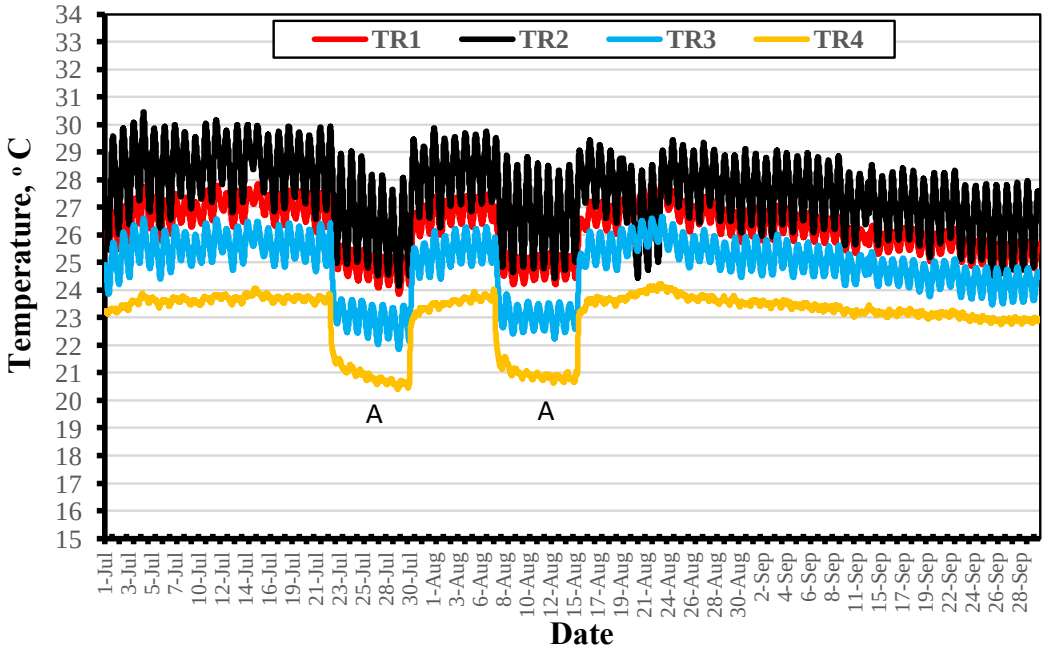

Figure 4.45: Inside surface temperature of North wall.

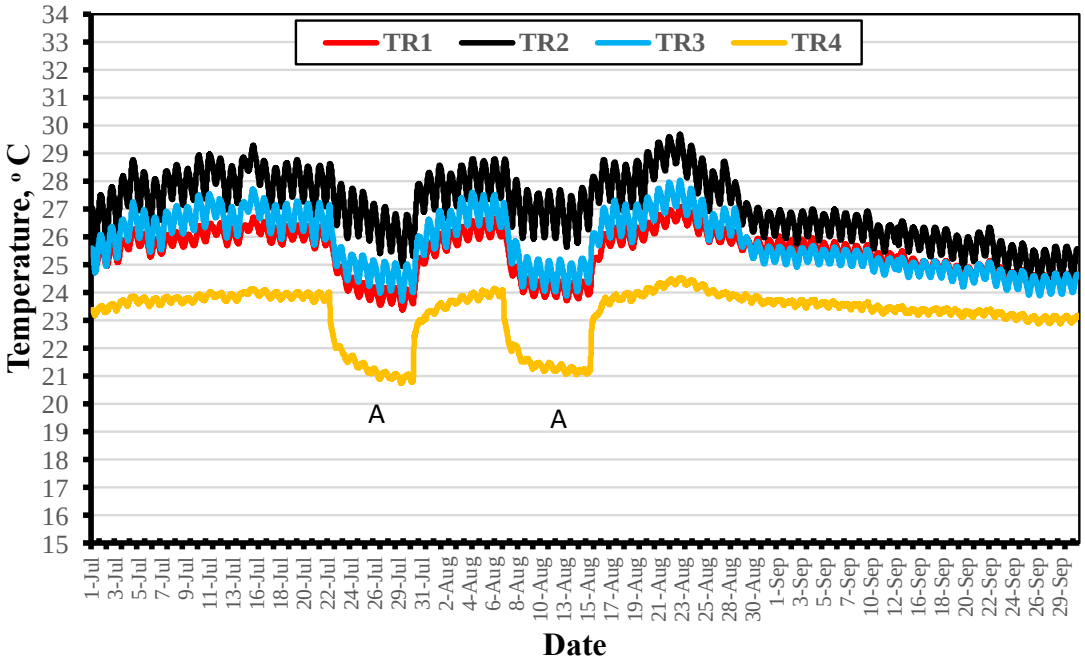

Figure 4.46: Inside surface temperature of roof.

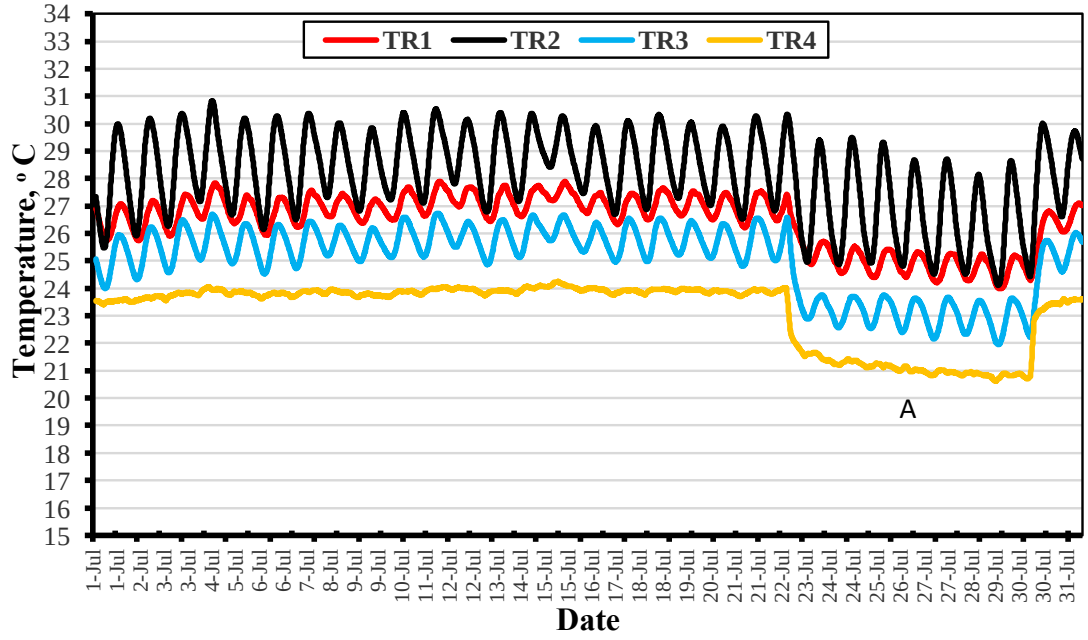

Figure 4.47: Inside surface temperature of roof during July.

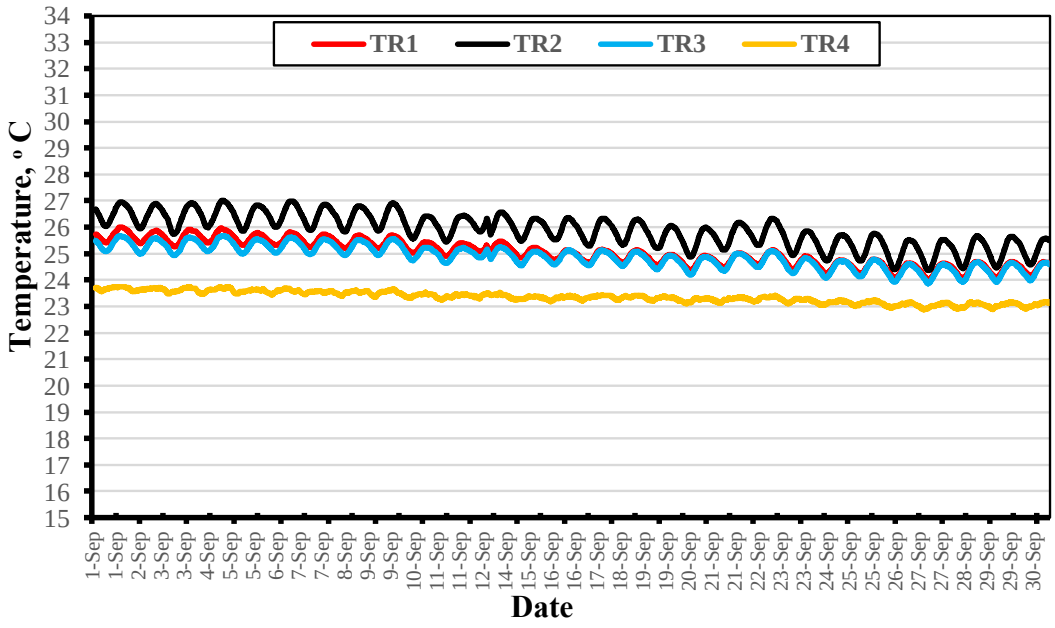

Figure 4.48: Inside surface temperature of roof during September.

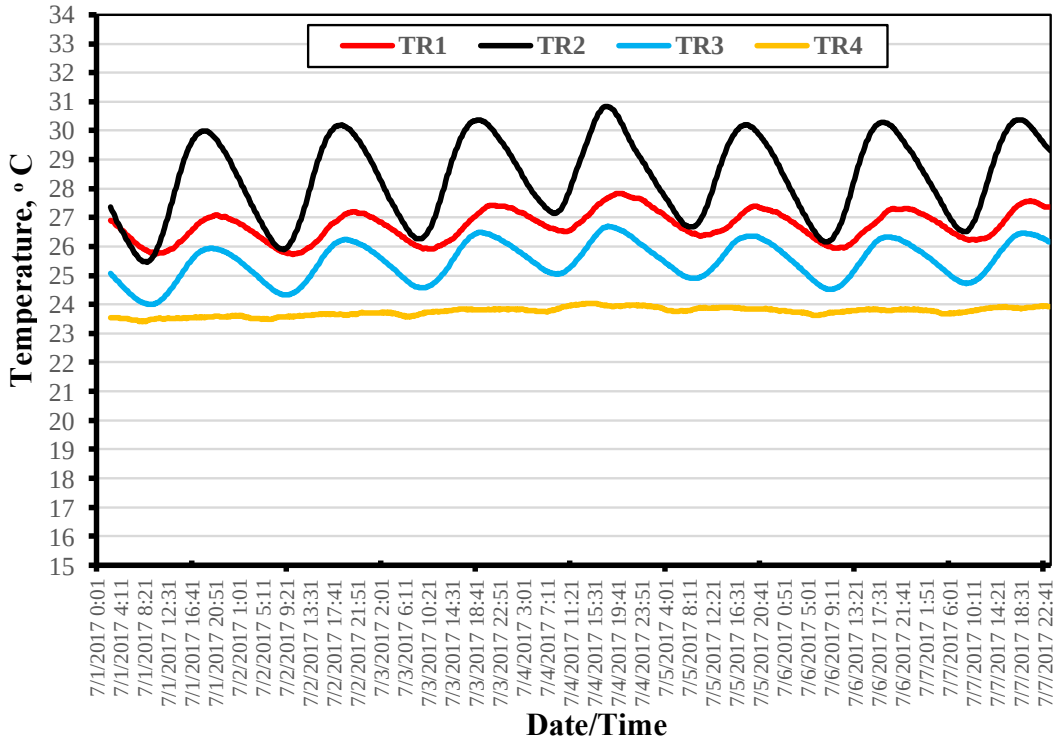

Figure 4.49: Typical inside surface temperature on representative week (1 to 7 July) of West wall.

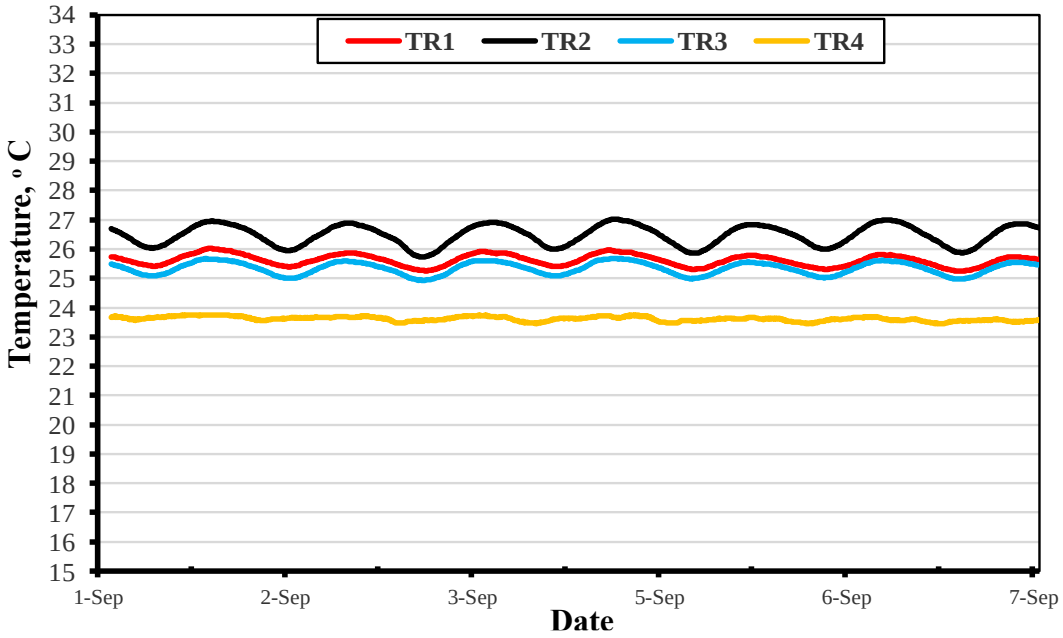

Figure 4.50: Typical inside surface temperature on a representative week (1 to 7 September) of roof.

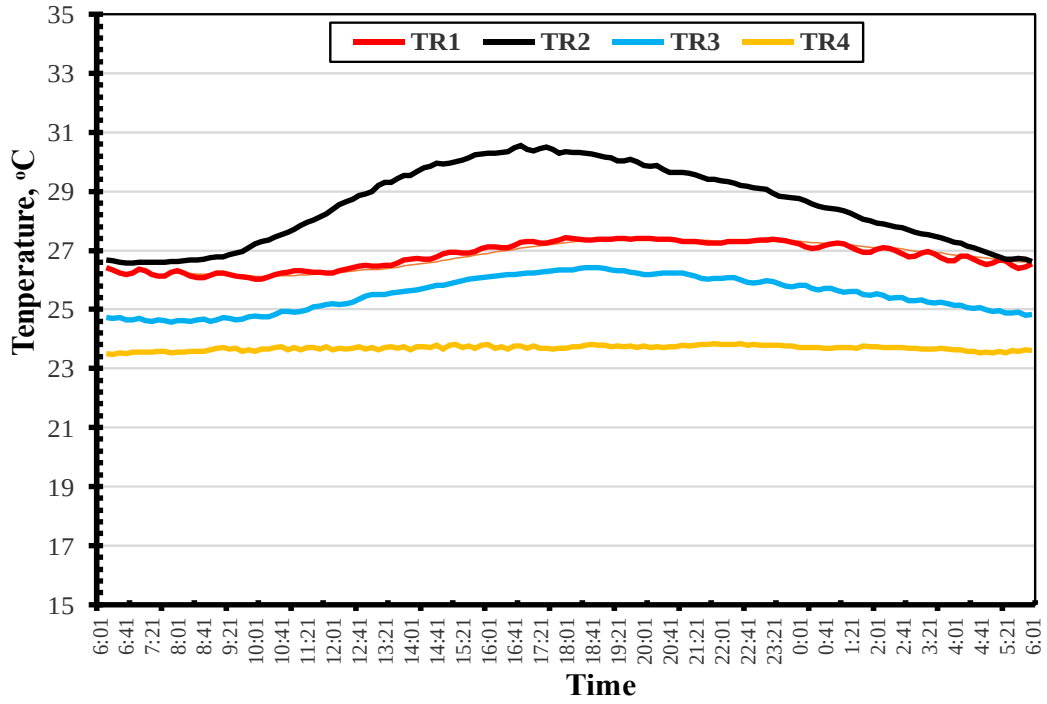

Figure 4.51: Typical inside surface temperature on a representative day; 1st August; of West wall.

4.8 Heat flux (heat flow) results

The heat flow through any material is a major parameter to express the thermal resistance of that material [79]. The data of heat flow through East and West walls during the selected summer periods, which was measured using FleuxTeq sensors with their special data loggers, are demonstrated in Figures 4.52 to 4.55. The heat flow through East and West walls of the Reference Room (TR2), which was without any insulation materials, was highly comparable with the other test rooms that are with different insulation materials. The heat flow though East and West walls in TR2 on August during the day was between 30 and 50 W/m² and it was between 20 and 35 W/m² on September. This reduction in heat flow on September was due to the low prevailing outside air temperature.

The insulation system used in TR4 was the most effective procedure to decelerate the heat flow and this effectiveness is clear from the heat flow data where the heat flow through East and West walls in this test room was the lowest among all the test rooms and it was almost less than 15 W/m² in all the walls and periods. The heat flow through East and West wall in TR1 and TR3, as explained in Figures 4.52 to 4.45, seems to be similar with a marginal preference for TR3 where the heat flow through East and West walls in TR3 was always less than that in TR1 at all periods. The heat flow through the walls in TR1 on August was between 10 and 25 W/m² and it was between 5 and 15 W/m² on September. However, through the walls in TR3 on August, it was between 5 and 20 W/m² and it was between 3 and 15 W/m² on September.

According to the heat flow results (Figures 4.52 to 4.55), the insulation system used in TR4 was the most effective to decrease heat transfer from outside environment followed by that used in TR3 and TR1. The details of surface temperature and heat flux of the walls in the test rooms during the monitoring period are presented in Appendix C.

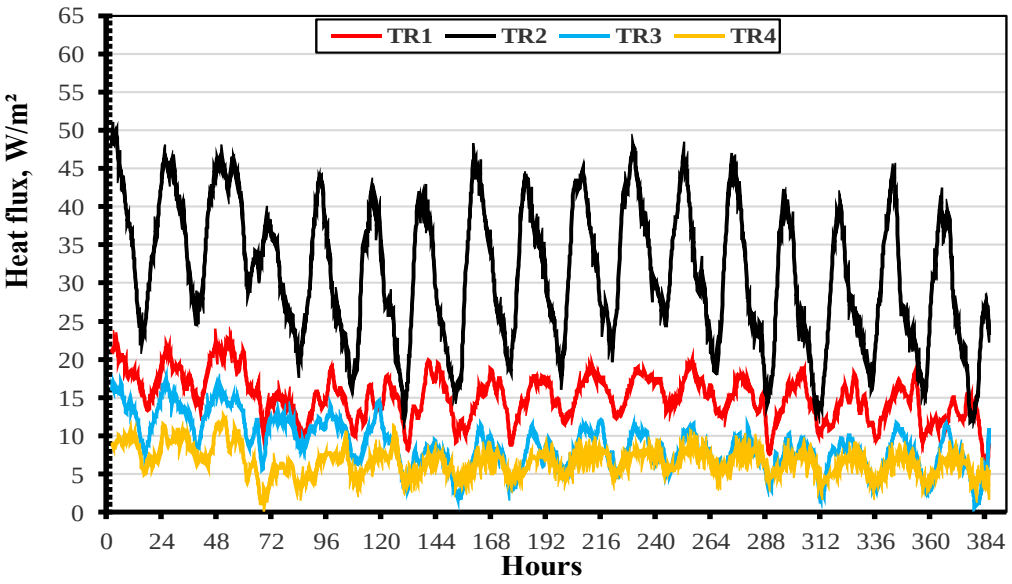

Figure 4.52: Heat flux during August, 12 to 28 of East wall.

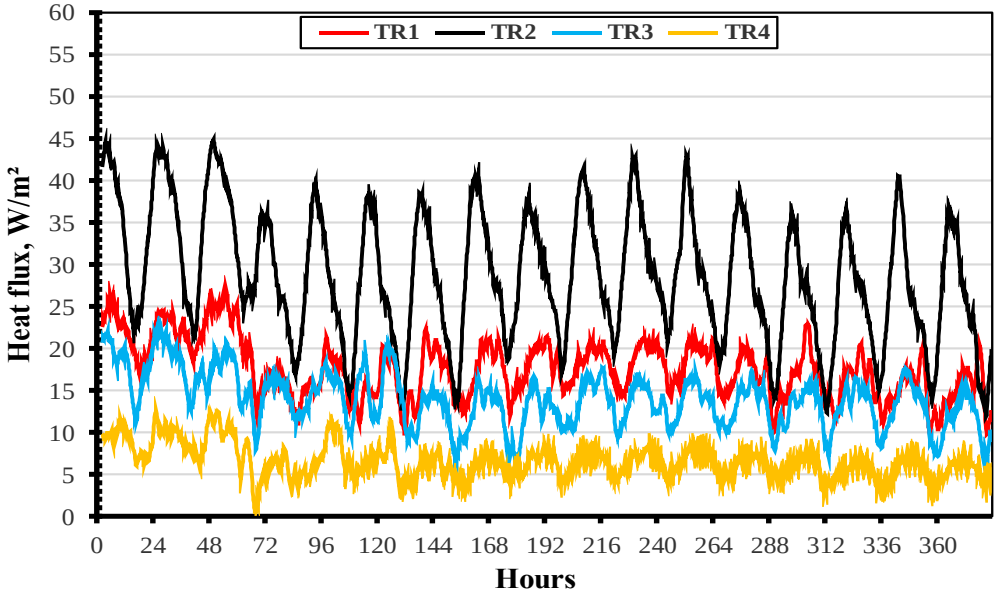

Figure 4.53: Heat flux during August, 12 to 28 of West wall.

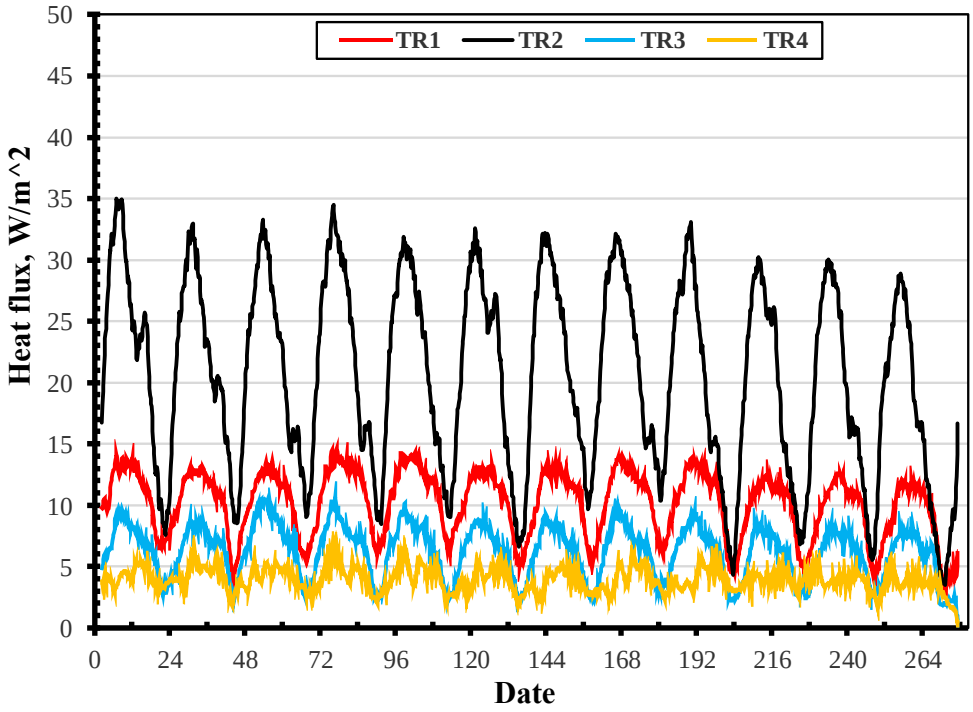

Figure 4.54: Heat flux during September, 14 to 26 of East wall.

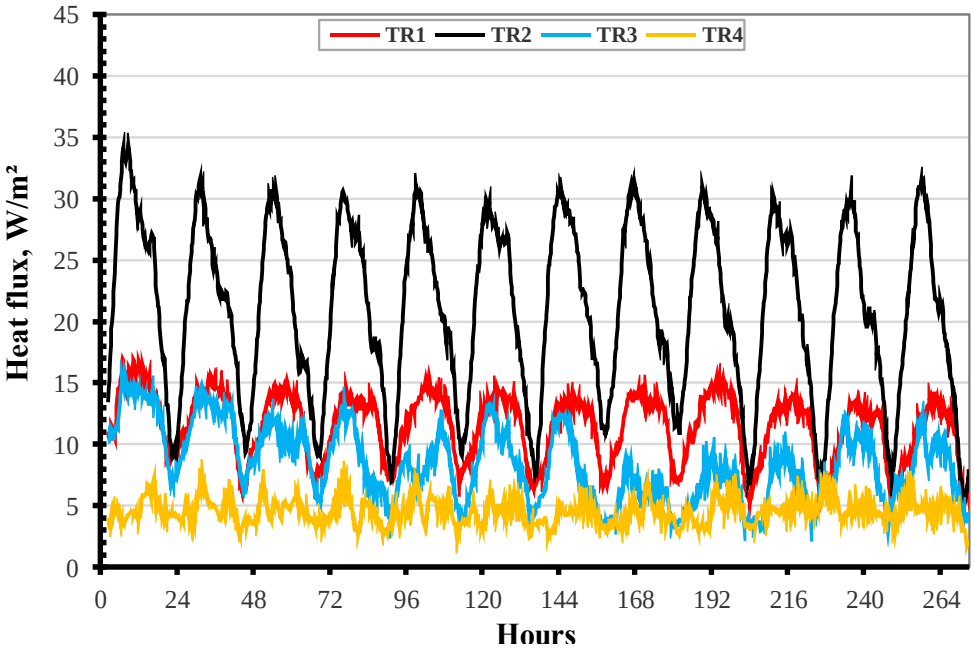

Figure 4.55: Heat flux during September, 14 to 26 of West all.

4.9 Calculations of thermal parameters

According to ASTM C1155-95 [86] and ISO 9869-1 [87], the thermal resistance, thermal conductance and thermal transmission could be calculated using the average method/summation technique and experimental measurement data as follows:

4.9.1 Thermal resistance (R-value)

The thermal resistance (surface to surface) of walls with and without insulation materials was calculated using the following equation [86,87]:

$$R = \frac{\sum_{j=1}^{m} \left(T_{soj} - T_{sij}\right)}{\sum_{j=1}^{m} q_j} \qquad 4.1$$

where:

R = Thermal resistance (surface to surface) (m^2.K/w).

q = Heat flux (W/m^2).

T_{soj} = Outside surface temperature of wall (K).

T_{sij} = Inside surface temperature of wall (K).

Figures 4.56 to 4.63 show the outside and inside surface temperatures of East and West walls during the selected period on August, while Figures 4.64 to 4.71 show the outside and inside surface temperatures of East and West walls during selected period on September in TR1, TR2, TR3 and TR4; respectively. The data from these figures were used to find the summation of the difference between the outside and inside surface temperatures of the walls and the summation of heat flux was calculated using the data in Figures 4.52 to 4.55. After that, the thermal resistance of walls was determined using

Equation 4.1 above and by taking the average of all periods. Finally, the thermal resistance results were drawn as presented in Figure 4.72.

The thermal resistance of TR4 walls was very high; 2.04 m².K/W; as compared with the thermal resistance of TR2 walls; 0.34 m².K/W. The thermal resistance of hollow concrete blocks walls in TR2 was almost similar to that of the hollow reinforced precast concrete walls which was 0.35 m².K/W [88]. The thermal resistance of TR4 walls was the highest between all the test rooms. The thermal resistance of TR3 walls was 1.15 m².K/W, while the thermal resistance of TR1 walls was 0.87 m².K/W. This indicates that the insulation system used in TR4 has the highest resistance for heat transfer through the walls followed by that is used in TR3 and TR1.

4.9.2 Thermal conductance (C-value)

The thermal conductance of walls with and without insulation materials was calculated using the following equation [86,87]:

$$C = \frac{\sum_{j=1}^{m} q_j}{\sum_{j=1}^{m} \left(T_{soj} - T_{sij}\right)} = \frac{1}{R} \qquad 4.2$$

where:

C = Thermal conductance [W/(m².K)].

The thermal conductance is just the inverse of the thermal resistance, as shown in Figure 4.73. Less thermal resistance means high thermal conductance. Walls of TR2 had the highest conductance for heat with rate of 2.93 W/m².K. The reflective coating on TR1 walls reduced this conductance to 1.15 W/(m².K), while TR3 walls with expanded

polystyrene boards had conductance of 0.87 W/m².K. The walls of TR4 were the lowest conductor for heat 0.49 W/(m².K).

4.9.3 Thermal transmittance (U-value)

The thermal transmittance (air to air) of walls with and without insulation materials was calculated using the following equation [86,87]:

$$U = \frac{\sum_{j=1}^{m} q_j}{\sum_{j=1}^{m} \left(T_{oj} - T_{ij}\right)} \quad 4.3$$

where:

U = Thermal transmittance (air to air) [W/(m².K)].

q = Heat flux (W/m²).

T_{oj} = Outside air temperature (K).

T_{ij} = Inside air temperature (K).

Figures 4.74 and 4.75 show the inside air temperature and outside air temperature of each test room during the selected periods on August and September, while Figures 4.76 and 4.77 present the difference between the inside and outside air temperatures in each test room for the same periods. The difference between the inside and outside air temperatures was not very big between all the test rooms because the inside temperature was controlled by A/C.

The data from these figures was used to find the summation of the difference between the outside and inside air in each test room and the summation of heat flux was determined using data in Figures 4.52 to 4.55. After that, the thermal transmittance of

walls was determined using Equation 4.3 and taking the average of all periods. Finally, the thermal transmittance results were drawn, as shown in Figure 4.78. The thermal transmittance of walls in TR1, TR2, TR3 and TR4 was 0.88, 2.03, 0.70 and 0.38 W/(m². K); respectively. Thermal transmittance of hollow concrete blocks walls in TR2 was close to that of hollow reinforced precast concrete walls which was 1.81 m².K/W [88]. The thermal transmittance was very high through the walls of TR2 which don't have insulation materials, whereas it was very low through the walls of TR4. The thermal transmittance through walls of TR1 and TR3 was about half and third; respectively; of that through walls of TR2. This indicates that insulation materials were effective to decrease heat transfer through the walls.

4.9.4 Total thermal resistance

The total thermal resistance (air to air) of walls with and without insulation materials was calculated using the following relation [86,87]:

$$R_T = \frac{1}{U} \qquad 4.4$$

where:

R_T = Total thermal resistance (air to air) (m². K/W).

The total thermal resistance is the ability of the insulation materials used in the walls to decrease the inside air temperature by reducing heat transfer through the wall and it can be found as the inverse of the thermal transmittance, as demonstrated in Equation 4.4. Figure 4.79 depicts the total thermal resistance of walls in each test. The thermal resistance of walls in TR1, TR2, TR3 and TR4 was 1.14, 0.49, 1.42 and 2.62 m².K/W;

respectively. The effectiveness of the insulation materials used in wall was in the following arrangement: TR4 followed by TR3 and finally TR1.

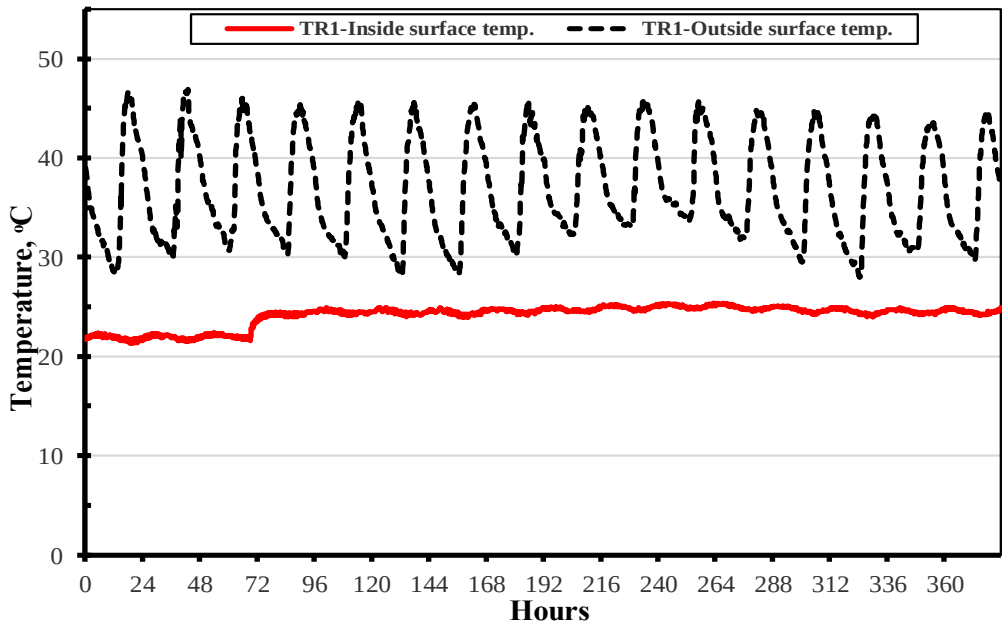

Figure 4.56: Inside and outside surface temperature; at August; of East wall in TR1.

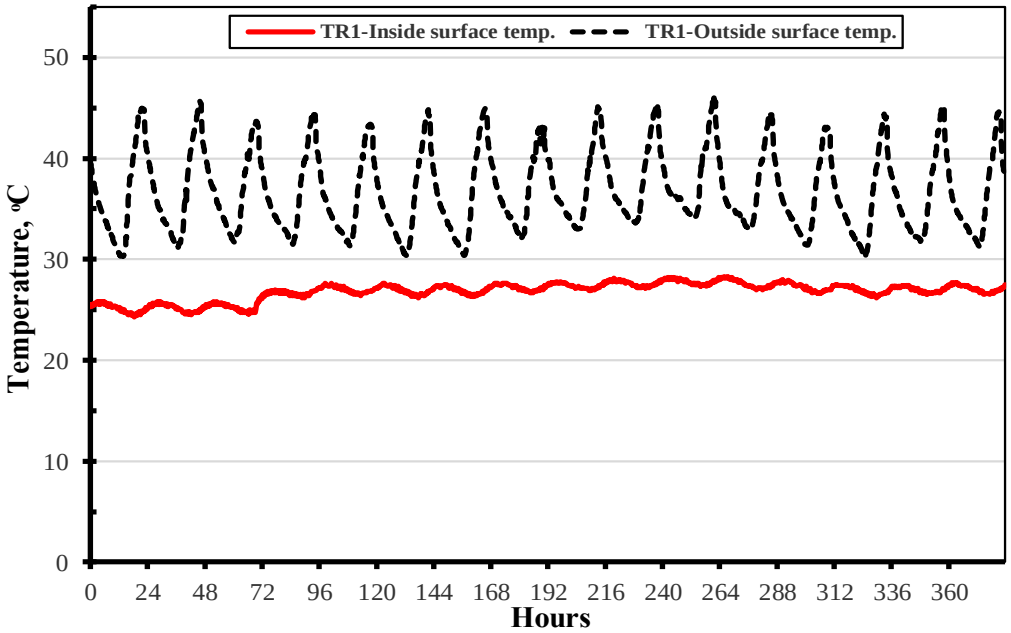

Figure 4.57: Inside and outside surface temperature; at August; of West wall in TR1.

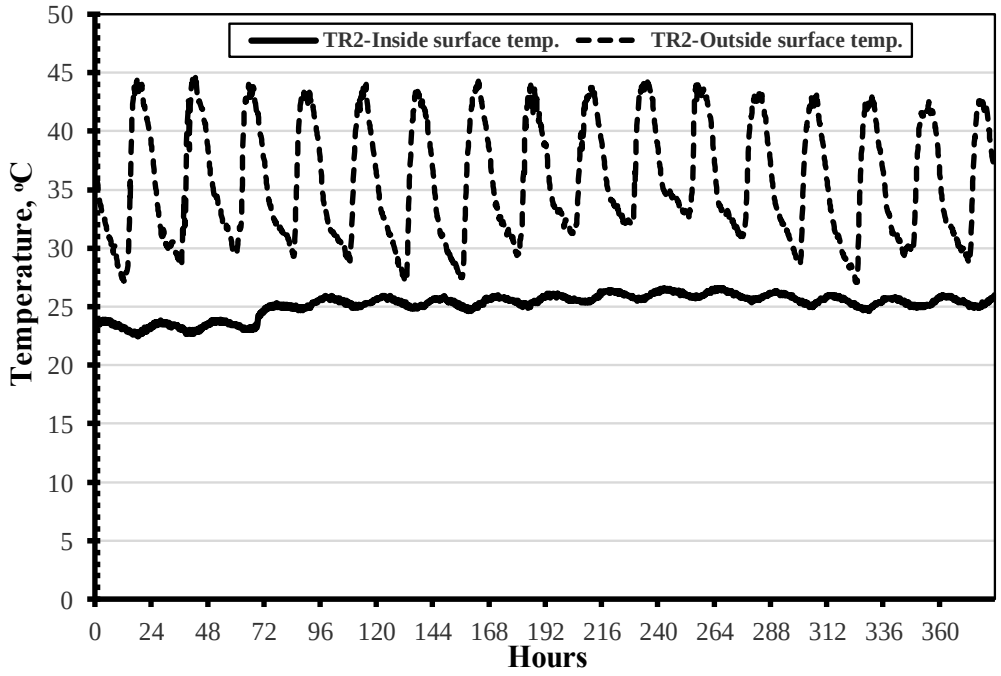

Figure 4.58: Inside and outside surface temperature; at August; of East wall in TR2.

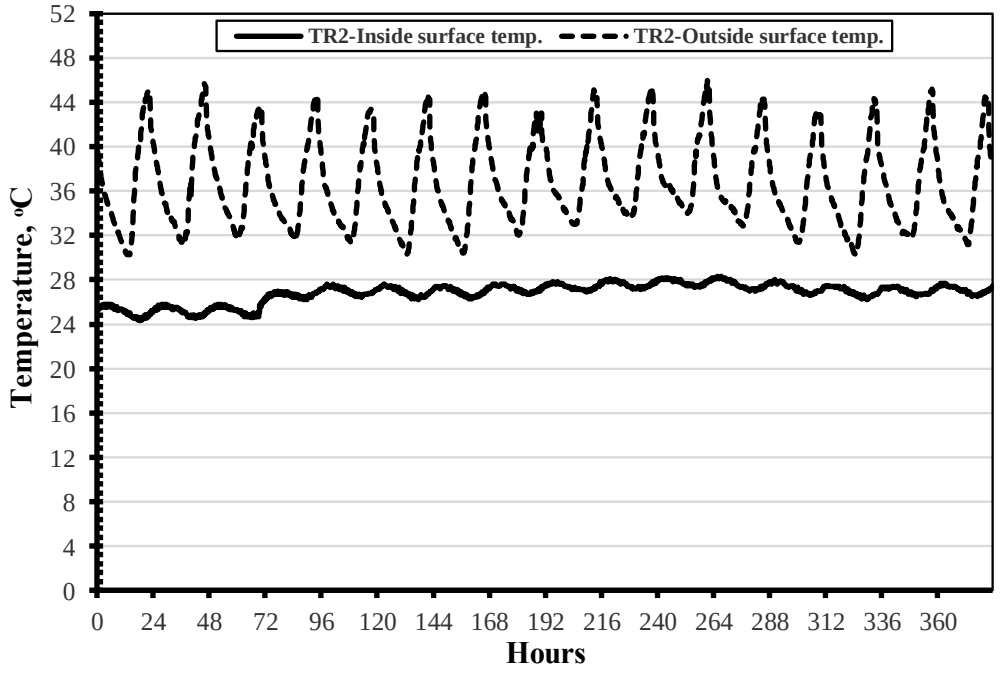

Figure 4.59: Inside and outside surface temperature; at August; of West wall in TR2.

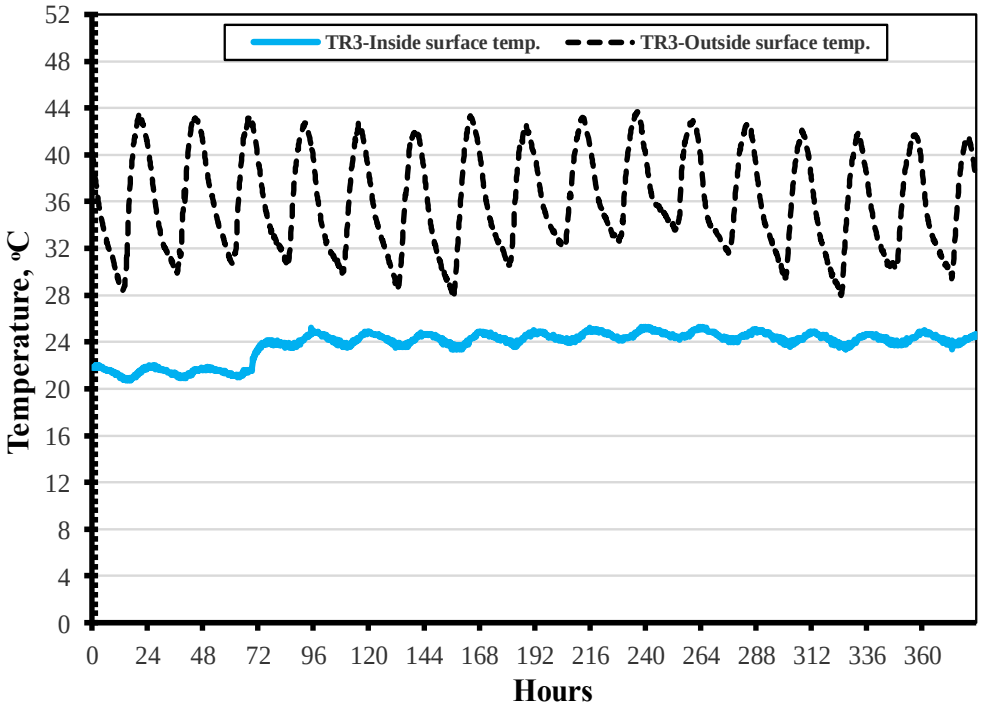

Figure 4.60: Inside and outside surface temperature; at August; of East wall in TR3.

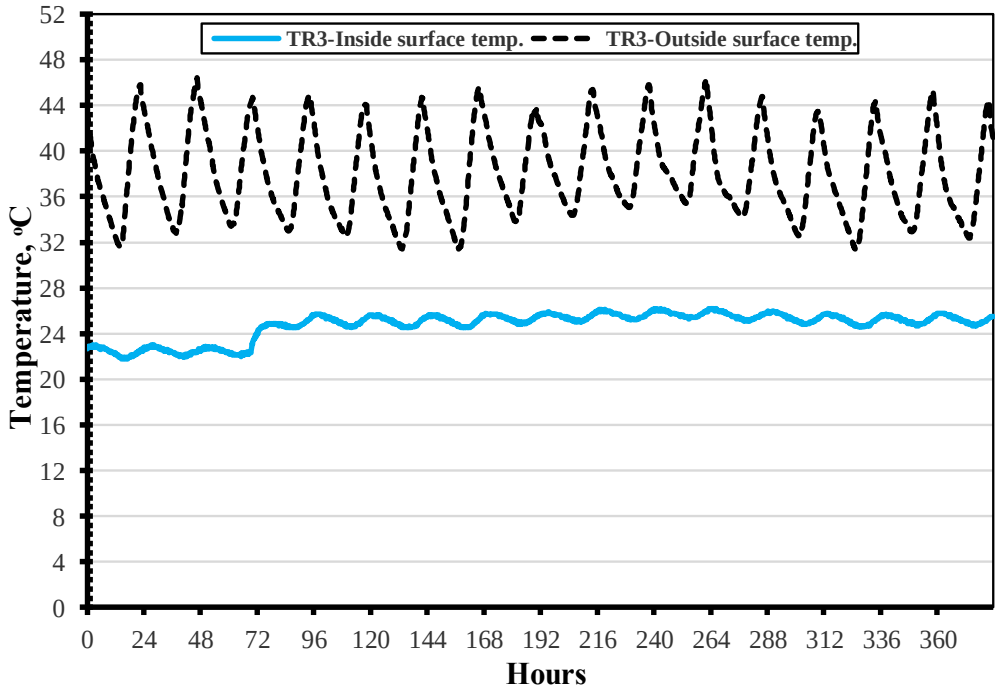

Figure 4.61: Inside and outside surface temperature; at August; of West wall in TR3.

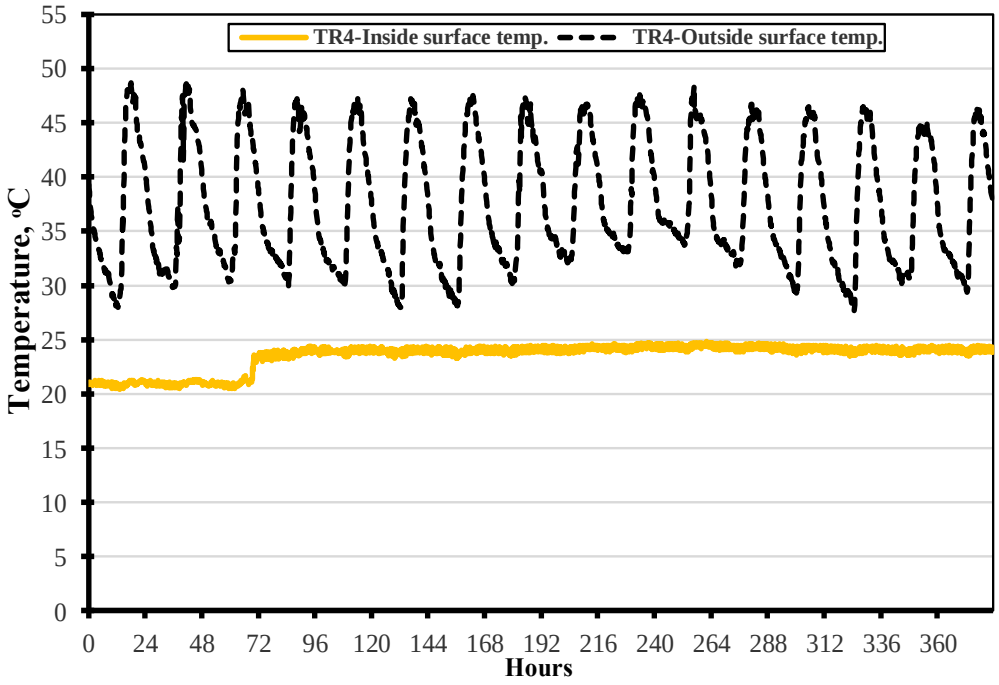

Figure 4.62: Inside and outside surface temperature; at August; of East wall in TR4.

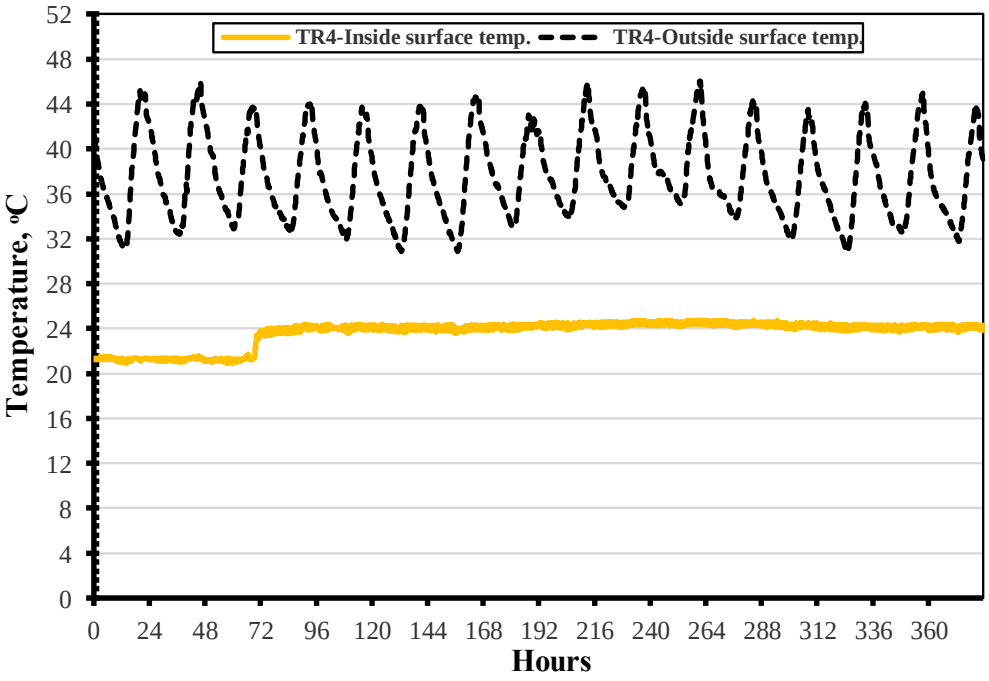

Figure 4.63: Inside and outside surface temperature; at August; of West wall in TR4.

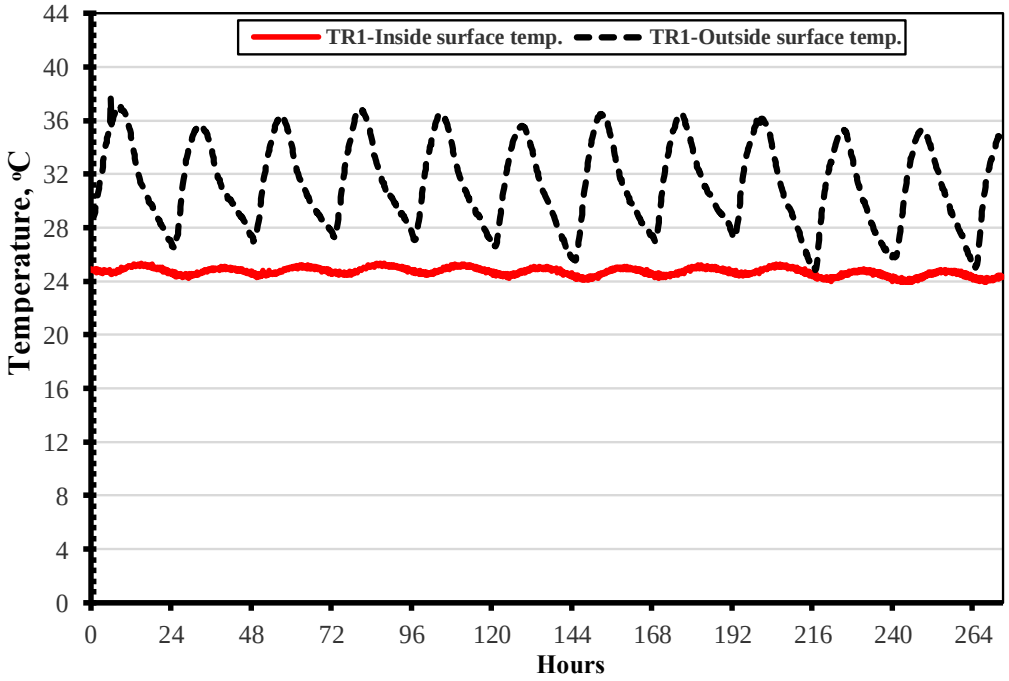

Figure 4.64: Inside and outside surface temperature; at September; of East wall in TR1.

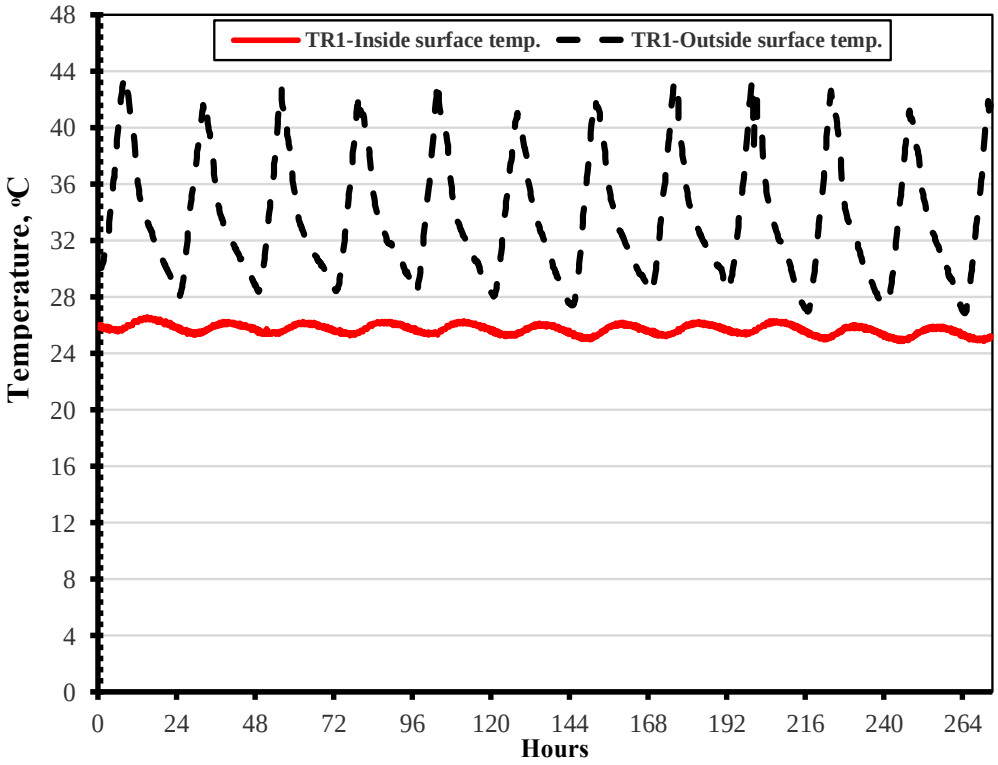

Figure 4.65: Inside and outside surface temperature; at September; of West wall in TR1.

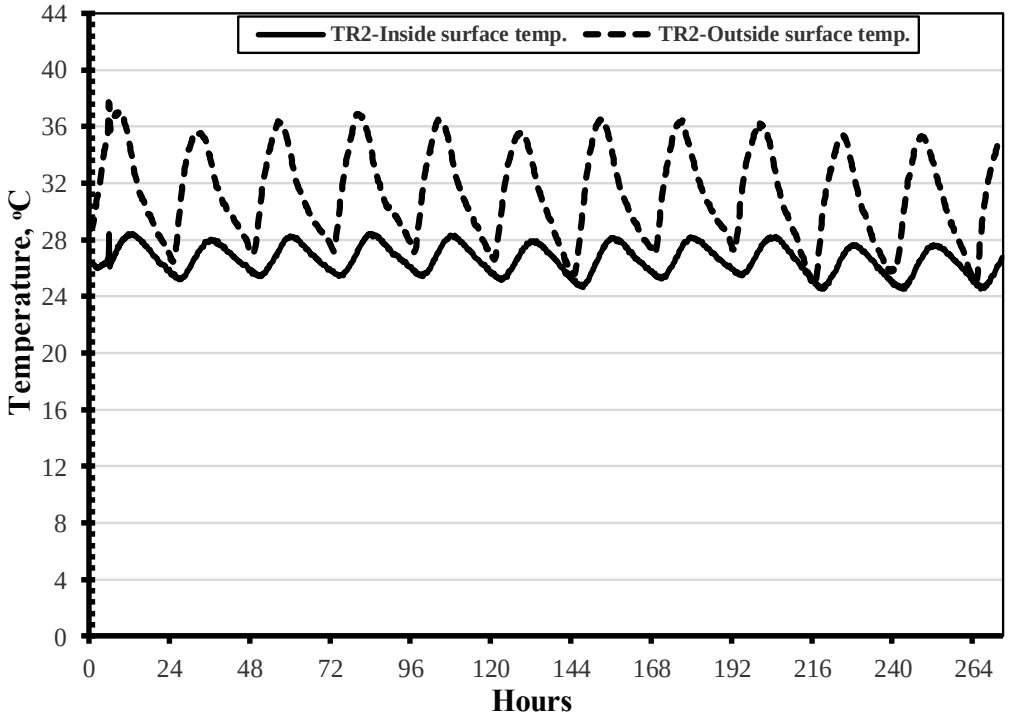

Figure 4.66: Inside and outside surface temperature; at September; of East wall in TR2.

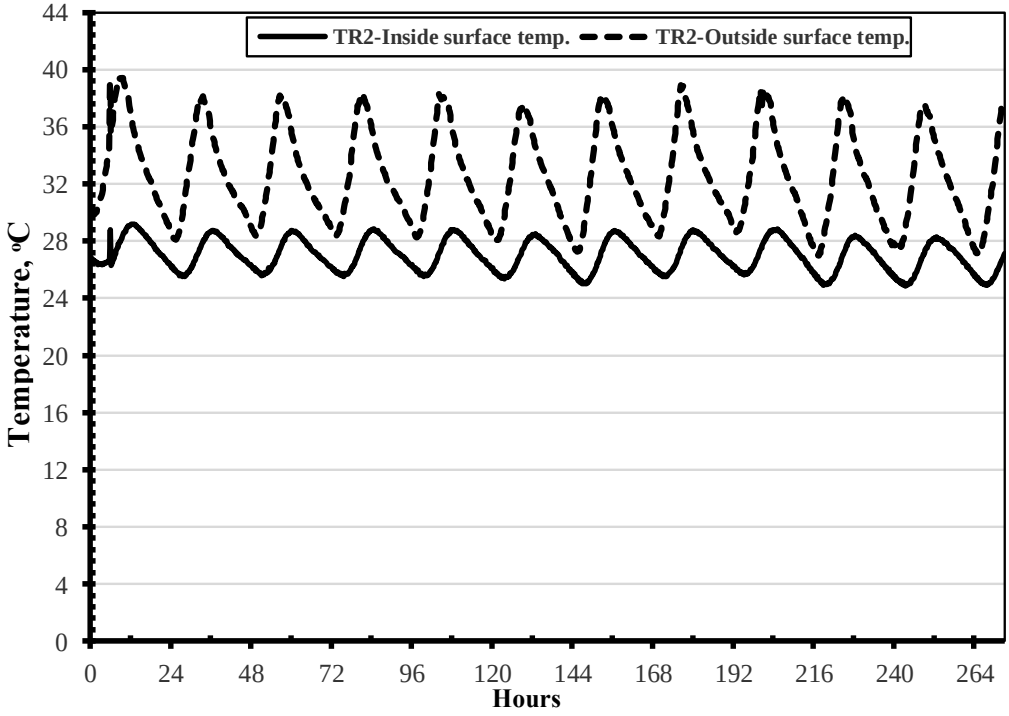

Figure 4.67: Inside and outside surface temperature; at September; of West wall in TR2.

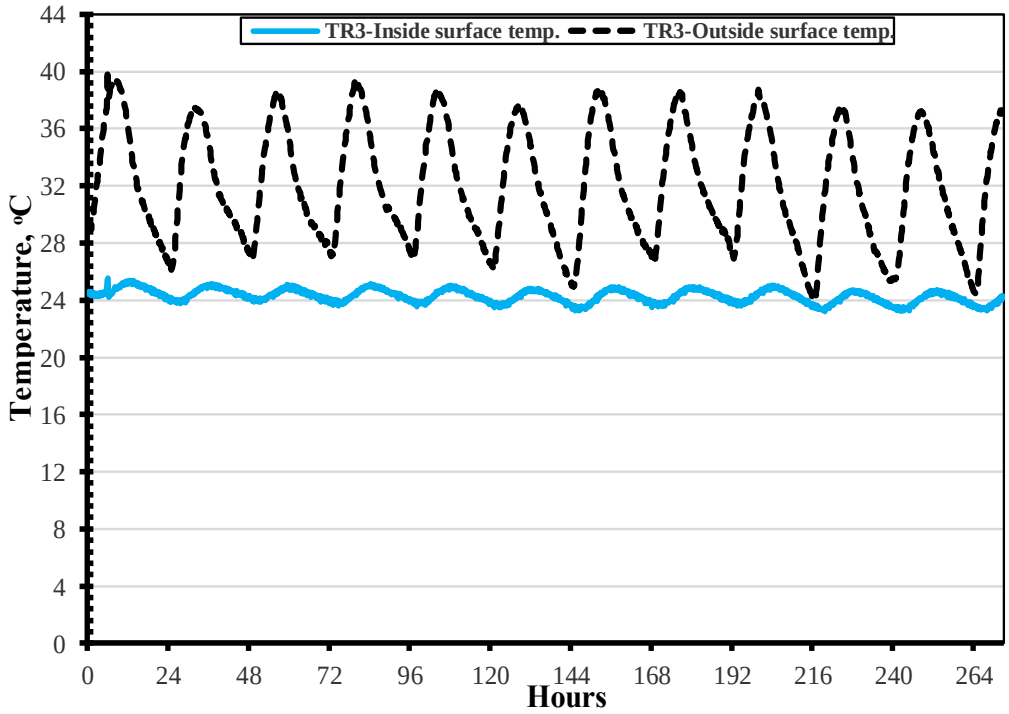

Figure 4.68: Inside and outside surface temperature; at September; of East wall in TR3.

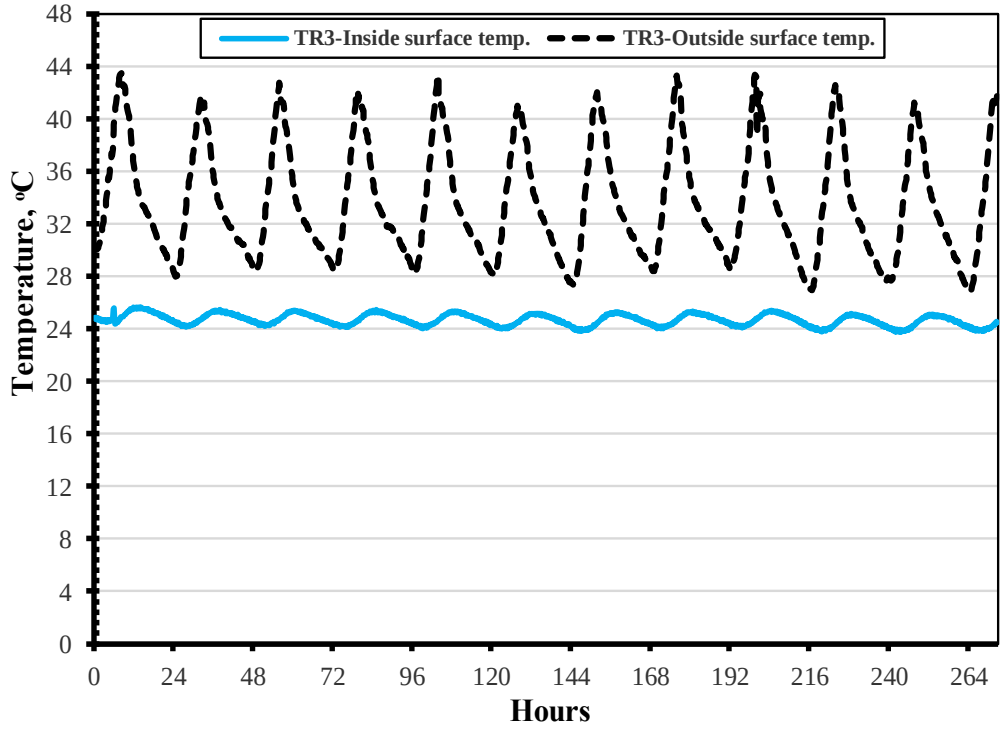

Figure 4.69: Inside and outside surface temperature; at September; of West wall in TR3.

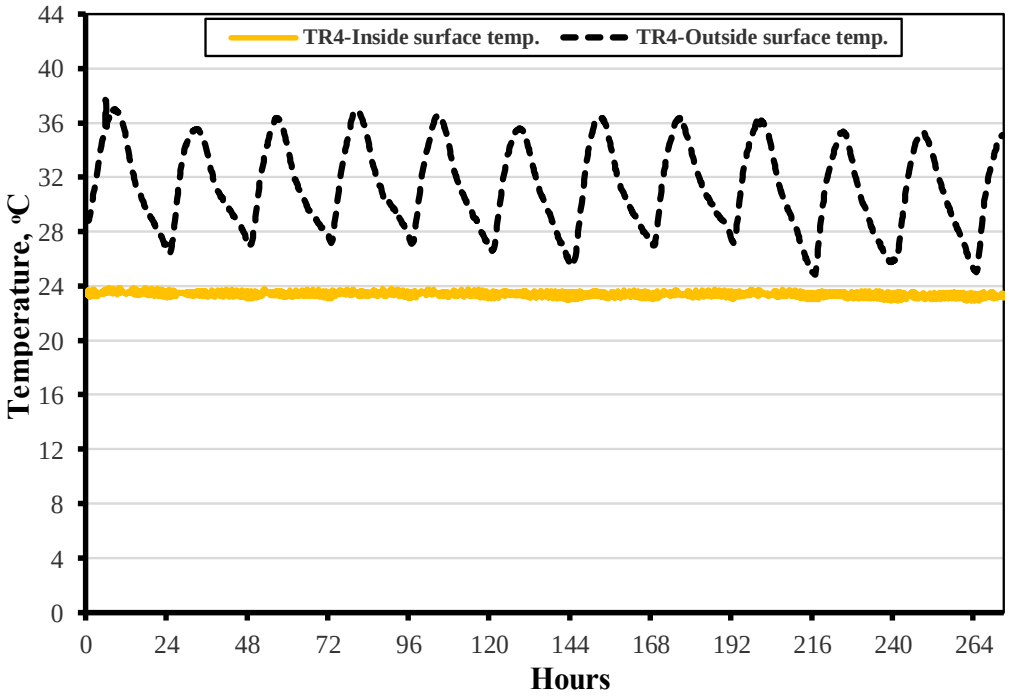

Figure 4.70: Inside and outside surface temperature; at September; of East wall in TR4.

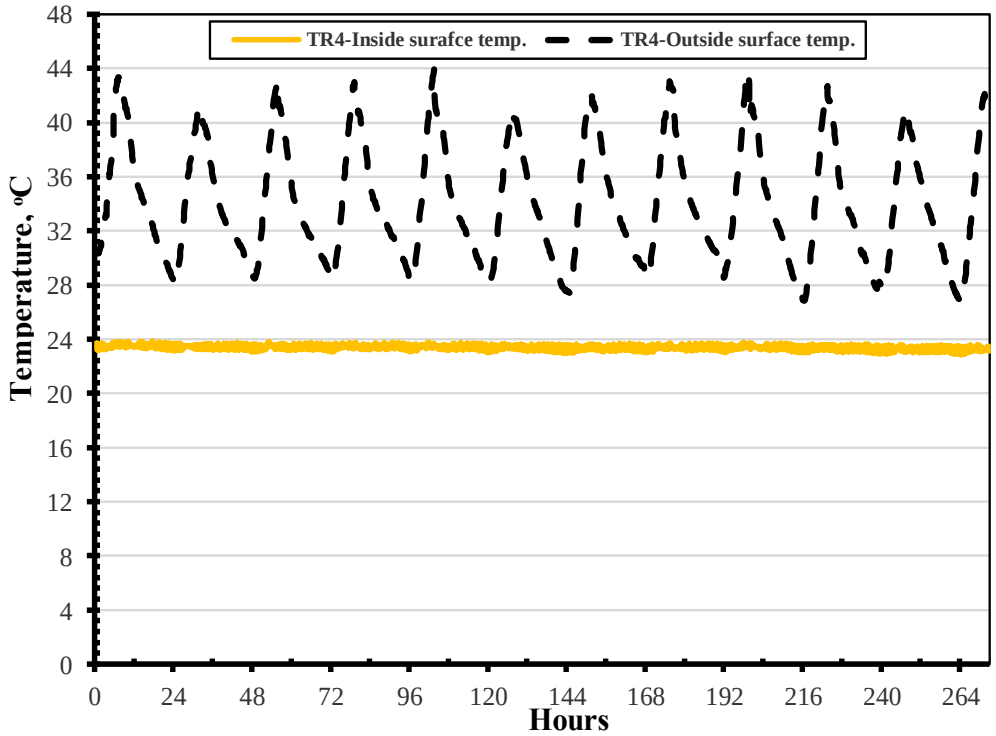

Figure 4.71: Inside and outside surface temperature; at September; of West wall in TR4.

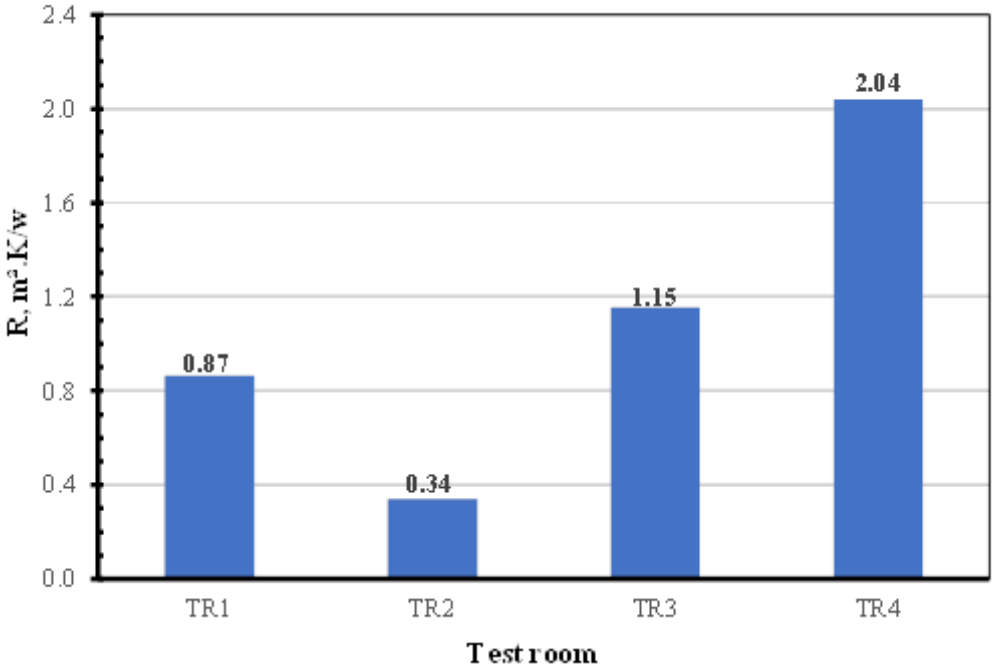

Figure 4.72: Thermal resistance of walls in test rooms.

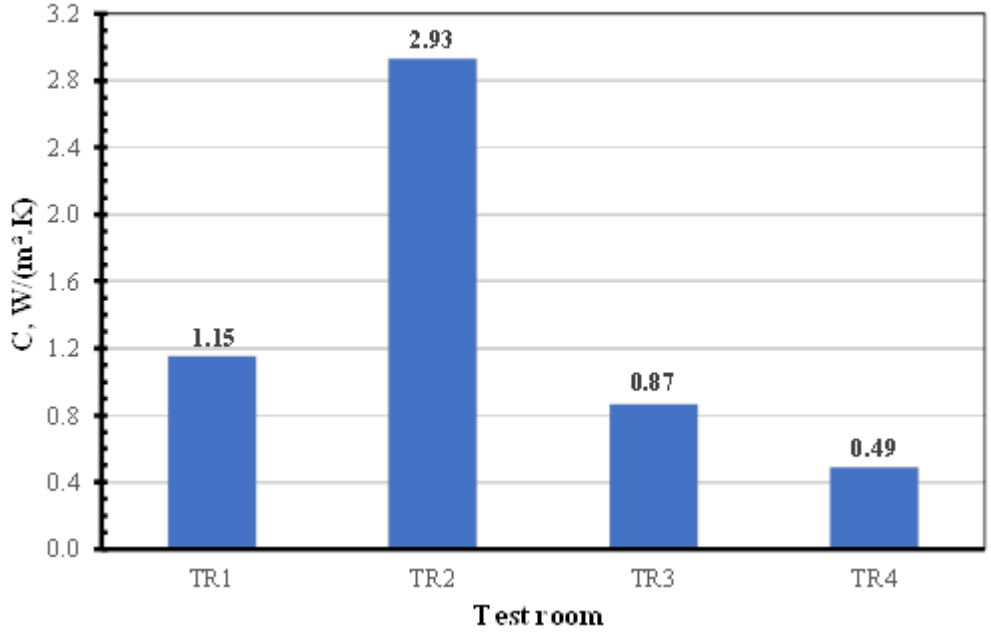

Figure 4.73: Thermal conductance of walls in test rooms.

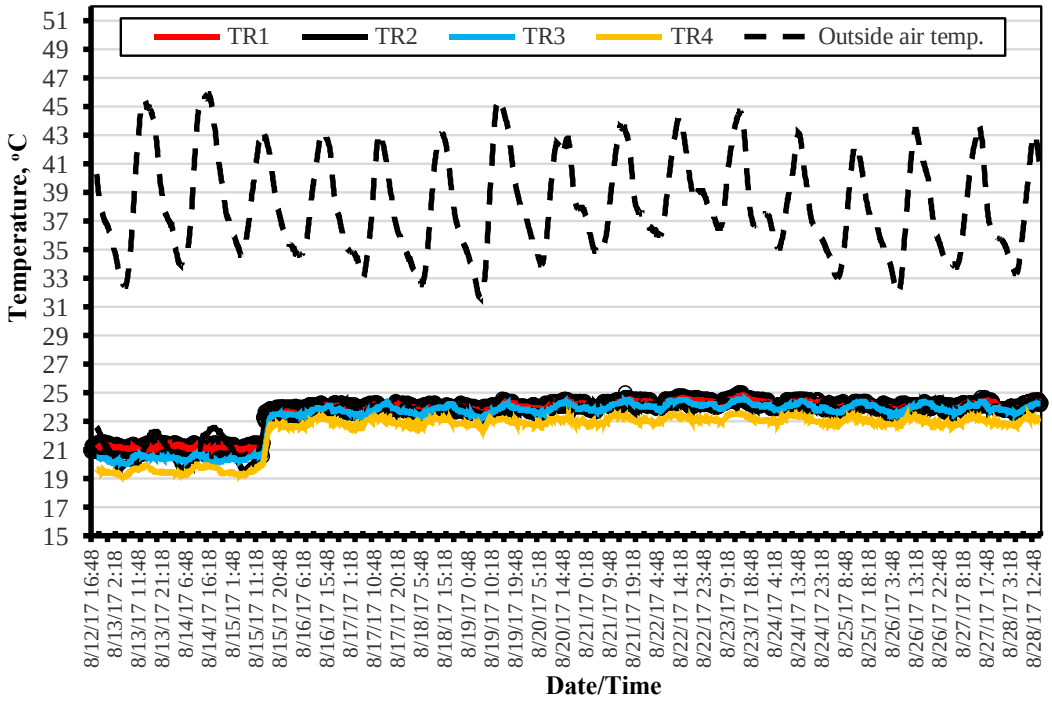

Figure 4.74: Inside air temperature of test rooms and outside air temperature; August.

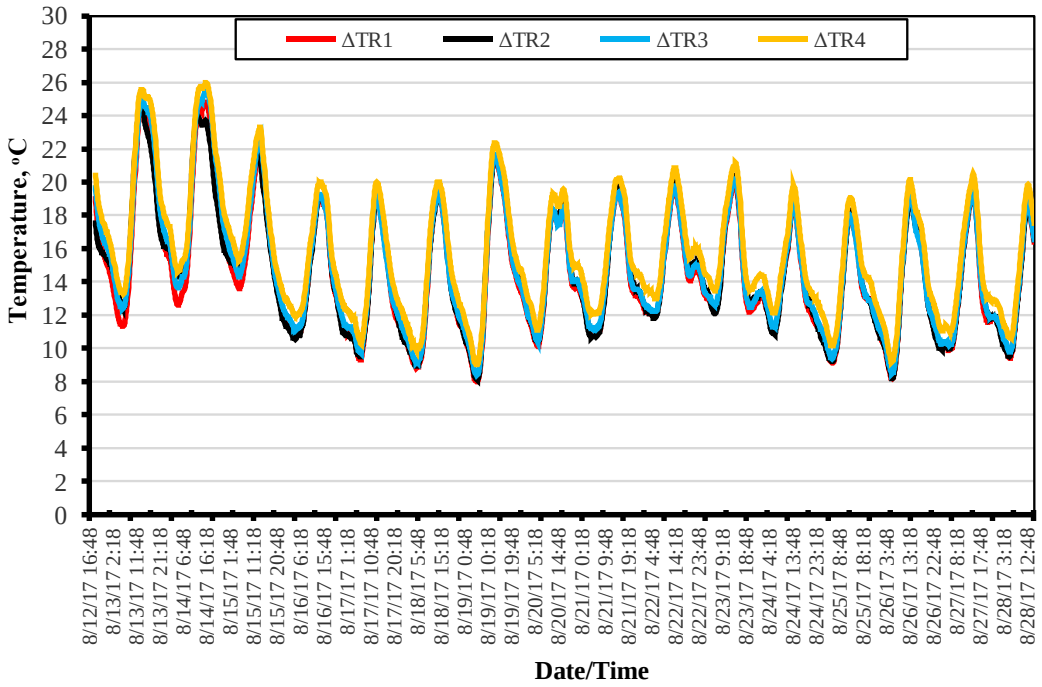

Figure 4.75: Difference between outside and inside air temperature; August.

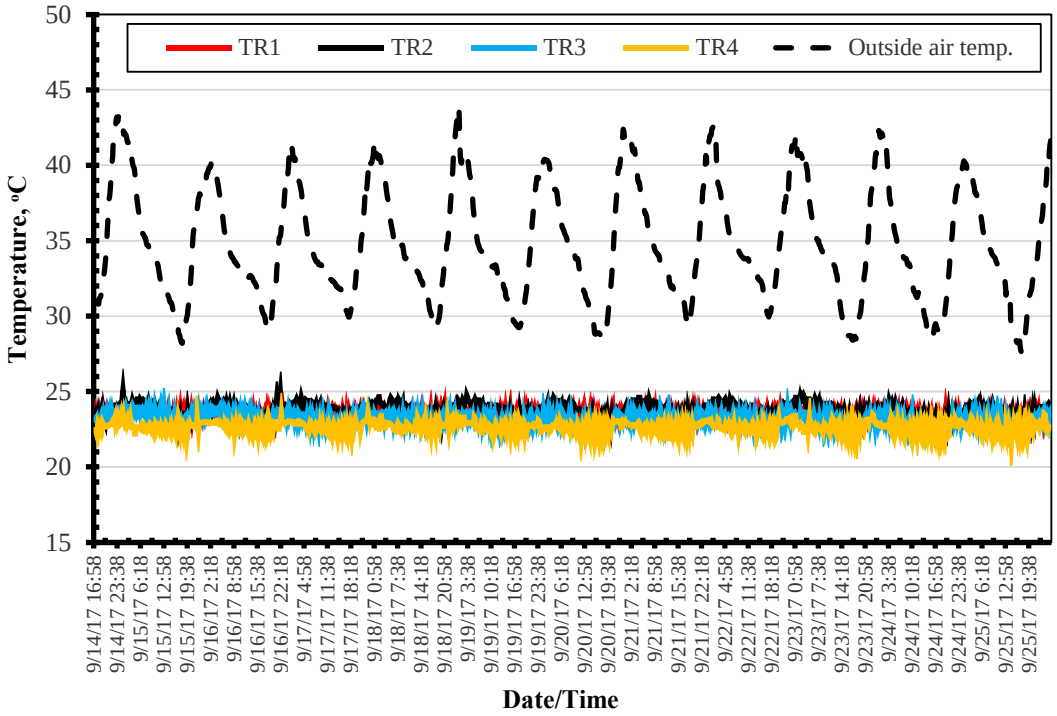

Figure 4.76: Inside air temperature of test rooms and outside air temperature; September.

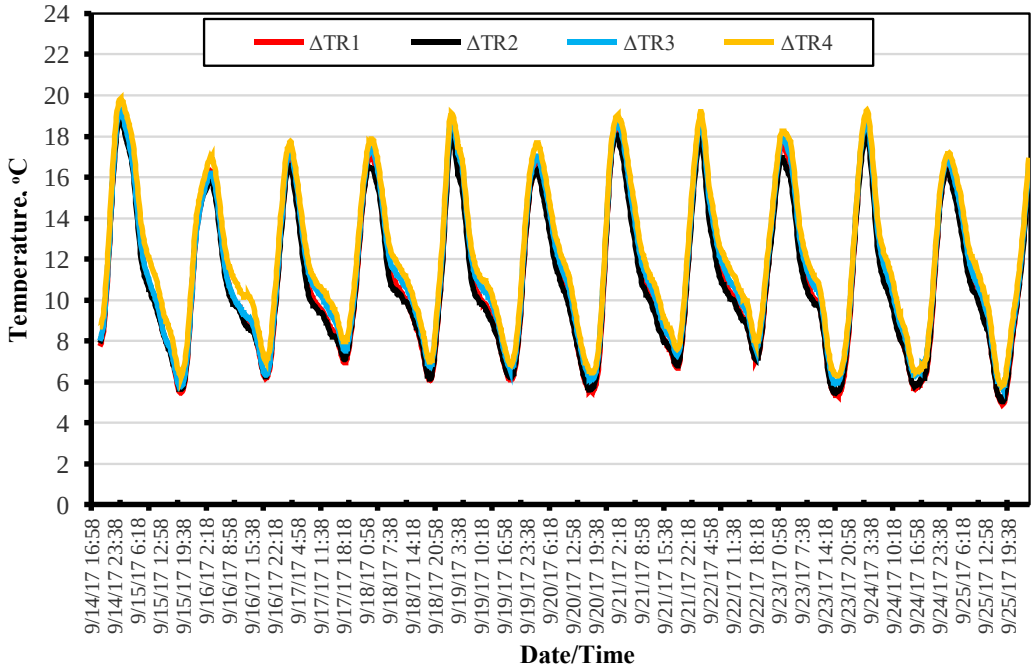

Figure 4.77: Difference between outside and inside air temperature; September.

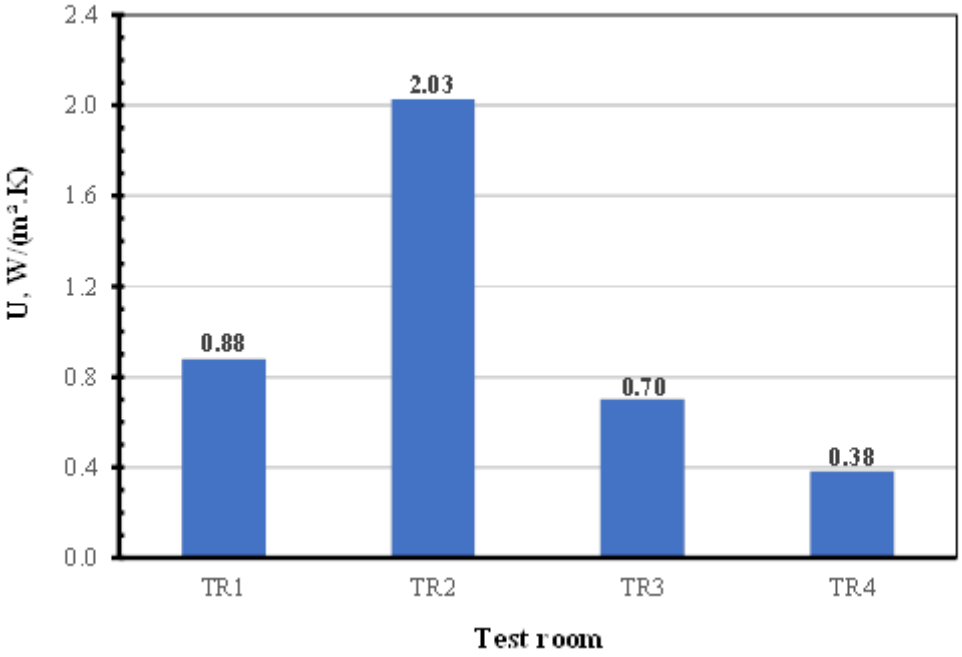

Figure 4.78: Thermal transmittance of walls in test rooms.

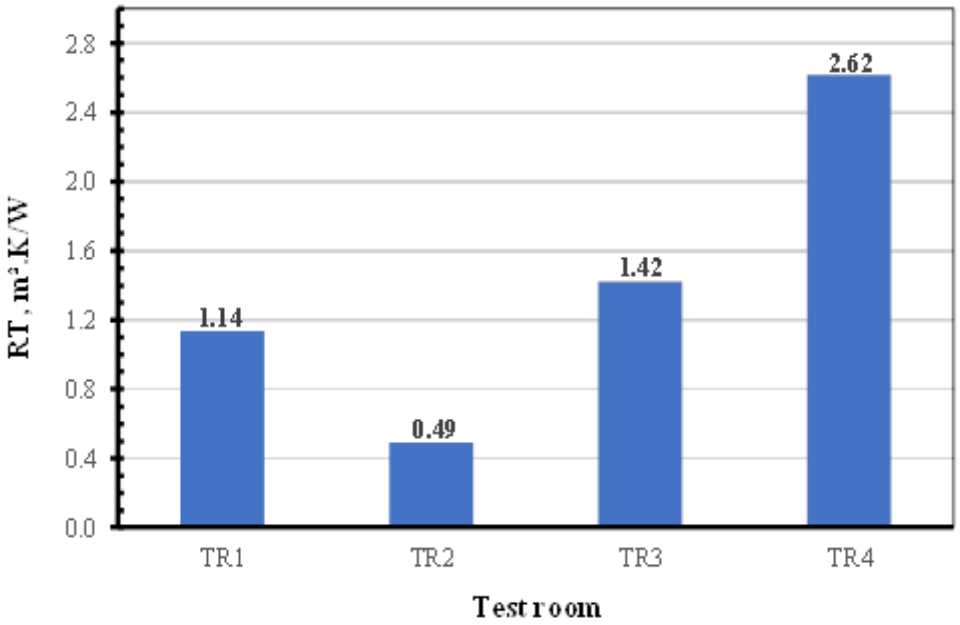

Figure 4.79: Total thermal resistance of walls in test rooms.

4.10 Thermal transmission measurement results

The thermal transmittance of walls in each test room was also evaluated using the U-value set (testo 635-2). The thermal transmittance measurement on walls in each test room was taken at many points, as explained in Chapter 3, and at the same periods of measuring the heat flux. After that, the average of all measurements was calculated. Figures 4.80 and 4.81 show the average values of all measurements for East and West walls, respectively, while Figure 4.82 depicts the final average values of all thermal transmittance measurements of all walls. The results of this test had the same trend for the results from the calculation method in the previous section where the maximum thermal transmittance was through walls of TR2; 1.5735 W/(m².K); and the minimum thermal transmittance was through walls of TR4; 0.4595 W/(m².K). The thermal transmittance of TR1 walls was 0.813 W/(m².K), while the thermal transmittance of TR3 walls was 0.556 W/(m².K).

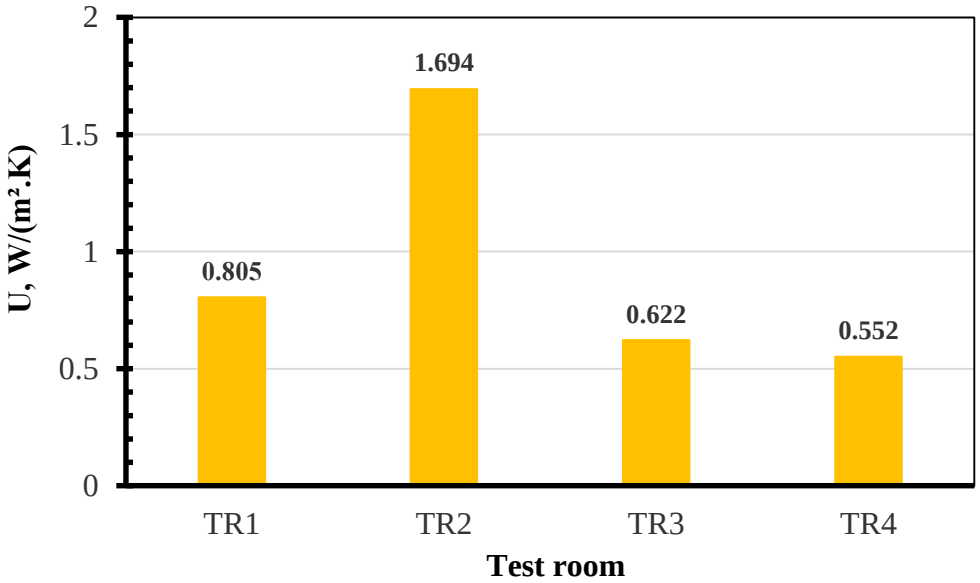

Figure 4.80: Thermal transmittance of East wall in test rooms.

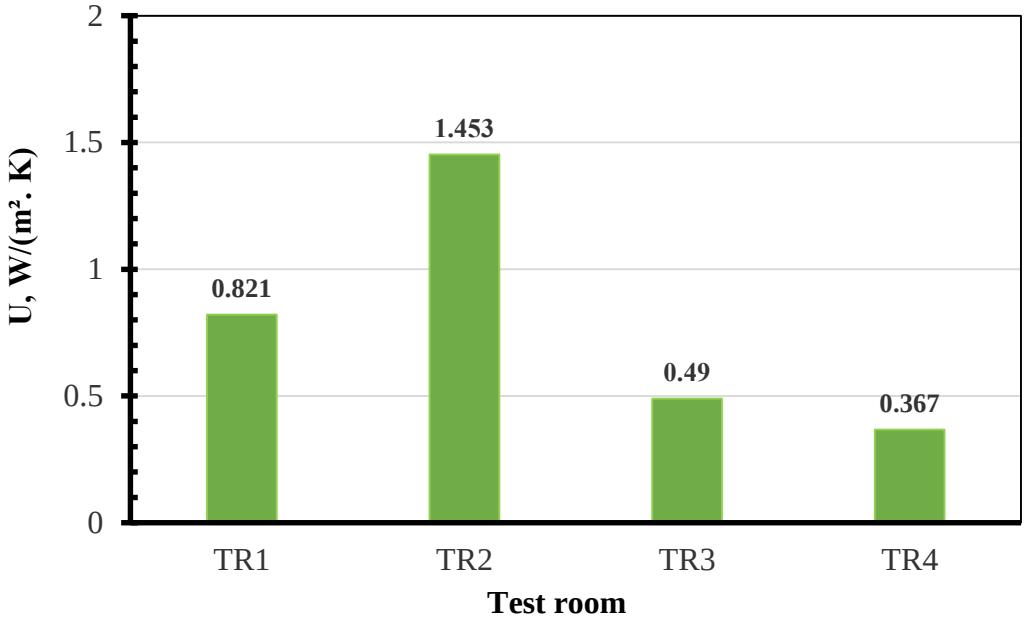

Figure 4.81: Thermal transmittance of West wall in test rooms.

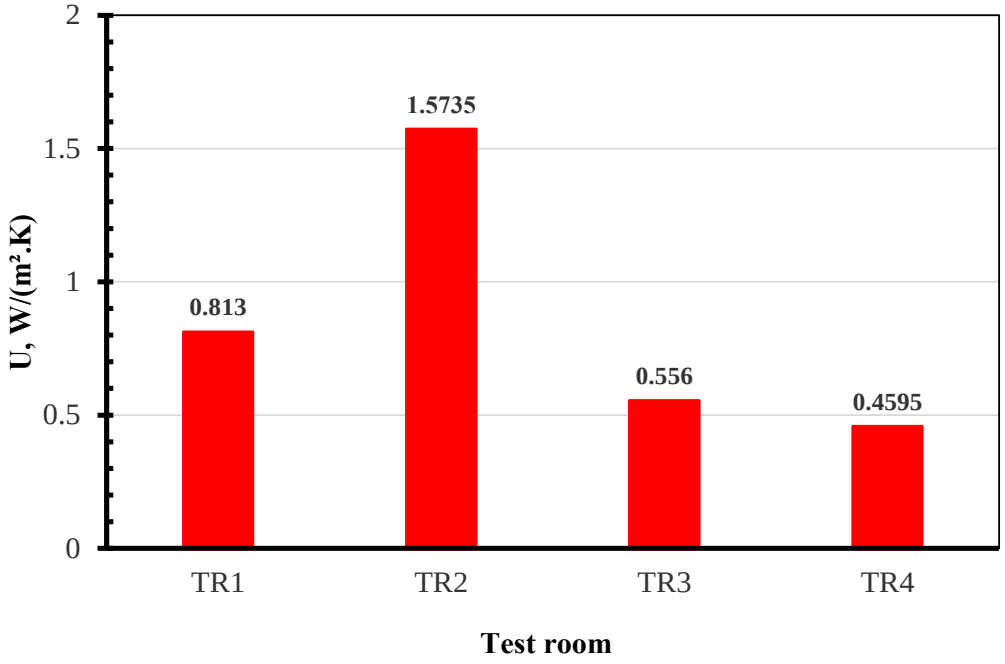

Figure 4.82: Thermal transmittance of walls in test rooms.

4.11 Comparison of thermal transmittance test results

According to ASTM C1155-95 [86] and ISO 9869 [87] calculation methods that use the heat flux and temperature difference results through walls, the average thermal transmittance of walls in TR1, TR2, TR3 and TR4 was 0.88, 2.03, 0.70 and 0.38 W/(m².K); respectively; while it was 0.813, 1.573, 0.556 and 0.4595 W/(m².K); respectively; using U-value set (testo 635-2). The thermal transmittance results from both methods had the same trend (the TR2 walls had the maximum thermal transmittance followed by TR1 and TR3 walls and finally the TR4 walls had the lowest thermal resistance) and this confirms the validation of the comparison between test rooms. However, the values of thermal transmittance that was determined from the calculation methods in TR1, TR2 and TR3 were more than those resulted from the U-value set and the value of thermal transmittance resulted from calculation methods in TR4 was less than that resulted from U-value set.

This difference in the thermal transmittance values is due to the accuracy of the two methods. Calculation methods are standard method to measure the thermal transmittance that depend on long-term monitoring results of heat flux and difference of temperature on walls at different times; day and night; and with different conditions of temperature, solar radiation, UV index, RH, wind speed and direction; while the U-value set measures the thermal transmittance at specific time and with certain conditions for short time (i.e. not more than one hour). Further, the U-value set (testo 635-2) used to measure the thermal transmission coefficient (U-value) uses sensors for measuring the inside and outside environmental temperatures and thermocouples for measuring the inside surface

temperatures. However, the heat flux is not measured. Simple theoretical and metrology fundamentals are used by testo 635-2 to calculate the U-value [80]. Therefore, it is obvious that the thermal transmittance values resulted from the calculation method are more accurate and comprehensive than those resulted from the U-value set method and this can also be concluded from comparing other tests results. Using the thermal transmittance values resulted from calculation method will be more precise for comparing the thermal performance of test rooms and drawing reliable conclusions [80].

4.12 Electricity consumption results

The electricity consumed by air conditioners (A/C's) inside the test rooms to keep the inside temperature like the setting temperature of A/C; 24°C or 20°C; was measured and recorded every 10 minutes as explained in the previous chapter. A summary of daily electricity consumption in test rooms is schematically presented in Figure 4.83. It should be noted that during the periods from 22th to 30th July and from 7th to 15th August, the A/C was set with 20°C. Therefore, the electricity consumption in these periods was expected to be more than the other periods of the three months where the A/C was set with 24°C.

The daily energy consumption in all the test rooms during July and August was more than that during September and this was due to the high outside temperature and RH. It is clear that the insulation system used in TR4 was the most effective insulation system to save electricity between all systems. The insulation system used in TR1 and TR3 have almost the same effect in saving electricity. The same observation can be noted from the day (6:00 am to 6:00 pm) and night (6:00 pm to 6:00 am) electricity consumption in all

the test rooms explained in Figures 4.84 and 4.85; respectively. The electricity consumption during the day was more than that during the night because of higher ambient temperature and solar radiation. The energy consumption in the test rooms during different periods and different setting temperatures of A/C is numerically presented in Table 4.5 and schematically depicted in Figure 4.86. The details of energy consumption in the test rooms during the monitoring period are presented in Appendix D.

Table 4.5: Energy consumption in test rooms during different periods and different setting temperatures of A/C.

Period	Number of days	A/C temp., °C	Energy consumption, kwh			
			TR1	TR2	TR3	TR4
1 to 21-July	21	24	398	666	430	264
22 to 30 July	9	20	228	330	244	154
31-Julu to 6 August	7	24	136	206	146	86
7 to 15 August	9	20	250	356	266	168
16 to 31 August	16	24	332	488	354	200
September	30	24	496	772	564	308
Total			1840	2818	2004	1180

The accumulative electricity consumption in each test room from the beginning of July up to the end September is shown in Figure 4.87. At the end of these three months of the summer, the electricity consumption in TR1, TR2, TR3 and TR4 was 1840, 2812, 2004 and 1180 kwh; respectively (see Table 4.5). In comparison with TR2, which is the reference test room, the saving of electrical energy due to the usage of the insulation materials in walls of TR1, TR3 and TR3 was 34.6, 28.7 and 58.0%; respectively. This indicates that the insulation system used in walls of TR4 was the most effective system to save electricity between all systems followed by that used in TR1 and then by TR3. These

results mean that the insulation system used in walls of TR1 decreases the heat transfer more than the insulation system used in the walls of TR3. However, other measurements demonstrated in the previous sections of this Chapter; thermograph assessment of walls, surface temperature of walls, heat flux through the walls, R, C and U measurements; indicate that the insulation system used in walls of TR3 tended to reduce the heat transfer more than the insulation system used in the walls of TR3. Therefore, the effectiveness of insulation coating on walls of TR1 is not only ascribed to its low thermal conductivity and its high reflectivity for solar radiation. However, it is also due to its low heat convective coefficient [22–26]. This critical issue will be thoroughly proven in Chapter 5 (Simulation of Test Rooms). The low heat convective coefficient of coating will explain why the surface temperatures on walls of TR1 were more than those on walls of TR3 despite the fact that the walls of TR1 saved more energy than those of TR3 [89–94].

According to ASTM C1155-95 [86] and ISO 9869-1 [87], the total thermal resistance can also be calculated using the following equation:

$$R_T = R_{os} + R + R_{is} \quad 4.6$$

where

R_T = Total thermal resistance of wall (m^2.K/W).

R = Thermal resistance (surface to surface of wall) (m^2.K/W).

R_{is} = Inner surface thermal resistance of wall (m^2.K/W).

R_{os} = Outer surface thermal resistance of wall (m^2.K/W).

$$R_{is} = \frac{1}{h_i} \quad (4.7)$$

where

h_i = Inside heat convective coefficient [(W/(m^2.K)].

and

$$R_{os} = \frac{1}{h_{os}} \quad (4.8)$$

where

h_{os} = Outside heat convective coefficient [W/(m^2.K)].

It is to be highlighted that the surface thermal resistance increases with the decrease of the heat convection coefficient thereby reducing the heat transfer through wall and decreasing the energy consumption of test room. [22–26]. Therefore, the heat convective coefficient of inner and outer surfaces of walls have to be considered for calculating the total thermal resistance when the nano-ceramic coating is used [22–26]. The effectiveness of insulate coating in increasing the surface thermal resistance will be demonstrated at the end of Chapter 5.

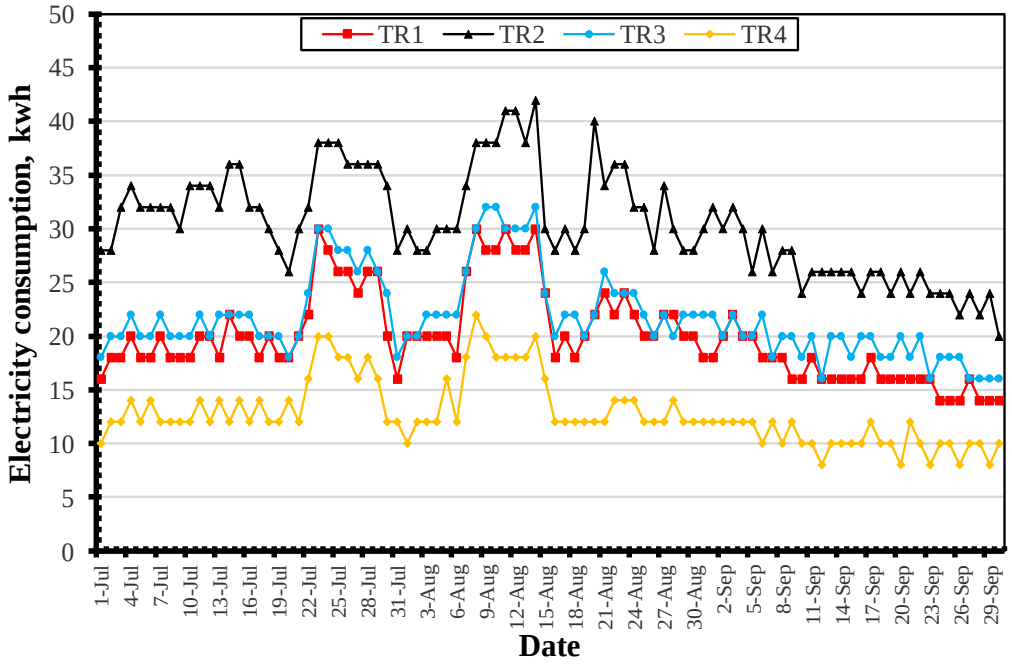

Figure 4.83: Daily energy consumption in test rooms during summer months.

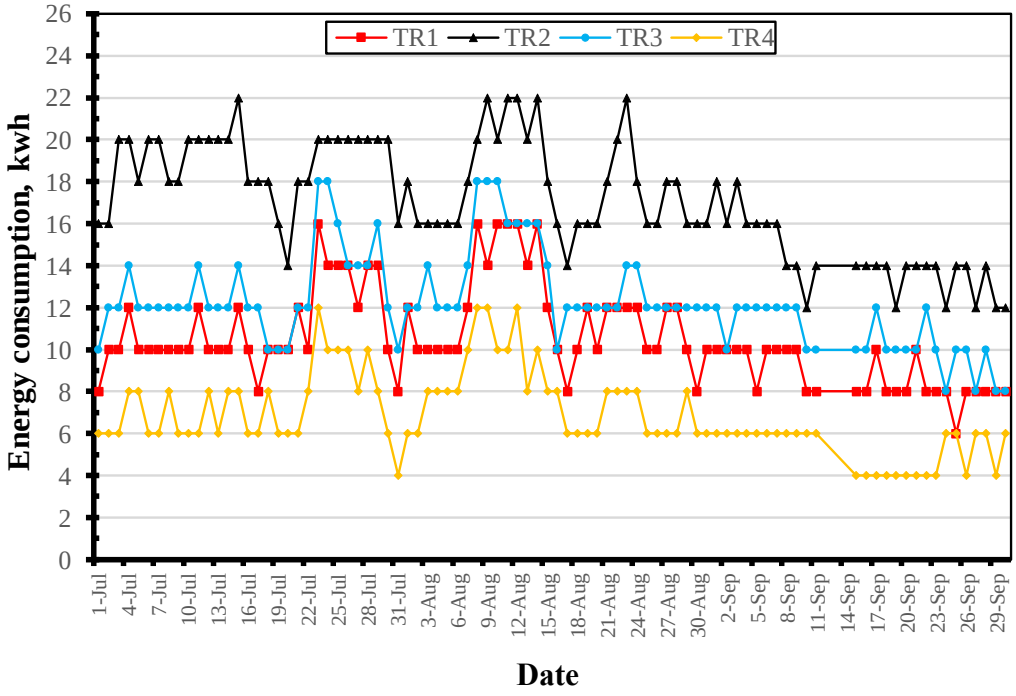

Figure 4.84: Energy consumption in test rooms during the day (6:00 am to 6:00 pm) for summer months.

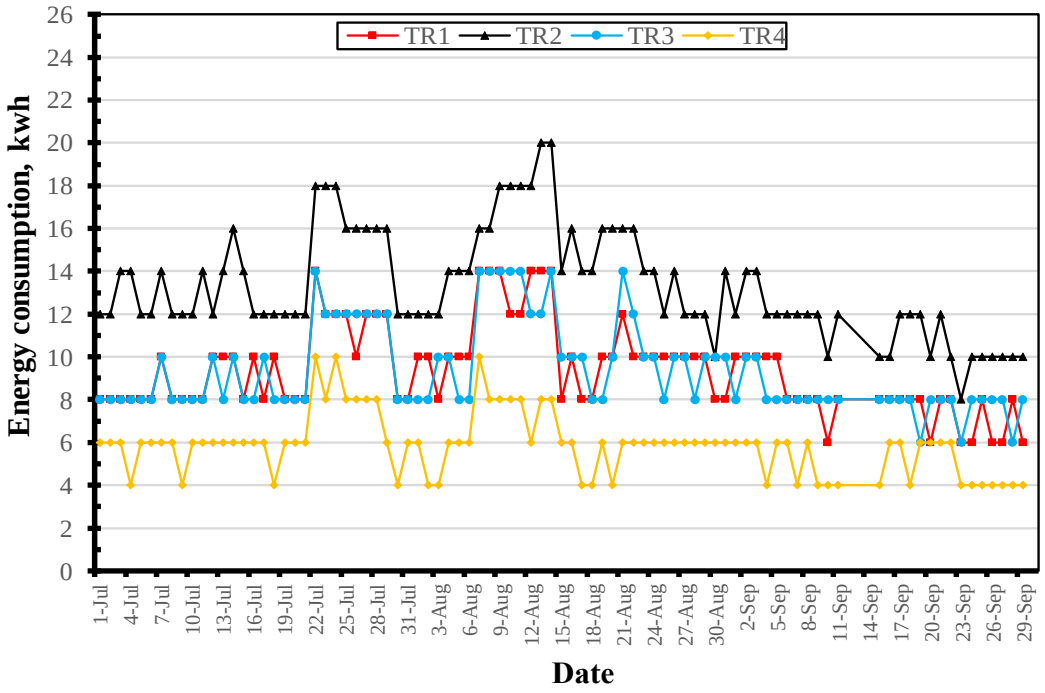

Figure 4.85: Energy consumption in test rooms during the night (6:00 pm to 6:00 am) for summer months.

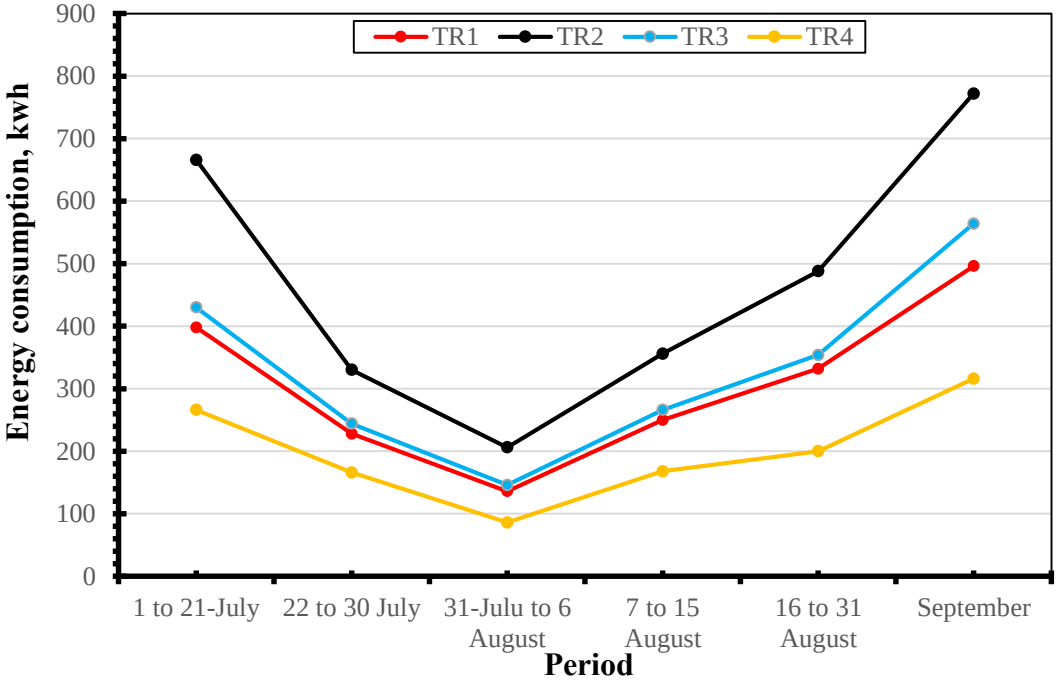

Figure 4.86: Energy consumption in test rooms with different temperatures of A/C.

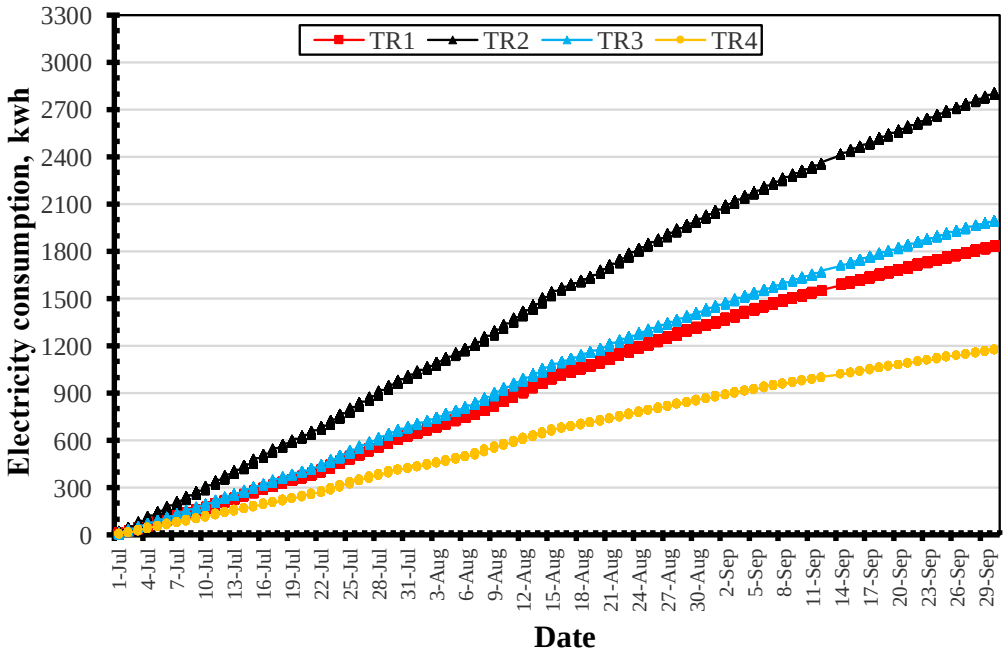

Figure 4.87: Energy consumption in test rooms during summer months.

CHAPTER FIVE

SIMULATION OF TEST ROOMS

5.1 General

Simulation is the process of modeling real buildings using software programs to obtain the performance of it without doing any actual measurement. Simulation nowadays has become an important tool to predict and estimate the thermal performance of building and thermal comfort that considers all the thermal factors including thermal properties of building materials, all activities of humans and the actual weather conditions [95–99]. Using simulation/modeling programs will certainly save time and effort consumed in the building's site for testing and evaluation. Many simulation/modeling software tools have been developed and published over the last two decades. Figure 5.1 shows the modeling and thermal insulation software tools and the exchange of data between them. One of the most utilized programs in UK and EUROPE, which provides trustworthy certificate and reports for its results, is the DesignBuilder [95–99].

5.2 DesignBuilder software

The DesignBuilder software is an advanced 3D graphical user interface that has been specially developed to run the powerful simulation engine which is EnergyPlus. This software tool is has been developed to simulate the physical conditions by treating time as the independent variable and solving a series of equation sets in discrete steps [99].

Energyplus is a whole building energy simulation program that engineers, architects, and researchers use to model energy consumption [100]. Designbuilder provides data

such as: energy consumption, comfort conditions, maximum summertime temperatures. Figure 5.2 depicts the scheme for simulation using Designbuilder [99].

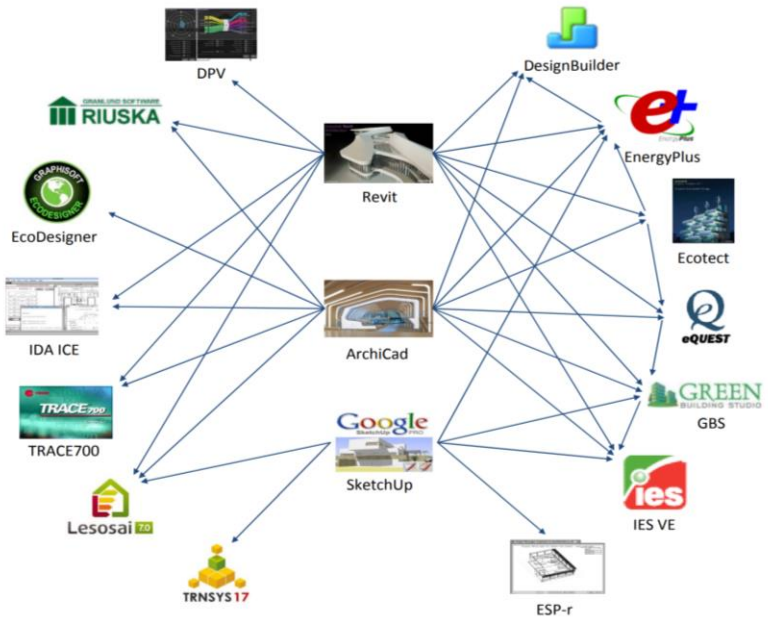

Figure 5.1: Modeling and thermal simulation software tools [101].

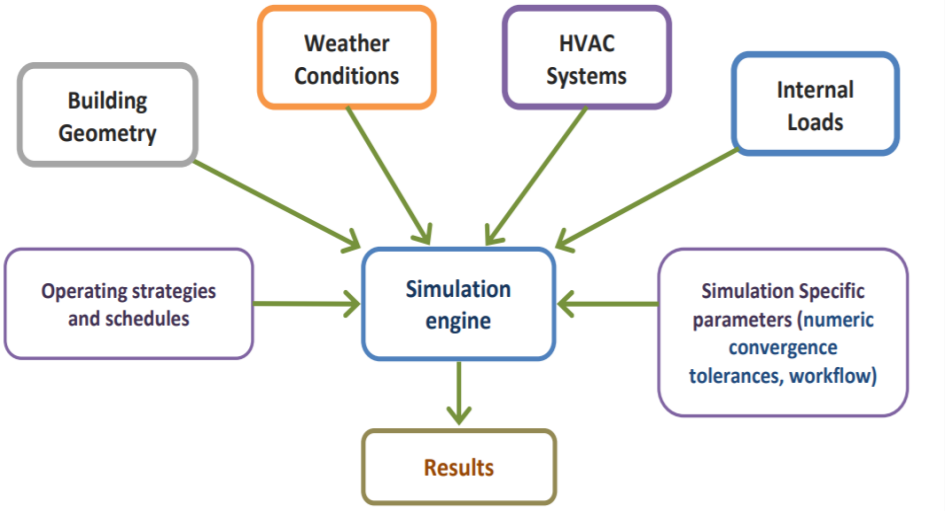

Figure 5.2: Simulation scheme using DesignBuilder [101].

5.3 EnergyPlus heat transfer calculations

The heat is transferred from outside buildings to inside during the summer session through walls, slabs, windows and doors by the following three processes; radiation, convection and conduction; or one of them as shown in Figure 5.3 [100].

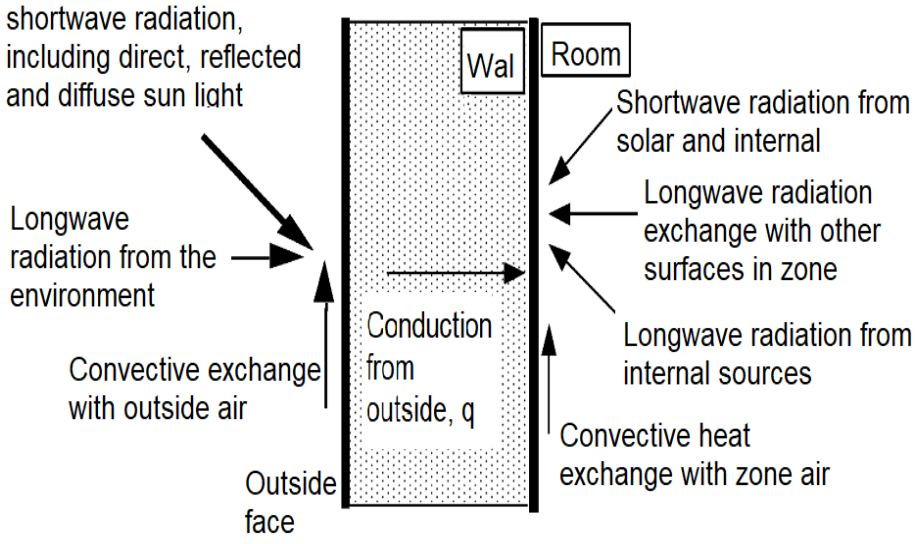

Figure 5.3: Heat transfer processes through wall [100].

5.3.1 Calculation of radiation

Heat transfer from surface radiation is modeled using the following classical formulation [100]:

$$Q_r = \varepsilon \, \sigma \, A \, (T^4_{surf} - T^4_{air}) \qquad 5.1$$

where:

Q_r = Radiation exchange formulation between the surface and air (W).

ε = Emittance of the surface.

σ = Stefan-Boltzmann constant [W/(m^2.K^4)].

A = area of surface (m^2).

T_{surf} = Surface temperature (K).

T_{air} = Air temperature (K).

5.3.2 Calculation of convection

Heat transfer from surface convection is modeled using the classical formulation:

$$Q_c = h_c A(T_{surf} - T_{air}) \quad 5.2$$

where:

Q_c = Rate of exterior convective heat transfer (W).

h_c = Convection coefficient ($W/(m^2.K)$).

A = Surface area (m^2).

T_{surf} = Surface temperature (K).

T_{air} = Air temperature (K).

5.3.3 Calculation of conduction transfer functions

Conduction transfer functions calculations in EnergPlus were achieved using the state space method which is defined by the following linear matrix equations:

$$\frac{d[x]}{dt} = [A][x] + [B][u] \quad 5.3$$

$$[y] = [C][x] + [D][u] \quad 5.4$$

where:

x = Vector of state variable.

u = Vector of inputs.

y = Vector of output.

t = Time.

A, B, C and D = Coefficient matrices.

The above formulation can be used to solve the transient heat conduction equation by enforcing a finite difference grid over the various layers in the building element being analyzed. In this case, the state variables are the nodal temperatures, while the environmental temperatures (interior and exterior) are the inputs, and the resulting heat fluxes at both surfaces are the outputs. Thus, the state space representation with finite difference variables would take the following form [100]:

$$\frac{d\begin{bmatrix} T_1 \\ \vdots \\ T_n \end{bmatrix}}{dt} = [\mathrm{A}]\begin{bmatrix} T_1 \\ \vdots \\ T_n \end{bmatrix} + [\mathrm{B}]\begin{bmatrix} T_i \\ T_o \end{bmatrix} \quad 5.5$$

$$\begin{bmatrix} q''_i \\ q''_o \end{bmatrix} = [\mathrm{C}]\begin{bmatrix} T_1 \\ \vdots \\ T_n \end{bmatrix} + [\mathrm{D}]\begin{bmatrix} T_i \\ T_o \end{bmatrix} \quad 5.6$$

where:

T1, T2, ..., Tn-1, Tn= Finite difference nodal temperatures.

n = Number of nodes.

T_i and T_o = Interior and exterior environmental temperatures (K).

q''_i and q''_o = Heat fluxes (W/m^2).

Figure 5.4 shows an example of a simple one-layer wall with two interior nodes and convection at both sides, and the resulting finite difference equations are given by:

$$C\frac{dT_1}{dt} = hA\left(T_o - T_1\right) + \frac{T_2 - T_1}{R} \tag{5.7}$$

$$C\frac{dT_2}{dt} = hA\left(T_i - T_2\right) + \frac{T_1 - T_2}{R} \tag{5.8}$$

$$q\text{“}_i = h\left(T_i - T_2\right) \tag{5.9}$$

$$q\text{“}_o = h\left(T_1 - T_o\right) \tag{5.10}$$

where:

$R = \frac{\ell}{kA}$,

$C = \frac{\rho c_p \ell A}{2}$

A = Surface area exposed to the environmental temperatures (m^2).

ρ = Density (kg/m^3).

C_p = Specific heat (J/K).

In matrix format:

$$\begin{bmatrix} \frac{dT_1}{dt} \\ \frac{dT_2}{dt} \end{bmatrix} = \begin{bmatrix} -\frac{1}{RC} - \frac{hA}{C} & \frac{1}{RC} \\ \frac{1}{RC} & -\frac{1}{RC} - \frac{hA}{C} \end{bmatrix} \begin{bmatrix} T_1 \\ T_2 \end{bmatrix} + \begin{bmatrix} \frac{hA}{C} & 0 \\ 0 & \frac{hA}{C} \end{bmatrix} \begin{bmatrix} T_o \\ T_i \end{bmatrix}$$

$$\begin{bmatrix} q''_o \\ q''_i \end{bmatrix} = \begin{bmatrix} 0 & -h \\ h & 0 \end{bmatrix} \begin{bmatrix} T_1 \\ T_2 \end{bmatrix} + \begin{bmatrix} 0 & h \\ -h & 0 \end{bmatrix} \begin{bmatrix} T_o \\ T_i \end{bmatrix} \tag{5.11}$$

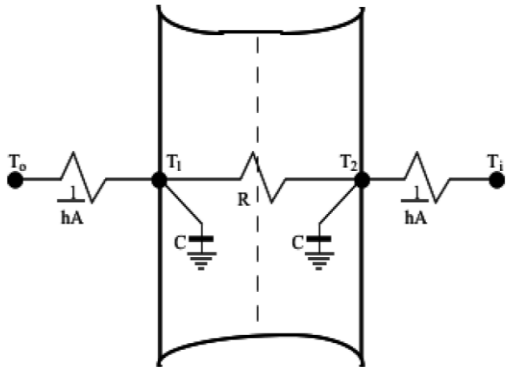

Figure 5.4: Two nodes state space example [100].

5.4 Simulation of test rooms using DesignBuilder

The steps of the simulation test rooms using Designbuilder software were as follows:

5.4.1 Input data

5.4.1.1 Location data

Region: Al-Faisaliah District, Dammam, Saudi Arabia.

Longitudinal: 50.04.

Latitude: 26.38.

Elevation: 17 m.

5.4.1.2 Weather file

The simulation of test rooms was achieved using the weather file which was created from the weather station data explained in Chapter 4. Figure 5.5 depicts the visualization of the test rooms with the surrounding weather.

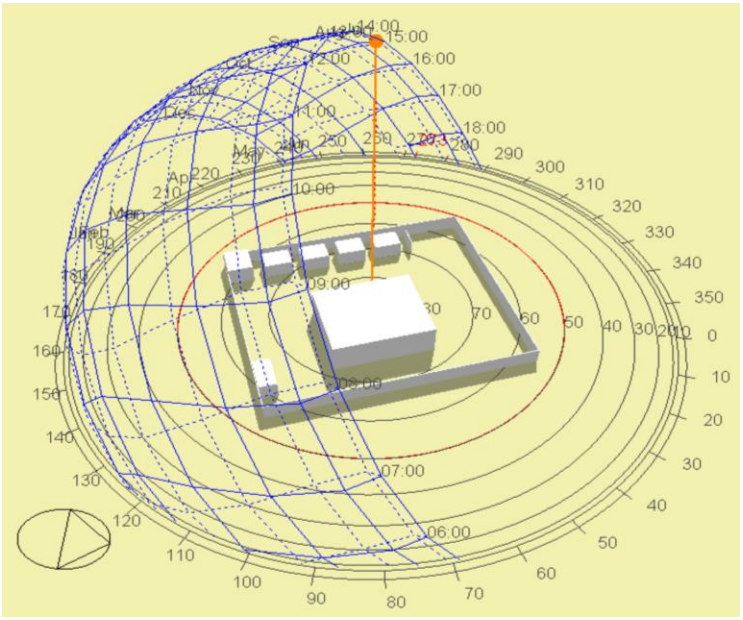

Figure 5.5: Visualization of test rooms with surrounding weather.

5.4.1.3 Test rooms geometry

The test rooms were drawn with the same dimensions, borders and shading in the site, as shown in Figure 5.6.

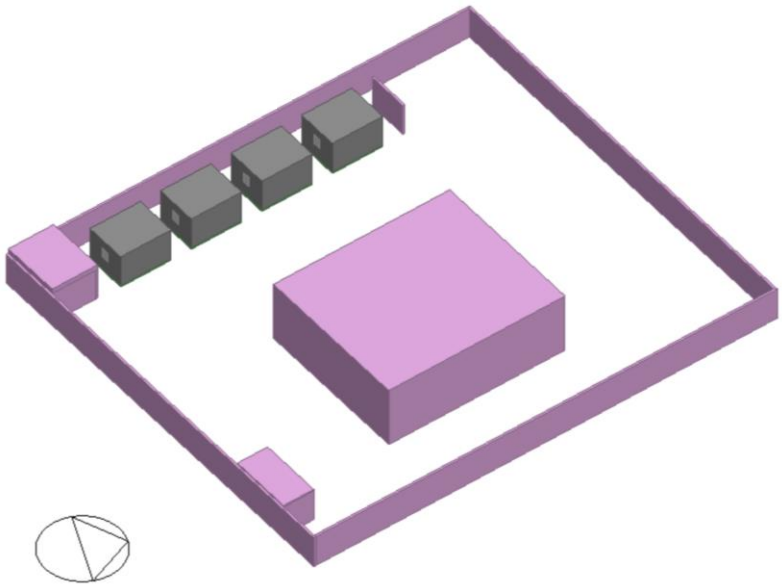

Figure 5.6: Geometry of test rooms.

5.4.1.4 Activities

The test rooms activities, that included room occupancy, equipment, computers and environmental control, were modeled exactly as they were in the site.

5.4.1.5 Test rooms construction

All walls, roof, window and door in each test room were modeled as they were in the site. Figures 5.7 to 5.10 show cross-sections of the walls in all test rooms from the models whereas Figure 5.11 depicts the cross section of the roof used in TR1 and TR4. The roof used in TR2 and TR3 was similar to the roof used in TR1 and TR4 except INSULATE coating was not applied.

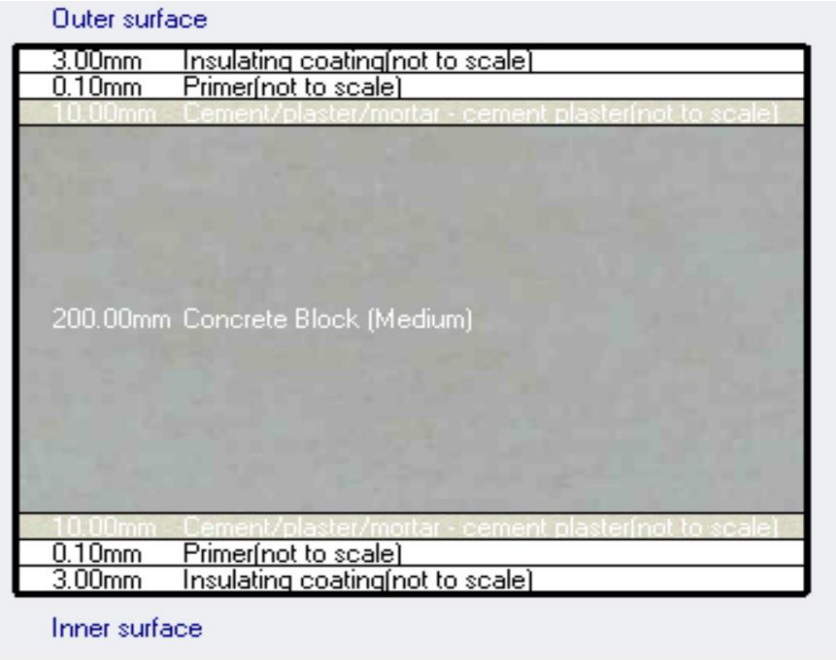

Figure 5.7: Cross section of TR1 walls.

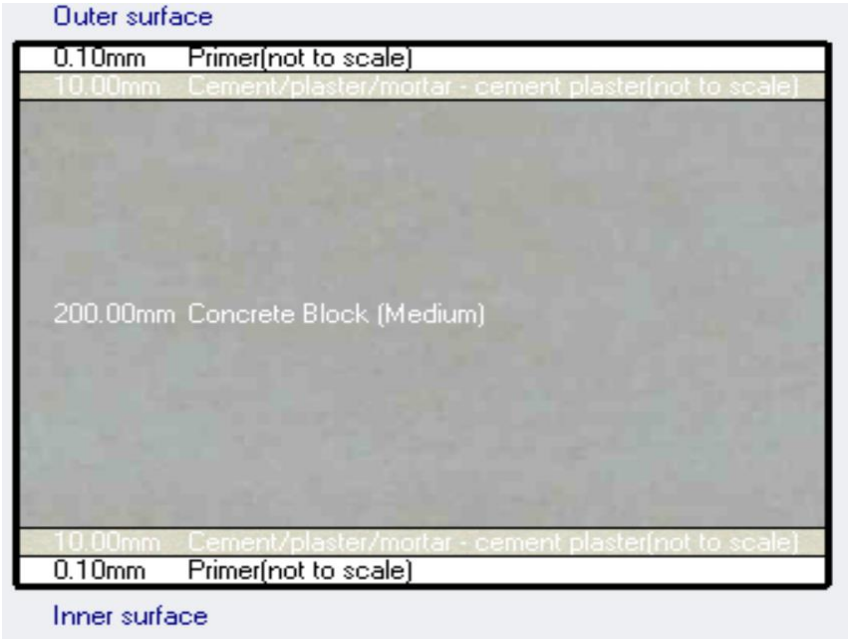

Figure 5.8: Cross section of TR2 walls.

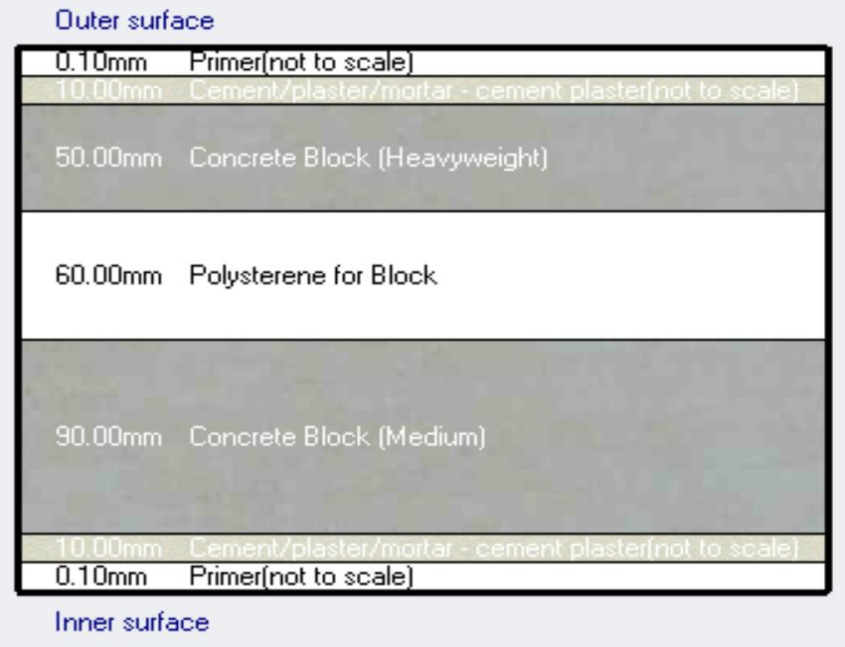

Figure 5.9: Cross section of TR3 walls.

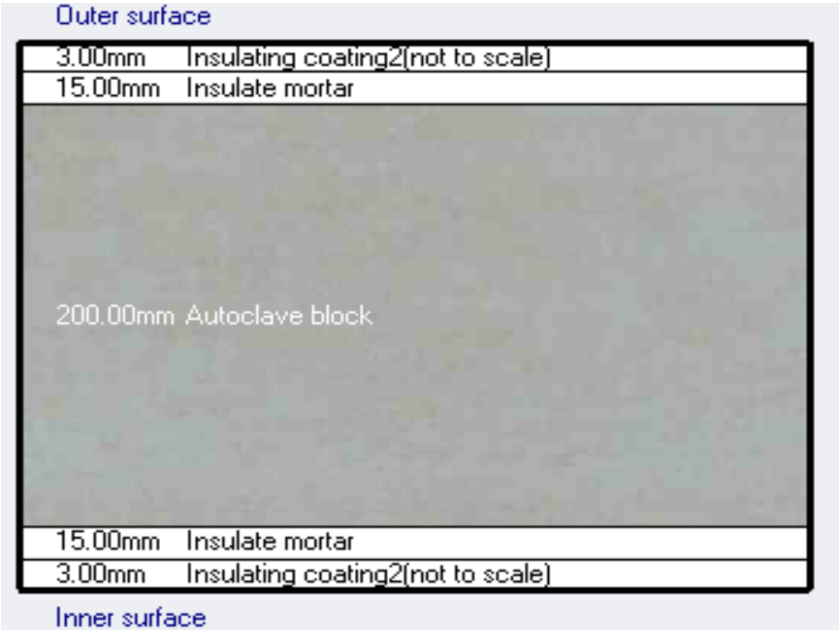

Figure 5.10: Cross section of TR4 walls.

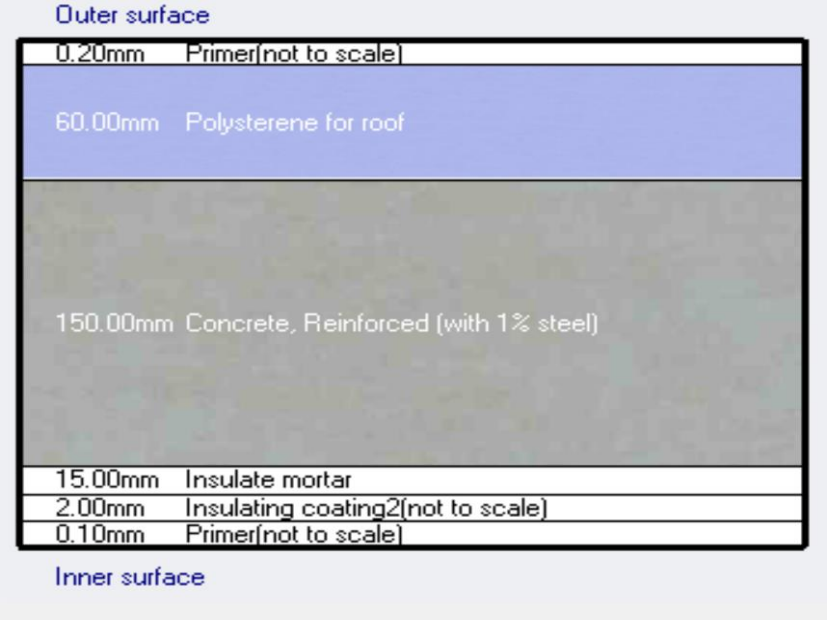

Figure 5.11: Cross section of the roof in TR1 and TR4.

5.4.1.6 Test rooms openings

The door and window were the same in all test rooms as explained in Chapter 3 and the same location as show in Figures 5.12 and 5.13.

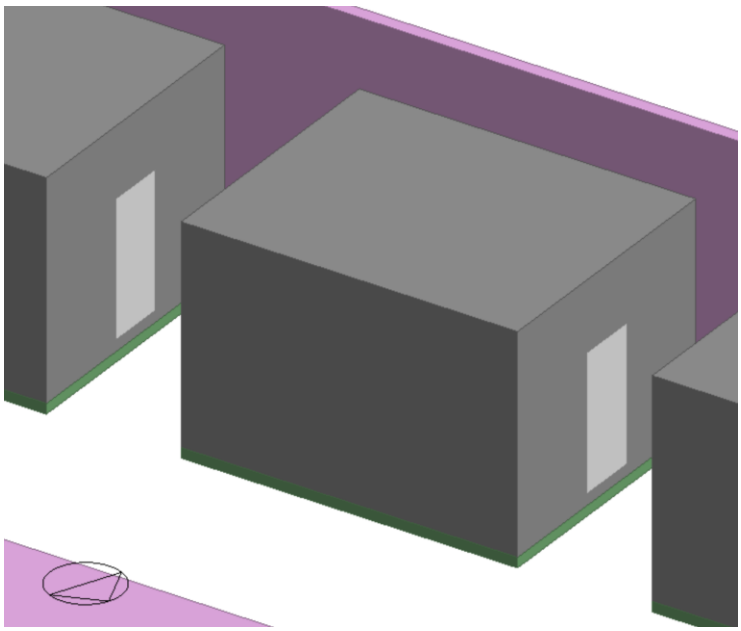

Figure 5.12: Doors of the test rooms in the model.

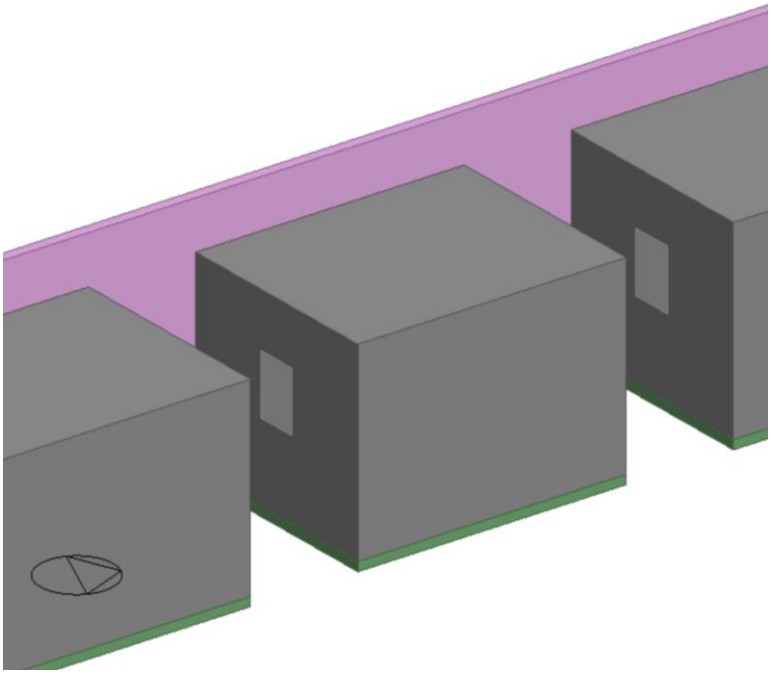

Figure 5.13: Windows of the test rooms in the model.

5.4.1.7 HVAC

Split air conditioner used in all the test rooms was modeled to run 24 hours on the summer season at 24°C and 20°C like it was set in the site.

5.4.2 Simulation results

5.4.2.1 TR1

5.4.2.1.1 Energy results

The energy consumption in TR1 at different periods with different setting temperature of A/C from the experimental test and modeling using Designbuilder are numerically presented in Table 5.1 and schematically depicted in Figure 5.14. The energy consumption values resulted from the experimental measurement and modeling are close to each other. The maximum difference between the results from actual measurement and

modeling during all periods and different setting temperature of A/C was 4.4% which is considered low from practical point of view thereby the agreement between the results can be considered as excellent. This is considered as excellent modeling validation for the experimental measurements. Therefore, the values of convective heat transfer coefficient of both outer and inner surfaces (h_i and h_o) of walls in TR1 obtained from modeling are acceptable.

Table 5.1: Energy consumption in TR1.

Period	A/C temp., °C	Energy consumption, kwh		% Difference between Modeling and Experimental results
		Modeling	Experimental	
1 to 21-July	24	402	398	1.00
22 to 30 July	20	229	228	0.44
31-Julu to 6 August	24	135	136	0.74
7 to 15 August	20	239	250	4.40
16 to 31 August	24	323	332	2.71
September	24	490	496	1.21

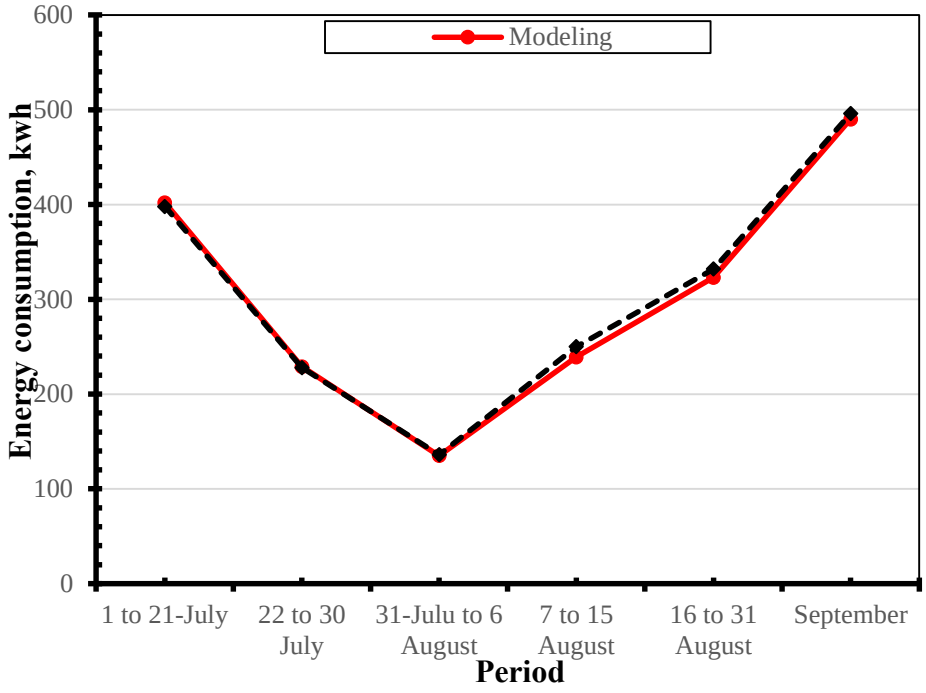

Figure 5.14: Energy consumption in TR1.

5.4.2.1.2 Temperature results

The inside surface temperature of the walls and roof in TR1 measured experimentally using thermocouples, as explained in Chapter 4, and calculated numerically using DesighnBuilder program during the period from 1st to 21th July with A/C setting temperature of 24°C are depicted in Figure 5.15. The temperature results from modeling show good agreement with the experimental measurement. This confirms that TRI model validates the experimental result and the values of convective heat transfer coefficient of both outer and inner surfaces (h_i and h_o) of walls in TR1 obtained from modeling are acceptable.

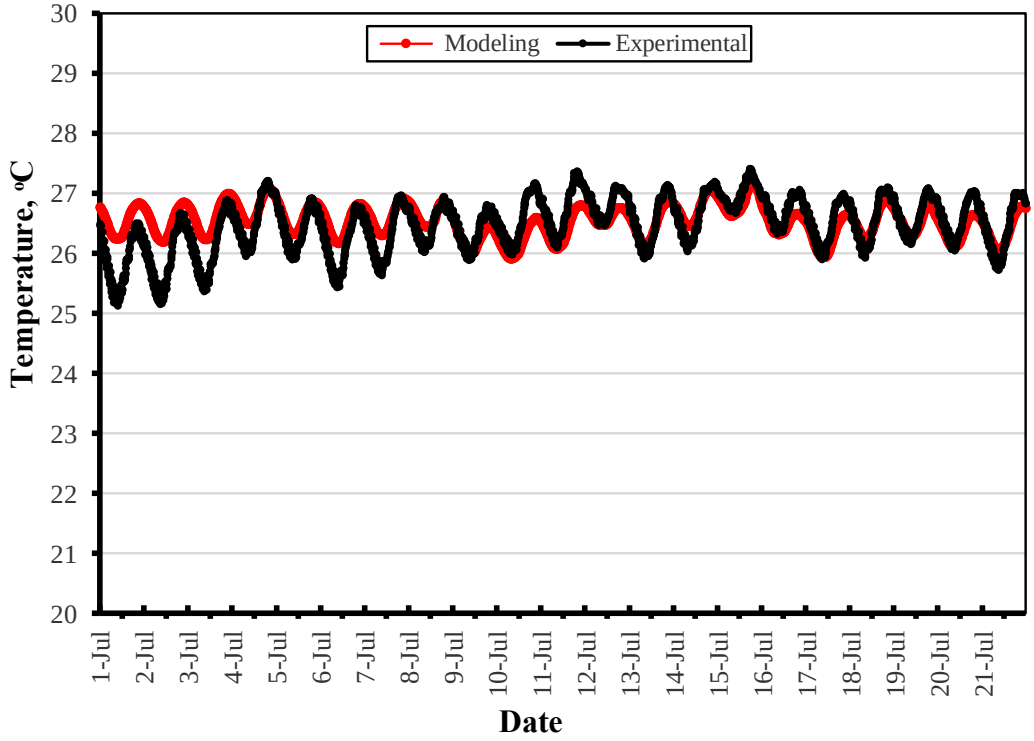

Figure 5.15: Comparison of inside surface temperatures of TR1 walls from experimental test and modeling.

The average convective heat transfer coefficient during each period of constant setting temperature of A/C obtained from TR1 modeling is summarized in Table 5.2.

Table 5.2: Convective heat transfer coefficients of both outer and inner surfaces (h_i and h_o) of walls in TR1.

Period	A/C temp., °C	h_i, W/(m²k)	h_o, W/(m²k)
1 to 21-July	24	1.55	20
22 to 30 July	20	1.70	20
31-Julu to 6 August	24	1.60	20
7 to 15 August	20	1.90	20
16 to 31 August	24	1.40	20
September	24	1.40	18

5.4.2.2 TR2

5.4.2.2.1 Energy results

The energy consumption results in TR2 (the Reference test room) at different periods with different setting temperature of A/C which was calculated using modeling, show good agreement with the experimental results as demonstrated numerically in Table 5.3 and depicted schematically in Figure 5.16. The maximum difference between the experimental measurement and modeling calculations was 2.83%, which is considered as low from practical point of view thereby the agreement between the results can be considered as excellent. The values of convective heat transfer coefficient of both outer and inner surfaces (h_i and h_o) of walls in TR2 obtained from modeling are acceptable because of the excellent modeling validation for the experimental measurements.

Table 5.3: Energy consumption in TR2.

Period	A/C temp., °C	Energy consumption, kwh		% Difference between Modeling and Experimental results
		Modeling	Experimental	
1 to 21-July	24	654	666	1.8
22 to 30 July	20	333	330	0.90
31-Julu to 6 August	24	212	206	2.83
7 to 15 August	20	360	356	1.11
16 to 31 August	24	502	488	2.79
September	24	759	772	1.68

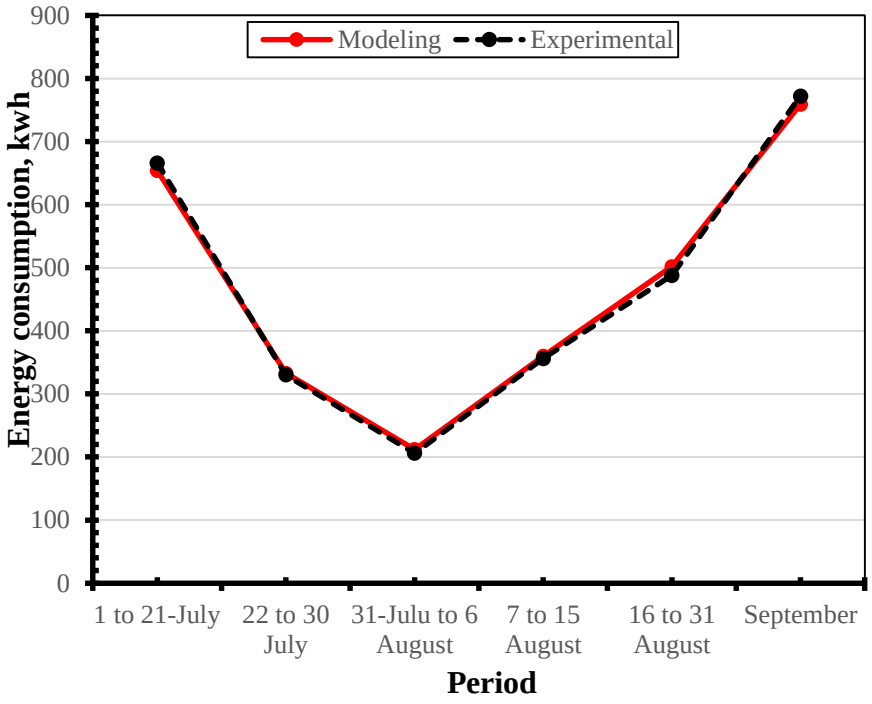

Figure 5.16: Energy consumption in TR2.

5.4.2.2.2 Temperature results

Figure 5.17 shows the inside surface temperatures of the walls during the period from 1st to 21th July with A/C setting temperature of 24°C from experimental measurement and modeling calculations. Good matching between the inside surface temperature values was obtained from the experimental measurement and modeling calculations. This proves the validation of TR2 model with the actual experimental work thereby proving that the values of convective heat transfer coefficient of both outer and inner surfaces (h_i and h_o) of walls TR2 obtained from modeling represent the exact values.

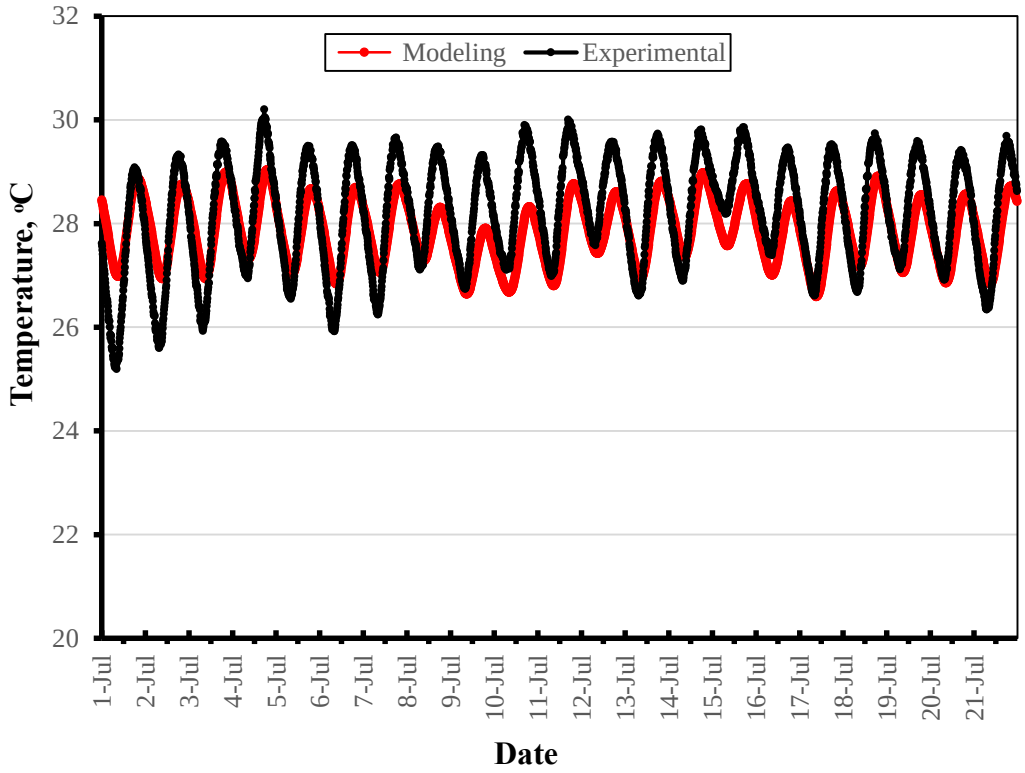

Figure 5.17: Comparison of inside surface temperatures of TR2 walls from experimental and modeling calculations.

The average convective heat transfer coefficient during each period with constant setting temperature of A/C obtained from TR2 modeling is summarized in Table 5.4.

Table 5.4: Convective heat transfer coefficient of both outer and inner surfaces (h_i and h_o) of walls in TR2.

Period	A/C temp., °C	h_i, W/(m²k)	h_o, W/(m²k)
1 to 21-July	24	2.55	25
22 to 30 July	20	2.50	25
31-Julu to 6 August	24	2.40	30
7 to 15 August	20	2.60	30
16 to 31 August	24	2.30	25
September	24	2.50	30

5.4.2.3 TR3

5.4.2.3.1 Energy results

The energy consumption in TR3 at different periods with different setting temperature of A/C from the experimental measurements and modeling calculations are numerically presented in Table 5.5 and schematically depicted in Figure 5.18. There was good matching between the energy consumption values from the experimental measurement and modeling calculations where the maximum difference between experimental and modeling calculations was less than 3.28% (except for September, which went up to 6.03%), which is considered relatively low from practical perspectives indicating that the agreement between the results can be considered as excellent. Due to this excellent modeling validation for experimental measurements, the values of convective heat transfer coefficient of both outer and inner surfaces (h_i and h_o) of walls in TR3 from modeling are acceptable and they represent the actual values.

Table 5.5: Energy consumption in TR3.

Period	A/C temp., °C	Energy consumption, kwh		% Difference between Modeling and Experimental results
		Modeling	Experimental	
1 to 21-July	24	424	430	1.40
22 to 30 July	20	236	244	3.28
31-Julu to 6 August	24	142	146	2.74
7 to 15 August	20	258	266	3.01
16 to 31 August	24	356	354	0.56
September	24	530	564	6.03

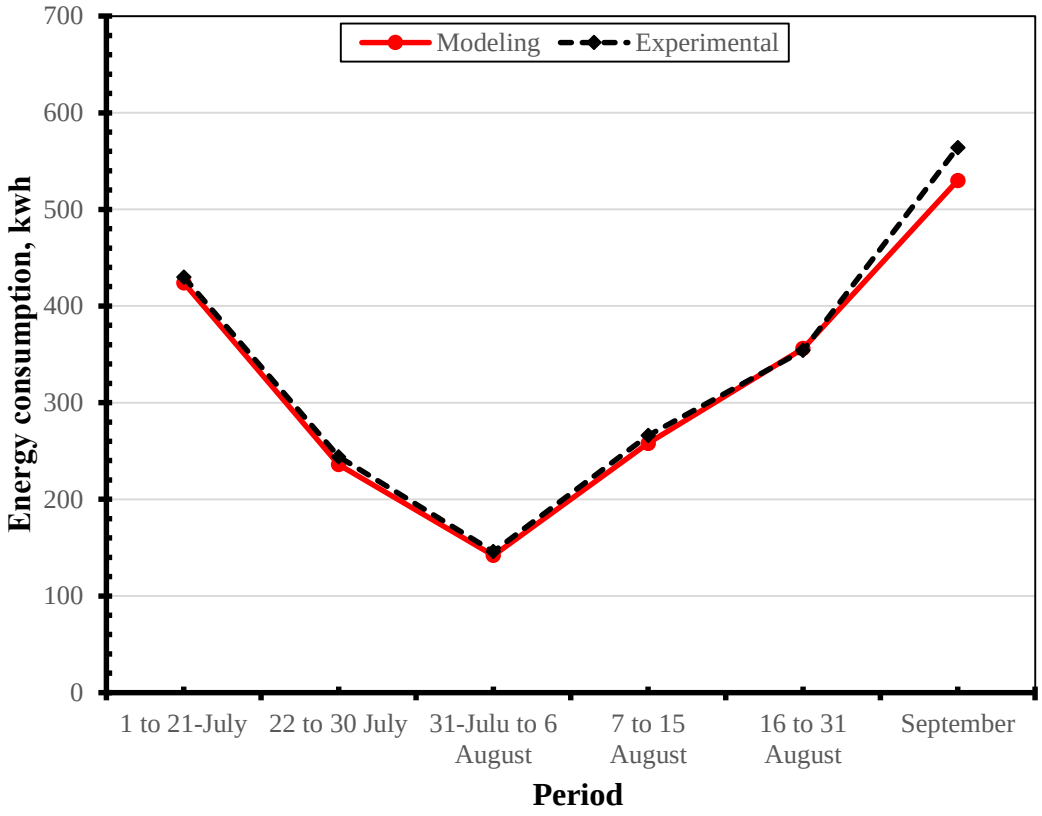

Figure 5.18: Energy consumption in TR3.

5.4.2.3.2 Temperature results

The inside surface temperature of walls and roof in TR3 measured experimentally; using thermocouples as explained in Chapter 4; and calculated numerically using DesighnBuilder program during the period from 1st to 21th July with A/C setting temperature of 24°C, are depicted in Figure 5.19. This good agreement between the results from experimental and modeling calculations confirm the ability of modeling techniques to simulate the actual conditions in the site. Therefore, the values of convective heat transfer coefficient of both outer and inner surfaces (h_i and h_o) of the walls in TR3 obtained from modeling represent the exact values.

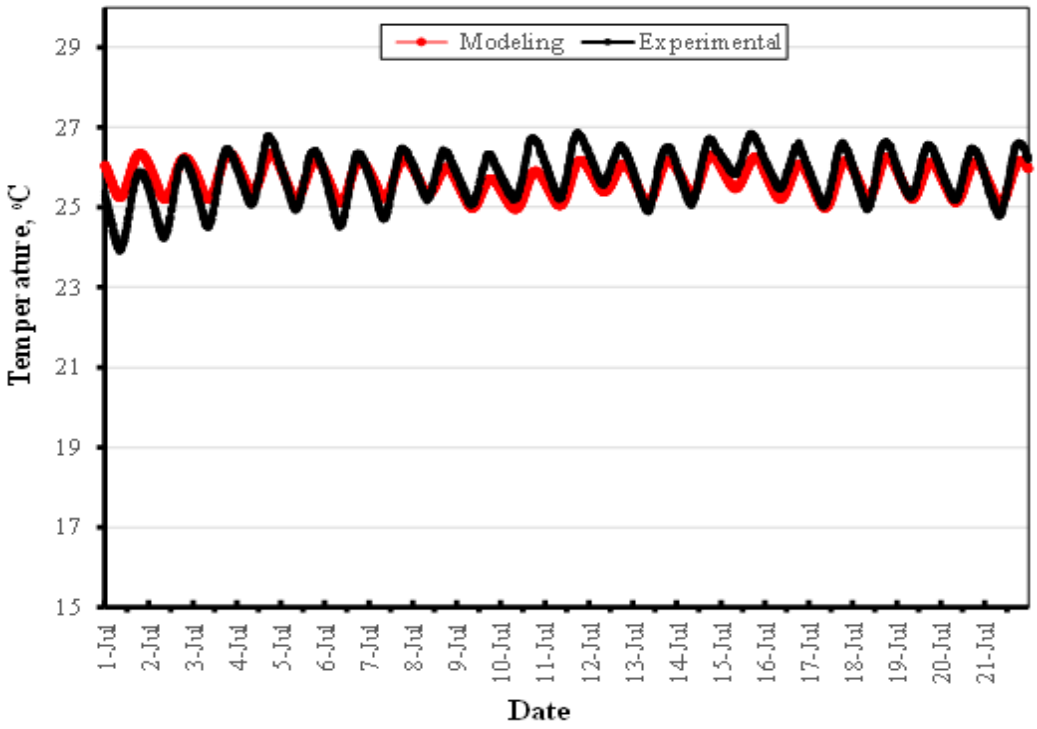

Figure 5.19: Comparison of inside surface temperatures of TR3 walls from experimental test and modeling.

The average convective heat transfer coefficient during each period with constant setting temperature of A/C obtained from TR3 modeling is summarized in Table 5.6.

Table 5.6: Convective heat transfer coefficient of both outer and inner surfaces (h_i and h_o) of walls in TR3.

Period	A/C temp., °C	h_i, W/(m²k)	h_o, W/(m²k)
1 to 21-July	24	2.9	25
22 to 30 July	20	3.2	25
31-Julu to 6 August	24	2.9	20
7 to 15 August	20	3.2	22
16 to 31 August	24	2.9	25
September	24	3.2	20

5.4.2.4 TR4

5.4.2.4.1 Energy results

The energy consumption in TR4 at different periods with different setting temperatures of A/C from the experimental measurements and modeling calculations are demonstrated in Table 5.7 and drawn in Figure 5.20. The maximum difference between the experimental and modeling calculations at different periods and different temperatures was 4.76%, which is considered low from practical point of view, hence, the agreement between the results can be considered as excellent. Therefore, the values of convective heat transfer coefficient of both outer and inner surfaces (h_i and h_o) of walls in TR4 obtained from modeling represent the actual values.

Table 5.7: Energy consumption in TR4.

Period	A/C temp., °C	Energy consumption, kwh		% Difference between Modeling and Experimental results
		Modeling	Experimental	
1 to 21-July	24	256	264	3.03
22 to 30 July	20	157	154	1.91
31-Julu to 6 August	24	85	86	1.16
7 to 15 August	20	167	168	0.60
16 to 31 August	24	210	200	4.76
September	24	304	308	3.80

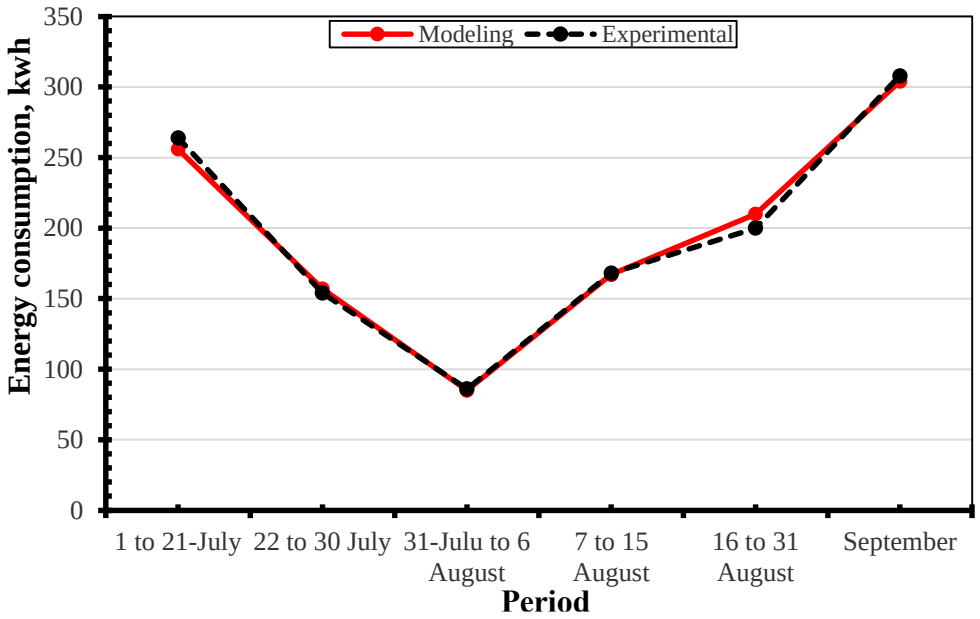

Figure 5.20: Energy consumption in TR4.

5.4.2.4.2 Temperature results

Figure 5.21 depicts the inside surface temperature of walls and roof in TR4 during a typical period from 1st to 21th July with A/C setting temperature of 24°C from experimental measurements and modeling calculations. The inside surface temperature values from walls and roof in TR4 measured experimentally was less than those resulted from modeling calculation by about 0.7°C because of the high RH inside TR4, as explained in Chapter 4, which was ascribed to high moisture content of insulation materials used in walls thereby decreasing the temperature on the walls. Modeling results are more accurate than those from the experimental measurements because the moisture content of the insulation materials in modeling is not high as it is in actual. Therefore, the values of convective heat transfer coefficient of both outer and inner surfaces (h_i and h_o) of walls in TR4 obtained from modeling represent the accurate values.

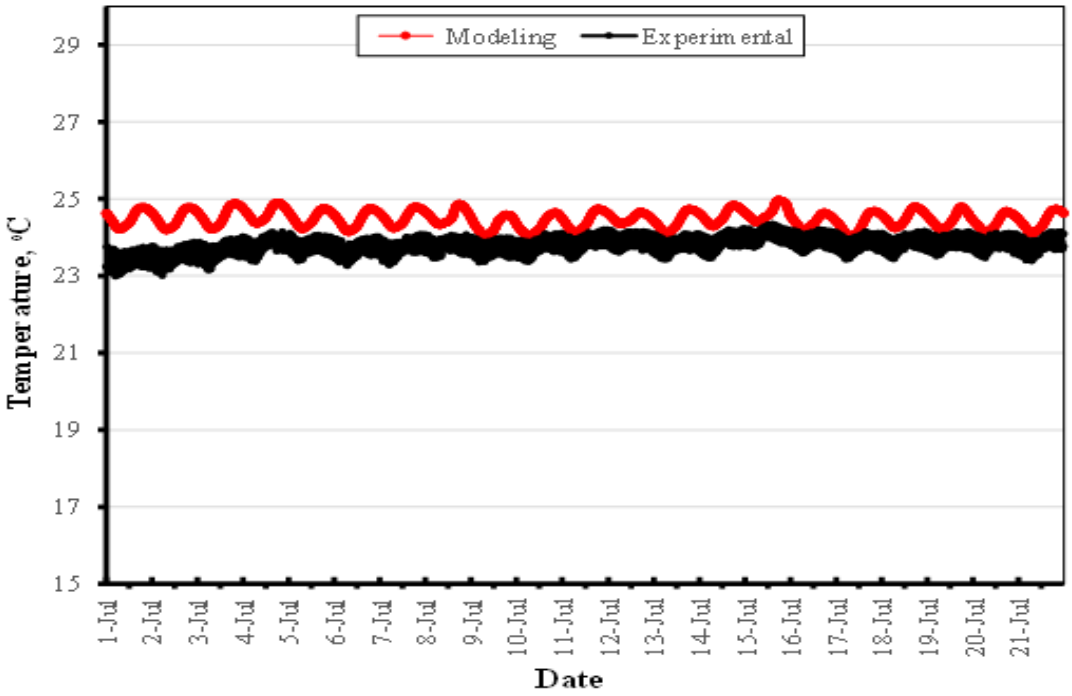

Figure 5.21: Comparison of inside surface temperatures of TR4 walls from experimental test and modeling.

The average convective heat transfer coefficient during each period with constant setting temperature of A/C obtained from TR4 modeling is summarized in Table 5.8.

Table 5.8: Convective heat transfer coefficient of both outer and inner surfaces (h_i and h_o) of walls in TR4.

Period	A/C temp., °C	hi, W/(m²k)	ho, W/(m²k)
1 to 21-July	24	2	20
22 to 30 July	20	2.2	20
31-Julu to 6 August	24	2	20
7 to 15 August	20	1.8	20
16 to 31 August	24	1.5	20
September	24	1.6	20

5.5 Total thermal resistance (R_T) of walls including the effect of heat convective coefficient

The heat convective coefficient of the inner and outer surfaces of walls in all test rooms obtained from modeling during the same period of which the surface resistance of walls was measured in the experimental work is presented in Table 5.9. The inner and outer surface resistances of walls calculated using Equations 4.7 and 4.8 is also presented in Table 5.9. The total thermal resistance of walls in all test rooms calculated using Equation 4.6, which is the summation of the inner and outer surface resistances of walls and the thermal resistance of walls (surface to surface) calculated using Equation 4.1, is presented in Table 5.10.

Table 5.9: The heat convective coefficient of the inner and outer surfaces of walls in all test rooms.

Test room	h_i, W/(m²k)	h_o, W/(m²k)	R_{is}, m²k/W	R_{os}, m²k/W
TR1	1.4	19	0.71	0.053
TR2	2.4	25	0.42	0.040
TR3	3.05	20	0.33	0.050
TR4	1.55	20	0.65	0.050

Table 5.10: Total thermal resistance of walls in all test rooms.

Test room	R_{is}, m²k/W	R_{os}, m²k/W	R, m²k/W	R_T, m²k/W
TR1	0.71	0.053	0.87	1.64
TR2	0.42	0.040	0.34	0.80
TR3	0.33	0.050	1.15	1.53
TR4	0.65	0.050	2.04	2.74

CHAPTER SIX

FINITE ELEMENT MODELING OF TEST ROOMS WALLS

6.1 General

A 3D finite element model (FEM) of each wall constructed in the four test rooms was developed using ABAQUS 6.13 software to find the inside/outside surface temperatures of walls. Moreover, FEM simulates the heat transfer through the different layers of the materials used for constructing the wall considering the thermal properties of these materials, the internal cavities and the actual thermal conditions around the wall. The effectiveness of different insulation materials used in the walls could be assessed by comparing the average inside surface temperature from walls.

The FEM of each test room wall considers the heat transfer through the wall by the following three processes: radiation, convection and conduction, which were explained in Section 5.3. The FEMs of test rooms walls were developed according to the following scheme:

6.2 Mathematical modeling

The heat is transferred from outside the building to inside during the summer through one or more of the following three processes: radiation, convection and conduction, as shown in Figure 6.1 [102,103]. The boundary conditions can be represented mathematically as follows:

At outside surface x=0,

$$q_{cond} = q_{rad.} + q_{solar} + q_{conv.} \quad (6.1)$$

$$-k\frac{\partial T}{\partial x} = q_{solar} + h_{co}\left(T_{air} - T_{surf}\right) + \varepsilon\sigma\ ({T^4}_{air} - {T^4}_{surf}) \quad (6.2)$$

where:

T = Temperature (K).

K = Thermal conductivity [W/(m.K)].

h_{co} = Convection coefficient of outside surface [W/(m².K)].

T_{surf} = Surface temperature (K).

T_{air} = Air temperature (K).

ε = Emittance of the surface.

σ = Stefan-Boltzmann constant [W/(m^2·K^4)].

At inside surface x=d (thickness of the wall),

$$-k\frac{\partial T}{\partial x} = h_{ci}\left(T_{surf} - T_{air}\right) + \varepsilon\sigma\ ({T^4}_{surf} - {T^4}_{air}) \quad (6.3)$$

where:

h_{ci}= Convection coefficient of inside surface [W/(m².K)].

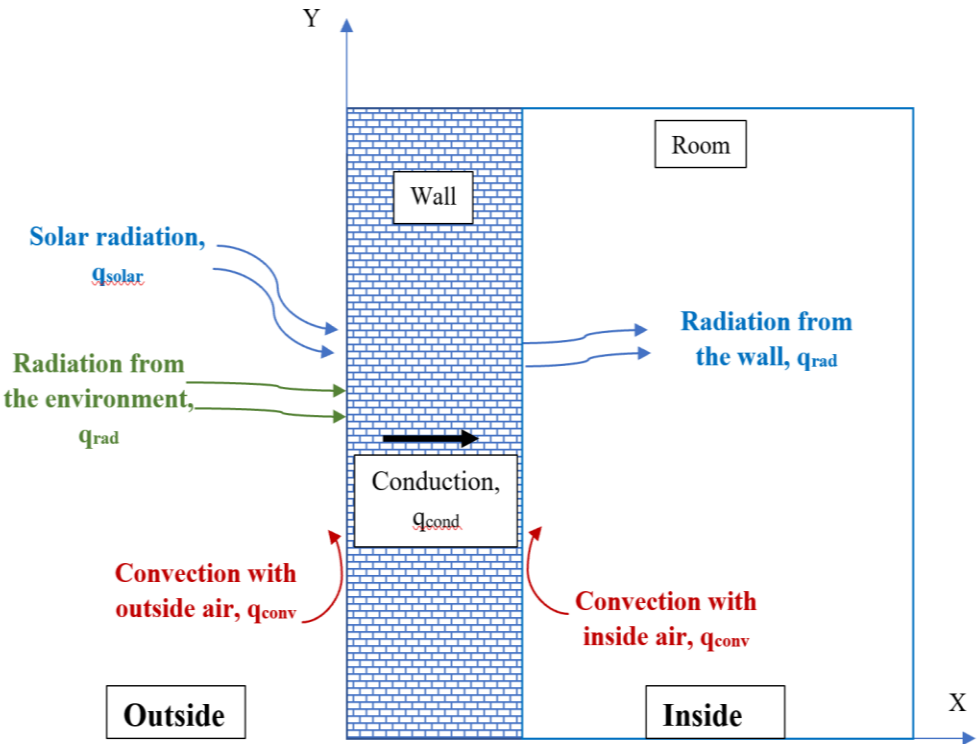

Figure 6.1: Modeling of thermal processes through wall.

6.3 Finite element model

The FEMs of test rooms walls were developed according to the following steps:

6.3.1 Geometry of the test rooms walls

The walls of the test rooms were modeled in ABAQUS 6.13 software by taking a typical surface on the middle of West wall; 1x1 m. The block size in TR1, TR2 and TR3 was 20x20x40 cm, while it was 20x20x60 cm in TR4. Therefore, two and half blocks in the length were considered in the length of this typical surface in TR1, TR2 and TR3. However, one and two thirds of blocks only were considered in TR4. Five rows of blocks in the height were included in this typical modeled surface. Figure 6.2 depict the geometry of the modeled normal hollow-core concrete used in TR1 and TR2.

The modeled insulate polystyrene block used in TR3 is shown in Figure 6.3. In the type of block, there were three parts; two parts of concrete blocks connected by the third part which was the polystyrene leaf. The interaction between these three parts was modeled as a tie contact to make certain the heat is transfered through the conduction process during the modeling.

Figure 6.4 depicts the modeled insulate aerated block used in TR4. The cement mortar model used in TR1, TR2 & TR3 and the insulate mortar model used in TR4 used in TR4 are depicted Figures 6.5 and 6.6; respectively. Figure 6.7 shows the cement plaster layer model used in TR1, TR2 and TR3, while Figure 6.8 depicts the insulate plaster model used in TR4. Figure 6.9 depicts the INSULATE coating layer model applied on the plaster in TR1. The model of paint applied on the plaster in TR2 and TR3 is shown in Figure 6.10. The 3D dimensions of all models were exact like what was done in the site during the construction as was explained in Chapter 3.

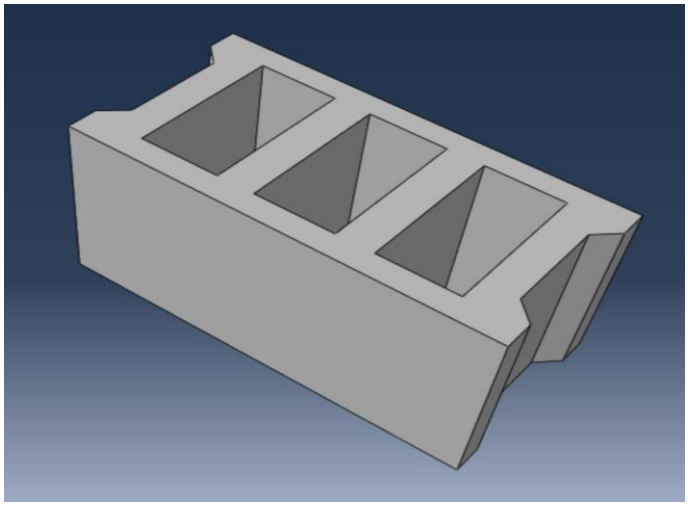

Figure 6.2: Model of block type used in TR1 and TR2.

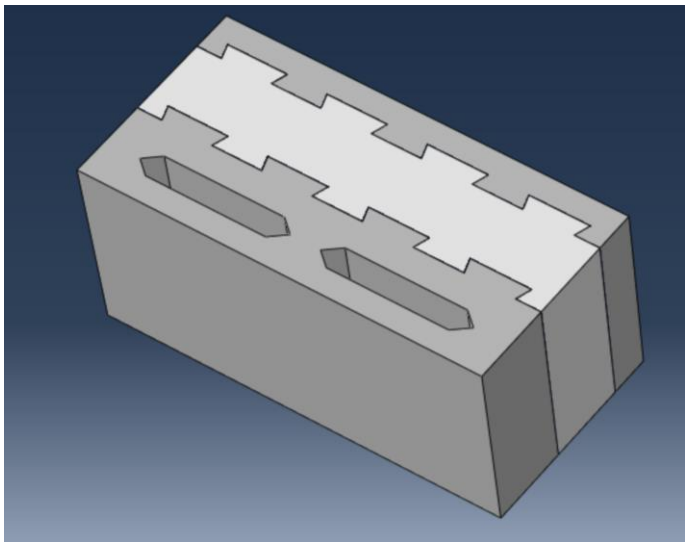

Figure 6.3: Model of block type used in TR3.

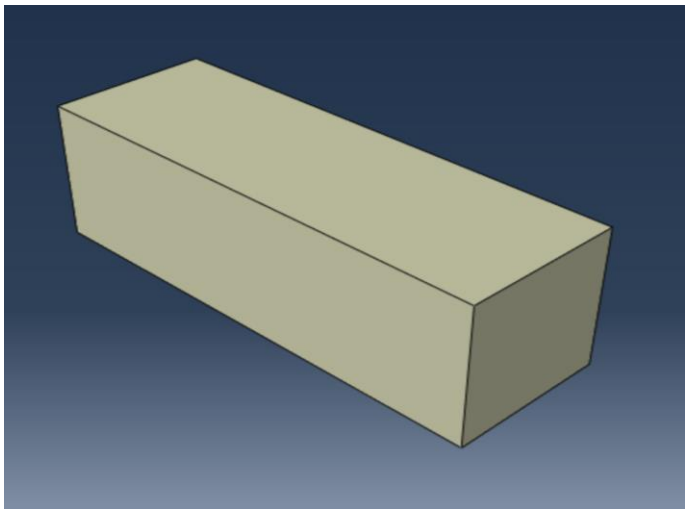

Figure 6.4: Model of block type used in TR4.

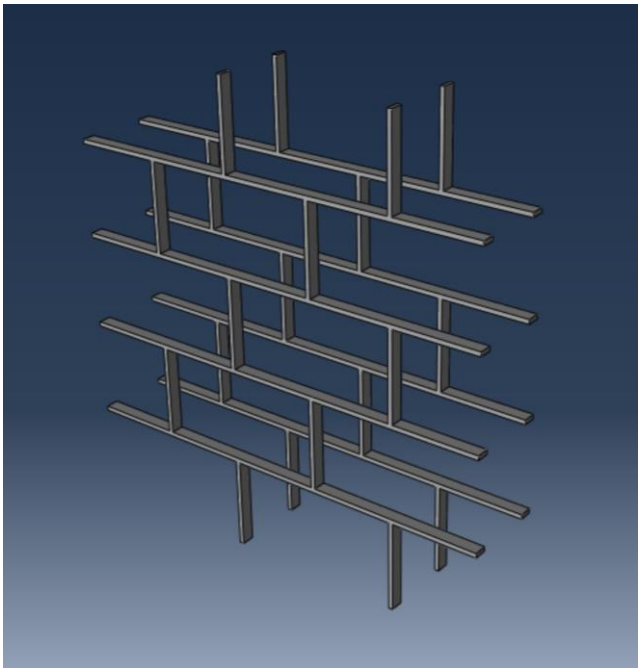

Figure 6.5: Model of mortar applied in TR1, TR2 and TR3.

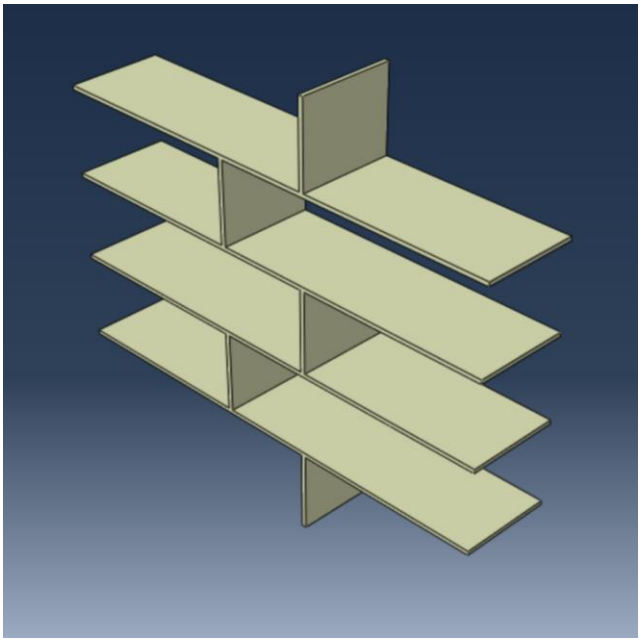

Figure 6.6: Model of insulate mortar applied in TR4.

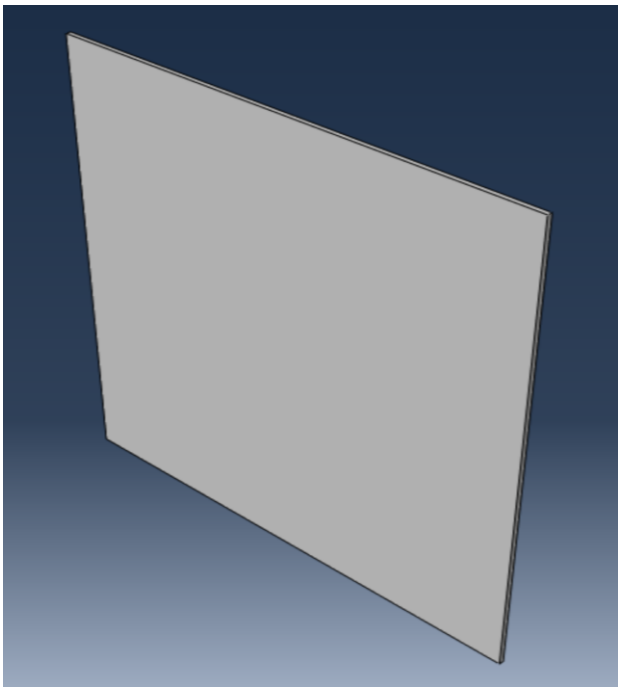

Figure 6.7: Model of plaster applied in TR1, TR2 and TR3.

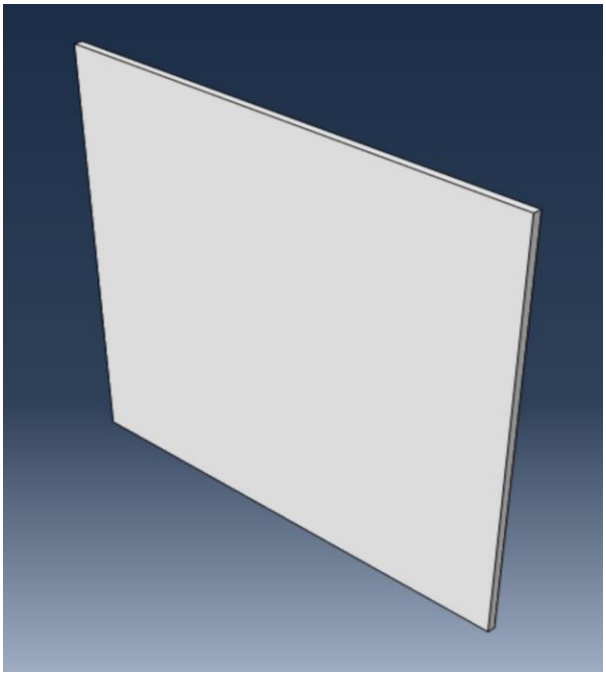

Figure 6.8: Model of insulate plaster applied in TR4.

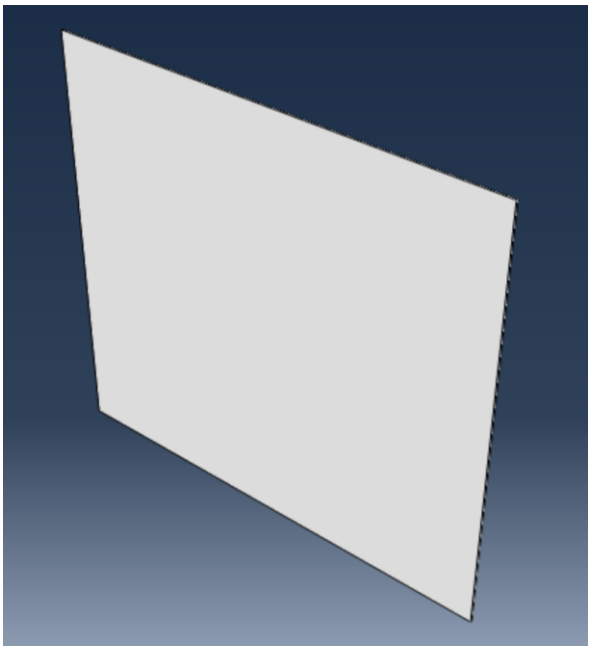

Figure 6.9: Model of insulate coating applied on plaster in TR1.

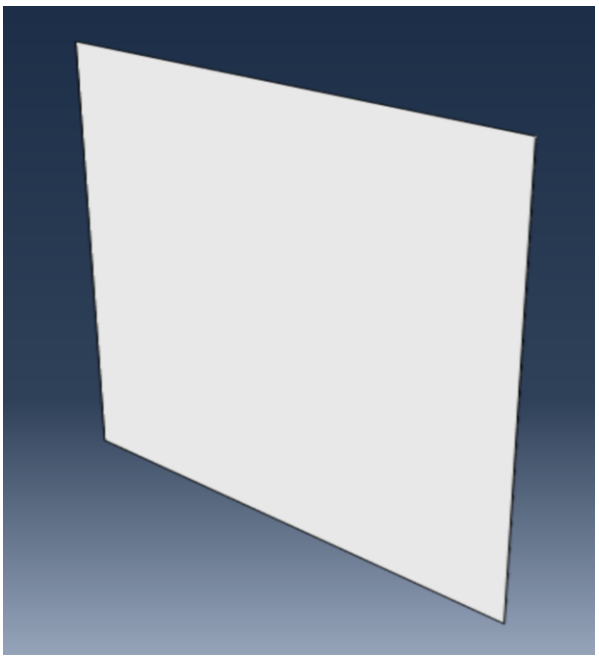

Figure 6.10: Model of paint applied on plaster in TR2 and TR3.

6.3.2 Thermal properties of materials

The thermal properties of the materials used in FEMs were obtained from the experimental test results and from the simulation of the test rooms in Chapter 5 which was done using DesignBuilder software. Thermal conductivity values of the materials are presented in **Table 6.1**.

Table 6.1: Thermal conductivity of materials used in FEMs.

Material	k, W/(m.K)
Hollow concrete block	0.720
Cement mortar	0.720
Cement plaster	0.720
Insulate block	0.163
Insulate coating	0.030
Insulate mortar	0.063
Insulate plaster	0.063
Primer paint	0.200
Polystyrene	0.060

The solar absorption (α) of the walls depends on the outer and inner layers of the wall which were painted by primer emulsion in TR2 and TR3, while they were treated with INSULATE coating in TR1 and TR4. The normal paint has low solar reflectivity; 30% [100]; whereas the INSULATE coating has high solar reflectivity; 90%; as explained in Chapter 4. Therefore, α was 0.7 in TR2 and TR3, while it was 0.1 in TR1 and TR4.

The emissivity (ε) of outside and inside surfaces was 0.9 in all rooms which was taken from thermal properties of outermost layer on wall [104,105]. Stefan-Boltzmann constant is equal to 5.67×10^{-8} [$W/(m^2 .K^4)$].

The film coefficient of inner and outer surfaces of the walls in all the test rooms was obtained from the simulation using Designbuilder software in Chapter 5. Table 6.2 presents the film coefficient of inner and outer surfaces of walls in all test room used in FEMs.

Table 6.2: Film coefficient of inner and outer surfaces of walls in all test rooms used in FEMs.

Test room	h_i, W/(m²k)	h_o, W/(m²k)
TR1	1.55	20
TR2	2.55	25
TR3	3.2	20
TR4	2	20

The convection and radiation for holes in the hollow concrete blocks in TR1 and TR2 were based on the equivalent film coefficient (h_{eq}), as reported in EN ISO 6946 standard [106].

$$h_{eq} = h_a + h_r \quad 6.4$$

where

h_a = Convection film coefficient which is higher value between 1.25 W/(m^{2}K) and $(\frac{0.025}{d})$.

where

d = Thickness of the air cavity (mm).

For unventilated airspaces with cavity length and cavity width both more than 10 times cavity thickness:

$$h_r = \frac{h_{r0}}{\frac{1}{\varepsilon_1} + \frac{1}{\varepsilon_2} - 1} \quad (6.5)$$

where

h_{ro} = Radiative coefficient for black body surface [W/(m².K)].

ε_1 = Emissivity of the hot surface of the air cavity.

ε_2 = Emissivity of the cold surface of the air cavity.

For small airspaces with a cavity width less than ten times its thickness:

$$h_r = \frac{h_{r0}}{\frac{1}{\varepsilon_1} + \frac{1}{\varepsilon_2} - 2 + \frac{2}{(1 + \sqrt{1 + \frac{d^2}{b^2}} - \frac{d}{b})}} \quad (6.6)$$

where

d = Thickness of the air cavity (mm).

b = Width of the air cavity (mm).

The equivalent film coefficient *(h_{eq})* has been estimated for hollow concrete block in TR1, TR2 and TR3 where it was 6 W/(m^2 K) [103].

6.3.3 Assembly and interaction of FEM

FEM of walls in each test room was constructed in dimensions of 1x1 m by assembling blocks, mortar, plaster and paint together as shown in Figures 6.11 to 6.13. The interaction between blocks, mortar, plaster, coating and paint was considered as tie contact to make certain the heat transfer through the thermal conduction process.

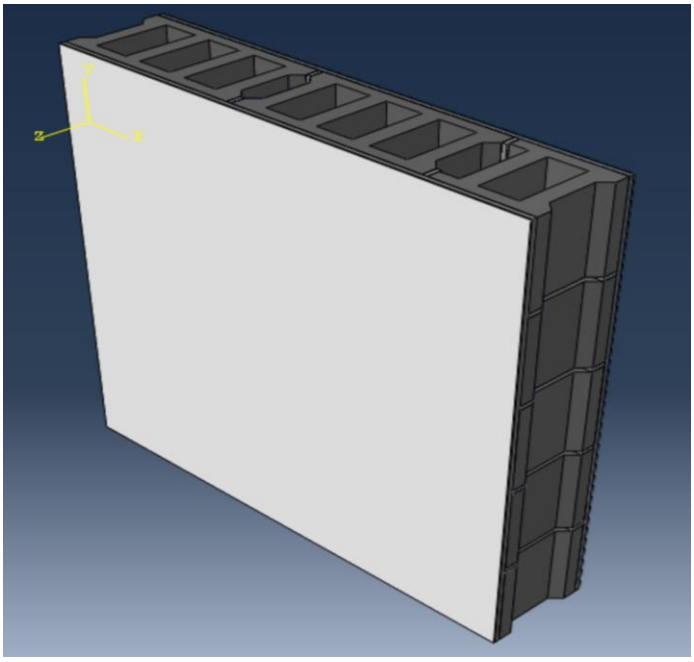

Figure 6.11: Model of wall in TR1 and TR2.

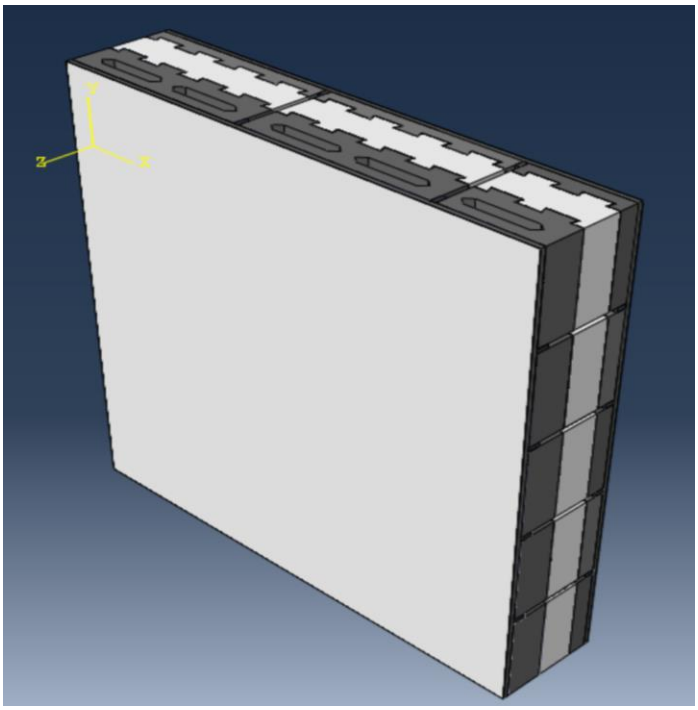

Figure 6.12: Model of wall in TR3.

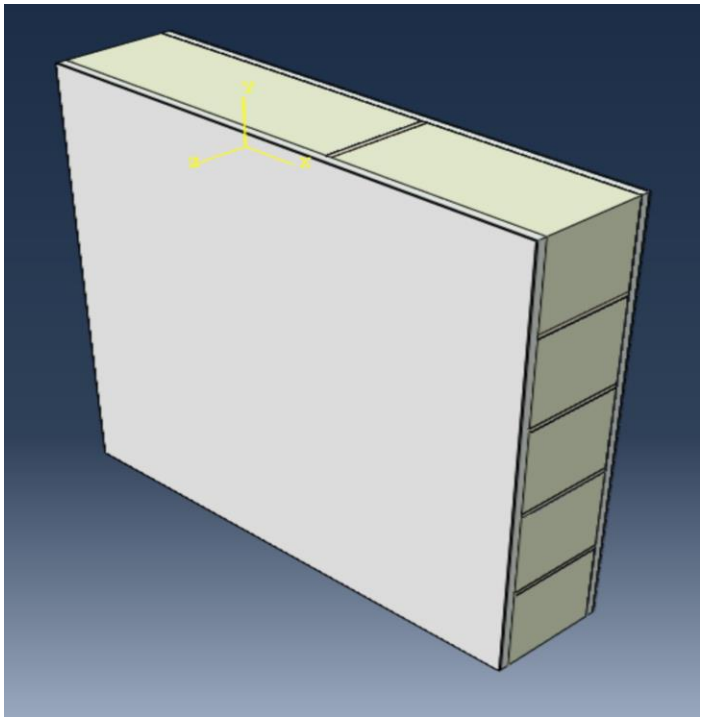

Figure 6.13: Model of wall in TR4.

6.3.4 Boundary conditions and loads for FEM

The three processes of heat transfer (i.e. radiation, convection and conduction) were considered in FEM. The boundary conditions, which were applied on FEM of walls, were taken from experimental measurement in specific location; middle of West wall; and at specific time; July 15 15:00. For the outside radiation and convection, the outside ambient temperature was 42°C (315°K) at that time and for the inside radiation and convection, the inside ambient temperature was 24°C (297°K). The film coefficient of the inside and outside surfaces of wall was taken from Table 5.9 in Chapter 5.

For the inside and outside radiation, the emissivity was 0.9. This value of the emissivity was taken from the energy simulation using DesignBuilder in Chapter 5. The convection and radiation for holes in the hollow concrete blocks in TR1 and TR2 were

based on equivalent film coefficient (h_{eq}) explained in Section 6.3.1. The equivalent film coefficient *(h_{eq})* in the hollow concrete blocks in TR1, TR2 and TR3 was (6 W/m^{2}K) when the sink temperature was 302, 306 and 301K in TR1, TR2 and TR3; respectively. These sink temperature values were found by calculating the average temperature between the inside two sides of block hole in each test room. The heat load, which was applied on FEM for this part of the West wall in all test rooms, was heat flux from the solar radiation applied at the time of investigation. The solar radiation on the west wall at 15:00 July 15 was 465 W/m².

6.3.5 Mesh optimization

In the preliminary simulation, mesh independence was conducted for each wall in each test room because the FEM results were changed with varying the geometry of the model. It was found that mesh size of 10 mm was the optimum to reduce the error and save time. Figure 6.14 shows the meshing of wall in TR1 and TR2, while Figures 6.15 and 16.6 depict the meshing of wall in TR3 and TR4; respectively.

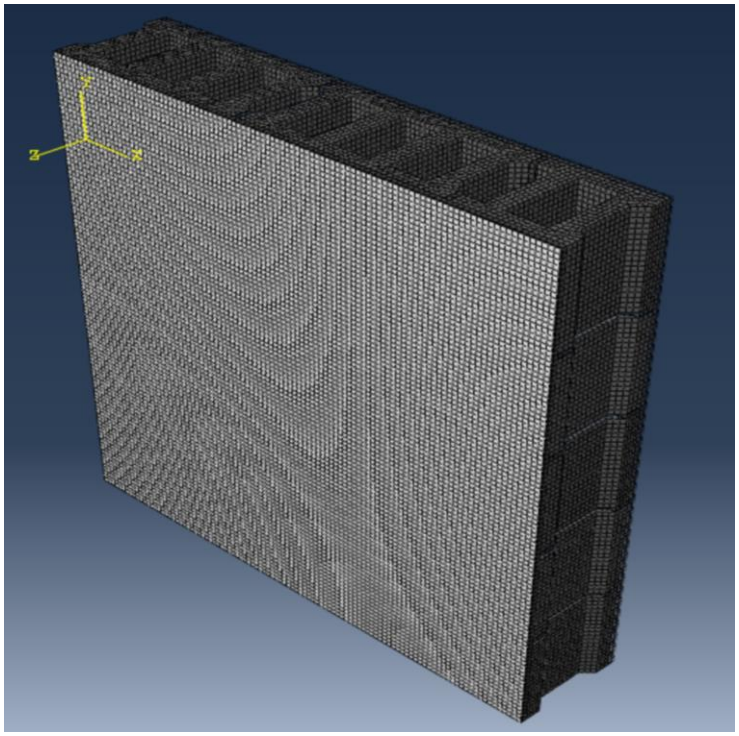

Figure 6.14: Meshing of wall in TR1 and TR2.

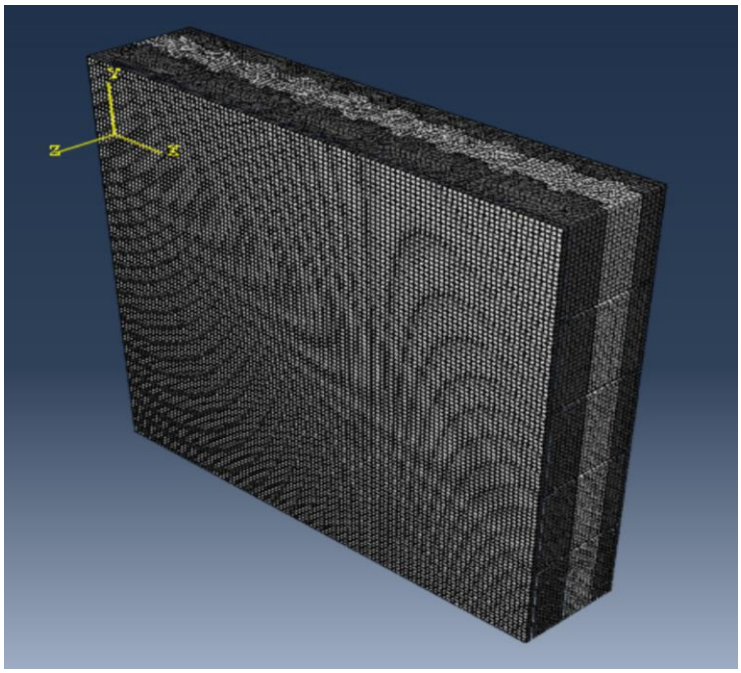

Figure 6.15: Meshing of wall in TR3.

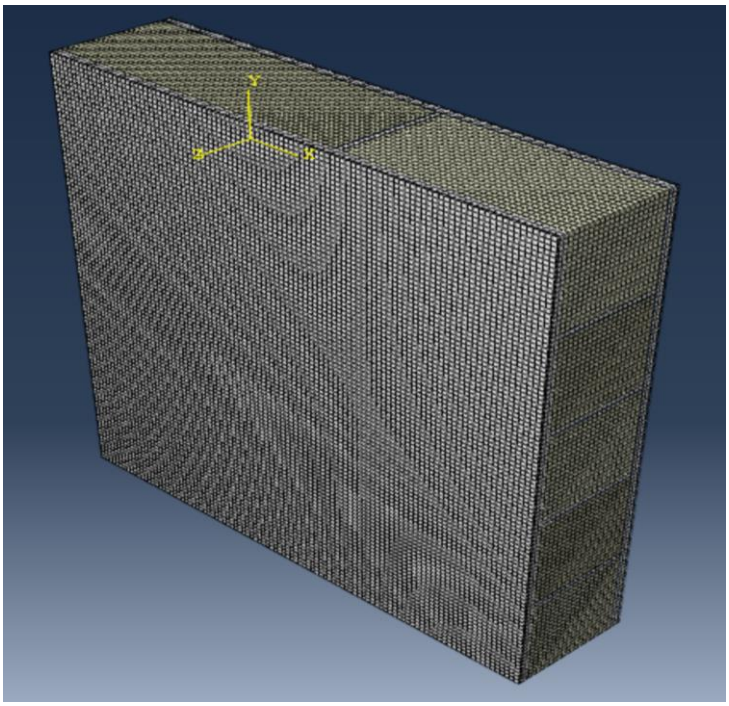

Figure 6.16: Meshing of wall in TR4.

6.3.6 Surface temperature results of Modeling

Figures 6.17 to 6.20 present he nodal temperature distribution (NT11) (in Kelvin scale) of the West wall in TR1, TR2, TR3 and TR4; respectively. The temperature distribution is depicted through the different colors from highest values (outer surface) to lowest values (inner surface) of the wall. The blue color indicates the lowest values, while the red color indicates the highest values of the surface temperatures. Comparison between the surface temperature results of inner and outer surface of the wall in each test room from experimental measurement and FE modeling is summarized in Table 6.3. The data in Table 6.3 indicates that there is good matching between the inner and outer surface temperature values from the experimental measurement and FE modeling

calculations where the maximum difference between experimental and modeling calculations in TR1, TR2 and TR3 was less than 2%. However, this difference was 5.43% for the inner surface temperature in TR4. This could be ascribed to the high moisture content of insulation materials used in walls, thereby decreasing the temperature on the walls as demonstrated in Chapter 5. The values of convective heat transfer coefficient of both outer and inner surfaces (h_i and h_o) of walls in TR3 obtained from FE modeling can be considered as reliable values with high percentage of accuracy because the agreement between experimental and modeling was excellent.

Table 6.3: Surface temperature results.

Test room	Surface temperature, °C				% Difference between Modeling and Experimental results	
	Experimental		Modeling			
	Inside	Outside	Inside	Outside	Inside	Outside
TR1	27.59	42.04	27.55	41.95	0.14	0.21
TR2	30.09	41.10	29.85	41.75	0.79	1.56
TR3	26.51	43.96	26.45	43.95	0.24	0.03
TR4	24.16	42.46	25.55	43.15	5.43	1.59

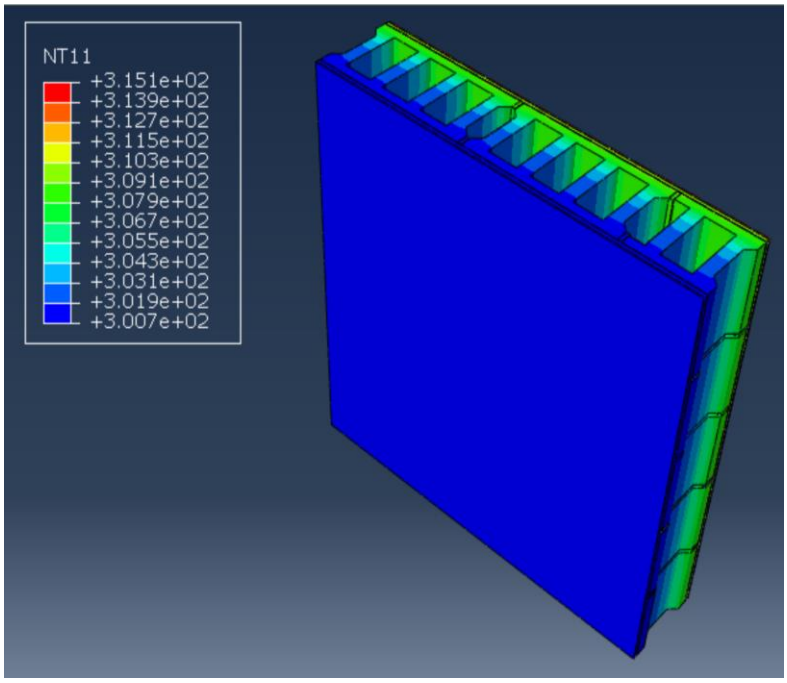

Figure 6.17: Nodal temperature distribution (NT11) (K) through the West wall in TR1.

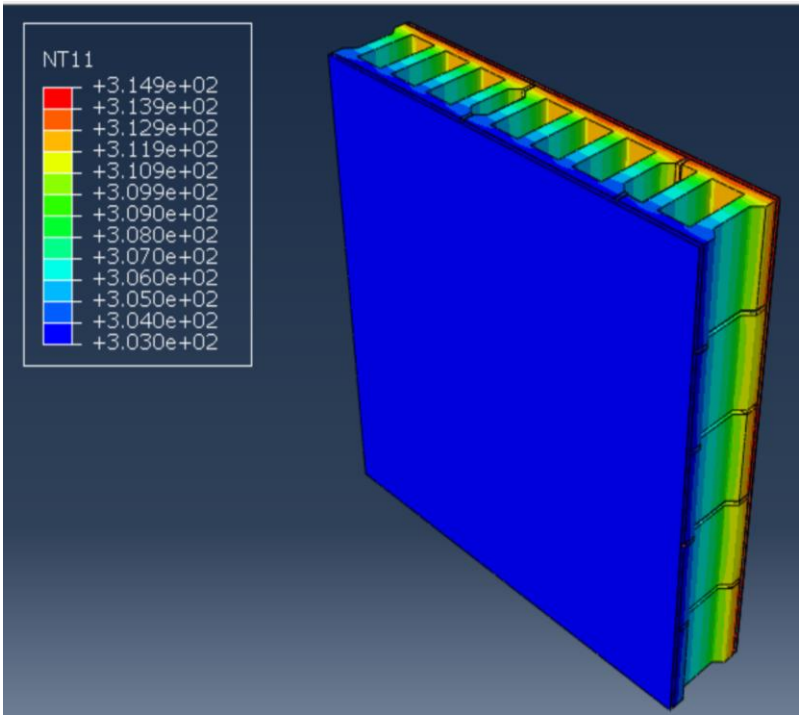

Figure 6.18: Nodal temperature distribution (NT11) (K) through the West wall in TR2.

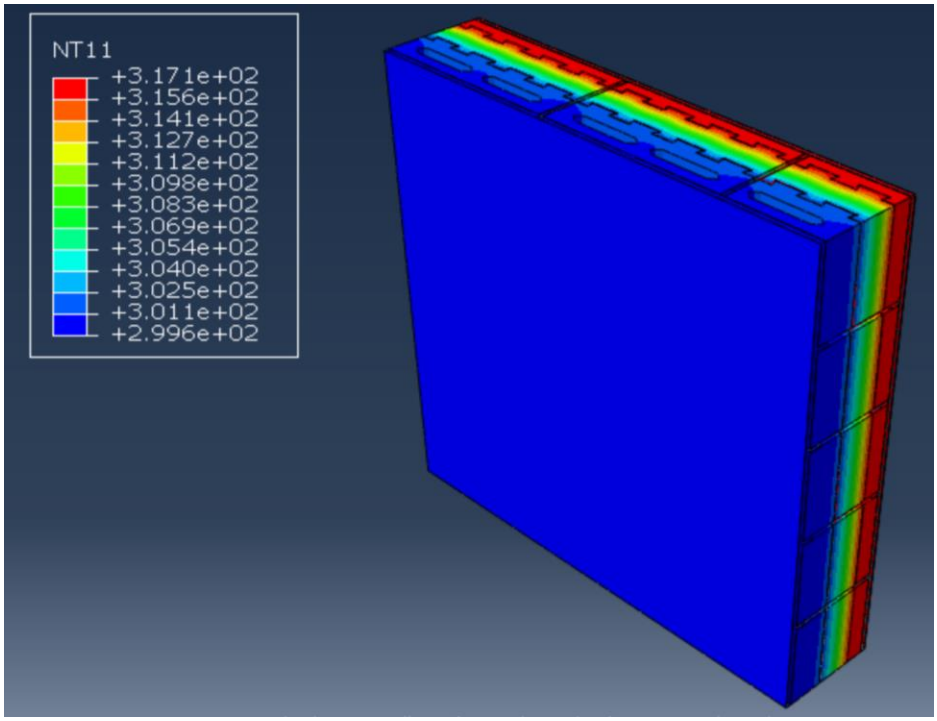

Figure 6.19: Nodal temperature distribution (NT11) (K) through the West wall in TR3.

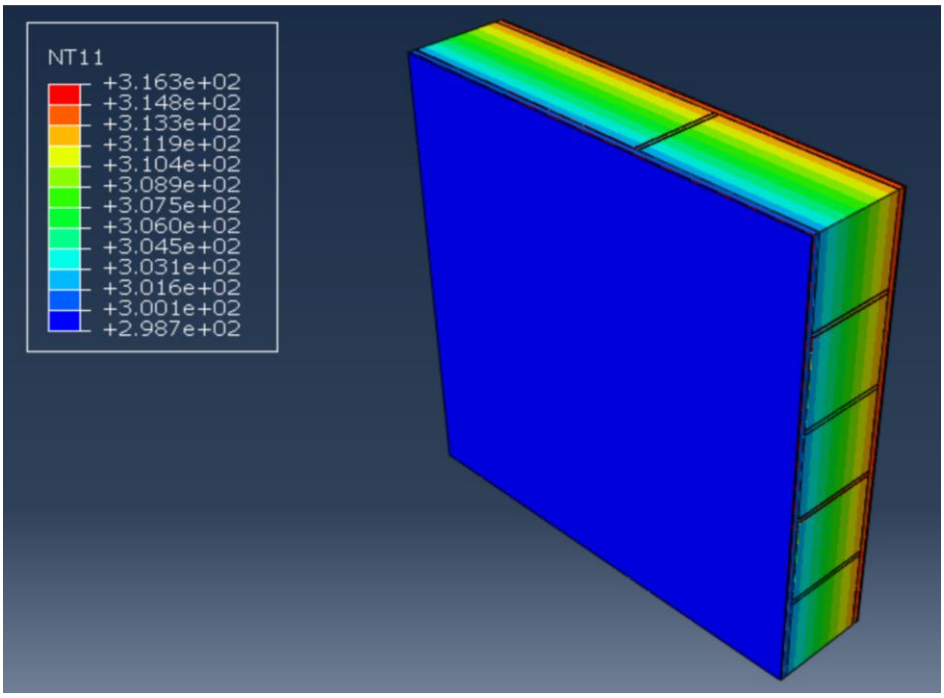

Figure 6.20: Nodal temperature distribution (NT11) (K) through the West wall in TR4.

CHAPTER SEVEN
CONCLUSIONS AND RECOMMENDATIONS

7.1 Conclusions

The study was conducted to assess the effectiveness of INSULATE coating applied on hollow concrete block walls in decreasing the heat transfer through the walls in buildings as compared with the walls constructed from normal hollow-core concrete blocks only, concrete block incorporating expanded polystyrene board or INSULATE aerated blocks with a plaster and INSULATE coating. The effectiveness of this insulation coating and other insulation materials in reducing the energy consumed to provide the thermal comfort for human during the summer session was experimentally and numerically investigated.

Four test rooms were constructed with these different insulation materials and were instrumented with temperature sensors, heat flux sensors, relative humidity sensors and energy meters. Further, a weather station was also installed in the site to measure the external environment parameters. The thermal performance and energy consumption of these test rooms with walls constructed with different insulation materials were monitored during the hottest summer months.

Based on the experimental tests and numerical simulation results developed in this investigation, the following conclusions could be drawn:

1. The performance of the four different test rooms was eventually assessed in term of the electricity consumption during the exposure period. Accordingly, the best performance was noted to be in TR4 (INSULATE aerated blocks, plaster and

coating) with a saving in electricity of 58% as compared with TR2 (the Reference Room), followed by TR1 (INSULATE coating) with 35% saving and then TR3 (concrete blocks incorporating expanded polystyrene board) with 29% of saving.

2. The superior performance of TR1 and TR4 is primarily ascribed to the presence of the hollow microspheres, which constitute the major component of the INSULATE coating layer in TR1 and TR4. These microspheres decreased both the heat flow and the thermal conductivity of this coating. They also enhanced the smoothness of the coating surface thereby reflecting most of the solar radiation.
3. 3-mm INSULATE coating layer on both sides of walls in TR1 constructed from normal hollow-core concrete blocks increases the total thermal resistance (R_T) of these walls by about 100%.
4. Based on the simulation using DesignBuilder software, the inside surface thermal resistance (R_{is}) of INSULATE coating in TR1 and TR4 was high compared with normal primer paint in TR2 and TR3 because this coating has very low heat convective coefficient. R_{is} of TR1, TR2, TR3 and TR4 was 0.71, 0.42, 0.33 and 0.65 m^2K/w; respectively.
5. The expanded polystyrene board embedded in concrete blocks in TR3 provides a significant barrier, reducing the heat flux through the walls and the inner surface temperature of walls by about 58% as compared with the walls constructed with hollow concrete blocks.
6. The total thermal resistance of walls constructed from hollow concrete blocks and 3-mm INSULATE coating layer on both sides is more than the total thermal resistance

(R_T) of walls constructed from concrete blocks incorporating expanded polystyrene boards by about 7%.

7. The surface temperature on INSULATE coating in TR1 and the heat flux measured on this coating were higher than those in TR3 because this coating has low heat convective coefficient which prevents exchanging the temperature between the surface of coating and the surrounding air in the room. This coating property is considered as an advantage because it leads to decrease the cooling load required to maintain the temperature inside the room.
8. The walls constructed from the new generation and state-of-the-art insulation system in TR4, which includes INSULATED aerated block, plaster and coating, have high thermal resistance compared with the single insulation coating system in TR1. The total thermal resistance of the walls constructed from this new insulation system is more than three times that of the total thermal resistance of walls constructed from hollow concrete block (TR2).
9. In comparison with the Reference room (TR2), the saving in energy due to the usage of the INSULATE coating on walls of the room TR1, concrete blocks incorporating expanded polystyrene board in walls of room TR3 and new insulation system in the walls of the room TR4 was 35, 29 and 58%; respectively.
10. The thermal transmittance calculated from inner and outer temperatures of test rooms and heat flux measured on walls of the test rooms was higher as compared to that computed using the commercial testo 635-2 U-value equipment. This is

attributed to the fact that commercial U-value equipment depends on simple theoretical and metrology fundamentals to calculate the U-value [80].

11. The 3D simulation of the test rooms using DesignBuilder software incorporating the measured metrological data, materials properties and electrical loads was carried out to validate the energy consumption results measured in the field thereby calculating the heat convective coefficients of the walls' surfaces. The agreement between the experimental measurements and the DesignBuilder simulation results was more than 90%, which is considered highly acceptable and reliable from practical point of view.

12. The 3D FE modeling of the walls of test rooms using ABAQUS software was performed to validate the surface temperatures of walls measured in the field using the heat convective coefficients of the walls' surfaces obtained from DesginBuilder simulation. The difference between the experimental measurements and the ABAQUS modeling results in all test rooms was marginal (i.e., the accuracy was more than 90%).

7.2 Recommendations

1. INSULATE coating has a small thickness. However, it has excellent thermal properties thereby it is highly recommended to be applied on walls in new buildings because it can reduce the energy consumption by about 35%. Further, this coating is recommended as an excellent solution for decreasing the energy

consumption in existing buildings, particularly for the walls that were constructed without the usage of any thermal insulation materials.

2. The new insulation system of walls in TR4, which includes INSULATED aerated block, plaster and coating, is highly recommended to be used in new buildings since it can reduce the energy consumption by about 58%.

3. The concrete blocks incorporating polystyrene board is recommended to be used for constructing walls in new buildings because it can reduce the energy consumption by about 29%.

7.3 Future work

As a continuation of this field experimental tests, simulation and modeling, the following studies are recommended to be conducted:

1. To study the thermal performance and energy efficiency of walls constructed from concrete blocks incorporating expanded polystyrene board and cement plaster and INSULATE coating on both surfaces of walls.

2. To study the thermal performance and energy efficiency of walls constructed from normal hollow-core concrete blocks and INSULATE plaster and coating on both surfaces of walls.

3. To study the thermal performance and energy efficiency of walls constructed from aerated concrete blocks and cement plaster and INSULATE coating on both surfaces of walls.

4. To study the thermal performance and energy efficiency of walls constructed from concrete blocks incorporating expanded polystyrene board and INSULATE plaster and coating on both surfaces of walls.

REFERENCES

[1] Annual Report - Ministry of Industry and Electricity for the Year 2016, Information and Statistics Department, Saudi Electricity Company, Riyadh, Kingdom of Saudi Arabia, 2016. https://www.se.com.sa/en-us/Pages/AnnualReports.aspx, Riyadh, Kingdom of Saudi Arabia, 2016.

[2] Special Report - Jeddah Economic Gateway, KCOR, Housing the Growing Population of the Kingdom of Saudi Arabia. Jeddah, 2013. http://center4affordablehousing.org/new/wp-content/uploads/2016/08/Saudi-Arabi-Population-and-Housing-Challenges.pdf.

[3] F. Alrashed, M. Asif, Trends in Residential Energy Consumption in Saudi Arabia with Particular Reference to the Eastern Province, *J. Sustain. Dev. Energy, Water Environ. Syst*. 2 (2014) 376–387. doi:10.13044/j.sdewes.2014.02.0030.

[4] A.M. Al-Shaalan, W. Ahmed, A. Alohaly, Design Guidelines for Buildings in Saudi Arabia Considering Energy Conservation Requirements, *Appl. Mech. Mater*. 548–549 (2014) 1601–1606. doi:10.4028/www.scientific.net/AMM.548-549.1601.

[5] Y. Alyousef, M. Abu-ebid, *Energy Efficiency Initiatives for Saudi Arabia on Supply and Demand Sides, Energy Effic. - A Bridg. to Low Carbon Econ*. Dr. Zoran Morvaj (Ed.), ISBN 978-953-51-0340- 0. (2012) 280–308. doi:10.5772/38660.

[6] M. Aksoezen, M. Daniel, U. Hassler, N. Kohler, Building Age as an Indicator for Energy Consumption, *Energy Build*. 87 (2015) 74–86. doi:10.1016/j.enbuild.2014.10.074.

[7] M. Santamouris, G. Mihalakakou, P. Patargias, N. Gaitani, K. Sfakianaki, Using Intelligent Clustering Techniques to Classify the Energy Performance of School Buildings, *Energy Build*. 39 (2007) 45–51. doi:10.1016/j.enbuild.2006.04.018.

[8] Y. Lu, Z. Huang, T. Zhang, Method and Case Study of Quantitative Uncertainty Analysis in Building Energy Consumption Inventories, *Energy Build*. 57 (2013) 193–198. doi:10.1016/j.enbuild.2012.10.046.

[9] V. Oree, A. Khoodaruth, H. Teemul, A Case Study for the Evaluation of Realistic Energy Retrofit Strategies for Public Office Buildings in the Southern Hemisphere, *Build. Simul*. 9 (2016) 113–125. doi:10.1007/s12273-015-0259-y.

[10] I. Petri, S. Kubicki, Y. Rezgui, A. Guerriero, H. Li, Optimizing energy efficiency in operating built environment assets through building information modeling: A case study, *Energies*. 10 (2017) 1–17. doi:10.3390/en10081167.

[11] L. Pe, A Review on Buildings Energy Consumption Information, *Energy Build*. 40 (2008) 394–398. doi:10.1016/j.enbuild.2007.03.007.

[12] B. Howard, L. Parshall, J. Thompson, S. Hammer, J. Dickinson, V. Modi, Spatial Distribution of Urban Building Energy Consumption by End Use, *Energy Build*. 45 (2012) 141–151. doi:10.1016/j.enbuild.2011.10.061.

[13] A. Uihlein, P. Eder, Policy Options Towards an Energy Efficient Residential Building Stock in the EU-27, *Energy Build*. 42 (2010) 791–798. doi:10.1016/j .enbuild.2009.11.016.

[14] M.S. Al-Homoud, Performance Characteristics and Practical Applications of Common Building Thermal Insulation Materials, *Build. Environ.* 40 (2005) 353–366. doi:10.1016/j.buildenv.2004.05.013.

[15] Precast Autoclave Concrete. http://espac.com/.

[16] Autoclave Aerated Concrete Http://chemistryofmaterials2013.wikidot.com/rahul-malhotra.

[17] K.S. Al-Jabri, A.W. Hago, A.S. Al-Nuaimi, A.H. Al-Saidy, Concrete Blocks for Thermal Insulation in Hot Climate, *Cem. Concr. Res*. 35 (2005) 1472–1479. doi:10.1016/j.cemconres.2004.08.018.

[18] S.C. Saveto conctruction Materials-Product Data Shee.

[19] Thermal Insulating Plaster, Plaster. http://www.plastimur.it/en/thermoisol.html.

[20] D. Bozsaky, Laboratory Tests with Liquid Nano-Ceramic Thermal Insulation Coating, *Procedia Eng*. 123 (2015) 68–75. doi:10.1016/j.proeng.2015.10.059.

[21] H. Shen, H. Tan, A. Tzempelikos, The Effect of Reflective Coatings on Building Surface Temperatures, Indoor Environment and Energy Consumption — An Experimental Study, *Energy Build*. 43 (2011) 573–580. doi:10.1016/j.enbuild .2010.10.024.

[22] D. Bozsaky, Application of Nanotechnology-based Thermal Insulation Materials in Building Construction, *Slovak Journal of Civil Eng*. 24 (2016) 17–23. doi:10.1515 /sjce-2016-0003.

[23] D. Bozsaky, Special Thermal Insulation Methods of Building Constructions with Nanomaterials, *Acta Technica Jaurinensis*. 9 (2016) 29–41. doi:10.14513/actatechj aur.v9.n1.391.

[24] D. Bozsaky, Special Thermal Insulation Methods of Building Constructions with Nanomaterials, *Acta Technica Jaurinensis*. 9 (2016) 29–41. doi:10.14513/actate chja ur.v9.n1.391.

[25] D. Bozsaky, Heat Transfer Resistance Experiments of Thermal Insulation Coatings Consisted of Hollow Nano-Ceramic Microspheres, *Nanotech*. 1 (2018) 10-18.

[26] D. Bozsaky, Series of Experiments with Thermal Insulation Coatings Consisted of Vacuum-Hollow Nano- Ceramic Microspheres, *Acta Technica Jaurinensis*. 11 (2018) 17–33. doi:10.14513/actatechjaur.v11.n1.447.

[27] T. Soubdhan, T. Feuillard, F. Bade, Experimental Evaluation of Insulation Material in Roofing System Under Tropical Climate, *Solar Energy*. 79 (2005) 311–320. doi:10.1016/j.sol ener.2004.10.009.

[28] G.A. Sheikhzadeh, A.A. Azemati, H. Khorasanizadeh, The Effect of Mineral Micro Particle in Coating on Energy Consumption Reduction and Thermal Comfort in a Room with a Radiation Cooling Panel in Different Climates, *Energy Build*. 82 (2014) 644–650. doi:10.1016/j.enbuild.2014.07.043.

[29] A. Joudi, H. Svedung, M. Cehlin, M. Rönnelid, Reflective Coatings for Interior and Exterior of Buildings and Improving Thermal Performance, *Appl. Energy*. 103 (2013) 562–570. doi:10.1016/j.apenergy.2012.10.019.

[30] J. Maia, N.M.M. Ramos, V.P. De Freitas, Â. Sousa, Laboratory Tests and Potential of Thermal Insulation Plasters, *Energy Procedia*. 78 (2015) 2724–2729. doi:10.1016/j.egypro.2015.11.613.

[31] I. Amara, A. Mazioud, I. Boulaoued, A. Mhimid, Experimental Study on Thermal Properties of Bio-composite (Gypsum Plaster Reinforced with Palm Tree Fibers) for building insulation, *Int. J. Heat Technol*. 35 (2017) 576–584. doi:10.18280/ijht.350314.

[32] C. Buratti, E. Moretti, E. Belloni, F. Agosti, Development of Innovative Aerogel Based Plasters: Preliminary Thermal and Acoustic Performance Evaluation, *Sustain*. 6 (2014) 5839–5852. doi:10.3390/su6095839.

[33] R. Walker, S. Pavía, Thermal Performance of a Selection of Insulation Materials Suitable for Historic Buildings, *Build. Environ.* 94 (2015) 155–165. doi:10.1016/j.buildenv.2015.07.033.

[34] K. Ghazi Wakili, E. Hugi, L. Karvonen, P. Schnewlin, F. Winnefeld, Thermal Behaviour of Autoclaved Aerated Concrete Exposed to Fire, *Cem. Concr. Compos*. 62 (2015) 52–58. doi:10.1016/j.cemconcomp.2015.04.018.

[35] C. Tasdemir, O. Sengul, M.A. Tasdemir, A comparative Study on the Thermal Conductivities and Mechanical Properties of Lightweight Concretes, *Energy Build*. 151 (2017) 469–475. doi:10.1016/j.enbuild.2017.07.013.

[36] R. Drochytka, J. Zach, A. Korjenic, J. Hroudová, Improving the Energy Efficiency in Buildings While Reducing the Waste Using Autoclaved Aerated Concrete Made from Power Industry Waste, *Energy Build*. 58 (2013) 319–323. doi:10.1016/j.enbuild.2012.10.029. doi:10.1016/j.enbuild.2012.10.029.

[37] H. Radhi, Viability of Autoclaved Aerated Concrete Walls for the Residential Sector in the United Arab Emirates, *Energy Build*. 43 (2011) 2086–2092. doi:10.1016/j.enbuild.2011.04.018..

[38] A.M. Othman, Experimental Investigations of the Effect of Some Insulating Materials on the Compressive Strength, Water Absorption and Thermal Conductivity of Building Bricks, *Jordan Journal of Mechanical and Industrial Engineering*. 4 (2010) 443–450.

[39] A. Castell, M. Medrano, I. Martorell, L.F. Cabeza, *Experimental Study on the Performance of Buildings with Different Insulation Materials*, Chapter 5: Monitoring and evaluation. (2008) 521–526.

[40] M.I. Emadi, The Role of Thermal Insulation in External Walls for Energy Consumption in the case of Famagusta, Adva. Env. Tech. Biotech. (2015) 81–90.

[41] M. Manzan, E. Zandegiacomo, D. Zorzi, W. Lorenzi, Experimental and Numerical Comparison of Internal Insulation Systems for Building Refurbishment, *Energy Procedia*. 82 (2015) 493–498. doi:10.1016/j.egypro.2015.11.853.

[42] C. Stjsao, Experimental Analysis of Thermal Comfort in an Air Conditioned Open Space Office, *Strojarstvo*. 52 (2010) 651–663.

[43] X. Chen, Q. Wang, J. Srebric, Occupant Feedback Based Model Predictive Control for Thermal Comfort and Energy Optimization : A Chamber Experimental Evaluat ion, *Appl. Energy*. 164 (2016) 341–351. doi:10.1016/j.apenergy.2015.11.065.

[44] B. Lin, Z. Wang, H. Sun, Y. Zhu, Q. Ouyang, Evaluation and Comparison of Thermal Comfort of Convective and Radiant Heating Terminals in Office build ings, *Build. Environ.* 106 (2016) 91–102. doi:10.1016/j.buildenv.2016.06.015.

[45] Y. Wang, Y. Liu, C. Song, J. Liu, Appropriate Indoor Operative Temperature and Bedding Micro Climate Temperature that Satisfies the Requirements of Sleep Thermal Comfort, *Build. Environ*. 92 (2015) 20–29. doi:10.1016/j.buildenv .2015.04.015.

[46] M.K. Singh, S. Mahapatra, S.K. Atreya, Thermal Performance Study and Evaluation of Comfort Temperatures in Vernacular Buildings of North-East India, *Build. Environ*. 45 (2010) 320–329. doi:10.1016/j.buildenv.2009.06.009.

[47] S.T. Elias-ozkan, F. Summers, N. Surmeli, A Comparative Study of the Thermal Performance of Building Materials, *23rd Conference on Passive and Low Energy Architecture*, Geneva, Switzerland. (2006) 6–8.

[48] S.5 Gendelis, A. Jakovi, L. Bandeniece, Experimental research of thermal comfort conditions in small test buildings with different types of heating, *Energy Procedia*. 78 (2015) 2929–2934. doi:10.1016/j.egypro.2015.11.669.

[49] M. Ozel, Thermal performance and optimum insulation thickness of building walls with different structure materials, *Appl. Therm. Eng*. 31 (2011) 3854–3863. doi:10.1016/j.applthermaleng.2011.07.033.

[50] A.E. Fiorato, Thermal Performance of Masonry Walls. *Vth International Brick Masonry Conference*., (n.d.) 664–674. http://www.hms.civil.uminho.pt/ibmac/1979/664.pdf.

[51] I. Danielski, M. Froling, Diagnosis of Buildings' Thermal Performance-a Quantitative Method Using Thermography Under Non-steady State Heat Flow, *Energy Procedia*. 83 (2015) 320–329. doi:10.1016/j.egypro.2015.12.186.

[52] F. Asdrubali, C. Buratti, F. Cotana, G. Baldinelli, M. Goretti, E. Moretti, C. Baldassarri, E. Belloni, F. Bianchi, A. Rotili, M. Vergoni, D. Palladino, D. Bevilacqua, Evaluation of Green Buildings' Overall Performance Through in Situ Monitoring and Simulations, *Energies*. 6 (2013) 6525–6547. doi:10.3390/en6126525.

[53] J. Terés-zubiaga, C. Escudero, C. García-gafaro, J.M. Sala, Methodology for Evaluating the Energy Renovation Effects on the Thermal Performance of Social Housing Buildings : Monitoring Study and Grey Box Model Development, *Energy Build*. 102 (2015) 390–405. doi:10.1016/j.enbuild.2015.06.010.

[54] S.S. Hung, C.Y. Chang, C.J. Hsu, S.W. Chen, Analysis of Building Envelope Insulation Performance Utilizing Integrated Temperature and Humidity Sensors, *Sensors*. 12 (2012) 8987–9005. doi:10.3390/s120708987.

[55] K. Horikiri, Y. Yao, J. Yao, *Numerical Optimisation of Thermal Comfort Improvement for Indoor Environment with Occupants and Furniture*, Faculty of Science , Engineering and Computing , Kingston University , London SW15 3DW, Faculty of Environment and Technology , University of the We, (2015) 303–315.

[56] S.H. Ho, *Numerical Simulation of Thermal Comfort and Contaminant Transport in Air Conditioned Rooms*, MS thesis, Department of Mechanical Engineering College of Engineering University of South Florida (2004).

[57] R.H. Mohammed, Numerical Investigation of Indoor Air Quality and Thermal Comfort in a Ventilated Room, *International Journal of Mechanical and Mechatronics Engineering*. 7 (2013) 876–882.

[58] S.A. Al-Sanea, M.F. Zedan, Improving Thermal Performance of Building Walls by Optimizing Insulation Layer Distribution and Thickness for Same Thermal Mass, *Appl. Energy*. 88 (2011) 3113–3124. doi:10.1016/j.apenergy.2011.02.036.

[59] C.P.O. Box, N. Scotia, Thermal Modeling in a Historical Building – Improving Thermal Comfort through the Siting of a Passive Mass of Phase Change Material,

*COMSOL Conference in Bosto*n. (2014) 1–7.

[60] A. Sabanskis, J. Virbulis, Experimental and Numerical Analysis of Air Flow, Heat Transfer and Thermal Comfort in Buildings with Different Heating Systems, *Latvian Journal of Physics and Technical Sciences*. (2016) 20–30. doi:10.1515/lpts-2016-0010..

[61] I. Wolf, I. Frankovic, I. Bonefacic, I. Wolf, B. Frankovic, Numerical Modelling of Thermal Comfort Conditions in an Indoor Space with Solar Radiation Sources, *Journal of Mechanical Engineering.* 61 (2015) 641–650. doi:10.5545/sv-jme.2015. 2493.

[62] A. Zhou, K. Wong, D. Lau, Thermal Insulating Concrete Wall Panel Design for Sustainable Built Environment, *The Scientific World Journal*. 2014 (2014) 12.

[63] M. Ibrahim, E. Wurtz, P. Henry, P. Achard, Performance Evaluation of Buildings with Advanced Thermal Insulation System : A Numerical Study, *Journal of Facade Design and Engineering*. 4 (2016) 19–34. doi:10.3233/FDE-160048.

[64] A.A. Azemati, B. Shirkavand Hadavand, H. Hosseini, A. Salemi Tajarrod, Thermal Modeling of Mineral Insulator in Paints for Energy Saving, *Energy Build*. 56 (2013) 109–114. doi:10.1016/j.enbuild.2012.09.036.

[65] X. Xu, Y. Zhang, K. Lin, H. Di, R. Yang, Modeling and Simulation on the Thermal Performance of Shape-stabilized Phase Change Material Floor Used in Passive Solar Buildings, *Energy Build*. 37 (2005) 1084–1091. doi:10.1016/j.enbuild .2004.12.016.

[66] G. Hu, R.K. Agarwal, *Accented Models : Evaluating Their Effectiveness in Building Energy Simulation*, Independent Study, Department of Mechanical Engineering & Materials Science, Washington University. (2016). http://openscho larship.wustl. edu/ mems500/2.

[67] N. Cardinale, G. Rospi, P. Stefanizzi, Energy and Microclimatic Performance of Mediterranean Vernacular Buildings: The Sassi District of Matera and the Trulli District of Alberobello, *Build. Environ*. 59 (2013) 590–598. doi:10.1016/j. buildenv.2012.10.006.

[68] M. Webb, Building Energy and Cfd Simulation To Verify Thermal Comfort in Under Floor Air Distribution (Ufad) Design, *Build. Simul.* (2013) 1885–1892.

[69] ASTM C518 – *Standard Test Method for Steady-State Thermal Transmission Properties by Means of the Heat Flow Meter Apparatus*, 2010.

[70] P. Akbari, H., Levinson, R., Berdahl, H. Akbari, R. Levinson, P. Berdahl, ASTM Standards for Measuring Solar Reflectance and Infrared Emittance of Construction Materials and Comparing their Steady-State Surface Temperatures, ACEEE

Summer Study Energy Effic. *Build*. 1 (1996) 1–9.

[71] A. Fernández-García, F. Sutter, L. Martínez-Arcos, C. Sansom, F. Wolfertstetter, C. Delord, Equipment and Methods for Measuring Reflectance of Concentrating Solar Reflector Materials, *Sol. Energy Mater. Sol. Cells*. 167 (2017) 28–52. doi:10.1016/j.solmat.2017.03.036.

[72] L.S. Facility, Jasco V-670 Absorption Spectrometer Operation Instructions, https://www.chem.uci.edu/~dmitryf/manuals/Instructions/Jasco%20V-670%20instructions.pdf

[73] ASTM C1723-16, *Standard Guide for Examination of Hardened Concrete Using Scanning Electron Microscopy*, (2010).

[74] ASTM C1365-18, *Standard Test Method for Determination of the Proportion of Phases in Portland Cement and Portland-Cement Clinker Using X-Ray Powder Diffraction Analysis*, 2010.

[75] K.O. Lee, *Experimental and Simulation Approaches for Optimizing the Thermal Performance of Building Enclosures Containing Phase Change Materials*, PhD thesis, Civil Engineering College of The University of Kansas, Lawrence, Kansas, USA, 2014.

[76] J. Jaworski, The infrared thermography of buildings proceeding its surrounding and their thermal performance, *9th Int. Conf. Quant. InfraRed Thermogr*. Krakow - Poland (2008).

[77] F. Bianchi, A.L. Pisello, G. Baldinelli, F. Asdrubali, Infrared Thermography Assessment of Thermal Bridges in Building Envelope: Experimental validation in a test room setup, *Sustain*. 6 (2014) 7107–7120. doi:10.3390/su6107107.

[78] ASTM C1060-11a-2015, *Standard Practice for Thermographic Inspection of Insulation Installations in Envelope Cavities of Frame Buildings*, Annual Book of ASTM Standards, Vol. 04.06. West Conshohocken, PA, USA, 2015.

[79] ASTM C 1046-95 (2013), *Standard Practice for In-situ Measurement of Heat Flux and Temperature on Building Envelope Components*, Annual Book of ASTM Standards, Vol. 04.06, West Conshohocken, PA, USA, 2013. 20 https://www.astm.org/Standards/C1046.htm.

[80] D. Bienvenido-Huertas, R. Rodríguez-Álvaro, J. Moyano, F. Rico, D. Marín, Determining the U-Value of Façades Using the Thermometric Method: Potentials and Limitations, *Energies*. 11 (2018) 360. doi:10.3390/en11020360.

[81] Reflectivity of Materilas. The Engineering Tool Box - https://www.engineeringtoolbox.com/light-material-reflecting-factor-d_1842.html.

[82] S.J.P.M. Sumirat, I., Ando, Y. & Shimamura, Theoretical consideration of the effect of porosity on thermal conductivity of porous materials, *J. Porous Mater*. 13 (2006) 439–443.

[83] Paint Background, http://www.madehow.com/Volume-1/Paint.html.

[84] Silicone-based Paints and Coatings for Industrial and Consumer Markets, https://silicones.elkem.com/EN/Our_offer/Market_And_Application/Pages/paint-and-coating.aspx.

[85] R.G. Mathey, W.J.J. Rossiter, A Review of Autoclaved Aerated Concrete Products, *NBS Publ*. (1988) 32. doi:10.6028/NBS.IR.87-3670.

[86] ASTMC1155-95(2013), *Standard Practice for Determining Thermal Resistance of Building Envelope Components from the In-Situ Data*, Annual Book of ASTM Standards, Vol. 04.06, West Conshohocken, PA, USA, 2013. 30 https://www.astm.org/Standards/C1155.htm 31.

[87] ISO9869-1(2014), *Thermal Insulation Building Elements-In-situ Measurement of Thermal Resistance and Thermal Transmittance-Part 1: Heat Flow Meter*, Geneve, Switzerland, 2014. https://www.iso.org/standard/59697.html 34 35.

[88] A. Ahmad, M. Maslehuddin, L.M. Al-Hadhrami, In Situ Measurement of Thermal Transmittance and Thermal Resistance of Hollow Reinforced Precast Concrete Walls, *Energy Build*. 84 (2014) 132–141. doi:10.1016/j.enbuild.2014.07.048.

[89] S.E.G. Jayamaha, N.E. Wijeysundera, S.K. Chou, Measurement of the Heat Transfer Coefficient for Walls, *Build. Environ.* 31 (1996) 399–407. doi:10.1016/0360-1323(96)00014-5.

[90] T. Defraeye, B. Blocken, J. Carmeliet, Convective Heat Transfer Coefficients for Exterior Building Surfaces : Existing correlations and CFD modelling, *Energy Build*. 32 (2010) 1–20.

[91] I. Beausoleil-morrison, An Algorithm for Calculating Convection Coefficients for Internal Building Surfaces for the Case of Mixed Flow in Rooms, *Energy Build*. 33 (2001) 351–361.

[92] S. Obyn, G. Van Moeseke, Variability and Impact of Internal Surfaces Convective Heat Transfer Coefficients in the Thermal Evaluation of Office Buildings, *Appl. Therm. Eng*. 87 (2015) 258–272. doi:10.1016/j.applthermaleng.2015.05.030.

[93] J. Gao, X. Zhang, J. Zhao, Numerical Determination of Convection Coefficients for Internal Surfaces in Buildings Dominated by Thermally Stratified Flows, *Journal of Building Physics*. 31 (2007). doi:10.1177/1744259107085400.

[94] M. Mirsadeghi, D. Cóstola, B. Blocken, J.L.M. Hensen, Review of External

Convective Heat Transfer Coefficient Models in Building Energy Simulation Programs : Implementation and Uncertainty, *Appl. Therm. Eng*. 56 (2013) 134–151. doi:10.1016/j.applthermaleng.2013.03.003..

[95] Georgios Georgiou, M. Heier, A.S. Muhaisen, H.R. Dabboor, H. Technologies, S. Hoffmann, C. Jedek, E. Arens, P. Kaul, A. Banerjee, U. Chand, S. Alvarez, J.L. Molina, New Buildings Institute, T. Vechaphutti, Daylight and thermal comfort in a Residential Passive House, *Best Build. Enclos. Sci. Technol. Conf*. 2002 (2012) 531–547.

[96] X. Zheng, *Thermal Comfort Research in a Naturally-Ventilated High-Rise*, MS thesis, Faculty of Civil Engineering and Geosciences, Delft University of Technology, Delft, The Netherlands, (2015).

[97] M. Tap, H.M. Kamar, A. Kadir, M. Nazri, K. Amry, M. Salimin, Simulation of Thermal Comfort of a Residential House, *Int. J. Comput. Sci*. 8 (2011) 200–208.

[98] C.D. Douglass, *Instructional Modules Demonstrating Building Energy Analysis Using a Building Information Model*, MS thesis, Systems and Entrepreneurial Engineering College, University of Illinois at Urbana-Champaign, 2010.

[99] DesignBuilder, DesignBuilder Software Ltd 2017. DesignBuilder Simulation + CFD Training Guide, (2017). https://www.designbuilder.co.uk/.

[100] EnergyPlus, EnergyPlus Documentation-Engineering Reference, The Reference to EnergyPlus Calculations; Pdf. https://energyplus.net/documentation.

[101] Y. Bahar, C. Pere, J. Landrieu, C. Nicolle, A Thermal Simulation Tool for Building and Its Interoperability through the Building Information Modeling (BIM) Platform, *Buildings*. 3 (2013) 380–398. doi:10.3390/buildings3020380.

[102] F.P. Incropera, D.P. DeWitt, T.L. Bergman, A.S. Lavine, Fundamentals of Heat and Mass Transfer, 2007. doi:10.1073/pnas.0703993104.

[103] A.S. Al-Tamimi, M.A. Al-Osta, O.S.B. Al-Amoudi, R. Ben-Mansour, Effect of Geometry of Holes on Heat Transfer of Concrete Masonry Bricks Using Numerical Analysis, *Arab. J. Sci. Eng*. 42 (2017) 3733–3749. doi:10.1007/s13369-017-2482-6.

[104] Electronic Temperature Instruments, Emissivity Table. https://thermometer.co.uk.

[105] M. Čekon, Spectral emissivity properties of reflective coatings, *Slovak J. Civ. Eng*. XX (2012) 1–7. doi:10.2478/v10189-012-0007-6.

[106] UNE EN ISO6946:2012, Building Components and Building Elements. Thermal Resistance and Thermal Transmittance. Calculation method (ISO 6946:2007).

APPENDICES

Appendix A: Weather station data

Average daily outside temperature, RH, wind speed, solar radiation and UV-index

Date	Outside temperature, °C	Outside RH, %	Wind speed, km/h	Solar Radiation, W/m^2	UV-Index
7/1/2017	38.89	15.03	3.82	289.51	1.41
7/2/2017	39.21	18.46	4.08	288.68	1.43
7/3/2017	39.90	23.46	3.96	279.03	1.31
7/4/2017	39.92	29.72	6.95	279.67	1.35
7/5/2017	39.28	28.34	4.26	274.35	1.25
7/6/2017	39.33	22.01	3.98	277.53	1.30
7/7/2017	39.72	26.38	4.30	270.48	1.23
7/8/2017	38.14	49.29	7.25	256.20	1.15
7/9/2017	37.35	59.65	5.51	240.09	1.11
7/10/2017	39.04	47.91	4.96	247.47	1.18
7/11/2017	40.13	41.67	5.23	243.82	1.09
7/12/2017	39.33	27.01	10.38	267.19	1.25
7/13/2017	40.55	13.44	4.45	264.74	1.19
7/14/2017	40.59	22.02	5.01	230.59	0.93
7/15/2017	39.45	41.05	7.91	233.94	0.86
7/16/2017	38.07	51.94	5.42	239.28	1.04
7/17/2017	39.11	40.81	2.98	255.10	1.12
7/18/2017	39.94	19.62	5.75	263.17	1.14
7/19/2017	38.32	51.41	6.44	262.00	1.21
7/20/2017	38.64	40.29	5.19	272.16	1.30
7/21/2017	39.85	29.44	2.61	272.72	1.27
7/22/2017	39.80	26.72	3.11	273.23	1.26
7/23/2017	39.58	35.29	3.86	267.78	1.16
7/24/2017	40.06	34.05	3.76	270.78	1.25
7/25/2017	39.99	31.46	4.78	265.71	1.18
7/26/2017	39.23	26.97	5.48	266.59	1.28
7/27/2017	39.28	25.28	5.33	268.33	1.18
7/28/2017	37.93	40.51	5.65	266.28	1.17
7/29/2017	38.20	42.62	4.10	264.65	1.19
7/30/2017	39.48	35.41	3.75	257.97	1.08
7/31/2017	38.40	34.90	7.05	265.35	1.30

Average daily outside temperature, RH, wind speed, solar radiation and UV-index

Date	Outside temperature, °C	Outside RH, %	Wind speed, km/h	Solar Radiation, W/m^2	UV-Index
8/1/2017	39.24	24.12	7.25	270.69	1.32
8/2/2017	38.18	32.59	5.25	262.38	1.22
8/3/2017	38.43	49.17	4.88	245.63	1.15
8/4/2017	39.38	37.01	3.51	247.17	1.11
8/5/2017	39.42	34.20	3.24	228.58	0.98
8/6/2017	38.96	43.15	3.80	260.28	1.18
8/7/2017	38.86	47.21	4.33	245.60	1.11
8/8/2017	38.92	41.83	3.77	255.63	1.17
8/9/2017	39.24	39.80	3.61	254.63	1.13
8/10/2017	39.19	44.44	3.82	252.10	1.09
8/11/2017	38.82	47.99	4.86	247.76	1.14
8/12/2017	38.80	49.03	4.89	248.82	1.17
8/13/2017	38.91	46.91	3.77	235.63	1.04
8/14/2017	39.80	43.47	4.50	231.79	0.97
8/15/2017	38.30	56.12	5.34	217.27	0.86
8/16/2017	38.05	57.16	4.16	232.02	1.02
8/17/2017	37.15	59.85	5.55	222.95	0.94
8/18/2017	37.22	55.99	3.16	237.72	1.09
8/19/2017	38.59	42.92	3.98	222.70	0.92
8/20/2017	38.43	53.54	3.14	208.67	0.84
8/21/2017	38.61	59.71	3.96	207.06	0.87
8/22/2017	39.42	47.26	4.33	209.94	0.88
8/23/2017	39.25	45.35	5.80	216.99	0.93
8/24/2017	38.01	54.16	4.57	207.26	0.84
8/25/2017	37.08	55.49	3.27	212.19	0.87
8/26/2017	37.25	50.28	2.95	222.77	0.93
8/27/2017	37.44	57.31	5.38	222.71	0.95
8/28/2017	37.09	53.92	4.36	222.43	0.95
8/29/2017	36.76	52.44	4.19	226.37	0.96
8/30/2017	36.75	53.06	3.55	227.72	0.97
8/31/2017	37.29	46.47	4.61	233.97	1.06

Average daily outside temperature, RH, wind speed, solar radiation and UV-index

Date	Outside temperature, °C	Outside RH, %	Wind speed, km/h	Solar Radiation, W/m^2	UV-Index
9/1/2017	37.45	48.60	3.99	234.42	1.04
9/2/2017	36.84	50.44	3.91	226.27	0.98
9/3/2017	38.77	28.18	3.00	238.69	1.06
9/4/2017	37.15	44.67	4.37	226.97	0.99
9/5/2017	36.52	47.65	3.53	215.70	0.87
9/6/2017	36.29	56.58	4.96	226.78	0.94
9/7/2017	35.90	56.51	4.02	224.85	0.95
9/8/2017	36.14	55.00	2.97	221.90	0.93
9/9/2017	35.70	53.26	4.72	211.31	0.82
9/10/2017	35.16	43.90	5.66	214.66	0.81
9/11/2017	34.69	62.44	3.34	207.60	0.81
9/12/2017	36.15	64.89	2.36	197.17	0.75
9/13/2017	37.29	44.68	2.76	217.54	0.85
9/14/2017	36.05	38.88	3.56	218.90	0.84
9/15/2017	34.25	65.06	5.12	212.21	0.87
9/16/2017	34.39	67.08	4.19	204.21	0.81
9/17/2017	35.08	61.89	4.72	194.46	0.71
9/18/2017	34.91	59.82	4.25	203.56	0.79
9/19/2017	34.66	57.55	3.66	190.18	0.67
9/20/2017	34.91	49.96	3.34	192.20	0.66
9/21/2017	34.95	56.53	4.40	204.17	0.80
9/22/2017	35.40	52.47	3.46	206.38	0.84
9/23/2017	34.17	47.42	2.93	213.85	0.84
9/24/2017	34.18	51.07	4.08	194.12	0.73
9/25/2017	34.13	49.65	2.61	201.81	0.78
9/26/2017	34.34	36.58	2.73	202.06	0.76
9/27/2017	34.71	33.38	3.07	204.73	0.78
9/28/2017	34.76	33.97	2.30	202.98	0.78
9/29/2017	34.12	47.10	5.04	200.36	0.83
9/30/2017	33.41	54.94	4.39	197.12	0.78

Appendix B: Inside temperature and RH of the test rooms

Average daily inside temperature (°C) in the test rooms

Date	TR1	TR2	TR3	TR4
7/1/2017	23.51	23.66	23.25	22.51
7/2/2017	23.60	23.76	23.44	22.62
7/3/2017	23.77	23.87	23.67	22.63
7/4/2017	24.12	24.02	23.85	22.80
7/5/2017	23.95	23.95	23.70	22.74
7/6/2017	23.77	23.82	23.57	22.67
7/7/2017	23.97	23.92	23.63	22.73
7/8/2017	24.00	24.15	23.75	22.79
7/9/2017	23.93	24.12	23.67	22.69
7/10/2017	24.04	24.08	23.82	22.76
7/11/2017	24.16	24.04	23.83	22.85
7/12/2017	24.16	24.24	23.82	22.82
7/13/2017	24.05	24.00	23.67	22.78
7/14/2017	24.11	24.00	23.75	22.80
7/15/2017	24.32	24.24	23.99	22.96
7/16/2017	24.14	24.18	23.82	22.79
7/17/2017	24.07	23.99	23.74	22.81
7/18/2017	24.06	23.87	23.73	22.81
7/19/2017	24.13	24.09	23.73	22.81
7/20/2017	24.00	24.10	23.75	22.81
7/21/2017	23.97	23.87	23.75	22.79
7/22/2017	23.44	23.58	23.12	22.22
7/23/2017	21.44	21.28	20.66	19.84
7/24/2017	21.30	21.25	20.55	19.64
7/25/2017	21.26	21.11	20.54	19.59
7/26/2017	21.25	20.76	20.50	19.48
7/27/2017	21.15	21.02	20.46	19.35
7/28/2017	21.14	20.45	20.48	19.37
7/29/2017	21.03	20.70	20.40	19.31
7/30/2017	22.45	22.35	21.98	21.17
7/31/2017	23.77	23.90	23.49	22.57

Average daily inside temperature (°C) in test rooms

Date	TR1	TR2	TR3	TR4
8/1/2017	23.91	23.89	23.63	22.66
8/2/2017	23.86	23.98	23.55	22.65
8/3/2017	24.06	24.14	23.79	22.72
8/4/2017	24.11	24.09	23.78	22.81
8/5/2017	24.07	24.04	23.87	22.85
8/6/2017	24.17	24.09	23.87	22.98
8/7/2017	23.29	23.60	22.92	22.03
8/8/2017	21.26	21.42	20.72	19.92
8/9/2017	21.14	21.20	20.36	19.67
8/10/2017	21.17	21.54	20.41	19.65
8/11/2017	21.15	21.21	20.31	19.58
8/12/2017	21.18	20.97	20.35	19.63
8/13/2017	21.15	20.82	20.37	19.50
8/14/2017	21.17	21.11	20.36	19.58
8/15/2017	22.15	21.91	21.64	20.81
8/16/2017	23.92	24.02	23.71	22.89
8/17/2017	23.97	23.94	23.74	22.92
8/18/2017	23.93	23.83	23.74	22.93
8/19/2017	23.98	23.62	23.71	22.90
8/20/2017	24.10	23.80	23.92	22.98
8/21/2017	24.24	24.05	24.05	23.10
8/22/2017	24.39	24.04	24.19	23.16
8/23/2017	24.45	24.17	24.20	23.22
8/24/2017	24.26	24.07	24.06	23.13
8/25/2017	24.08	24.10	23.97	22.99
8/26/2017	24.03	24.05	23.89	22.95
8/27/2017	24.13	23.96	23.92	22.99
8/28/2017	24.07	24.10	23.89	22.95
8/29/2017	23.96	23.94	23.77	22.92
8/30/2017	23.92	23.95	23.75	22.90
8/31/2017	23.89	23.82	23.68	22.80

Average daily inside temperature (°C) in the test rooms

Date	TR1	TR2	TR3	TR4
9/1/2017	23.97	23.77	23.74	22.93
9/2/2017	23.93	23.82	23.66	22.86
9/3/2017	23.91	23.71	23.72	22.85
9/4/2017	24.00	23.98	23.71	22.81
9/5/2017	23.85	23.85	23.65	22.83
9/6/2017	23.85	23.90	23.71	22.77
9/7/2017	23.81	23.89	23.62	22.70
9/8/2017	23.78	23.88	23.63	22.72
9/9/2017	23.76	23.84	23.63	22.71
9/10/2017	23.65	23.67	23.50	22.67
9/11/2017	23.65	23.79	23.55	22.67
9/12/2017	23.86	23.93	23.79	22.77
9/13/2017	23.79	23.92	23.68	22.72
9/14/2017	23.62	23.81	23.51	22.65
9/15/2017	23.51	23.65	23.47	22.68
9/16/2017	23.63	23.84	23.26	22.66
9/17/2017	23.67	23.85	23.15	22.69
9/18/2017	23.65	23.84	23.09	22.73
9/19/2017	23.54	23.73	23.03	22.57
9/20/2017	23.51	23.70	23.02	22.61
9/21/2017	23.58	23.84	23.08	22.63
9/22/2017	23.62	23.91	23.11	22.68
9/23/2017	23.46	23.61	22.97	22.58
9/24/2017	23.40	23.57	22.92	22.55
9/25/2017	23.42	23.70	22.95	22.55
9/26/2017	23.29	23.54	22.89	22.45
9/27/2017	23.29	23.49	22.85	22.51
9/28/2017	23.33	23.60	22.94	22.51
9/29/2017	23.34	23.55	22.88	22.49
9/30/2017	23.37	23.49	22.86	22.54

Average daily inside RH (%) in the test rooms

Date	TR1	TR2	TR3	TR4
7/1/2017	57.30	52.48	61.02	72.38
7/2/2017	57.82	51.02	60.26	72.73
7/3/2017	58.98	49.25	60.80	72.25
7/4/2017	57.60	47.11	59.50	71.97
7/5/2017	58.05	48.74	60.68	71.28
7/6/2017	57.65	49.23	60.29	71.57
7/7/2017	57.56	48.87	60.19	71.56
7/8/2017	57.94	48.88	61.11	71.61
7/9/2017	58.97	50.20	61.71	71.74
7/10/2017	58.77	47.81	60.39	71.70
7/11/2017	57.30	46.68	59.66	71.50
7/12/2017	56.95	46.78	59.31	70.92
7/13/2017	55.83	48.48	59.36	70.44
7/14/2017	56.26	46.71	60.30	70.90
7/15/2017	56.89	45.61	58.55	71.09
7/16/2017	58.13	48.41	59.89	70.94
7/17/2017	58.75	49.23	62.00	71.09
7/18/2017	56.91	46.88	59.76	70.43
7/19/2017	58.89	47.96	60.38	71.12
7/20/2017	56.53	48.86	61.03	71.11
7/21/2017	58.68	48.65	61.19	71.30
7/22/2017	53.23	46.03	55.63	69.16
7/23/2017	47.63	39.00	48.53	64.58
7/24/2017	50.26	40.05	50.76	65.80
7/25/2017	51.03	39.58	51.14	66.78
7/26/2017	51.79	39.82	52.64	67.98
7/27/2017	52.05	41.45	53.47	67.91
7/28/2017	52.61	40.44	54.41	68.33
7/29/2017	53.21	42.38	54.29	68.95
7/30/2017	58.47	45.48	58.63	72.15
7/31/2017	60.88	51.88	62.96	74.71

Average daily inside RH (%) in the test rooms

Date	TR1	TR2	TR3	TR4
8/1/2017	58.59	48.31	61.14	73.02
8/2/2017	57.89	50.01	61.21	72.45
8/3/2017	59.90	49.26	61.18	72.88
8/4/2017	58.71	47.90	60.45	72.26
8/5/2017	57.48	48.66	60.56	69.85
8/6/2017	58.33	47.83	60.93	71.35
8/7/2017	52.94	45.62	55.12	67.44
8/8/2017	47.71	40.12	49.35	64.06
8/9/2017	49.49	40.35	50.34	66.25
8/10/2017	50.79	41.30	51.41	67.08
8/11/2017	49.00	40.39	51.40	67.95
8/12/2017	50.20	40.47	51.95	68.36
8/13/2017	51.58	41.68	52.96	67.78
8/14/2017	50.87	41.54	51.65	67.70
8/15/2017	56.65	44.57	59.13	71.81
8/16/2017	62.39	50.28	62.49	74.78
8/17/2017	60.58	50.11	61.86	74.08
8/18/2017	59.82	49.88	62.31	74.30
8/19/2017	60.00	49.85	62.32	73.27
8/20/2017	58.60	48.50	60.79	73.16
8/21/2017	56.80	47.37	59.80	73.23
8/22/2017	56.28	45.90	58.17	72.26
8/23/2017	56.69	46.41	58.07	71.87
8/24/2017	56.08	47.58	58.72	71.79
8/25/2017	57.75	49.71	60.79	71.89
8/26/2017	58.39	51.50	61.96	72.52
8/27/2017	59.49	49.07	61.12	73.10
8/28/2017	57.55	50.57	62.17	73.62
8/29/2017	60.41	51.41	62.81	73.25
8/30/2017	60.11	52.49	62.55	73.30
8/31/2017	60.78	51.83	62.45	72.93

Average daily inside RH (%) in the test rooms

Date	TR1	TR2	TR3	TR4
9/1/2017	60.10	49.90	63.35	74.16
9/2/2017	60.67	52.05	64.24	74.29
9/3/2017	60.48	51.46	64.73	73.46
9/4/2017	59.92	52.47	63.50	73.77
9/5/2017	61.42	53.41	64.66	74.03
9/6/2017	61.32	53.16	64.62	74.24
9/7/2017	61.90	54.48	64.86	74.13
9/8/2017	62.32	54.59	64.80	74.54
9/9/2017	61.88	53.80	65.08	74.14
9/10/2017	63.03	55.98	64.98	75.02
9/11/2017	64.08	57.27	66.24	75.56
9/12/2017	63.11	53.57	65.20	75.38
9/13/2017	62.27	54.19	65.06	75.23
9/14/2017	62.43	55.97	65.21	74.74
9/15/2017	64.64	57.27	67.17	75.40
9/16/2017	65.12	57.88	67.47	75.96
9/17/2017	65.20	57.48	67.61	76.64
9/18/2017	64.97	57.48	66.94	76.44
9/19/2017	65.33	57.94	67.84	75.13
9/20/2017	66.15	58.38	67.81	75.97
9/21/2017	65.42	57.59	67.30	75.88
9/22/2017	64.91	56.91	67.01	75.88
9/23/2017	65.61	58.95	68.04	75.19
9/24/2017	67.07	59.68	69.01	76.07
9/25/2017	67.08	59.85	69.15	76.34
9/26/2017	66.76	60.75	68.81	75.68
9/27/2017	66.98	59.87	69.21	76.15
9/28/2017	66.56	59.80	69.31	76.06
9/29/2017	67.72	59.76	69.72	76.73
9/30/2017	67.81	60.05	69.55	77.19

Appendix C: Surface temperature and heat flux of the walls in the test rooms

Average inside surface temperature on walls of the test rooms during different periods and different setting temperature of A/C

Wall	Test Room	Inside Surface Temperature (°C)		
		A/C-24°C	A/C-20°C	A/C-24°C
		1 to 21-July	22 to 30-July	31-July to7-August
North wall	TR1	26.9	25.1	26.8
	TR2	28.5	26.7	28.3
	TR3	25.6	23.3	25.4
	TR4	23.6	21.3	23.5
South wall	TR1	26.8	24.8	26.6
	TR2	27.8	26.1	27.8
	TR3	25.7	23.4	25.5
	TR4	23.6	21.2	23.5
West wall	TR1	27	25.2	26.9
	TR2	28.6	26.9	28.5
	TR3	25.7	23.5	25.6
	TR4	23.9	21.5	23.7
East wall	TR1	25.8	23.9	25.7
	TR2	28.3	26.6	28
	TR3	25.4	23.1	25.2
	TR4	23.9	21.5	23.8

Average inside surface temperature on walls of the test rooms during different periods and different setting temperature of A/C

Wall	Test Room	Inside Surface Temperature (°C)		
		A/C-20	A/C-24	A/C-24
		8to15-August	16 to 31-August	1 to 30-September
North wall	TR1	24.9	26.9	25.8
	TR2	26.7	27.7	27
	TR3	23.1	25.6	24.7
	TR4	21.1	23.7	23.2
South wall	TR1	24.5	26.7	25.8
	TR2	26.2	27.8	26.5
	TR3	22.9	25.6	24.8
	TR4	21	23.9	23.4
West wall	TR1	24.9	26.8	25.9
	TR2	27	28.5	27.2
	TR3	23.1	25.7	24.9
	TR4	21.3	24	23.5
East wall	TR1	23.7	25.8	24.8
	TR2	26.5	27.6	26.7
	TR3	22.9	25.5	24.5
	TR4	21.3	24.1	23.5

Average heat flux through East and West walls of the test rooms during different periods of August and September and different setting temperature of A/C

Wall	Test Room	Heat Flux (w/m2)		
		August		September
		A/C-20°C	A/C-24°C	A/C-24°C
West	TR1	21.2	16.6	11.5
	TR2	34	37.4	20.9
	TR3	17.1	13.1	8.4
	TR4	8.4	6	4.5
East	TR1	17.6	14.5	10.3
	TR2	36.9	29.7	20.5
	TR3	12.8	7.8	6.3
	TR4	7.8	6.3	4

Appendix D: Energy consumption in the test rooms

Daily energy consumption in test rooms during summer months.

Date	TR1	TR2	TR3	TR4
7/1/2017	16	28	18	10
7/2/2017	18	28	20	12
7/3/2017	18	32	20	12
7/4/2017	20	34	22	14
7/5/2017	18	32	20	12
7/6/2017	18	32	20	14
7/7/2017	20	32	22	12
7/8/2017	18	32	20	12
7/9/2017	18	30	20	12
7/10/2017	18	34	20	12
7/11/2017	20	34	22	14
7/12/2017	20	34	20	12
7/13/2017	18	32	22	14
7/14/2017	22	36	22	12
7/15/2017	20	36	22	14
7/16/2017	20	32	22	12
7/17/2017	18	32	20	14
7/18/2017	20	30	20	12
7/19/2017	18	28	20	12
7/20/2017	18	26	18	14
7/21/2017	20	30	20	12
7/22/2017	22	32	24	16
7/23/2017	30	38	30	20
7/24/2017	28	38	30	20
7/25/2017	26	38	28	18
7/26/2017	26	36	28	18
7/27/2017	24	36	26	16
7/28/2017	26	36	28	18
7/29/2017	26	36	26	16
7/30/2017	20	34	24	12
7/31/2017	16	28	18	12

Daily energy consumption in test rooms during summer months.

Date	TR1	TR2	TR3	TR4
8/1/2017	20	30	20	10
8/2/2017	20	28	20	12
8/3/2017	20	28	22	12
8/4/2017	20	30	22	12
8/5/2017	20	30	22	16
8/6/2017	18	30	22	12
8/7/2017	26	34	26	18
8/8/2017	30	38	30	22
8/9/2017	28	38	32	20
8/10/2017	28	38	32	18
8/11/2017	30	41	30	18
8/12/2017	28	41	30	18
8/13/2017	28	38	30	18
8/14/2017	30	42	32	20
8/15/2017	24	30	24	16
8/16/2017	18	28	20	12
8/17/2017	20	30	22	12
8/18/2017	18	28	22	12
8/19/2017	20	30	20	12
8/20/2017	22	40	22	12
8/21/2017	24	34	26	12
8/22/2017	22	36	24	14
8/23/2017	24	36	24	14
8/24/2017	22	32	24	14
8/25/2017	20	32	22	12
8/26/2017	20	28	20	12
8/27/2017	22	34	22	12
8/28/2017	22	30	20	14
8/29/2017	20	28	22	12
8/30/2017	20	28	22	12
8/31/2017	18	30	22	12

Daily energy consumption in test rooms during summer months.

Date	TR1	TR2	TR3	TR4
9/1/2017	18	32	22	12
9/2/2017	20	30	20	12
9/3/2017	22	32	22	12
9/4/2017	20	30	20	12
9/5/2017	20	26	20	12
9/6/2017	18	30	22	10
9/7/2017	18	26	18	12
9/8/2017	18	28	20	10
9/9/2017	16	28	20	12
9/10/2017	16	24	18	10
9/11/2017	18	26	20	10
9/12/2017	16	26	16	8
9/13/2017	16	26	20	10
9/14/2017	16	26	20	10
9/15/2017	16	26	18	10
9/16/2017	16	24	20	10
9/17/2017	18	26	20	12
9/18/2017	16	26	18	10
9/19/2017	16	24	18	10
9/20/2017	16	26	20	8
9/21/2017	16	24	18	12
9/22/2017	16	26	20	10
9/23/2017	16	24	16	8
9/24/2017	14	24	18	10
9/25/2017	14	24	18	10
9/26/2017	14	22	18	8
9/27/2017	16	24	16	10
9/28/2017	14	22	16	10
9/29/2017	14	24	16	8
9/30/2017	14	20	16	10
Total	1840	2812	2004	1180

Energy consumption in test rooms during the day for summer months.

Date	TR1	TR2	TR3	TR4
7/1/2017 6:03	8	16	10	6
7/2/2017 6:04	10	16	12	6
7/3/2017 6:05	10	20	12	6
7/4/2017 6:05	12	20	14	8
7/5/2017 6:06	10	18	12	8
7/6/2017 6:07	10	20	12	6
7/7/2017 6:07	10	20	12	6
7/8/2017 6:08	10	18	12	8
7/9/2017 6:09	10	18	12	6
7/10/2017 6:10	10	20	12	6
7/11/2017 6:10	12	20	14	6
7/12/2017 6:11	10	20	12	8
7/13/2017 6:12	10	20	12	6
7/14/2017 6:13	10	20	12	8
7/15/2017 6:13	12	22	14	8
7/16/2017 6:14	10	18	12	6
7/17/2017 6:15	8	18	12	6
7/18/2017 6:16	10	18	10	8
7/19/2017 6:16	10	16	10	6
7/20/2017 6:17	10	14	10	6
7/21/2017 6:18	12	18	12	6
7/22/2017 6:18	10	18	12	8
7/23/2017 6:19	16	20	18	12
7/24/2017 6:20	14	20	18	10
7/25/2017 6:21	14	20	16	10
7/26/2017 6:21	14	20	14	10
7/27/2017 6:22	12	20	14	8
7/28/2017 6:23	14	20	14	10
7/29/2017 6:23	14	20	16	8
7/30/2017 6:24	10	20	12	6
7/31/2017 6:25	8	16	10	4

Energy consumption in test rooms during the day for summer months.

Date	TR1	TR2	TR3	TR4
8/1/2017 6:26	12	18	12	6
8/2/2017 6:26	10	16	12	6
8/3/2017 6:27	10	16	14	8
8/4/2017 6:28	10	16	12	8
8/5/2017 6:28	10	16	12	8
8/6/2017 6:29	10	16	12	8
8/7/2017 6:30	12	18	14	10
8/8/2017 6:31	16	20	18	12
8/9/2017 6:31	14	22	18	12
8/10/2017 6:32	16	22	18	10
8/11/2017 6:33	16	20	16	10
8/12/2017 6:34	16	20	16	12
8/13/2017 6:34	14	20	16	8
8/14/2017 6:35	16	22	16	10
8/15/2017 6:36	12	16	14	8
8/16/2017 6:36	10	14	10	8
8/17/2017 6:37	8	8	12	6
8/18/2017 6:38	10	12	12	6
8/19/2017 6:39	12	12	12	6
8/20/2017 6:39	10	22	12	6
8/21/2017 6:40	12	18	12	8
8/22/2017 6:41	12	20	12	8
8/23/2017 6:42	12	22	14	8
8/24/2017 6:42	12	18	14	8
8/25/2017 6:43	10	16	12	6
8/26/2017 6:44	10	16	12	6
8/27/2017 6:44	12	18	12	6
8/28/2017 6:45	12	18	12	6
8/29/2017 6:46	10	16	12	8
8/30/2017 6:46	8	16	12	6
8/31/2017 6:47	10	16	12	6

Energy consumption in test rooms during the day for summer months.

Date	TR1	TR2	TR3	TR4
9/1/2017 6:48	10	18	12	6
9/2/2017 6:48	10	16	10	6
9/3/2017 6:49	10	18	12	6
9/4/2017 6:50	10	16	12	6
9/5/2017 6:51	8	16	12	6
9/6/2017 6:51	10	16	12	6
9/7/2017 6:52	10	16	12	6
9/8/2017 6:53	10	14	12	6
9/9/2017 6:53	10	14	12	6
9/10/2017 6:54	8	12	10	6
9/11/2017 6:55	8	14	10	6
9/15/2017 6:04	8	14	10	4
9/16/2017 6:05	8	14	10	4
9/17/2017 6:05	10	14	12	4
9/18/2017 5:58	8	14	10	4
9/19/2017 5:59	8	12	10	4
9/20/2017 6:00	8	14	10	4
9/21/2017 6:00	10	14	10	4
9/22/2017 6:01	8	14	12	4
9/23/2017 6:02	8	14	10	4
9/24/2017 6:03	8	12	8	6
9/25/2017 6:03	6	14	10	6
9/26/2017 6:04	8	14	10	4
9/27/2017 6:05	8	12	8	6
9/28/2017 6:06	8	14	10	6
9/29/2017 6:06	8	12	8	4
9/30/2017 6:07	8	12	8	6

Energy consumption in test rooms during the night for summer months.

Date	TR1	TR2	TR3	TR4
7/1/2017	8	12	8	6
7/2/2017	8	12	8	6
7/3/2017	8	14	8	6
7/4/2017	8	14	8	4
7/5/2017	8	12	8	6
7/6/2017	8	12	8	6
7/7/2017	10	14	10	6
7/8/2017	8	12	8	6
7/9/2017	8	12	8	4
7/10/2017	8	12	8	6
7/11/2017	8	14	8	6
7/12/2017	10	12	10	6
7/13/2017	10	14	8	6
7/14/2017	10	16	10	6
7/15/2017	8	14	8	6
7/16/2017	10	12	8	6
7/17/2017	8	12	10	6
7/18/2017	10	12	8	4
7/19/2017	8	12	8	6
7/20/2017	8	12	8	6
7/21/2017	8	12	8	6
7/22/2017	14	18	14	10
7/23/2017	12	18	12	8
7/24/2017	12	18	12	10
7/25/2017	12	16	12	8
7/26/2017	10	16	12	8
7/27/2017	12	16	12	8
7/28/2017	12	16	12	8
7/29/2017	12	16	12	6
7/30/2017	8	12	8	4
7/31/2017	8	12	8	6

Energy consumption in test rooms during the night for summer months.

Date	TR1	TR2	TR3	TR4
8/1/2017	10	12	8	6
8/2/2017	10	12	8	4
8/3/2017	8	12	10	4
8/4/2017	10	14	10	6
8/5/2017	10	14	8	6
8/6/2017	10	14	8	6
8/7/2017	14	16	14	10
8/8/2017	14	16	14	8
8/9/2017	14	18	14	8
8/10/2017	12	20	14	8
8/11/2017	12	22	14	8
8/12/2017	14	20	12	6
8/13/2017	14	26	12	8
8/14/2017	14	22	14	8
8/15/2017	8	14	10	6
8/16/2017	10	16	10	6
8/17/2017	8	12	10	4
8/18/2017	8	12	8	4
8/19/2017	10	16	8	6
8/20/2017	10	14	10	4
8/21/2017	12	16	14	6
8/22/2017	10	16	12	6
8/23/2017	10	14	10	6
8/24/2017	10	14	10	6
8/25/2017	10	12	8	6
8/26/2017	10	14	10	6
8/27/2017	10	12	10	6
8/28/2017	10	12	8	6
8/29/2017	10	12	10	6
8/30/2017	8	10	10	6
8/31/2017	8	14	10	6

Energy consumption in test rooms during the night for summer months.

Date	TR1	TR2	TR3	TR4
9/1/2017	10	12	8	6
9/2/2017	10	14	10	6
9/3/2017	10	14	10	6
9/4/2017	10	12	8	4
9/5/2017	10	12	8	6
9/6/2017	8	12	8	6
9/7/2017	8	12	8	4
9/8/2017	8	12	8	6
9/9/2017	8	12	8	4
9/10/2017	6	10	8	4
9/11/2017	8	12	8	4
9/15/2017	8	10	8	4
9/16/2017	8	10	8	6
9/17/2017	8	12	8	6
9/18/2017	8	12	8	4
9/19/2017	8	12	6	6
9/20/2017	6	10	8	6
9/21/2017	8	12	8	6
9/22/2017	8	10	8	6
9/23/2017	6	8	6	4
9/24/2017	6	10	8	4
9/25/2017	8	10	8	4
9/26/2017	6	10	8	4
9/27/2017	6	10	8	4
9/28/2017	8	10	6	4
9/29/2017	6	10	8	4
9/30/2017	6	10	6	4

Resume

Personal Information:

Ahmed Abdullah Alawi Al-Naghi

King Fahd University of Petroleum & Minerals, Kingdom of Saudi Arabia

(+966) 580-040-067

alnghi2006@gmail.com; g201002620@kfupm.edu.sa

Date of birth: 9-10-1979 AD

Nationality: Yemeni

Profile

I am an organized person who enjoys making sure that jobs are done in a timely and efficient manner.

Qualifications

2014 – 2018 King Fahd University of Petroleum & Minerals, Saudi Arabia
PhD
Civil Engineering (Structures)
GPA: 3.81 / 4 [First honor]

2011 –2014 King Fahd University of Petroleum & Minerals, Saudi Arabia
Master
Civil Engineering (Structures)
GPA: 3.72 / 4

2000 –2005 Thamar University, Yemen
Bachelor
Civil Engineering (Structures)
GPA (91.16 %) [First honor]

Research Experience

- Saving Energy in Building Using Thermal Insulation Materials
- Simulation of Energy Consumption in Buildings
- Modeling of Thermal Performance of Buildings

- Strengthening of Beam-Column Joints in Buildings
- Protection of Concrete Structures in Aggressive Environment

Work Experience

- Research Engineer, May 2016-May 2018
  King Fahad University of Petroleum & Minerals, Dhahran, Saudi Arabia
- Graduate Assistant, July 2005-Septemper 2010
  Thamar University-Faculty of Engineering, Thamar, Yemen
- Engineer Designer, July 2005-Septemper 2010
  National and Private sectors, Yemen
- Consultant Engineer, May 2007-Septemper 2010
  Fund Community Contracting, Sana'a, Yemen
- Consultant Engineer, July 2006-Septemper 2010
  Social Fund for Development, Thamar, Yemen

Teaching Experience

At Thamar University, Yemen, I taught the following:

- Concrete Technology
- Design of Reinforced Concrete
- Theory of Structures
- Engineering Mechanics
- Strength of Materials

Short Courses &Workshops

- ACI (American Concrete Institute) membership, 2015, Saudi Arabia
- Protection of Reinforced Concrete Structures in Hot and Aggressive Exposures, 2014, KFUPM, Saudi Arabia
- Concrete Deterioration and Its Prevention, 2013, KFUPM, Saudi Arabia
- Laboratory Equipment Operation, 2006, Taiz

University, Yemen

-The Seventh Training Course of Outstanding Students in Arabic Universities, 2004, Faculty of Engineering, Al-Mania, Egypt

Technical Skills

-Microsoft Office

-ABAQUS, DesignBuilder, Mathmatica, AutoCAD and STAAD Pro